Investigations on the Oxygen Atom Transfer Reaction Mediated through a Bio-Inspired $Fe^{V}(O)$ Complex

Thesis Submitted to AcSIR For the Award of
the Degree of
DOCTOR OF PHILOSOPHY
In Chemical Sciences

By
Kundan Kumar Singh Sagar
(10CC11A26047)

Under the guidance of
Dr. Sayam Sen Gupta

CSIR-National Chemical Laboratory, Pune (India)

राष्ट्रीय रासायनिक प्रयोगशाला
(वैज्ञानिक तथा औद्योगिक अनुसंधान परिषद)
डॉ. होमी भाभा रोड, पुणे - 411 008. भारत
NATIONAL CHEMICAL LABORATORY
(Council of Scientific & Industrial Research)
Dr. Homi Bhabha Road, Pune - 411008. India

CERTIFICATE

This is to certify that the work incorporated in the thesis entitled "**Investigations on the Oxygen Atom Transfer Reaction Mediated through a Bio-Inspired $Fe^{V}(O)$ Complex**" submitted by **Kundan Kumar Singh Sagar** to **Academy of Scientific & Innovative Research (AcSIR)** in fulfillment of the requirements for the award of the degree of Doctor of Philosophy has been carried out by him under my supervision at Chemical Engineering & Process Development Division, CSIR-National Chemical Laboratory, Pune-411008, India. I further certify that this work has not been submitted to any other University or Institution in part or full for the award of any degree or diploma. All the materials from the other sources have been duly acknowledged in the thesis. Any text, illustration, table etc., used in the thesis from other sources, have been duly cited and acknowledged.

Kundan Kumar Singh Sagar

(Reg. No. **10CC11A26047**)

Dr. Sayam Sen Gupta

(Supervisor)

Date: 27 June 2017

Place: Pune

Communications Channels ☎ +91 20 25902000 +91 20 25893300 +91 20 25893400 Fax +91 20 25902601 (Director) +91 20 25902660 (Admin.) +91 20 25902639 (Business Development) URL : www.ncl-india.org

DECLARATION

I hereby declare that the thesis entitled "**Investigations on the Oxygen Atom Transfer Reaction Mediated through a Bio-Inspired $Fe^{V}(O)$ Complex**" submitted to **Academy of Scientific & Innovative Research (AcSIR)** for the Award of the **Degree of Doctor of Philosophy (Ph. D.) in Chemical Sciences (Chemistry)**, has been carried out by me at CSIR-National Chemical Laboratory, Pune-411008, India, under the supervision of Dr. Sayam Sen Gupta. The work is original and has not been submitted in part or full by me for any other degree or diploma to this or any other University.

Pune

June 2017

Kundan Kumar Singh Sagar

To my Parents

Acknowledgement

First and foremost, I would like to express my gratitude to my supervisor, Dr. Sayam Sen Gupta, for his guidance, scientific surroundings, and supports throughout my years in his group. I see myself privileged to have the opportunity to work under him where I learned different facets of life during the science and beyond the science.

I also need to thank my doctoral advisory committee Dr. Kumar Vanka (Chairman), Dr. Benudhar Punji and Dr. Rahul Banerjee for scientific discussions during my whole research study at NCL. I would like to thank the University Grants Commission, New Delhi, India, for the award of a research fellowship. I am thankful to Dr. S. Pal, Ex-Director, and Prof. Ashwini Nangia, Director, CSIR-National Chemical Laboratory, Pune, for extending all possible infrastructural facilities to complete my research work.

I sincerely thank Dr. Kumar Vanka and Mr. Mrityunjay Tiwari for their endless effort by DFT calculation during some of my collaborative work.

I would like to express my heartfelt thanks to all the scientific members of CSIR-NCL. I need to express my thanks to the support group and all the staff members, especially Mr. Raheja for his valuable cooperation and help to process all the official work. I acknowledge all the staffs and in charge of the central facility (NMR, and J wing's instrument room of PAML building).

I feel blessed to get the opportunity to interact with Prof. D. S. Pandey (BHU, Varanasi), Dr. Biswajit Ray (BHU, Varanasi), Dr. Jyotishamn Das (TIFR, Mumbai), and Dr. G. Rajaraman (IIT, Bombay), at some point in time during my Ph.D. tenure. I am very much thankful to Anant Kumar Srivastava (IISER, Pune) for his help in X-ray crystallography, Dr. Ajit Singh for mass spectrometry (Venture Centre, NCL-Pune) and Sujoy Rana (IIT, Bombay) for EPR measurement.

I would like to thank my labmates, Dr. B. Malvi, Dr. Mrityunjoy Kar, Dr. Debasis Pati, Dr. Chaka Dola Panda, Dr. Sushma Kumari, Dr. Munmun Ghosh, Soumen Das, Vinita Dhaware, Santanu Pattanayak, Bhawana Pandey, Praveen Korra, Dr. Raj Kumar Das, Dr. Debasree Das, Nimisha Parekh, Bittu Chandra, Sandipan Jana, Basudev Mondal, Maria and Mayur with whom my time in the lab overlapped in day to day life and for making a pleasant and healthy work environment. I have learned something from each and every one of you. However, my additional thanks to Dr. Chaka Dola Panda, Dr. Munmun Ghosh, and Dr. Basab Bijoyi Dhar, with whom I often discussed my results and got helped wherever

was required. Especially, I want to thank Dr. Basab Bijoyi Dhar, who taught me the kinetic measurement. I greatly acknowledge every one of present and past members in the D-wing of PAML building for making a friendly working atmosphere.

I found a memorable friendship with Brijesh Sharma and Mrityunjay Tiwari that I will treasure forever. Thank you to the friends, Neha Tiwari, Sayan Pal, Rajendra Meena, Manoj Sharma, Kshirodra K. Patra, and Santosh Kumar Singh from NCL and Aditya Raj, Abhishek Kumar, Vikas Ranjan, Abadh Kishor Jha, Anil Kumar, Rohit Ritesh, Sunil Rai and Bikas Shaw from other educational institutions as well as from different part of life. All of you have helped me to keep my life balanced during this time.

I offer my sincere regards to my school and college teachers who blessed me with all aspects of education.

I am ever so thankful to my family. I feel fortunate to be a son of Sri Ajay Kishor Singh and Smt. Manikraj Devi who provided me immense love and support at every step of success and failure in life. I have been blessed to have parents who believed in me and encouraged me to take a fresh and boost start after each of my failure. I express my deepest gratitude to my elder brothers, Er. Sunil Kumar Singh and Munna Kumar Singh, who have supported and encouraged me endlessly at every ups and down.

Kundan

Table of Contents

Particulars	Page
Acknowledgements	
List of figures	v
List of schemes	x
List of tables	xi
List of abbreviations	xiii
Abstract of the thesis	xv

Chapter I: Introduction on High-Valent Metal Complex in O-Atom Transfer Reaction			
1.1	Importance of C-H and C=C bond functionalization		1
1.2	Common methods for C=C bond functionalization		3
1.3	Biological systems (iron containing enzymes) in oxygen atom transfer reactions		6
1.4	Synthetic iron porphyrin complexes for hydroxylation and epoxidation reaction		10
1.5	Key intermediates in catalytic cycle of transition metal catalyzed epoxidation reaction		12
1.6	Synthetic approach for the formation of Fe-Oxo intermediate		13
1.7	Objective and motivation		15
1.8	References		19
Chapter II: Tuning the Reactivity of $Fe^{V}(O)$ towards C-H Bonds at Room Temperature: Effect of Water			
2.1	Abstract		26
2.2	Introduction		27
2.3	Experimental section		
	2.3.1	Materials	29
	2.3.2	General instrumentation	30
	2.3.3	Preparation of $Fe^{V}(O)$ in different H_2O/CH_3CN mixtures	31
	2.2.4	Kinetic measurements for the stability of $Fe^{V}(O)$ in different H_2O/CH_3CN mixtures	31
	2.3.5	Kinetic measurements for the reactivity of $Fe^{V}(O)$ toward toluene oxidation	31
	2.3.6	Product quantification	32
	2.3.7	Computational methods	32
2.4	Results and discussion		
	2.4.1	Formation and characterization of (bTAML)$Fe^{V}(O)$ complex in H_2O/CH_3CN mixture	34
	2.4.2	Stability of $Fe^{V}(O)$ species in different H_2O/CH_3CN mixtures	36
	2.4.3	Reactivity of $Fe^{V}(O)$ in different H_2O/CH_3CN mixtures towards toluene oxidation	38

	2.4.4	Kinetic isotope effect (KIE) and source of O-atom (^{18}O-labelling) in product formation	39
	2.4.5	Thermodynamic parameters for toluene oxidation by $Fe^{V}(O)$	41
	2.4.6	Density Functional Theory (DFT) Studies for Toluene Hydroxylation by $Fe^{V}(O)$	43
2.5		Conclusions	50
2.6		References	50
Chapter III: On the Mechanism of Oxygen Atom Transfer from $Fe^{V}(O)$ to Olefins at Room Temperature			
3.1	Abstract		55
3.2	Introduction		56
3.3	Experimental section		
	3.3.1	Materials	59
	3.3.2	General instrumentation	60
	3.3.3	Second order rate constant (k_2) determination for the reaction of $Fe^{V}(O)$ with alkenes	60
	3.3.4	Single-turnover reaction of $Fe^{V}(O)$ with alkenes	61
	3.3.5	Cyclic voltammetry (CV) measurement	62
	3.3.6	Catalytic reaction of $Fe^{V}(O)$ with alkenes	62
	3.3.7	^{18}O Incorporation Experiment	63
	3.3.8	Computational details	63
3.4	Results and discussion		
	3.4.1	Kinetics of *cis*-cyclooctene epoxidation under single-turnover condition	63
	3.4.2	Rate of reaction (k_2) for the epoxidation of various alkenes under single-turnover conditions	65
	3.4.3	Reactivity of μ-oxo-$(Fe^{IV})_2$	68
	3.4.4	Investigations on the different possible pathways for the epoxidation of C=C bond involving $Fe^{V}(O)$ species	70
	3.4.5	Mechanistic Insite by Density Functional Theory (DFT)	76
	3.4.6	Molecular Mechanism of Epoxidation by $Fe^{V}(O)$	78
	3.4.7	Catalytic activity	80
	3.4.8	Proposed catalytic cycle	81
3.5	Conclusion		81
3.6	References		82
Chapter IV: Reductive Activation of O_2 by a Bioinspired Fe-Complex for Catalytic Epoxidation Reactions			
4.1	Abstract		85
4.2	Introduction		86
4.3	Experimental section		
	4.3.1	Materials	89
	4.3.2	General instrumentation	89
	4.3.3	Electron paramagnetic resonance (EPR) measurements	90
	4.3.4	Catalytic reaction of (bTAML)$Fe^{III}(OH_2)$ with alkenes under oxygen pressure	90

	4.3.5	Catalytic reaction of (bTAML)$Fe^{III}(OH_2)$ with alkenes at atmospheric pressure and at different temperature	90
	4.3.6	Reaction of (bTAML)$Fe^{III}(OH_2)$ with thioanisole and styrene in the presence of $^{18}O_2$	91
	4.3.7	Reaction of (bTAML)$Fe^{III}(H_2O)$ with styrene in the presence of $H_2{}^{18}O$ in air	91
	4.3.8	Synthesis of complex Et_4N[(bTAML)Fe^{IV}(Cl)]	91
	4.3.9	Synthesis of Complex (bTAML)Fe^{III}(superoxide)	92
	4.3.10	Computational Details	93
4.4	Results and discussion		
	4.4.1	UV-vis Spectroscopic observations for μ-Oxo-$(Fe^{IV})_2$ dimer formation using O_2 and (bTAML)$Fe^{III}(H_2O)$	93
	4.4.2	Product analysis after reaction of (bTAML)$Fe^{III}(H_2O)$ with alkenes using O_2	95
	4.4.3	Hammett plot	97
	4.4.4	^{18}O Labelling experiments	98
	4.4.5	Fate of the catalyst	100
	4.4.6	Mechanistic Investigations for O_2 Interaction with Iron Center of Complex (bTAML)$Fe^{III}(H_2O)$	100
	4.4.7	EPR Spectroscopic observations	102
	4.4.8	Reason for the reactivity of $[\{(bTAML)Fe^{IV}\}_2$-μ-oxo$]^{2-}$ dimer	104
	4.4.9	Evidence for the involvement of $Fe^{V}(O)$ species in the epoxidation reaction	105
4.5	Conclusion		107
4.6	References		107
Chapter V: Valence Tautomerization in High-Valent $Fe^{V}(O)$-bTAML Complex: Effect of Acid on Secondary Coordination Sphere			
5.1	Abstract		111
5.2	Introduction		112
5.3	Experimental section		
	5.3.1	Materials	113
	5.3.2	General instrumentation	114
	5.3.3	Synthesis of complex [(bTAML)$Fe^{V}(O)]^{-}$	114
	5.3.4	Synthesis of complex [(H-bTAML•+)$Fe^{IV}(O)$]	114
	5.3.5	Electron paramagnetic resonance (EPR) measurements	114
	5.3.6	Kinetic measurements for reaction of [(bTAML)$Fe^{V}(O)]^{-}$ with 9,10-Dihydroanthacene	115
	5.3.7	Kinetic measurements for reaction of [(H-bTAML•+)$Fe^{IV}(O)$] with 9,10-Dihydroanthacene	116
5.4	Results and discussion		
	5.4.1	Formation and characterization of [(H-bTAML•+)$Fe^{IV}(O)$] complex	117
	5.4.2	Comparative reactivity of complex [(bTAML)$Fe^{V}(O)]^{-}$ and (H-bTAML•+)$Fe^{IV}(O)$ for hydrogen atom transfer (HAT) reaction	118
5.5	Conclusion		121
5.6	References		122

Chapter VI: Conclusion and Future Perspective		
6.1	Conclusion	125
6.2	Future Perspective	128
6.3	References	130

Appendix A 131

Appendix B 150

Appendix C 173

Appendix D 182

List of Figures

Figure 1.1	Examples of natural products possessing hydroxyl (OH) and epoxide functional group	2
Figure 1.2	Introduction of function group by ring opening of epoxide with various nucleophiles	3
Figure 1.3	Active site of cytochrome P450 (reactive intermediate Compound 1)	7
Figure 1.4	Two possible pathways for hydroxylation (A), and epoxidation (B) reaction by cytochrome P450 enzyme	8
Figure 1.5	The common structural motif "2-His-1-carboxylate facial triad" for non-heme mononuclear rieske dioxygenase (Left) and dinuclear methane monooxygenase (MMO) (Right) iron enzyme	9
Figure 1.6	Few examples of *meso*-substituted synthetic porphyrin iron complexes used for the study of hydroxylation and epoxidation reaction	11
Figure 1.7	Influence of axial ligand for the generation of $Fe^{IV}(O)$ or $Fe^{IV}(O)$-radical cation in synthetic iron complex of substituted porphyrin	11
Figure 1.8	Proposed intermediates for reaction of alkenes with transition metal oxo and peroxo species	13
Figure 1.9	(A) Formation of (porphyrin)$Fe^{IV}(O)$-radical-cation during catalytic cycle of cytochrome P450 for hydroxylation reaction (NADP as an electron source and O_2 as an O-atom source). (B) Two different pathway for the formation of high valent iron-oxo intermediate in model complexes, either use of two electron reduced oxo donor reagents (mCPBA, PhIO, H_2O_2 etc.) or use of sacrificial reductant with O_2	15
Figure 1.10	Examples of $Fe^{IV}(O)$ intermediate synthesized by Fe(II) complex of ligand cyclam-acetate (**1**), TMC (**2**), TPA (**3**), and N4Py (**4**)	16
Figure 1.11	Examples of $Fe^{V}(O)$ intermediate synthesized by Iron complex of ligand Pytacn (**1**), Corrole (**2**), TAML (**3**)	17
Figure 1.12	Formation of (bTAML)$Fe^{V}(O)$ and catalytic cycle for cyclohexane hydroxylation	18
Figure 2.1	UV–vis spectral changes associated with the reaction of **2** with toluene to Fe^{IV} / Fe^{III} in 50% H_2O/CH_3CN mixture at 25 ^oC (in left). Kinetic traces for reaction of **2** with toluene at various toluene concentrations in 30% H_2O/CH_3CN (in right). The kinetic traces were fitted to the equation, $[(A_t = A_\alpha - (A_\alpha - A_o)e^{(-kobst)}]$ for obtaining k_{obs} values	32
Figure 2.2	(A) UV−vis spectral changes of **1** (10^{-4} M) (orange) upon the addition of 0.5 equiv of NaOCl (5×10^{-5} M) in CH_3CN forming the μ-Oxo-Fe^{IV} dimer species (violet). Addition of another 0.5 equiv of NaOCl (5×10^{-5}M) to the preformed μ-Oxo-Fe^{IV}dimer species produces the spectrum of $Fe^{V}(O)$ (**2**, green). (B) UV-vis spectra of $Fe^{V}(O)$ in different H_2O/CH_3CN mixtures. (C) EPR spectra of $Fe^{V}(O)$ (**2**) in acetonitrile (2 mM) at 21 K. Black = experimental, red = simulated. (D) Mössbauer spectra of ^{57}Fe-enriched [$Fe^{V}(O)$] (**2**) in acetonitrile (2 mM) at 4.2 K. The solid lines are spectral simulations	35

Figure 2.3	HR-MS of **2** in 30% H_2O/CH_3CN mixture. Calculated m/z of **2** is 429.0730	36
Figure 2.4	(A) First-order rate constant $k_{5/4,3}$ varies with water concentration. Inset shows initial rate *vs* [$Fe^{V}(O)$]. (B) Second-order rate constant k_2 for toluene oxidation *vs* the percentage of water content in the H_2O/CH_3CN mixture	37
Figure 2.5	Linear fit of toluene concentration [Toluene] against k_{obs} to determine second order rate constant (k_2)	39
Figure 2.6	GC-MS trace for the product formed upon reaction of **2** (10^{-4} M) with toluene (1000 equivalent) in 50% $H_2{}^{18}O$-CH_3CN mixture	40
Figure 2.7	Plot of k_{obs} vs. [toluene] (red dots) and [d_8-toluene-] (black dots) showing pronounce KIE at 25 ^oC (A) in 50% H_2O-CH_3CN mixture; (B) in 70% H_2O-CH_3CN mixture	41
Figure 2.8	Plot of ln(k_2/ T) *vs* 1/ T for toluene oxidation in 100 % CH_3CN and in 70:30 of H_2O/CH_3CN in the temperature range of 283-300 K	42
Figure 2.9	(A) Gas phase free energy profile for the hydroxylation of toluene by **2** at the UB3LYP/6-31G*, LANL2DZ (Fe) level of theory. Violet and black colors represent energy profiles at S = 3/2 and S = 1/2 spin states, respectively. All of the values are in kcal mol^{-1}; (B) Electronic energy profile for the rate-determining step of toluene hydroxylation catalyzed by **2**. All of the values correspond to gas-phase data. Values outside and inside the parentheses correspond to the the ROM062X/6-31G*, LANL2DZ (Fe) and UB3LYP/6-31G*, LANL2DZ (Fe) levels of theory, respectively. Black, green, and yellow colors represent the energy profile with zero, one, and two explicitly added water molecules, respectively, (i, ii, and iii) UB3LYP optimized transition state structures for the hydrogen atom abstraction rate-determining step (RDS) with zero, one, and two explicitly added water molecules, respectively. Hydrogen atoms not involved in the reaction coordinate are removed for clarity. All of the values are in kcal mol^{-1}. All the atom-atom distances are in Å	49
Figure 3.1	Plot of k_{obs} vs [substrate] for *cis*-stilbene, *trans*-stilbene, methyl *trans*-cinnamate, and norbornene). k_2 value determined for each substrate is the slope of the linear plot	61
Figure 3.2	Cyclic voltammogram of complex 2, $Fe^{V}(O)$, in acetonitrile using glassy carbon as working electrode.$E_{1/2}$ ($Fe^{V/IV}$) = 1.01 V *vs*. SCE	62
Figure 3.3	(A) UV–vis spectral changes upon reaction of **2** (4×10^{-5} M) with *cis*-cyclooctene (2.5×10^{-3} M); (B) absorbance *vs* time plot at 396 nm for reaction of **2** (4×10^{-5} M) with *cis*-cyclooctene (2.5×10^{-3} M) (●) indicates experimental data point; (red line) first-order fit according to the equation [$(A_t = A_\alpha - (A_\alpha - A_o)e^{(-kobst)}$]. Reaction was performed at RT in acetonitrile solvent under nitrogen atmosphere. (C) Plot of k_{obs} vs substrate concentration [*cis*-cyclooctene] to determine k_2 value from slope of the linear plot.	64
Figure 3.4	(A) HR-MS of **2** in CH_3CN after 3 hrs incubation in H_2O^{18} at -22 ^oC. Calculated m/z of **2** after ^{18}O incorporation = 431.0763. (B) The HR-MS spectra of *cis*-cyclooctene epoxide product obtained after reaction with *cis*-cyclooctene and ^{18}O labelled complex **2** in CH_3CN	66

Figure 3.5	(A) UV–vis spectral changes upon reaction of μ-Oxo-Fe^{IV}dimer (2×10^{-5} M) with *cis*-cyclooctene (4×10^{-3} M); (B) the absorbance *vs* time plot at 957 nm for reaction of μ-Oxo-Fe^{IV}dimer (2×10^{-5} M) with *cis*-cyclooctene (4×10^{-3} M); (● indicates experimental data point; the red line is the first-order fit according to the equation [($A_t = A_\alpha - (A_\alpha - A_o)e^{(-kobst)}$]. Reaction was performed at RT in acetonitrile solvent under inert condition. (C) The plot of initial rate *vs* concentration of Fe^{III}, complex **1**, added for reaction of μ-Oxo-Fe^{IV}dimer (2×10^{-5} M) with 4-methoxy styrene (5×10^{-4} M). k_1 (100) and k_{-2} (24196) were obtained by non-linear curve fit according to the equation obtained from proposed reaction scheme of μ-Oxo-Fe^{IV}dimer in presence alkene	69
Figure 3.6	Plot of the log of the second-order rate constant (k_2) for the epoxidation with Fe^{V}(O) (**2**) vs. the $E_{1/2}$ for 1e oxidation of the alkenes.[25] The alkenes are color coded: styrene (cyan), 4-methoxystyrene (black), 4-chlorostyrene (blue), 4-cyanostyrene (yellow), *cis*-cyclooctene (brown), *cis*-stilbene (red), *trans*-stilbene (green), norbornene (magenta)	72
Figure 3.7	(A) Hammett plots of log k_2^{rel} against *para*- σ^+ for the epoxidation of styrene and its *para*-substituted derivatives by Fe^{V}(O) at RT in CH_3CN. Hammett value ρ is -0.56; $k_2^{rel} = k_2^X/k_2^H$, (k_2^X and k_2^H are second-order rate constants for *para*-substituted styrene and styrene, respectively). (B), (C), (D), and (E) are plots of k_{obs} *vs* substrate concentration for 4-methoxystyrene, styrene, 4-chlorostyrene, and 4-cyanostyrene, respectively. k_2 value determined for each substrate is the slope of the linear plot	75
Figure 3.8	Gas-phase energy profile with optimized geometries of the intermediates and transition states for the epoxidation of styrene by **2** at the UB3LYP/6-31G*, LANL2DZ (Fe) level of theory from doublet and quartet surfaces for (A) α pathway; (B) β pathway (Dis and A denote distance and angles, respectively; superscripts 2 and 4 represent geometries in the doublet and quartet spin states)	78
Figure 3.9	Molecular orbital pictures of the HOMO and LUMO of reactant, intermediate, and product, and orbital occupancy for styrene epoxidation by Fe^{V}(O) at the ROB3LYP/6-31G*, LANL2DZ (Fe) level of theory in the gas phase	79
Figure 4.1	Examples of iron containing metalloenzymes and intermediates during their biological function, Hemoglobin (in left) and Cytochrome P450 (in right)	86
Figure 4.2	Example for aerobic epoxidation without use of coreductant (A) $Ru^{IV}(TMP)(O)_2$ {TMP = 5, 10, 15, 20-(tetramesityl)porphyrin}; (B) Ruthenium substituted polyoxometalate, $\{[WZnRu_2(OH)(H_2O)](ZnW_9O_{34})_2\}$	88
Figure 4.3	TON of styreneoxide trace with time at different temperature; 25 ˚C (green), 50 ˚C (red), and 70 ˚C (blue)	91
Figure 4.4	UV-vis spectrum of complex $[(bTAML)Fe^{IV}(Cl)]^-$ in dichloromethane formed by the reaction of $[(bTAML)Fe^{III}(Cl)]^{2-}$ with $(NH_4)_2Ce(NO_3)_6$ at room temperature (RT, 25 ˚C)	92
Figure 4.5	(A) UV-vis spectra of $[(bTAML)Fe^{III}(Cl)]^{2-}$ (black line) and $[(bTAML)Fe^{III}(O_2^{\cdot-})]^{2-}$ (red line) in DCM at -40 ˚C. (B) UV-vis	93

	spectra of $[(TAML)Fe^{III}(Cl)]^{2-}$ (black line) and $[(TAML)Fe^{III}(O_2^{\cdot-})]^{2-}$ (red line)	
Figure 4.6	(A) UV–vis spectral changes for reversible O_2 binding with complex **1** in DCM at room temperature (25 °C) and (B) the UV-vis spectral scan for the formation of dimer complex **2** by the reaction of complex **1** (3×10^{-4} M) in DCM with air (10 min reaction time, 25 °C and atmospheric pressure)	94
Figure 4.7	(A) UV-vis spectra of reaction mixure after completion of reaction with complex **1** and styrene at 5 bar O_2 pressure. The UV-vis obsereved is similar to the $[(bTAML)Fe^{IV}(Cl)]^{-}$ complex. (B) HR-MS of reaction mixture after completion of reaction with complex **1** and styrene at 5 bar O_2 pressure. Calculated m/z of $[(bTAML)Fe^{IV}(Cl)]^{-}$ is 448.0475. Observed m/z 448.0498	95
Figure 4.8	UV-vis spectral change for the reaction of $[(bTAML)Fe^{V}(O)]^{-}$ (1×10^{-4} M) with 100 equiv. of CH_2Cl_2 in acetonitrile. Monomeric $[(bTAML)Fe^{IV}(Cl)]^{-}$ was formed at the end of the reaction	96
Figure 4.9	Hammett plots of logk^{rel} against *para*- σ^{+} for the epoxidation of styrene and its *para*-substituted derivatives obtained from the reaction of complex **1** in DCB at 50 °C. Hammett value ρ is -0.87; $k^{rel} = k^X/k^H$, where k^X and k^H are concentration of epoxide product for *para*- substituted styrene and concentration of epoxide product for styrene respectively	98
Figure 4.10	GC-MS spectra of product after 60 min. of reaction with complex **1** and styrene in presence of $^{18}O_2$	99
Figure 4.11	GC-MS spectra of product after 10 min. of reaction with complex **1** and thioanisole in presence of $^{18}O_2$	99
Figure 4.12	GC-MS spectra of product after 60 min. of reaction with complex **1** and styrene in presence of $H_2{}^{18}O$ and air ($^{16}O_2$)	100
Figure 4.13	Plot of initial rate *vs* square of complex **1** concentration. k_{obs} was obtained by linear fit according to the equation: rate = k_{obs}[catalyst]^2. Reaction was performed under air in dichloromethane at 25 °C	101
Figure 4.14	(A) UV–vis spectral changes upon lowering the temperature from 25 °C to -40 °C for complex Fe-O_2 (**1**) in DCM. (B) UV-vis spectral scan for dimer (**2**) formations upon increasing temperature from -40 °C to 25 °C	103
Figure 4.15	UV–vis spectral changes of Fe^{IV}-Cl complex (5×10^{-5}M) upon reductive binding of superoxide (excess KO_2) in DCM; (B) X-band EPR signal of resulting solution Fe^{III}-O_2 adduct after reaction of Fe^{IV}-Cl and KO_2; at 100 K, in DCM	103
Figure 4.16	(A) X-band EPR of complex **1** (8.0 mM) in degassed dichloromethane (DCM) at 100 K; (B) X-band EPR of complex **1** (8.0 mM) in oxygenated DCM at 100 K	104
Figure 4.17	At the B3LYP/6-31G*, LANL2DZ (Fe) level of theory, gas-phase optimized geometries of (A) $[\{(TAML)Fe^{IV}\}_2$-μ-oxo$]^{2-}$, [9(a)] and (B) $[\{(bTAML)Fe^{IV}\}_2$-μ-oxo$]^{2-}$	105
Figure 4.18	HR-MS of $[(bTAML)Fe^{V}(O)]^{-}$ and $[(NO_2\text{-}bTAML)Fe^{V}(O)]^{-}$ complexes which are formed after incubation of $[\{(bTAML)Fe^{IV}\}_2$-μ-Oxo$]^{2-}$ dimer (**2**) solution with a nitro substituted complex, $[(NO_2\text{-}bTAML)Fe^{III}(Cl)]^{2-}$. Calculated m/z of $[(bTAML)Fe^{V}(O)]^{-}$	106

	and $[(NO_2\text{-bTAML})Fe^{V}(O)]^{-}$ is 429.0730 and 474.0581 respectively	
Figure 5.1	(A) UV–vis spectral changes upon reaction of $Fe^{V}(O)$ (4×10^{-5} M) with 9,10-dihydroanthracene (5×10^{-4} M); (inset) Absorbance *vs.* time plot at 857 nm (● indicates experimental data point; the red line is the first order fit according to the equation $[(A_t = A_\alpha - (A_\alpha - A_o)e^{(-k_{obs}t)}]$. Reaction was performed in acetonitrile solvent at -40 ˚C	115
Figure 5.2	(A) UV–vis spectral changes with time upon reaction of [(H-bTAML•+)$Fe^{IV}(O)$] (5.5×10^{-5} M) and DHA (5.5×10^{-4} M); (B) the initial rare (at 630 nm) *vs* [DHA] plot for reaction of [(H-bTAML•+)$Fe^{IV}(O)$] (5.5×10^{-5} M) with DHA (5.5×10^{-4} - 5.5×10^{-3} M); (● indicates experimental data point; the red line is the linear fit according to the equation k_{obs} = initial rate / [DHA]. Reaction was performed at -40 ˚C in acetonitrile solvent	116
Figure 5.3	(A) UV–vis spectral changes for the formation of **3** upon addition of 3 equiv of $B(C_6F_5)_3$ to **2** (1.0×10^{-4} M) at -40 ˚C in acetonitrile; (B) X-band EPR of complex **2** (2.0 mM) at 100 K;[13] (C) X-band EPR of complex **3** (2.0 mM) in acetonitrile at 100 K	118
Figure 5.4	UV-vis spectral change for axial ligand substitution in complex $[(bTAML)Fe^{IV}(Cl)]^{-}$ upon titration with NaOH at 25 ˚C in acetonitrile	120
Figure 5.5	(A) UV-vis spectral change upon redox titration of complex **3** (1.5×10^{-4} M) (green): after addition of 1 equiv ferrocene (red), after addition of 2 equiv ferrocene (orange). (B) UV-vis spectral scan for 1 electron oxidation of $[(bTAML)Fe^{III}(OH_2)]^{2-}$ (**1**) (3.0×10^{-4} M) (orange spectrum) with oxidant tris(4-bromophenyl)aminiumyl hexachlorideoantimonate (magic blue) (1 equiv) to form a proposed $[(bTAML)Fe^{IV}(OH_2)]$ complex at -40 ˚C in acetonitrile	121
Figure 6.1	Proposed bTAML modified Fe^{III} complex	129

List of Schemes

Scheme 1.1	General scheme for ring opening of epoxide in presence of nucleophile.	2
Scheme 1.2	Various methods for epoxide formation from alkene without using metal catalyst	4
Scheme 1.3	General scheme of Sharpless epoxidation reaction	5
Scheme 1.4	General scheme of Jacobsen-Katsuki epoxidation reaction	6
Scheme 2.1	The complex of $CytP450_{StaP}$ Cpd I with chromopyrolic acid	28
Scheme 2.2	Formation of $Fe^{V}(O)$ species in H_2O/CH_3CN mixture and its reaction towards toluene.	29
Scheme 3.1	(A) Different type of Intermediates Suggested for the Reaction of Cpd I and Olefins, (B) Representative Example for Possible Product Distribution Pattern during the Reaction of Cpd I and Olefins (Theoretical Investigation for Spin State Dependency)	57
Scheme 3.2	Proposed Mechanism for Oxidation of Olefins by Non-heme Iron Catalyst	58
Scheme 3.3	Catalytic Scheme for the Epoxidation of *cis*-Cyclooctene by $[(bTAML)Fe^{V}(O)]^{-}$	59
Scheme 3.4	Detailed Mechanistic Scheme for the Epoxidation of Alkenes by $[(bTAML)Fe^{V}(O)]^{-}$	71
Scheme 3.5	Proposed Catalytic Cycle for Epoxidation with Complex **1** and NaOCl	81
Scheme 4.1	Use of O_2 by Dioxygenases in Oxygen Atom Transfer Reaction	87
Scheme 4.2	Aerobic Catalytic Epoxidation with **1**	89
Scheme 4.3	Proposed Mechanism for the Formation of **2** by Reaction of Complex **1** and O_2	101
Scheme 5.1	Synthesis of complex **[**$(H\text{-}bTAML^{\bullet+})Fe^{IV}(O)]$	113
Scheme 5.2	Comparative Reaction Profile for Complex **2** and **3**	119

List of Tables

Table 1.1	Influence of axial ligands on reactivity of [Fe(tpfpp)X] complexes towards C-H and C=C bonds	12
Table 2.1	Stability and Reactivity of the $Fe^{V}(O)$ Intermediate for Toluene Oxidation in Various H_2O/CH_3CN mixtures	37
Table 2.2	SKIE Value [$k_2(H_2O)$/ $k_2(D_2O)$] of $Fe^{V}(O)$ for Toluene Oxidation in Various Mixtures of H_2O and D_2O in CH_3CN	41
Table 2.3	(A) Rate constant (k_2) values for toluene oxidation in CH_3CN and in 70 % of H_2O/CH_3CN mixture at different temperature. (B) Thermodynamic parameters ($\Delta H^{\#}$, $\Delta S^{\#}$ & $\Delta G^{\#}$) values at 300 K for toluene oxidation in CH_3CN and in 70 % of H_2O/CH_3CN mixture in temperature range of 283-300 K	42
Table 2.4	The relative gas phase reaction energies in kcal mol^{-1} at the UB3LYP/6-31G*, LANL2DZ (Fe) level of theory for toluene hydroxylation catalyzed by $Fe^{V}(O)$ (**2**)	44
Table 2.5	The relative gas phase energies of the intermediate complex $Fe^{IV}(OH)$ in singlet and triplet electronic states in kcal mol^{-1} at the UB3LYP/6-31G*, LANL2DZ (Fe) and ROM062X/6-31G*, LANL2DZ (Fe) level of theories. Values outside the parenthesis are in gas phase and inside the parenthesis are in solvent phase	44
Table 2.6	The relative reaction energies in kcal mol^{-1} for the rate determining step of toluene hydroxylation catalysed by $Fe^{V}(O)$ (**2**) in dielectric continuum of acetonitrile and water at the CPCM/UB3LYP/6-31G*, LANL2DZ (Fe) and CPCM/ROM062X/6-31G*, LANL2DZ (Fe) level of theories	44
Table 2.7	The relative gas phase reaction energies in kcal mol^{-1} for the rate determining step of toluene hydroxylation catalyzed by $Fe^{V}(O)$ (**2**) with explicitly added water molecules at the UB3LYP/6-31G*, LANL2DZ (Fe) and ROM062X/6-31G*, LANL2DZ (Fe) level of theories	45
Table 2.8	Fe-O distances (in Å) in water bound reactant, transition state and intermediate structures obtained by geometry optimization at the UB3LYP/6-31G*, LANL2DZ (Fe) level of theory	47
Table 2.9	Mulliken population analysis of reactant, TS1 and intermediate with and without explicit water at UB3LYP/6-31gG*, LANL2DZ(Fe) level of theory	48
Table 3.1	Epoxidation of Different Alkenes by $Fe^{V}(O)^{a}$ at RT in CH_3CN Solvent under Air	67
Table 3.2	Epoxidation of Alkenes by μ-Oxo-Fe^{IV} dimer[a] at RT in CH_3CN Solvent under Air	70
Table 3.3	Calculated Values of the Free Energy of Formation of the Transition State (ΔG^{a}) and Standard Free Energy (ΔG^{o}) for the One-Electron Transfer in the Transition	73

	State during the Reaction of $Fe^{V}(O)$ with Alkene at Temperature 25^{o}C in Acetonitrile	
Table 3.4	The gas phase relative reaction energies in kcal/mol at the UB3LYP/6-31G*, LANL2DZ (Fe) level of theory for styrene epoxidation catalyzed by $[(bTAML)Fe^{V}(O)]^{-}$	77
Table 3.5	Summary of the Catalytic Epoxidation[a] of Different Alkenes by **1** at RT in CH_3CN under Air	80
Table 4.1	Epoxidation of Different Alkenes by Complex **1** and O_2 in DCB at 50 °C	97

List of Abbreviations

*m*CPBA	*meta*-chloroperbenzoic acid
DMB	2,3-Dimethylbutane
His	Histidine
MMO	Methane monooxygenase
NADPH	Nicotinamide adenine dinucleotide (phosphate)
NDO	Naphthalene dioxygenase
EXAFS	X-ray absorption fine structure
Cpd I	Compound I
HRP	Horseradish peroxidase
TON	Turnover number
UV-vis	Ultraviolet-visible
EPR	Electron paramagnetic resonance
ESI-MS	Electron spray ionization mass spectrometry
HPLC	High performance liquid chromatography
LCMS	Liquid chromatography mass-spectrometry
TMP	*meso*-Tetramesityl porphyrin
TPFPP	*meso*-tetrakis(pentaflurophenyl) porphyrin
TDFPP	*meso*-tetrakis(2,6-difluorophenyl)porphyrin
TDCPP	*meso*-tetrakis(2,6-dichlorophenyl)porphyrin
rds/RDS	Rate determining step
RT	Room temperature
UV-vis	Ultraviolet-visible
NMR	Nuclear magnetic resonance
GC	Gas chromatography
GC-MS	Gas chromatography mass spectrometry
HR-MS	High resolution mass spectrometry
TPA	Tris(2-pyridylmethyl)amine
TACN	1,4,7-Triazacyclononane
PyTACN	1-(2´-pyridylmethyl)-4,7-dimethyl-1,4,7-triazacyclononane
N_4Py	1,1-di(pyridine-2-yl)-N,N-bis(pyridine-2-ylmethyl)methanamine
TMC	1,4,8,11-tetramethyl-1,4,8,11-tetraazacyclotetradecane
BPMEN	N,N´-*bis*-(2-pyridylmethyl)-ethane-1,2-diamine
Bn-tpen	N-benzyl-N,N,N´,N´-tris(2-pyridylmethyl)-1,2-diaminoethane
TBP_8Cz	octakis(p-tert-butylphenyl) corrolazinato
TAML	Tetraamido macrocyclic ligand
bTAML	Biuret-tetraamido macrocyclic ligand
Cyclam	1,4,8,11-tetraazacyclotetradecane
OTf	Trifluoromethanesulfonate anion
Triflate	Trifluoromethanesulfonate
MHz	Megahertz
ppm	Parts per million
CV	Cyclic voltammetry
THF	Tetrahydrofuran

Et_3N	Triethylamine
CH_3CN	Acetonitrile
n-BuLi	n-Butyl lithium
DCM	Dichloromethane
DCB	Dichlorobenzene
PCET	Proton coupled electron transfer
NaOCl	Sodium hypochlorite
$t_{1/2}$	Half-life
OD	Optical density
CytP450	Cytochrome P450
α-KG	α-ketogluterate dependent hydroxylase
equiv	Equivalent
eq	Equation
H_2O_2	Hydrogen peroxide
KIE	Kinetic isotope effect
SKIE	Secondary kinetic isotope effect
min	Minute
sec	Second
kcal	Kilocalorie
PhIO	Iodosyl benzene
TBHP	Tertiary butyl peroxide
ET	Electron transfer
OAT	Oxygen atom transfer
HAT	Hydrogen atom transfer
Py	Pyridine
DFT	Density functional theory
CPCM	Conductor-like polarizable continuum model
RDB	Rate-determining barrier
RDTS	Rate-determining transition state
HOMO	Highest occupied molecular orbital
LUMO	Lowest unoccupied molecular orbital
MO	Molecular orbital
Cys	Cysteine
Hb	Haemoglobin
Mb	Myoglobin
DHA	9,10-dihydroanthracene
Fc	Ferrocene

Abstract of the Thesis

The presence of O-atom as an alcohol and epoxide moiety in an organic molecule has high significance in chemical industries for the production of drugs. Several methods that oxidize hydrocarbons have been known where metal or non-metal mediated processes have been well explored. However, the traditional use of oxidants, such as peroxides, $KMnO_4$, OsO_4, and $K_2Cr_2O_7$ creates hazardous waste. Other approaches of transition metal mediated oxidations using peroxides as oxidants have limitations due to their very sensitive nature to the radical-chain reaction and are also subject to self-decomposition at higher concentrations following a catalase-like activity of the catalyst activator. Hence, the direct oxidation of hydrocarbons is a field of both academic and industrial importance and challenge in the quest of regio- and chemo-selectivity. Biological enzymes have already perfected this type of synthetic precision to develop and utilize the natural products in the biological process. The most potent tool for C-H bond hydroxylation and C=C bond epoxidation found in the natural systems involve enzymes such as cytochrome P450. The involvement of high-valent metal-oxo species as a reactive intermediate is a common consensus for their highly selective and efficient nature. However, the exact nature of these oxidants and the mechanism of oxygen atom transfer from the intermediates to organic substrates remain elusive. Although several models of $Fe^{IV}(O)$ intermediates have been synthesized and their reactivity have been explored, but very few reports about the reactivity of $Fe^{V}(O)$, isoelectronic of (porphyrin)$Fe^{IV}(O)$-radical cation (compound I), are available due to its high instability at ambient temperature. Hence, understanding of reaction mechanisms of $Fe^{V}(O)$ may lead to a new insight in biocatalysis and drug design as well as the development of new approaches for industrial catalysis.

Among very few examples, Fe-TAML is the first complex to generate spectroscopically characterized $Fe^{V}(O)$ species at -40 ˚C. However, instability of (TAML)$Fe^{V}(O)$ complex above -40 ˚C hampers its reactivity as well as its utility in mechanistic studies. In a recent work of our laboratory, the Fe(III) complex of a biuret-amide based macrocyclic ligand which was designed by replacing the tail $-CMe_2$ moiety of tetraamido macrocyclic ligands (TAML) by an –NMe group (assigned as bTAML, biuret modified-tetraamido macrocyclic ligand). The corresponding Fe^{III} complex shows 10^5 folds enhanced stability in aqueous acidic medium and also exhibits 10-fold lower deactivation rates for H_2O_2 activation in water compared to the corresponding Fe-TAML. Electrochemical studies of (bTAML)Fe displayed Fe(IV)/Fe(III) couple 230 mV lower than

the corresponding Fe-TAML complex which favors for the formation of high-valent iron species. It was hypothesized that higher donating ability of the deprotonated amide-biuret macrocyclic ligand in addition to its robustness towards oxidative degradation might help to stabilize Fe^{V}=O complex at room temperatures. This improved stability of the Fe^{V}=O complex ($t_{1/2}$ = 3 hrs) allowed for oxidation of unactivated C-H bonds of cyclohexane, having bond dissociation energy 99.3 kcal/mol.

This thesis work entitled "Investigations on the Oxygen Atom Transfer Reaction Mediated through a Bio-Inspired Fe^{V}(O) Complex" comprises of the detail mechanistic investigations on the O-atom transfer reactions for C-H bond hydroxylation and C=C bond epoxidation using Fe^{V}(O) species as a terminal oxidant. Inspired by the enzymatic systems, we have successfully generated Fe^{V}(O) complex in aqueous media. Further, the role of water on the reactivity of Fe^{V}(O) during C-H bond hydroxylation has been described. Thereafter, we elucidated the mechanism of direct O-atom transfer in the course of the reaction of Fe^{V}(O) with alkenes to form the corresponding epoxide. The mechanism of each step of the reaction was evaluated using various spectroscopic and kinetic methods. Then, we used $[(bTAML)Fe^{III}(H_2O)]^-$ complex for the reductive activation of O_2 where molecular O_2 has been shown as an oxygen source for catalytic epoxidation reaction without the use of any sacrificial reductant. Latter, the effect of Lewis acid on Fe^{V}(O) complex has been demonstrated. The redox non-innocent nature of the ligand of $[(bTAML)Fe^{V}(O)]^-$ complex has been observed to generate Fe^{IV}(O)-radical-cation in the presence of Lewis acid. The reactivity difference in hydrogen atom abstraction from C-H bond has been studied using these two valence tautomers, Fe^{V}(O) and Fe^{IV}(O)-radical cation.

Chapter I presents an overview of the existing literature on the importance of high-valent Fe-oxo intermediate in bio-inspired oxidations reactions. It describes the mechanism of various metal catalyzed C-H bond hydroxylation and C=C bond epoxidation reaction. A brief outline of synthetic heme and non-heme ligand systems which generate Fe^{IV}(O) and Fe^{V}(O) complexes has been introduced.

Chapter II shows the formation of a Fe^{V}(O) complex at room temperature in an H_2O/CH_3CN mixture that contains up to 90% water using NaOCl as the oxidant. The stability of Fe^{V}(O) decreases with increasing water concentration. We show that the reactivity of Fe^{V}(O) toward the oxidation of C-H bonds, such as those in toluene, can be tuned by varying the amount of water in the H_2O/CH_3CN mixture. Rate acceleration of up to 60 times is observed for the oxidation of toluene upon increasing the water concentration. The role of water in accelerating the rate of the reaction has been studied using kinetic

measurements, isotope labeling experiments, and density functional theory (DFT). A kinetic isotope effect of ~13 was observed for the oxidation of toluene and d_8-toluene showing that C-H abstraction was involved in the rate-determining step. Activation parameters determined by using Eyring plots for toluene oxidation in H_2O/CH_3CN mixtures showed a gain in enthalpy with a concomitant loss in entropy. This points to the formation of a more-ordered transition state involving water molecules. To further understand the role of water, we performed a careful DFT study, concentrating mostly on the rate-determining hydrogen abstraction step. The DFT-optimized structure of the starting $Fe^{V}(O)$ and the transition state indicates that the rate enhancement is due to the transition state's favored stabilization over the reactant due to enhanced hydrogen bonding with water.

Chapter III discloses detail study on the mechanism of O-atom transfer to alkenes using the $Fe^{V}(O)$ complex of biuret-modified Fe-TAML at room temperature. The second-order rate constant (k_2) for the reaction of different alkenes with $Fe^{V}(O)$ was determined under single turnover conditions. An 8000-fold rate difference was found between electron-rich (4-methoxystyrene; k_2 = 216 $M^{-1}s^{-1}$) and electron-deficient (Methyl *trans*-cinnamate; k_2 = 0.03 $M^{-1}s^{-1}$) substrates. This rate difference indicates the electrophilic character of $Fe^{V}(O)$. The use of *cis*-stilbene as a mechanistic probe leads to the formation of both *cis*- and *trans*-stilbene epoxides (73:27). This suggests the formation of a radical intermediate, which would allow C-C bond rotation to yield both stereoisomers of stilbene-epoxide. Additionally, a Hammett ρ value of –0.56 was obtained for the *para*-substituted styrene derivatives. Detailed DFT calculations show that the reaction proceeds via a two-step process through a doublet spin surface. Formation of epoxidation proceeds via generation of the radical intermediate through an electrophilic attack on alkene followed by a fast ring closing step Finally, using biuret-modified Fe-TAML as the catalyst and NaOCl as the oxidant under catalytic conditions epoxide was formed with modest yields and turnover numbers.

Chapter IV discusses the aerobic epoxidation of olefins catalyzed by iron complexes without the use of sacrificial coreductant. We report the reductive activation of O_2 by a bioinspired $[(bTAML)Fe^{III}(H_2O)]^-$ complex to catalyze the epoxidation of alkenes with TONs of up to 80. Due to the low redox potential of metal center in $[(bTAML)Fe^{III}(OH_2)]^-$ complex, Fe^{III} itself can act as an electron source to reduce the O_2 molecule, and both the oxygen atom get transferred to the substrate. The $[(bTAML)Fe^{III}(OH_2)]^-$ complex serve as a mimic of the dioxygenase enzymes, which is very uncommon in model systems. Spectroscopic and kinetic evidence indicates the

involvement of $Fe^{V}(O)$ as the active oxidant during the reaction. Mechanistic studies using UV-vis and EPR spectroscopy showed Fe-O_2 adduct formation upon O_2 interaction with the iron center.

Chapter V exhibits the formation of a mononuclear (H-bTAML)$Fe^{IV}(O)$-radical cation by reaction of $[(bTAML)Fe^{V}(O)]^{-}$ complex with Lewis acid ($B(C_6F_5)_3$) in acetonitrile at -40 ˚C. DFT calculations suggested for the addition of H^{+} in ligand moiety due to the higher nucleophilicity of the carbonyl oxygen than that of the oxygen of the $Fe^{V}(O)$. The reactivity of the $[(H\text{-}bTAML^{\bullet+})Fe^{IV}(O)]$ complex is compared to that of the $[(bTAML)Fe^{V}(O)]^{-}$ in hydrogen atom transfer reaction using 9,10-dihydroanthacene (DHA) as substrate. Reaction of DHA with $[(H\text{-}bTAML^{\bullet+})Fe^{IV}(O)]$ (k_2 = 0.24 M^{-1} s^{-1}) showed ~720 fold slower reaction rate than the reaction rate of its isoelectronic complex $[(bTAML)Fe^{V}(O)]^{-}$ (k_2 = 173 M^{-1} s^{-1}). The presence of kinetic isotope effect (KIE) for both the species in reaction with deuterated 9,10-dihydroanthacene confirms that hydrogen atom abstraction is the rate determining step.

Chapter VI presents an overall summary of the work and describes the major findings of the studies. Future perspective of this work is also discussed.

Chapter I

Introduction on High-Valent Metal Complex in O-Atom Transfer Reaction

1.1 Importance of C-H and C=C bond functionalization

The presence of O-atom as an alcohol and epoxide moiety in an organic molecule has high significance for the production of drugs.[1] The position and functionality of the prevalence of the O-atom in an organic molecule lead to extreme differences in their chemical and physical properties in view of their usefulness. The direct oxidation of hydrocarbons is a field of both academic and industrial importance and challenge in the quest of regio- and chemo-selectivity. Hence, selective methods for the introduction of O-atom into the C-H and C=C bonds are desirable. Biological enzymes have already perfected this type of synthetic precision to develop and utilize the natural products in the biological process.[2] The most potent tool for C-H bond hydroxylation and C=C bond epoxidation found in the natural systems involve enzymes such as cytochrome P450.[2,3] Hence, inspiration from the biological enzymes led to significant development in the field of catalytic oxygen atom transfer reactions, where catalysis by metal complexes play a central role in the selective and partial oxidation of both saturated and unsaturated hydrocarbons. In this introductory chapter, the motivation and general methods of C-H bond hydroxylation and C=C bond epoxidation, as well as the development of biomimetic catalyst towards these reactions, are discussed.

Oxygen atom transfer reaction with saturated hydrocarbons results in useful hydroxylated products whereas olefins give dihydroxylation as well as epoxide product. The selective functionalization of hydrocarbons represent an essential industrial processes for transforming fossil fuels into value added products.[4] However, functionalization of unactivated aliphatic C–H bonds remain a challenge, and there are very few methods which are routinely used to functionalize such bonds. Similarly, epoxides represent another significant intermediate in organic synthesis. Epoxidation reaction is attractive during asymmetric synthesis since it can lead to two chiral carbons in one step. Hence, such types of oxygen atom transfer reactions have attracted much attention. Many natural products possess these functional groups as an essential structural moiety for their biological activities which include Triptolide (hormone of American cockroach) and Brevetoxin-B (Figure 1.1).[5]

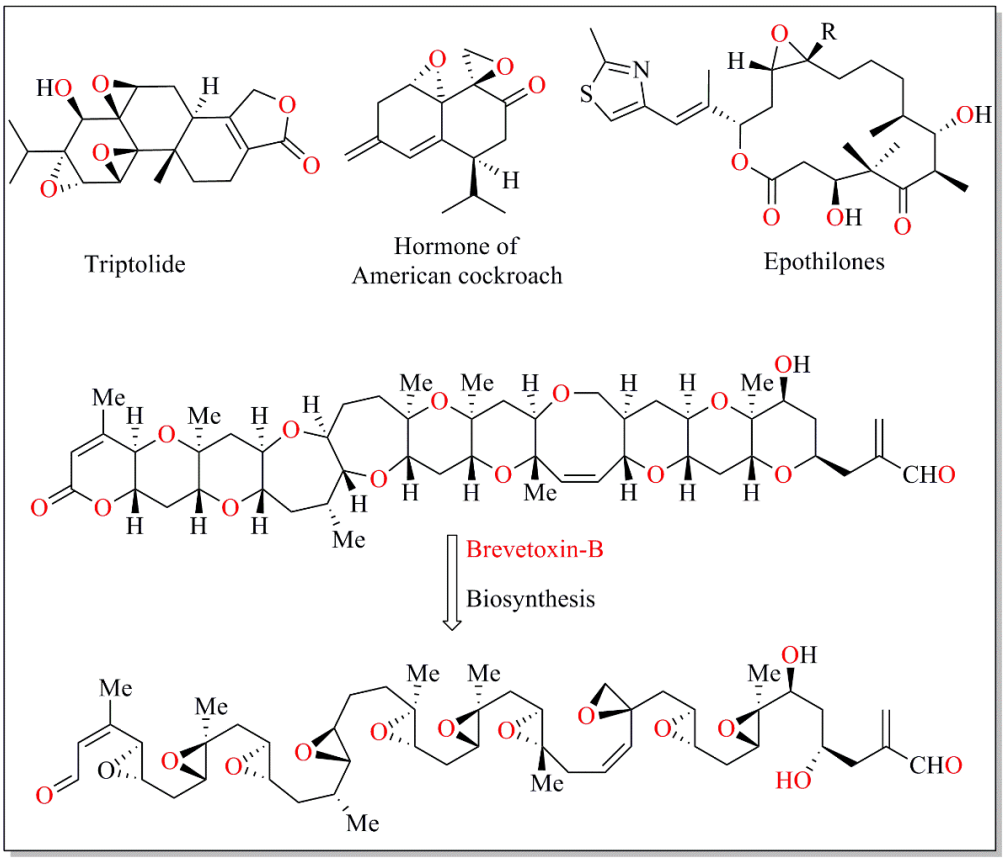

Figure 1.1. Examples of natural products possessing hydroxyl (OH) and epoxide functional group.[5]

The introduction of an epoxide moiety affords immense synthetic possibilities. This efficacy of epoxide is due to the presence of strained three-membered ring which can readily react with a variety of nucleophiles, resulting in organic products containing different functional groups.[6] Ring opening of epoxides is an important synthetic strategy for the construction of natural products and other organic compounds.

Scheme 1.1. General scheme for ring opening of epoxide in the presence of nucleophile.

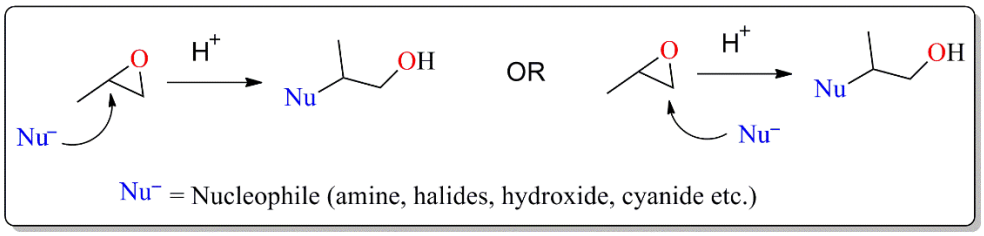

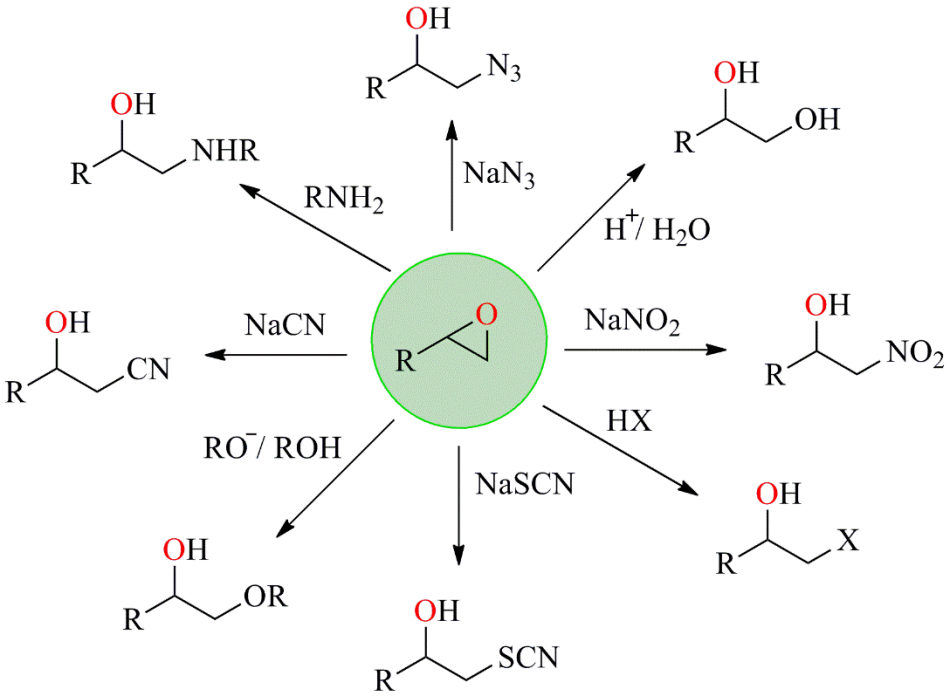

Figure 1.2. Introduction of function group by ring opening of epoxide with various nucleophiles.

1.2 Common methods for C=C bond functionalization

Epoxides have high synthetic importance both to synthetic chemists as well as to chemical industries. For example, propylene oxide has an annual demand of more than 6 million tonnes globally. Traditionally, propylene oxide was synthesized by intramolecular etherification of chlorohydrin intermediates (Scheme 1.2 (A)).[7] This route has severe environmental liabilities and requires a huge capital cost for an efficient effluent treatment.

Epoxidation by peroxy acid has been known since 1909, which is known as Prilezhaev reaction after first reported by Nikolause Prileschajew (Scheme 1.2 (B)).[8] This methodology has found wide usage for epoxide formation in organic laboratories. The kinetic rate of the reaction between peroxy acid and olefins is not very sensitive to the steric substitution of the substrate but is sensitive to the electronic changes. Reaction is faster for substrates have electron rich double bonds because peroxy acids act as an electrophile whereas alkene double bonds are best viewed as a nucleophile. [9] Hence, this method is not an efficient reagent in the case of electron deficient alkenes.

For the epoxidation of electron poor alkenes, the use of a nucleophilic reagent such as hydrogen peroxide in an alkaline solution gives α,β-epoxyketone in good yield. Under basic conditions, the anion of hydrogen peroxide (HOO^-) attacks the substrate and generates

the corresponding enolate. Consequently, due to the nucleophilic nature of enolate, weak O-O bond of peroxide break and form epoxide (Scheme 1.2 (C)).[10]

Over the past 25 years, dioxiranes have been shown to be powerful and versatile oxidants for epoxidation. Epoxidation mediated by dioxiranes are efficient towards both electron deficient and electron rich olefins (Scheme 1.2 (D)).[11] However, disadvantage of this method arises from its intolerance towards C-H bonds and heteroatoms present in the substrates.

To summarize, the major drawbacks of those mentioned above non-metal based epoxidation reactions are generation of side products, excess use of oxidants, overoxidation and harsh reaction conditions.

Scheme 1.2. Various methods for epoxide formation from alkene without using a metal catalyst.

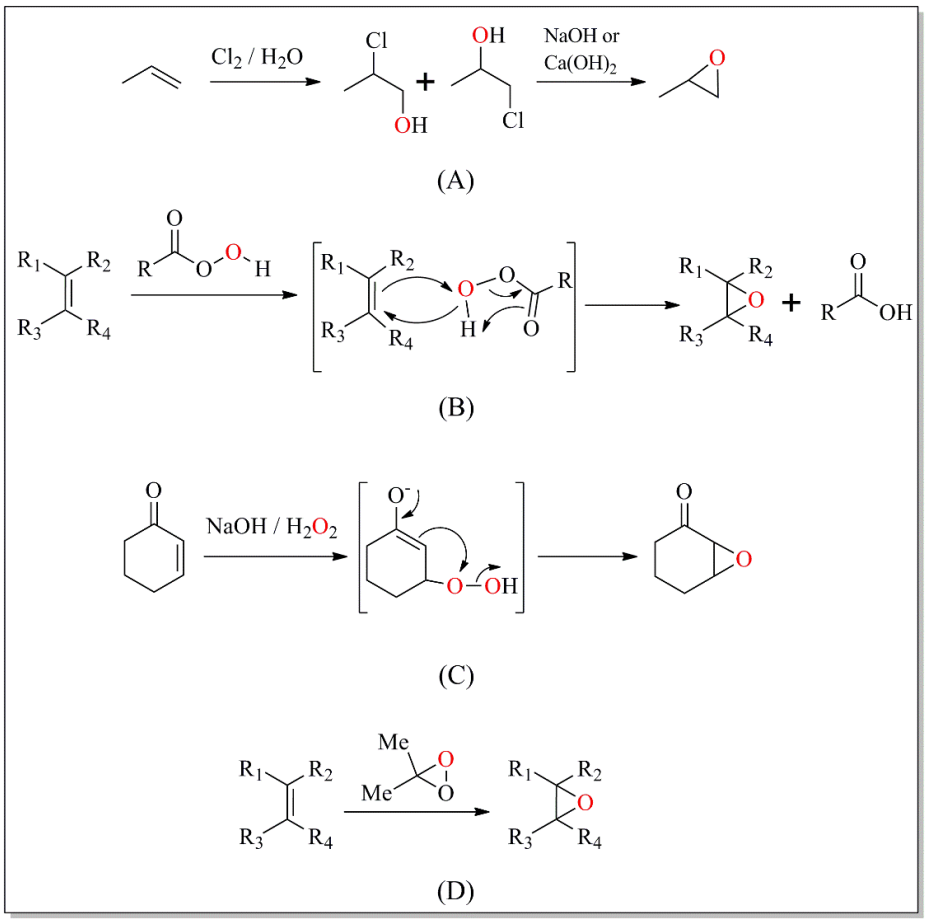

The use of transition metal complexes as a catalyst for alkene epoxidation has received increased attention during the past few decades. There are many reasons for this growing interest: e.g. the requirement for the functionalization of lower alkenes, the interest

in understanding the reaction of biological importance, the need of partial, stereo- and chemo-selective oxidation. The origin of the metal catalyzed epoxidation was inspired by Milas`s work on metal-catalyzed dihydroxylation of olefins with hydrogen peroxide and metal oxides (e. g. OsO_4, RuO_4, V_2O_5, MoO_3 and CrO_3).[12] The metal peroxide was proposed as an actual epoxidizing agent, which was formed by the reaction of metal oxide catalyst and hydrogen peroxide. In 1950, Hawkins first mentioned the metal catalyzed epoxidation with an alkyl hydroperoxide (cumene hydroperoxide) in the presence of V_2O_5.[13] Latter, several groups have studied the epoxidation of olefins with alkyl hydroperoxide in the presence of catalytic amount of soluble Mo, Cr, V complexes which afforded the corresponding epoxide in high yield. Metals with low oxidation potential and high Lewis acidity in their highest oxidation state have proved to be superior as catalysts, showing the following order of reactivity: Mo > W > Ti, V (Mo^{VI}, W^{VI}, Ti^{IV}, V^{V}).[14] However, first row transition metals (Co, Mn, Fe, Cu) which readily decompose peroxide are incompetent catalyst.[15] Use of peroxides as oxidants have limitations since these are very sensitive to the radical-chain reaction and are also subject to self-decomposition at higher concentrations following a catalase-like activity of the catalyst activator. Various transition metal based catalysts are known to activate these oxidants to afford very fast and selective epoxidation as accomplished by Sharpless and Jacobsen. The best known metal catalyzed epoxidation reaction (asymmetric epoxidation) where use of titanium (IV) tetraisopropoxide, tertiarybutyl hydroperoxide (TBHP), and (+)- or (-)-diethyl tartrate with allylic alcohol results in to epoxy alcohol with high enantiomeric excess (ee >90 %), known as the Sharpless epoxidation (Scheme 1.3).[16]

Scheme 1.3. General scheme of Sharpless epoxidation reaction.

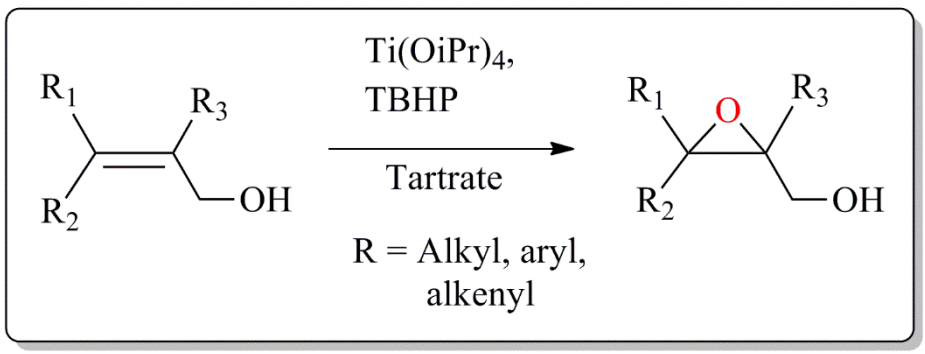

An important preparative methodology which has developed rapidly over the last few years is the (Salen)Mn-mediated epoxidation of alkenes (the Jacobsen-Katsuki

epoxidation). The first report on the epoxidation of unfunctionalized alkenes using achiral salen complex were published by Kochi *et al* in 1985.[17] Later, chiral Mn(III)-Salen complexes for asymmetric alkene epoxidation was reported simultaneously by Jacobsen and Katsuki in 1990.[18] The stereochemistry of the oxygen transfer from the Oxo-Mn-Salen to the alkene depends on the electronic environment around the oxo-manganese center. $Mn^{V}(O)$ was proposed as a catalytically active species.[18(a)]

Scheme 1.4. General scheme of Jacobsen-Katsuki epoxidation reaction.

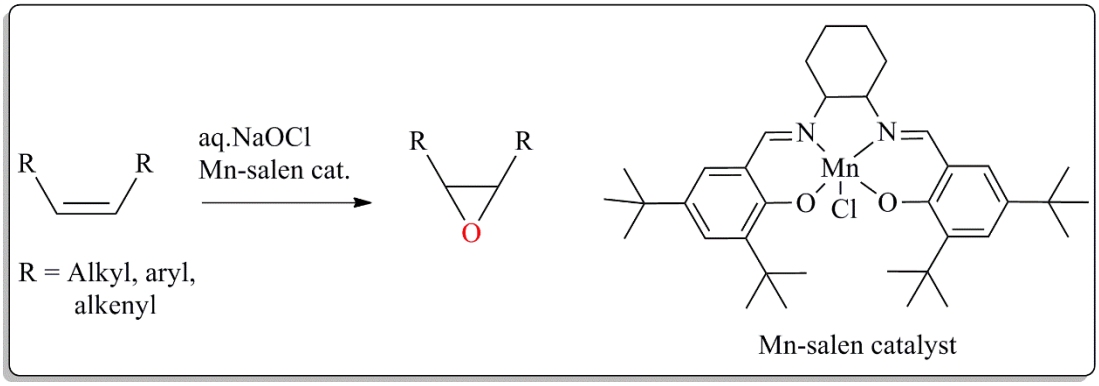

1.3 Biological systems (iron-containing enzymes) in oxygen atom transfer reactions

In nature, metalloenzymes utilize oxidants like dioxygen and hydrogen peroxide to catalyze a variety of oxidation reactions involving O-atom transfer to C–H and C=C bonds.[19,2(a,b)] The region-selectivity and stereo-selectivity of the transformations are controlled by both the metal co-factor in the active site as well as the protein environment surrounding it. These enzymes utilize earth abundant transition metals like iron, copper, and manganese in their active site. Among these, iron-containing enzymes have received widespread attention owing to their ability to catalyze various oxidation reactions such as hydroxylation, epoxidation, N-, S- and O-dealkylations, N-oxidations, sulfoxidation, and dehalogenations.[20] The most widely held heme-containing enzyme Cytochrome P450 (CytP450) has been studied in particular detail over several decades. The P450s are probably nature's most versatile enzymes regarding both their vast substrate range and the different type of biochemical transformations e.g. significant role in metabolism as well as the biosynthesis of steroid, vitamins and other bioactive molecules.[21] The reactions are very selective under mild conditions which are in contrast to the current industrial processes where a high temperature and pressure is required. The active site has been explored through the X-ray crystal structure of CytP450-camphor (Figure 1.3).[22] Its active site

consists of an iron-heme moiety which is ligated by two axial ligands; thiol group of Cys357 and an exchangeable nitrogen ligand from histidine. The β sheet of protein moiety around the porphyrin ring tunes the redox potential of iron.

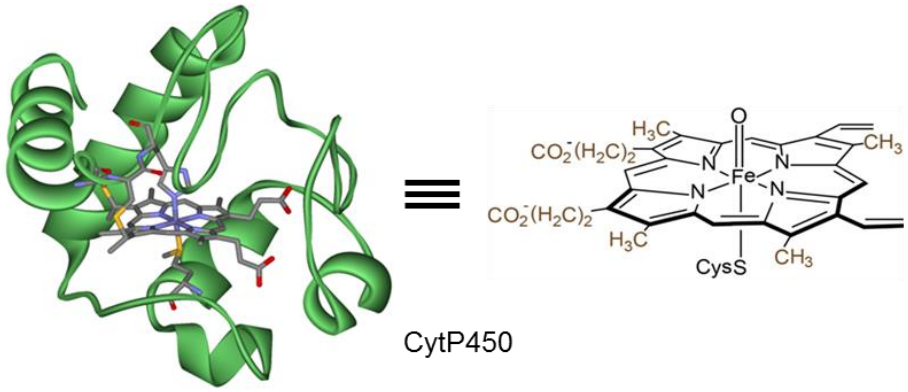

Figure 1.3. Active site of cytochrome P450 (reactive intermediate Compound 1).[19(d)]

Hydroxylation of saturated hydrocarbons is one of the most difficult reactions to achieve with a catalyst at room temperature. Mainly two mechanisms have been proposed in CytP450, oxygen rebound mechanism (cage control radical mechanism) and concerted mechanism. The most accepted 'rebound mechanism' consists of H atom abstraction from the substrate by higher oxidized iron-oxo species Fe^{IV}(O)-radical cation, known as Compound I, to form the corresponding Fe(IV)-hydroxo and a carbon radical. New C-O bond is formed after "rebound" of the 'OH' from the Fe^{IV}-OH which results in the formation of the hydroxylated product. Upon "rebound" the iron-center comes back to its resting state which is a precursor for catalytic oxidation (Figure 1.4(A)).[23] Similarly, olefin epoxidation with cytochrome P450 also has different possible pathways, where retention of stereochemistry in epoxide product of *cis*-olefins strongly suggests a concerted mechanism. However, in terminal alkene sometime it forms irreversible porphyrin N-alkylation products which indicated olefin epoxidation is not always concerted process (Figure 1.4(B)).[23(e)]

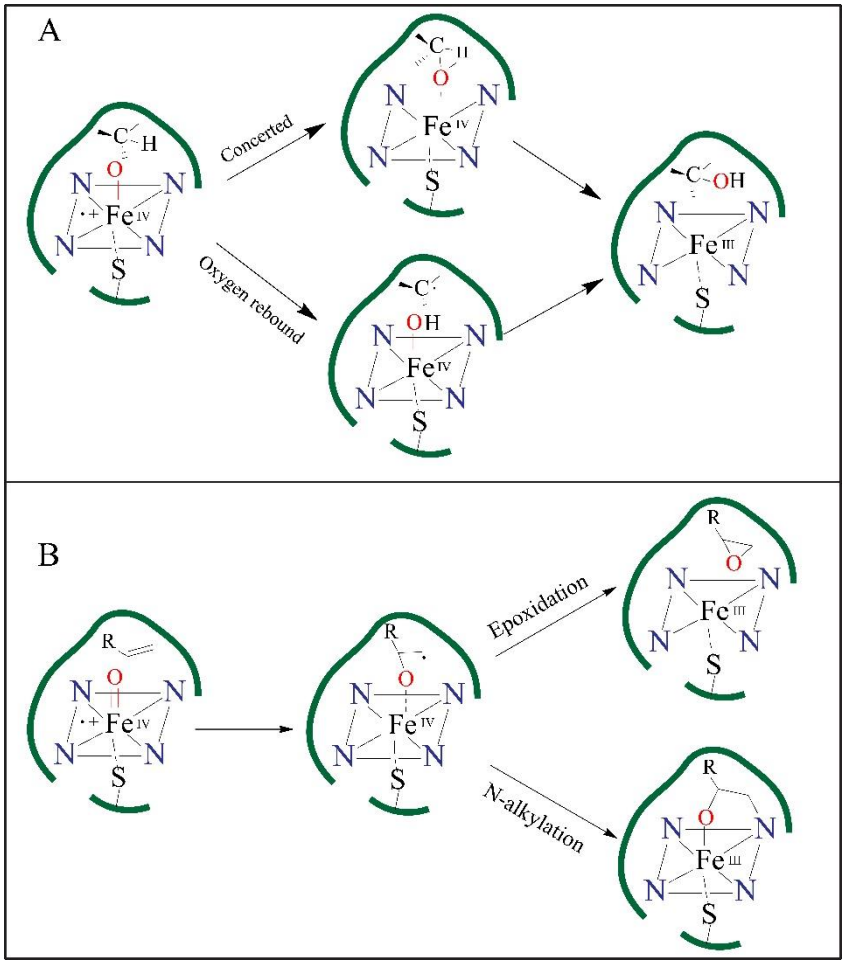

Figure 1.4. Two possible pathways for hydroxylation (A), and epoxidation (B) reaction by cytochrome P450 enzyme.

Non-heme enzymes (Fe-containing enzymes) are broadly classified into two types based on whether the active metal center is mononuclear or dinuclear. In the case of non-heme enzymes, amino acid residues form the coordinating environment which is in contrast to the heme-enzymes that contain porphyrin cofactor. As per the available structural data, a common structural motif consisting of a mononuclear Fe(II) metal center coordinated by two histidine residues and one carboxylate residue in a facial mode.[24] The carboxylate ligand can either be a glutamate or aspartate residue. An example of mononuclear iron enzymes is Rieske dioxygenase and Naphthalene 1,2-dioxygenase (NDO), whereas dinuclear non-heme enzymes include methane monooxygenases (MMO), toluene monooxygenase and tyrosinases.

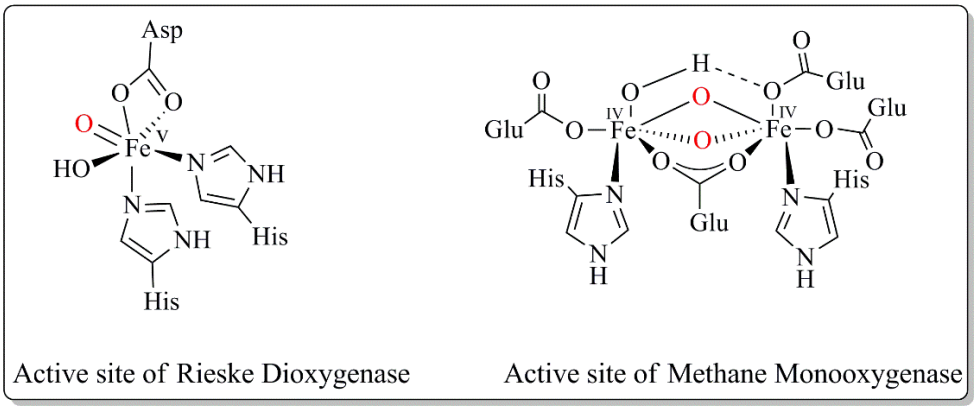

Figure 1.5. The common structural motif "2-His-1-carboxylate facial triad" for non-heme mononuclear Rieske dioxygenase (Left) and dinuclear methane monooxygenase (MMO) (Right) iron enzyme.[24]

Rieske dioxygenase is the most versatile non-heme enzyme analog of CytP450 which catalyzes the enantioselective *cis*-hydroxylation of an arene, a transformation which is challenging in organic synthesis.[21(a), 25] It can also catalyze benzylic hydroxylation, desaturation, sulfoxidation, O- and N- alkylation. The iron(II) center coordinated by 2-His-1-carboxylate facial triad with two histidines and an aspartate moiety. Unlike CytP450 (redox non-innocent porphyrin cofactor), the formation of $Fe^{V}(O)(OH)$ has been proposed for this type of enzyme where redox innocent nature of the amino acid residues allow these enzymes to store two oxidizing equivalents in the iron atom, thereby facilitating the formation of a $Fe^{V}(O)$ oxidant. Till now no direct spectroscopic evidence for a non-heme $Fe^{V}(O)$ species has been obtained during the enzymatic cycle. However, the iron(III)–peroxo precursor has been characterized by X-ray crystallography.[26] It has been proposed that the side-on peroxo moiety attacks either the arene double bond directly or first isomerizes to a $Fe^{V}(O)(OH)$ species.[27]

The di-iron enzyme methane monooxygenase (MMO) activates O_2 to catalyze the conversion of methane to methanol via di-iron(III)–peroxo and diiron(IV) intermediates.[28] Although the peroxo intermediate has been implicated as the oxidant in the epoxidation of electron-rich alkenes such as ethyl vinyl ether, the terminal oxo species has been demonstrated to be kinetically competent for methane hydroxylation. A di(μ-oxo)-di-iron(IV) core (popularly known as diamond core) has been confirmed by extended X-ray absorption fine structure (EXAFS) analysis for the di-iron(IV) species.[29] Methane monooxygenase oxidizes methane to methanol as part of the metabolism of methanotrophs.

Although these enzymes perform oxidations very efficiently and selectively during the biological process, their poor activity towards non-natural substrates, inability to withstand in an organic solvent and tedious isolation process limits their practical applications.

1.4 Synthetic iron porphyrin complexes for hydroxylation and epoxidation reaction

Development of biomimetic porphyrin catalysts was evolved through an iterative design process leading to the successive generations of porphyrin ligands. The first generation "flat metalloporphyrins" with no substituents at the meso positions were rapidly discarded because of very fast oxidation of the ligand framework. The structural features of flat porphyrins render them very reactive towards meso cleavage *via* self-oxidation to form a meso-hydroxy porphyrin derivative.[30] In the second generation of metalloporphyrins, the introduction of phenyl (and related) groups at the meso position proved to be a key structural feature to ensure efficient catalytic oxidations by protecting these highly reactive sites, and by providing steric protection that prevents the formation of catalytically inactive oxo-bridged dimers.[31] In 1979, Groves reported the synthesis of α,β,ϒ,δ-tetraphenylporphinatoiron(III) and chlorodimethylferiprotoporphyrin IX complexes which in the presence of iodosylbenzene catalyzed C-H bond hydroxylation and C=C bond epoxidation reaction. Analysis of reaction mixture showed the conversion of cyclohexene to cyclohexene oxide (55%), cyclohexenol (15%) and a trace amount of cyclohexenone. The complete retention of configuration in *cis*- and *trans*- stilbene epoxidation was found.[31(e)] Further, iron(III)porphyrins with electron withdrawing substituents on phenyl ring such as Fe(TPFPP)Cl [TPFPP = *meso*-tetrakis(pentafluorophenyl) porphyrin], Fe(TDFPP)Cl [TDFPP = *meso*-tetrakis(2,6-difluorophenyl) porphyrin], and Fe(TDCPP)Cl [TDCPP = *meso*-tetrakis(2,6 dichlorophenyl)porphyrin], complexes were synthesised to see the effect of substituent on the electronics structure and oxygen reactivity of model compound I complexes.[31(a)-(d)] Notably, the electron withdrawing power of the substituent attached to the meso position of porphyrin showed a remarkable yield improvement in epoxidation and hydroxylation reactions. Further, these effects were studied by using meso-substituted porphyrins with various aryl groups (Figure 1.6). It was concluded that the catalysts with higher oxidation potential were more reactive than those with the lower oxidation potential.

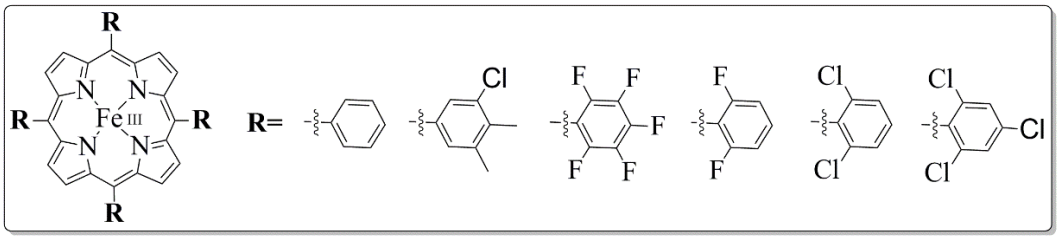

Figure 1.6. Few examples of *meso*-substituted synthetic porphyrin iron complexes used for the study of hydroxylation and epoxidation reaction.

The effect of axial ligands has also been demonstrated as a pronounced influence on the hydroxylation as well as epoxidation reaction in an aprotic solvent. The donor ability of axial ligand dictates for the generation of either of the two reactive intermediates, $Fe^{IV}(O)$ or $Fe^{IV}(O)$-radical cation (equivalent to $Fe^{V}(O)$). These intermediates are the consequence of two different methods of O-O bond breakage of peroxide oxidant. A strong axial donation (e.g. ^{-}OH, ^{-}OAc, Cl^{-}) assists homolysis of O-O bond whereas weak donor axial ligand (e.g. $CF_3SO_3^{-}$, ClO_4^{-}, NO_3^{-}) promotes heterolysis. Consequently they generate $Fe^{IV}(O)$ or $Fe^{IV}(O)$-radical cation, respectively (Figure 1.7).[32(a)-(c)] The reactivity and the catalytic efficiency of the [Fe(tpfpp)X] complexes have been revealed as a pronounced influence of axial ligand.[32(d)] The reactivity decreases in the order: $X^{-} = NO_3^{-} > CF_3SO_3^{-} > ClO_4^{-} >> OAc^{-}$, $Cl^{-} > OH^{-}$ (Table 1.1)[32(d)] attributed to the involvement of different intermediate species ($Fe^{IV}(O)$ or $Fe^{IV}(O)$-radical cation) due to the influence of axial ligand. Moreover, the regioselectivity of C=C epoxidation versus C–H hydroxylation in the oxygenation of cyclohexene, dramatically depend on the reaction temperatures, electronic nature of the iron porphyrins, and substrates.

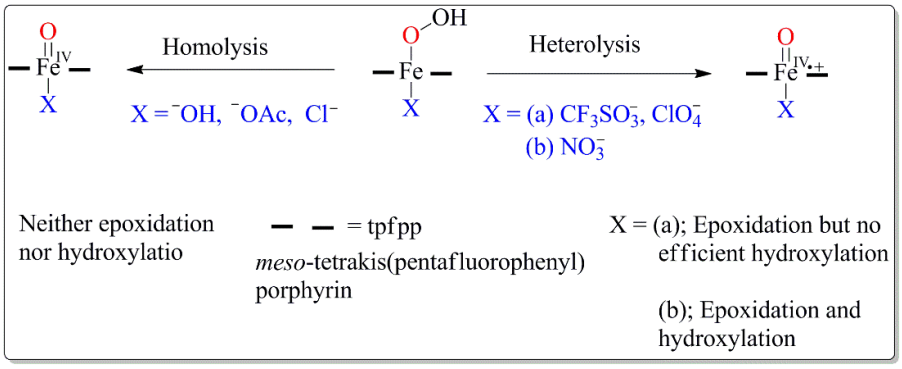

Figure 1.7. Influence of axial ligand for the generation of $Fe^{IV}(O)$ or $Fe^{IV}(O)$-radical cation in a synthetic iron complex of substituted porphyrin.

Table 1.1. Influence of axial ligands on reactivity of [Fe(tpfpp)X] complexes towards C-H and C=C bonds.[32(d)]

Substrate	Products	Products Yield (%)					
		X = $^-$OH	$^-$OAc	$^-$Cl	$CF_3SO_3^-$	ClO_4^-	NO_3^-
Olefins							
Cyclohexene	Cyclohexene oxide	< 2	< 2	< 2	65	68	78
cis-stilbene	*cis*-stilbene oxide	< 2	9	14	78	76	74
Alkanes							
Cyclohexane	Cyclohexenol	< 1	< 1	< 1	6	6	30

1.5 Key intermediates in catalytic cycle of transition metal catalyzed epoxidation reaction

Three main types of transition metal intermediate complexes are involved in the transfer of an oxygen atom to the alkenes: (i) metal-peroxo (ii) oxo-metal complex and (iii) metal mediated peroxo radical. The metal-peroxo complexes are formed in the early transition metal series, where the transition metals are in highest oxidation state such as Ti (IV), V (V), Mo (VI) and W (VI).[33] These metal-peroxo intermediates can catalyze epoxidation reaction with a variety of alkenes. The proposed mechanism for the transfer of the O-atom from metal-peroxo to alkene shows intermediate *via* interaction of the C=C with one of the electrophilic peroxygens or formation of a peroxometallacycle *via* interaction of C=C with the metal center and O-atom of peroxygen (Figure 1.8(i)).[33] Furthermore, the oxo-metal complexes from the middle of the transition metal series (e.g. Cr, Mn, Fe) are the main reactive intermediate towards the alkene epoxidation.[34,17(b)] The metal center in these complexes have partly filled d-electron which can be perturbed by structural and electronic changes through ligand modification to originate several possible spin state of the metal. Similar to the metal peroxo, two type of intermediates have also been proposed for the transfer of oxygen atom from oxo-metal complex to an alkene: interaction of the oxygen atom of oxo-metal with C=C or interaction of the alkene with both oxygen atom and the metal center to form a metallacycle (Figure 1.8(ii)).[35] The peroxo radicals are mainly operating where the systems can undergo electron-transfer process (Co, Ni) and the epoxidation takes place for alkenes in which abstraction of allylic hydrogen is disfavored compared to addition of C=C double bond.[36]

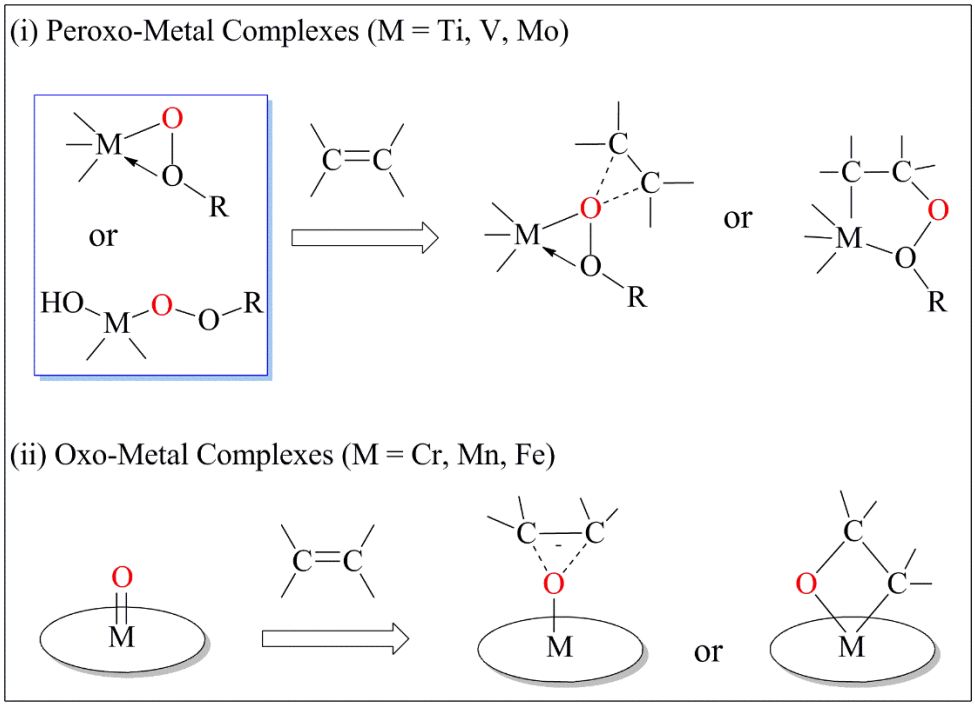

Figure 1.8. Proposed intermediates for the reaction of alkenes with transition metal oxo and peroxo species.

1.6 Synthetic approach for the formation of Fe-Oxo intermediate

Metal-oxo species when the metal is present to the left of Fe in the transition metal series of the periodic table are stable and isolable in many cases whereas metal (Co, Ni, Cu) to the right of the Fe do not form high valent metal-oxo species. This phenomenon, known as the "oxo wall," leads to most metal-catalyzed oxidation (for metals to the right of Fe) occurring through radical intermediates.[36] In the case of Cr and Mn, metal-oxo intermediate has a tendency to decompose oxidants (e.g., alkyl peroxide, hydrogen peroxide) due to their high Lewis acidity.[34,17(b)] However, high valent Fe-Oxo intermediates has unique properties of having reactivity towards oxygen atom transfer to C-H and C=C bonds. Therefore, plenty of iron catalyst has been reported which generate high-valent Fe-Oxo species as a reactive intermediate towards hydroxylation and epoxidation reaction.[37,31(e)] Reduced oxygen species such as PhIO, ClO^-, alkyl hydroperoxide, H_2O_2, *etc*. have been used to achieve the Fe-Oxo species (Figure 1.9(B)).[37,31(e)] However, the use of O_2 as the oxygen source for oxidation reactions, such as the one observed in monooxygenases such as cytochrome P450, is most desirable in our quest for the development of green oxidation reactions.

The study of cytochrome P450 reveals an NADP-dependent reductive dioxygen activation where NADP (coenzyme) function as an exogenous electron source (Figure

1.9(A)).[2(a,c),38] In synthetic small molecule systems, oxygenation reaction (hydroxylation or epoxidation) via reductive activation of dioxygen have been reported, but each require the consumption of at least stoichiometric amounts of a reducing agent (hydride, H_2/Pt, ascorbic acid, etc.) (Figure 1.9(B)).[39] However, the additional use of chemical as a sacrificial reductant and their secondary reaction with highly reactive intermediate overshadow the advantage of using O_2. Therefore, development of metal complexes, in particular with cheap and environmentally friendly metal Fe, for oxidation reactions without the use of sacrificial reductant is desirable. Such system, where the metal center of the complex itself can act as an electron source to reduce the O_2 molecule, and both the oxygen atom get transferred to the substrate, can serve as a mimic of the dioxygenase enzymes.[40] Although in a biomimetic approach a plenty of model iron complexes have been generated to activate molecular oxygen, none of them are proven as a potential epoxidation catalyst where molecular oxygen can be used as a terminal oxidant without the use of reductant.[41] However, for the first time in 1985, a ruthenium porphyrin complex, $Ru^{IV}(TMP)(O)_2$ {TMP = 5, 10, 15, 20-(tetramesityl)porphyrin}, was reported for aerobic epoxidation of olefins without using any coreductant.[42] Absence of such an iron complex in literature, prompted us to look in to the use of (bTAML)Fe complex[43] (developed in our group) for reductive dioxygen activation to catalyze epoxidation reaction. The detail mechanistic investigation of O_2 interaction with the iron center and its use for epoxidation reaction has been discussed in chapter 4.

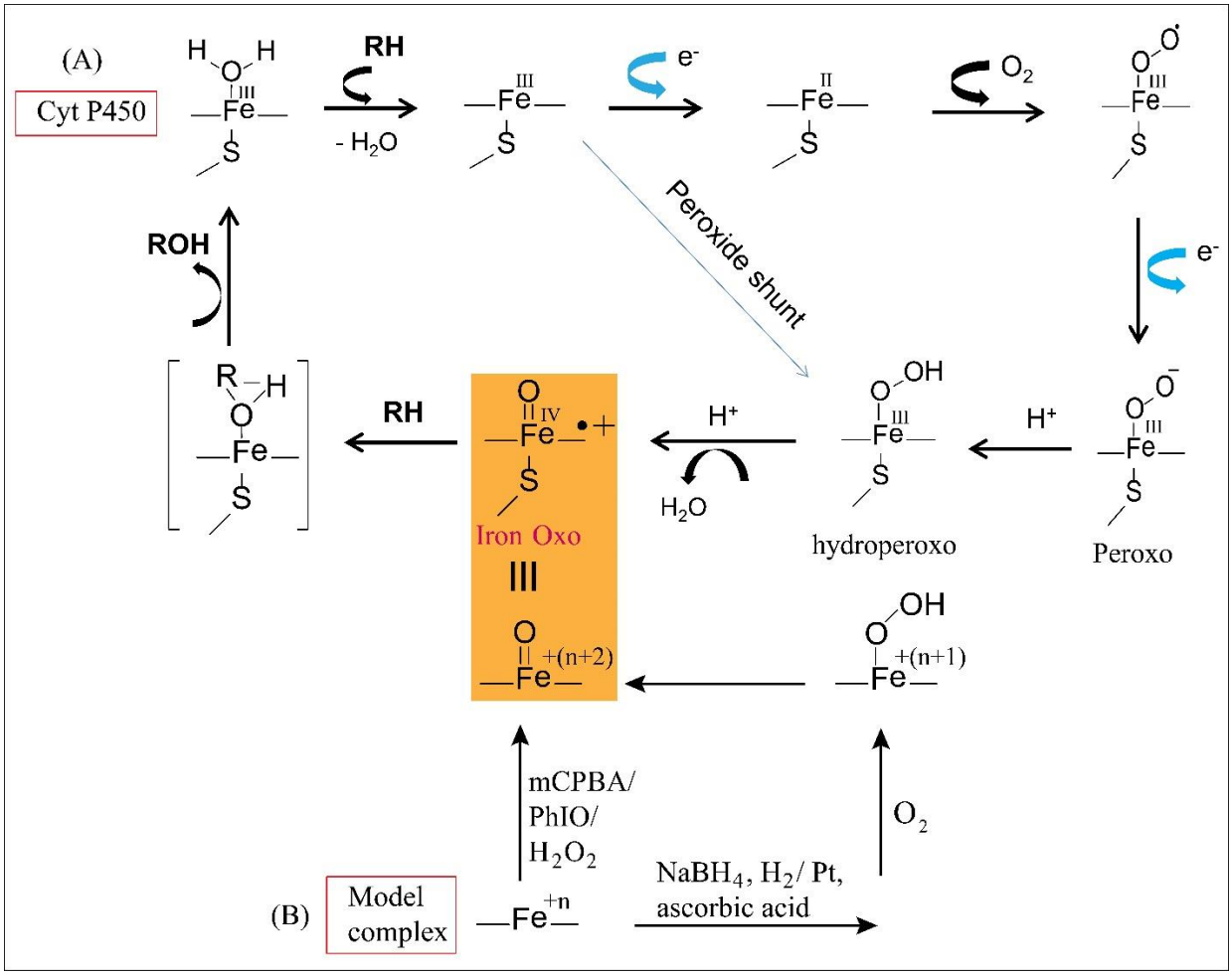

Figure 1.9. (A) Formation of (porphyrin)Fe^{IV}(O)-radical-cation during the catalytic cycle of cytochrome P450 for hydroxylation reaction (NADP as an electron source and O_2 as an O-atom source). (B) Two different pathway for the formation of high valent iron-oxo intermediate in model complexes, either the use of two electrons reduced oxo donor reagents (mCPBA, PhIO, H_2O_2, etc.) or use of sacrificial reductant with O_2.

1.7 Objective and Motivation

Based on the above literature survey on bio-inspired oxygenation reactions (epoxidation and hydroxylation), it has been noticed that the chemical reactions performed by enzymatic systems are very efficient and selective. The active site of these enzymes contain a high-valent (Porphyrin)Fe^{IV}(O)-radical-cation as a reactive intermediate which does the oxygen atom transfer to the substrate.[44] Therefore, over an extended period of time, many metal complexes (heme and non-heme) have been designed by several scientific groups to mimic the structural and functional aspects of this highly reactive intermediate. The first report of a mononuclear nonheme Fe(IV)-oxo species, postulated as

$[Fe^{IV}(O)(cyclam\text{-}acetate)]$ [cyclam-acetate = 1-(carboxymethyl)-1,4,8,11-tetraazacyclotetradecane][45] (Figure 1.10(1)), was formed by the reaction of the corresponding Fe(II) complex and ozone at –80 °C. Later, mononuclear nonheme complex of $Fe^{IV}(O)$ species was demonstrated with various ligand systems, such as $[Fe^{IV}(O)(TMC)(NCCH_3)](OTf)_2$ (TMC = 1,4,8,11-tetramethyl-1,4,8,11-tetraazacyclotetradecane; OTf = CF_3SO_3)[46] (Figure 1.10(2)) and $[Fe^{IV}(O)(TPA)][ClO_4]_2$ (tetradentate tripodal ligand TPA)[47] (Figure 1.10(3)). While the TMC complex could execute oxygen-atom transfer only to PPh_3 at -40 °C, the TPA complex was capable of cyclooctene epoxidation at this temperature. Furthermore, the synthesis and characterization of corresponding $Fe^{IV}(O)$ complexes of the pentadentate N_5 ligands N_4Py (Figure 1.10(4))[48] and Bn-tpen[49] display striking similarities in their properties such as their room temperature stability and ability to hydroxylate strong C-H bonds such as cyclohexane (C-H bond strength of 99.3 kcal/mol).

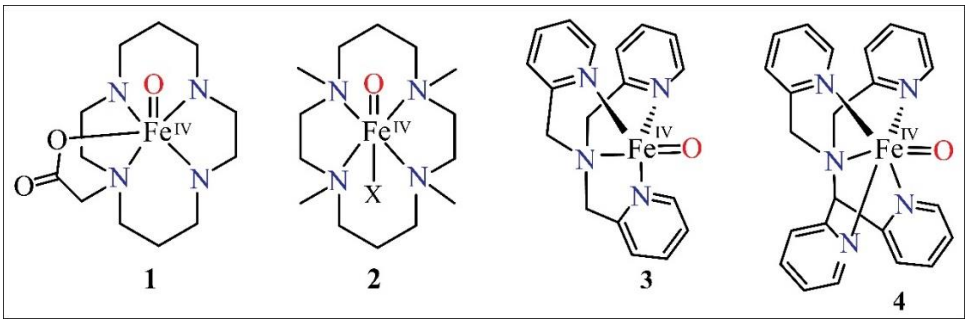

Figure 1.10. Examples of $Fe^{IV}(O)$ intermediate synthesized by Fe(II) complex of ligand cyclam-acetate (**1**), TMC (**2**), TPA (**3**), and N4Py (**4**).

The synthesis of Fe(V)-Oxo Complexes, which are isoelectronic to the naturally occurring $Fe^{IV}(O)(P^{+\bullet})$ species, Compound I) would be more noteworthy in view of its enhanced oxidizing properties. The role of $Fe^{V}(O)$ has also been proposed in the intermediate Q species of the methane monooxygenase enzyme where a di(μ-oxo)diiron(IV) ($Fe_2^{IV}(\mu\text{-}O)_2$) core has been as the active intermediate for methane hydroxylation.[26,27] Another important enzyme is Rieske dioxygenase which catalyzes the initial steps during biodegradation of aromatic hydrocarbons. A (hydroxo)oxo-iron(V) ($HO\text{-}Fe^{V}=O$) intermediate has been hypothesized which catalyzes the *cis*-dihydroxylation of arene double bonds.[50] However, unlike $Fe^{IV}(O)$, the direct role of $Fe^{V}(O)$ during various steps of the hydroxylation and epoxidation reaction is unmapped. This is primarily due to the paucity of well-defined $Fe^{V}(O)$ system. In synthetic iron(II) complex of Pytacn ligand

(Figure 1.11(1)), the involvement of iron(V) species for the *cis*-dihydroxylation of C=C bonds was postulated by variable temperature mass analysis.[51] In another example, a transient formation of Fe^{V}-Oxo species was optically detected through laser flash photolysis experiments of an iron-corrole complex and cytochrome P450 mutant CYP 119 (Figure 1.11(2)).[52] For synthetic small molecule mimics, Terrence J. Collins and co-workers have reported tetraamido macrocyclic ligands (TAMLs) which have the ability to stabilize a variety of high-valent iron complexes.[53] The deprotonated TAML have four exceptionally strong amido-N σ-donors atoms that is bonded to the iron center. Therefore, this macrocyclic ligand displays the capability of stabilizing an oxo-iron(V) complex at -40 °C (Figure 1.11(3)).[54] This represented the first example of a fully spectroscopically characterized iron(V)-oxo complex $[(TAML)Fe^{V}(O)]^{-}$ (EPR, Mössbauer, ESI-MS, x-ray absorption spectroscopies and DFT). $[(TAML)Fe^{V}(O)]^{-}$ was shown as a strong oxidizing iron-oxo complex for various reaction, such as oxygen atom transfer reaction to the triphenylphosphine, thioanisole, styrene, and cyclooctene. However, its instability above -40 °C hindered mechanistic studies especially for hydroxylation reaction for strong unactivated C-H bonds (these rates were comparable their rate of self-decay).

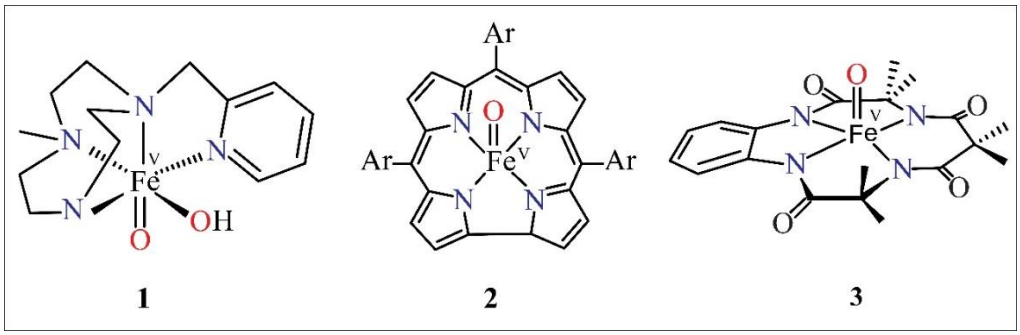

Figure 1.11. Examples of $Fe^{V}(O)$ intermediate synthesized by Iron complex of ligand Pytacn (**1**), Corrole (**2**), TAML (**3**).

We have recently reported the Fe(III) complex of a biuret-amide based macrocyclic ligand which was designed by replacing the tail -CMe_2 moiety of tetraamido macrocyclic ligands (TAML) by an –NMe group, (assigned as bTAML, biuret modified-tetraamido macrocyclic ligand).[43] The corresponding Fe^{III} complex shows 10^5 folds enhanced stability in aqueous acidic medium and also exhibits 10-fold lower deactivation rates for H_2O_2 activation in water compared to the corresponding Fe-TAML.[43] Electrochemical studies of (bTAML)Fe displayed Fe(IV)/Fe(III) couple 230 mV lower than the corresponding Fe-TAML complex which favors for the formation of high-valent iron species. It was

hypothesized that higher donating ability of the deprotonated amide-biuret macrocyclic ligand in addition to its robustness towards oxidative degradation might help to stabilize Fe^{V}=O complex at room temperatures. (bTAML)Fe^{V}(O) complex has been formed with [(bTAML)Fe^{III}] and *m*CPBA as oxidant (1:1.2) at room temperature and was characterized by UV-Vis spectra, EPR and HRMS.[55] This improved stability of the Fe^{V}=O complex ($t_{1/2}$ = 3 hrs) allowed for oxidation of unactivated C-H bonds of cyclohexane, having bond dissociation energy 99.3 kcal/mol (Figure 1.12).

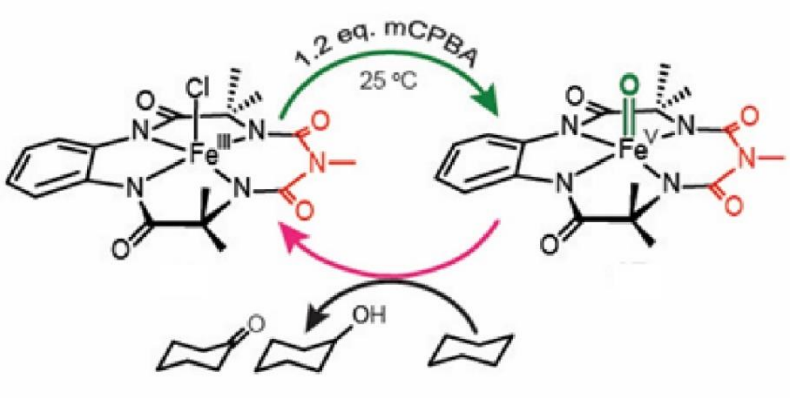

Figure 1.12. Formation of (bTAML)Fe^{V}(O) and catalytic cycle for cyclohexane hydroxylation.[55]

Further, the use of (bTAML)Fe^{V}(O) has been extended to catalytic reactions, where selective oxidation of tertiary C-H bonds over secondary C-H bonds were observed in a wide range of organic substrates. The mechanism of C–H bond and O–H bond oxidation, as well as the role of FeV(O) in water oxidation, has also been achieved using (bTAML)Fe complex.[56] However, mechanistic studies on C=C bond epoxidation involving the direct role of Fe^{V}(O) complex has not been explored. Also, the effect of water during C-H bond hydroxylation using Fe^{V}(O) complex is unknown. Therefore, the main objective of this work is:

1. To generate Fe^{V}(O) in aqueous medium and to see its effect on the reactivity for C-H bond hydroxylation reaction
2. Mechanistic investigation on O-atom transfer from Fe^{V}(O) to C=C bond
3. Use of cost effective and environmentally friendly oxidant, such as NaOCl and O_2 for catalytic epoxidation reaction.
4. Generation of different high-valent intermediate species of Fe-bTAML complex, such as $Fe^{IV}OFe^{IV}$, Fe^{IV}(Cl), Fe^{IV}(O)-radical-cation, and comparison of their properties with Fe^{V}(O).

It is important to understand the effect of water on the rate of reaction for the oxidation of C-H bonds by Fe-Oxo because water has been shown to play a critical role during oxidation of organic substrates in heme-containing enzymes such as cytochrome P450. Chapter 2, entitled "Tuning the Reactivity of $Fe^{V}(O)$ towards C-H Bonds at Room Temperature: Effect of Water," verify the stability of $Fe^{V}(O)$ in H_2O/CH_3CN mixtures containing up to 90% water. The effect of water on the reactivity of $Fe^{V}(O)$ during C-H activation has been studied both experimentally and theoretically.[57] In chapter 3, entitled "On the Mechanism of Oxygen Atom Transfer from $Fe^{V}(O)$ to Olefins at Room Temperature," we elucidated the mechanism of direct O-atom transfer during the reaction of $Fe^{V}(O)$ with alkenes to form the corresponding epoxide.[58] For the first time, we have studied the mechanism of O-atom transfer to alkenes using the $Fe^{V}(O)$ complex of biuret-modified Fe-TAML at room temperature. Subsequently, we show the use of molecular O_2 as an oxygen source for catalytic epoxidation reaction with (bTAML)Fe complex, without the use of any sacrificial reductant. The use of cheap and environmentally friendly metal Fe for epoxidation reaction, without the use of sacrificial reductant, was unprecedented.[59] This has been discussed in chapter 4, entitled "Reductive Activation of O_2 by Bioinspired Fe-Complex for Catalytic Epoxidation Reactions". The effect of Lewis acid on $Fe^{V}(O)$ results in valence tautomerism to generate $Fe^{IV}(O)$-radical cation due to extended π-conjugation in the bTAML ligand. This redox non-innocent nature of the ligand causing valence tautomerization has been discussed in chapter 5.

1.8 References:

1. (a) Yang, D. *Acc. Chem. Rev.* **2004**, *37*, 497. (b) Vollhardt, K. P. C. C.; Schore, N. E. *Química Orgánica, Ed. Omega* **1996**, *467*. (c) Lindsley, C. W. *ACS Chem. Neurosci*. **2013**, *4*, 905. (d) Yamaguchi, J.; Yamaguchi, A. D.; Itami, K. *Angew. Chemie Int. Ed.* **2012**, *51*, 8960.
2. (a) Meunier, B.; de Visser, S. P.; Shaik, S. *Chem. Rev.* **2004**, *104*, 3947. (b) Ortiz de Montellano, P. R. *Chem. Rev.* **2010**, *110*, 932. (c) Rittle, J.; Green, M. T. *Science*. **2010**, *330*, 933. (d) Groves, J. T. *J. Inorg. Biochem.* **2006**, *100*, 434. (e) Guengerich, F. P. *Chem. Res. Toxicol*. **2008**, *21*, 70. (f) Denisov, I. G.; Makris, T. M.; Sligar, S. G.; Schlichting, I. *Chem. Rev*. **2005**, *105*, 2253.
3. (a) Shaik, S.; Kumar, D.; de Visser, S. P.; Altun, A.; Thiel, W. *Chem. Rev*. **2005**, *105*, 2279. (b) Bell, S. R.; Groves, J. T. *J. Am. Chem. Soc*. **2009**, *131*, 9640.

4. (a) Shilov, A. E.; G. B. S. p. *Activation and Catalytic Reactions of Saturated Hydrocarbons in the Presence of Metal Complexes*, Springer Netherlands: **2002**; Vol. 21. (b). Arndtsen, B. A.; Bergman, R. G.; Mobley, T. A.; Peterson, T. H. *Acc. Chem. Res.* **1995,** *28*, 154. (c) Bergman, R. G. *Nature* **2007**, *446*, 391. (d) Cornell, C. N.; Sigman, M. S., *Molecular Oxygen Binding and Activation: Oxidation Catalysis. In Activation of Small Molecules*, Wiley-VCH Verlag GmbH & Co. KGaA: **2006**; p 159-186. (e) Labinger, J. A.; Bercaw, J. E. *Nature* **2002**, *417*, 507. (f) Olah, G. A.; Molnar, A. *Hydrocarbon chemistry*. John Wiley & Sons: **2003**. (g) Sheldon, R. A.; Kochi, J. K. *Metal-Catalyzed Oxidations of Organic Compounds.* **1981,** Academic Press, New York.
5. (a) Taylor, S. K.; Hopkins, J. A.; Spangenberg, K. A. *J. Org. Chem.* **1991**, *56*, 5951. (b) Mori, K. *Tetrahedron* **1989**, *45*, 3233. (c) Paddon-Jones, G. C.; Mamdapur, V. R.; Chadha, M. S. *Tetrahedron Lett*. **1997**, *38*, 4379.
6. Parker, R. E.; Isaacs, N. S. *Chem. Rev*. **1959**, *59*, 737.
7. Weissermel, K.; Arpe, H. -J., *Industrial Organic Chemistry*, Wiley: New York, **2003**.
8. (a) Prileschajew, N. *Eur. J. Inorg. Chem*. **1909**, *42*, 4811. (b) Swern, D. *Organic Peroxides;* Wiley: New York, Chapter V, **1972**, 11. (c) Metelitsa, D. I. *Russ. Chem. Reu. (Engl. Transl.)* **1972**, *41*, 807. (d) Hiatt, R.; Augustine, R. L., Trecker, D. J. *Eds.; Marcel Dekker*: New York, Vol. 2, **1971**.
9. (a) Bartlett, P. D. *Record of Chemical Progress* **1950**, *11*, 47. (b) Edwards, J. O. "Peroxide Reaction Mechanisms", *Interscience*, New York, **1962**, p. 67–106. (c) Donohoe, T. J. *Oxidation and Reduction in Organic Synthesis*, Oxford University Press **2000**, pp. 13. (d) Angelis, Y. S.; Orfanopoulos, M. *J. Org. Chem*. **1997**, *62*, 6083. (e) Plesnicar, B.; Patai, S., Ed.; Wiley: New York, **1983**; p 521.
10. (a) de Visser, S. P.; Kaneti, J.; Neumann, R.; Shaik, S. *J. Org. Chem*. **2003**, *68*, 2903. (b) Dowd, P.; Ham, S. W.; Marchand, A. P.; Rajapaksa, D. *J. Org. Chem*. **1992**, *57*, 3514. (c) Arai, S.; Oku, M.; Miura, M.; Shioiri, T. *Synlett* **1998**, 1201.
11. (a) Narsaiah, A. V. *Synlett* **2002**, *7*, 1178. (b) Adam, W.; Hadjiarapoglou, L. P.; Wang, X. *Tetrahedron Lett*. **1991**, *32*, 1295. (c) Dushin, R. G.; Danishefsky, S. J. *J. Am. Chem. Soc*. **1992**, *114*, 3471. (d) Murray, R. W. *Chem. Rev*. **1989**, *89*, 1187.
12. Milas, N. A.; Sussman, S. *J. Am. Chem. Soc*. **1936**, *58*, 1302.
13. Hawkins, E. G. E. *J. Chem. Soc. (London)* **1950**, *2*, 169.
14. Ugo, R., *Aspects of Homogeneous Catalysis*, Vol. 4, **1981**, p 3-70.
15. Sheldon, R. A.; Van Doorn, J. A. *J. Catalysis* **1973**, *31*, 427.

16. (a) Katsuki, T.; Sharpless, K. B. *J. Am. Chem. Soc.* **1980**, *102*, 5974. (b) Hanson, R. M.; Sharpless, K. B. *J. Org. Chem.* **1986**, *51*, 1922. (c) Gao, Y.; Hanson, R. M.; Klunder, J. M.; Ko, S. Y.; Masamune, H.; Sharpless, K. B. *J. Am. Chem. Soc.* **1987**, *109*, 5765.
17. (a) Srinivasan, K.; Michaud, P.; Kochi, J. K. *J. Am. Chem. Soc.* **1986**, *108*, 2309. (b) Samel, E. G.; Srinivasan, K.; Kochi, J. K. *J. Am. Chem. Soc*. **1985**, *107*, 7606. (c) Yoon, H.; Borrows, C. J. *J. Am. Chem. Soc.* **1988**, *110*, 4087.
18. (a) Zhang, W.; Loebach, J. L.; Wilson, S. R.; Jacobsen, E. N. *J. Am. Chem. Soc.* **1990**, *112*, 2801. (b) Irie, R.; Noka, K.; Ito, Y.; Matsumoto, N.; Katsuki. T. *Tetrahedron Lett.* **1990**, *31*, 7345.
19. (a) Costas, M.; Mehn, M. P.; Jensen, M. P.; Que, L., Jr. *Chem. Rev*. **2004**, *104*, 939. (b) Que, L., Jr.; Tolman, W. B. *Nature* **2008**, *455*, 333. (c) Poulos, T. L. *Chem. Rev*. **2014**, *114*, 3919. (d) Smith, L. J.; Kahraman, A.; Thornton, J. M., *Proteins: Struct. Funct. Genet*. **2010**, *78*, 2349.
20. Sono, M.; Roach, M. P.; Coulter, E. D.; Dawson, J. H. *Chem. Rev*. **1996**, *96*, 2841.
21. (a) Ortiz de Montellano, P. R., *Cytochrom P-450: Structure, Mechanism, and Biochemistry*, Plenum New York, **1986**. (b) Lee, S.-K.; Fox, B. G.; Froland, W. A.; Lipscomb, J. D.; Münck, E. *J. Am. Chem. Soc.* **1993**, *115*, 6450. (c) Lee, S.-K.; Nesheim, J. C.; Lipscomb, J. D. *J. Biol. Chem*. **1993**, *268*, 21569. (d) Liu, K. E. *et al*. *J. Am. Chem. Soc*. **1994**, *116*, 7465. (e) Feig, A. L.; Lippard, S. J. *Chem. Rev*. **1994**, *94*, 759. (f) Que, L., Jr.; True, A. E. *Prog. Inorg. Chem*. **1990**, *38*, 97. (g) Sánchez-Ferrer, A.; Rodríguez-López, J. N.; García-Cánovas, F.; García-Carmona, F. *Biochim. Biophys. Acta* **1995**, *1*, 1247. (h) Nordlund, P.; Sjöberg, B.-M.; Eklund, H. *Nature* **1990**, *345*, 593. (i) Bollinger, J. M., Jr. *J. Am. Chem. Soc*. **1994**, *116*, 8024.
22. Schlichting, I.; Berendzen, J.; Chu, K.; Stock, A. M.; Maves, S. A.; Benson, D. E.; Sweet, R. M.; Ringe, D.; Petsko, G. A.; Sligar, S. G. *Science* **2000**, *287*, 1615.
23. (a) Gelb, M. H.; Heimbrook, D. C.; Malkonen, P.; Sligar, S. G. *Biochemistry* **1982**, *21*, 370. (b) Hjelmeland, L. M.; Aronow, L.; Trudell *J. Biochem. Biophys. Res. Commun.* **1977**, *76*, 541. (c) Groves, J. T.; McClusky, G. A. *J. Am. Chem. Soc*. **1976**, *98*, 859. (d) Ortiz de Montellano, P. R. *Cytochrome P450*: *Structure, Mechanism and Biochemistry*; *Ed.;* Plenum: New York, **1995**. (e) Mayer, J. M., In. *Biomimetic Oxidations Catalyzed by Transition Metal Complexes*; *Meunier, B.,* Ed.; Imperial College Press: London, **2000**; Chapter 1, pp 1-43.

24. (a) Que, L. *Nat. Struct. Mol. Biol.* **2000**, *7*, 182. (b) Prof. dr. R. J. M. Klein Gebbink, P. d. i. B. M. W., Prof. dr. G. van Koten, Structural and Functional Models of Non-Heme Iron Enzymes. In.
25. (a) Bruijnincx, P. C. A.; van Koten, G.; Klein-Gebbink, R. J. M. *Chem Soc Rev.* **2008**, *37*, 2716. (b) Gibson, D. T.; Resnick, S. M.; Lee, K.; Brand, J. M.; Torok, D. S.; Wackett, L. P.; Schocken, M. J.; Haigler, B. E. *J. Bacteriology*, **1995**, *177*, 2615. (c) Wolfe, M. D.; Parales, J. V.; Gibson, D. T.; Lipscomb, J. D. *J Bio Chem.* **2001**, *276*, 1945. (d) Kauppi, B. R.; Lee, K.; Carredano, E.; Parales, R. E.; Gibson, D. T.; Eklund, H.; Ramaswamy, S. *Structure* **1998**, *6*, 571. (e) Crutcher, S. E.; Geary, P. J. *Biochemical J.* **1979**, *177*, 393. (f) Pavel, E. G.; Martins, L. J.; Ellis, W. R.; Solomon, E. I. *Chemistry & Biology* **1994**, *1*, 173.
26. Karlsson, A.; Parales, J. V.; Parales, R. E.; Gibson, D. T.; Eklund, H.; Ramaswamy, S. *Science* **2003**, *299*, 1039.
27. McDonald, A. R.; Que, L., Jr. *Nature Chem.* **2011**, *3*, 761.
28. (a) Merkx, M.; Kopp, D. A.; Sazinsky, M. H.; Blazyk, J. L.; Müller, J.; Lippard, S. J. *Angew Chem Int Ed.* **2001**, *40*, 2782. (b) Beauvais, L. G.; Lippard, S. J. *J Am Chem Soc.* **2005**, *127*, 7370. (c) Shu, L.; Nesheim, J. C.; Kauffmann, K.; Münck, E.; Lipscomb, J. D.; Que, L., Jr. *Science* **1997**, *275*, 515. (d) Siegbahn, P. E. M.; Crabtree, R. H. *J. Am. Chem. Soc*. **1997**, *119*, 3103. (e) Xue, G.; De Hont, R.; Münck, E.; Que, L. *Nat. Chem*. **2010**, *2*, 400.
29. (a) Rosenzweig, A. C.; Frederick, C. A.; Lippard, S. J.; Nordlund, P. *Nature* **1993**, *366*, 537. (b) Lipscomb, J. D.; Que, L., Jr. *J. Biol. Inorg. Chem*. **1998**, *3*, 331. (c) Lieberman, R. L.; Rosenzweig, A. C. *Nature* **2005**, *434*, 177.
30. Chang, C. K.; Kuo, M.-S. *J. Am. Chem. Soc.* **1979,** *101*, 3413.
31. (a) Chang, C. K.; Ebina, F. *J. Chem. Soc., Chem. Comm.* **1981**, 778. (b) Bortolini, O.; Meunier, B. *J. Chem. Soc., Chem. Comm.* **1983**, 1364. (c) Traylor, P. S.; Dolphin, D.; Traylor, T. G. *J. Chem. Soc., Chem. Comm.* **1984**, 279. (d) de Poorter, B.; Meunier, B. *Tetrahedron Letters* **1984,** *25*, 1895. (e) Groves, J. T.; Nemo, T. E.; Myers, R. S. *J. Am. Chem. Soc.* **1979**, *101*, 1032.
32. (a) Traylor, T.G.; Kim, C.; Richards, J. L.; Xu, F.; Perrin, C. L. *J. Am. Chem. Soc*. **1995**, *117*, 3468. (b) Nam, W.; Goh, Y. M.; Lee, Y. J.; Lim, M. H.; Kim, C. *Inorg. Chem* **1999**, *38*, 3238. (c) Bartoli, J. F.; Bathioni, P.; De Foor, W. R.; Mansuy, D. *J. Chem. Soc. Chem. Commun*. **1994**, 23. (d) Nam, W.; Lim, M. H.; Ho, S.-Y.; Lee, J. H.; Kim, C.; Shin, W. *Angew. Chem. Int. Ed.* **2000**, *39*, 3646.

33. (a) Sheldon, R. A., In, *Aspects of Homogeneous Catalysis; Ugo, R., Ed.; D. Reidel: Dordrecht*, **1991**, *4*, 3. (b) White, P. J.; Kaus, M. J.; Edwards, J. O.; Rieger, P. H. *J. Chem. Soc., Chem. Commun*. **1976**, 419. (c) Bradley, D. C.; Mehrotra, R. C.; Gaur, D. P., In, *Metal Alkoxides*, Academic Press: New York, **1978**, Chapter 4. (d) Clark, R. J. H. *The Chemistry of Titenium and Vanadium*; Elsevier: Amasterdam, **1968**.
34. (a) Groves, J. T.; Kruper, W. J.; Haushalter, R. C. *J. Am. Chem. Soc*. **1980**, *102*, 6375. (b) Groves, J. T.; Nemo, T. E. *J. Am. Chem. Soc*. **1983**, *105*, 5786.
35. (a) Rappé, A. K.; Goddard, W. A. *J. Am. Chem. Soc*. **1982**, *104*, 3287. (b) Walba, D. M.; De Puy, C. H.; Grabowski, J. J.; Bierbaum, V. M. *Organometallics* **1984**, *3*, 498. (c) Kafafi, Z. H.; Hauge, R. H.; Billups, W. E.; Margrave, J. L. *J. Am. Chem. Soc*. **1987**, *109*, 4775. (d) Collman, J. P.; Brauman, J. I.; Meunier, B.; Hayashi, T.; Kodadek, T.; Raybuck, S. K. *J. Am. Chem. Soc*. **1985**, *107*, 2000. (e) Sevin, A.; Fontecave, M. *J. Am. Chem. Soc*. **1986**, *108*, 3266.
36. (a) Koola, J. D.; Kochi, J. K. *J. Org. Chem*. **1987**, *52*, 4545. (b) Nam, W.; Kim, H. J.; Kim, S. H.; Ho, R. Y. N.; Valentine, J. S. *Inorg. Chem*. **1996**, *35*, 1045. (c) Lim, S. Y.; Kang, M.; Kim, J.; Lee, I.-M. *Bull. Korean Chem. Soc*. **2005**, *26*, 887.
37. (a) Mas-Balleste, R.; Que, L., Jr. *J. Am. Chem. Soc*. **2007**, *129*, 15964. (b) Ostović, D.; Bruice, T. C. *Acc. Chem. Res*. **1992**, *25*, 314. (c) Stephenson, N. A.; Bell, A. T. *J. Am. Chem. Soc*. **2005**, *127*, 8635. (d) Traylor, T. G.; Miksztal, A. R. *J. Am. Chem. Soc*. **1989**, *111*, 7443. (e) Green, M. T. *J. Am. Chem. Soc*. **1999**, *121*, 7939. (f) Harris, D. L.; Loew, G. H. *J. Am. Chem. Soc*. **1998**, *120*, 8941. (g) Antony, J.; Grodzicki, M.; Trautwein, A. X. *J. Phys. chem. A* **1997**, *101*, 2692. (h) Ogliaro, F.; Harris, N.; Cohen, S.; Filatov, M.; de Visser, S. P.; Shaik, S. J. *Angew. chem. Int. Ed*. **2000**, *39*, 3855.
38. (a) Poulos, T. L.; Finzel, B. C.; Howard, A. J. *J. Mol. Bio*. **1987**, *195*, 687. (b) Sligar, S. G.; Cinti, D. L.; Gibson, G. G.; Schankman, J. B. *Biochem. Biophy. Res. Commun.* **1979**, *90*, 925. (c) Ortiz de Montellano, P. R. *Cytochrom P-450: Structure, Mechanism, and Biochemistry* **2005**, New York: Kluwer (3rd Ed.).
39. (a) Tabushi, I.; Yazaki, A. *J. Am. Chem. Soc*. **1981**, *103*, 7371. (b) Mansuy, D.; Fontecave, M.; Bartoli, J.-F. *J. Chem. Soc., Chem. Commun*. **1983**, *6*, 253. (c) Battioni, P.; Bartoli, J. F.; Leduc, P.; Fontecave, M.; Mansuy, D. *J. Chem. Soc., Chem. Commun*. **1987**, *791*. (d) Evans, S.; Smith, J. R. L. *J. Chem. Soc., Perkin Trans* **2000**, *2*, 1541. (e) Lyons, J. E.; Ellis, P. E.; Myers, H. K. *J. Catal*. **1995**, *155*, 59. (f) Che, C.-M.; Lo, V. K.-Y.; Zhou, C.-Y.; Huang, J.-S. *Chem. Soc. Rev*. **2011**,

40, 1950. (g) Ellis, P. E.; Lyons, J. E. *Coord. Chem. Rev*. **1990**, *105*, 181. (h) Grinstaff, M. W.; Hill, M. G.; Labinger, J. A.; Gray, H. B. *Science* **1994**, *264*, 1311.

40. (a) Leitgeb, S.; Nidetzky, B. *Biochem. Soc. Trans*. **2008**, *36*, 1180. (b) Abu-Omar, M. M.; Loaiza, A.; Hontzeas, N. *Chem. Rev*. **2005**, *105*, 2227. (c) de Visser, S.; Kumar, D. *Iron-containing enzymes versatile catalysts of hydroxylation reactions in nature, Royal Soc. Chem*. **2011**.
41. (a) Lee, Y.-M.; Hong, S.; Morimoto, Y.; Shin, W.; Fukuzumi, S.; Nam, W. *J. Am. Chem. Soc.* **2010**, *132*, 10668. (b) He, Y.; Goldsmith, C. R. *Chem. Commun*. **2012**, *48*, 10532. (c) Sheet, D.; Paine, T. K. *Chem. Sci.* **2016**, *7*, 5322. (d) Sahu, S.; Goldberg, D. P. *J. Am. Chem. Soc.* **2016**, *138*, 11410. (e) Kim, S. O.; Sastri, C. V.; Seo, M. S.; Kim, J.; Nam, W. *J. Am. Chem. Soc.* **2005**, *127*, 4178. (f) Momenteau, M.; Reed, C. A. *Chem. Rev*. **1994**, *94*, 659. (g) Kitajima, N.; Tamura, N.; Amagai, H.; Fukui, H.; Moro-oka, Y.; Mizutani, Y.; Kitagawa, T.; Mathur, R.; Heerwegh, K.; Reed, C. A.; Randall, C. R.; Que, L., Jr.; Tatsumi, K. *J. Am. Chem. Soc.* **1994**, *116*, 9071. (h) Ookubo, T.; Sugimoto, H.; Nagayama, T.; Masuda, H.; Sato, T.; Tanaka, K.; Maeda, Y.; Okawa, H.; Hayashi, Y.; Uehara, A.; Suzuki, M. *J. Am. Chem. Soc*. **1996**, *118*, 701. (i) Dong, Y.; Yan, S.; Young, V. G., Jr.; Que, L., Jr. *Angew. Chem. Int. Ed. Engl.* **1996**, *35*, 618. (j) Thibon, A.; England, J.; Martinho, M.; Young, V. G., Jr.; Frisch, J. R.; Guillot, R.; Girerd, J.-J.; Münck, E.; Que, L., Jr.; Banse, F. *Angew. Chem. Int. Ed.* **2008**, *47*, 7064. (k) Nam, W. *Acc. Chem. Res*. **2015**, *48*, 2415. (l) Chatterjee, S.; Paine, T. K. *Angew. Chem. Int. Ed.* **2015**, *54*, 9338.
42. Groves, J. T.; Watanabe, Y. *J. Am. Chem. Soc*. **1986**, *108*, 7834.
43. Panda, C.; Ghosh, M.; Panda, T.; Banerjee, R.; Sen Gupta, S. *Chem. Comm.* **2011**, *47*, 8016.
44. (a) Fruetel, J. A.; Collins, J. R.; Camper, D. L.; Loew, G. H.; Ortiz de Montellano, P. R. *J. Am. Chem. Soc*. **1992**, *114*, 6987. (b) Vaz, A. D. N.; McGinnity, D. F.; Coon, M. J. *Proc. Natl. Acad. Sci. USA*. **1998**, *95*, 3555. (c) Kumar, D.; de Visser, S. P.; Shaik, S. *Chem. Eur. J*. **2005**, *11*, 2825. (d) Groves, J. T.; Myers, R. S. *J. Am. Chem. Soc*. **1983**, *105*, 5791. (e) Song, W. J.; Ryu, Y. O.; Song, R.; Nam, W. *J. Biol. Inorg. Chem*. **2005**, *10*, 294. (f) Fusii, H. *Coord. Chem. Rev*. **2002**, *226*, 51.
45. Grapperhaus, C. A.; Mienert, B.; Bill, E.; Weyhermu¨ller, T.; Wieghardt, K. *Inorg. Chem.* **2000**, *39*, 5306.

46. Rohde, J.-U.; In, J.-H.; Lim, M. H.; Brennessel, W. W.; Bukowski, M. R.; Stubna, A.; Nam, W.; Que, L., Jr. *Science* **2003**, *299*, 1037.
47. Lim, M. H.; Rohde, J.-U.; Stubna, A.; Bukowski, M. R.; Costas, M.; Ho, R. Y. N.; Munck, E.; Nam, W.; Que, L., Jr. *Proc. Natl. Acad. Sci. USA* **2003** , *100*, 3665.
48. Fukuzumi, S.; Morimoto, Y.; Kotani, H.; Naumov, P. e.; Lee, Y.-M.; Nam, W. *Nat. Chem.* **2010**, *2*, 756.
49. Que, L. *Acc. Chem. Res.* **2007**, *40*, 493.
50. (a) Moelands, M. A. H.; Nijsse, S.; Folkertsma, E.; de Bruin, B.; Lutz, M.; Spek, A. L.; Klein-Gebbink, R. J. M. *Inorg. Chem*. **2013**, *52*, 7394. (b) Tiwa, T.; Nakada, M. *J. Am. Chem. Soc*. **2012**, *134*, 13538. (c) Feng, Y.; England, J.; Que, L., Jr. *Acs. Catal*. **2011**, *1*, 1035. (d) Krebs, C.; Fujimori, D. G.; Wals, C. T.; Bollinger, J. M. *Acc. Chem. Res*. **2007**, *40*, 484.
51. Prat, I.; Mathieson, J. S.; Güell, M.; Ribas, X.; Luis, J. M.; Cronin, L.; Costas, M. *Nat. Chem.* **2011**, *3*, 788.
52. Zhang, R.; Newcomb, M. *Nat. chem.* **2011**, *3*, 761.
53. Collins, T. J.; Ryabov, A. D. *Chem. Rev*. **2017**, DOI: 10.1021/acs.chemrev.7b00034.
54. de Oliveira, F. T.; Chanda, A.; Banerjee, D.; Shan, X.; Mondal, S.; Que, L., Jr.; Bominaar, E. L.; Münck, E.; Collins, T. J. *Science* **2007**, *315*, 835.
55. Ghosh, M.; Singh, K. K.; Panda, C.; Weitz, A.; Hendrich, M. P.; Collins, T. J.; Dhar, B. B.; Sen Gupta, S. *J. Am. Chem. Soc.* **2014**, *136*, 9524.
56. (a) Ghosh, M.; Nikhil, Y. L. K.; Dhar, B. B.; Sen Gupta, S. *Inorg. Chem.* **2015,** *54*, 11792. (b) Panda, C.; Debgupta, J.; Díaz, D. D.; Singh, K. K.; Sen Gupta, S.; Dhar, B. B. *J. Am. Chem. Soc.* **2014,** *136*, 12273.
57. Singh, K. K.; Tiwari, M. k.; Ghosh, M.; Panda, C.; Weitz, A.; Hendrich, M. P.; Dhar, B. B.; Vanka, K.; Sen Gupta, S. *Inorg. Chem.* **2015**, *54*, 1535.
58. Singh, K. K.; Tiwari, M. k.; Dhar, B. B.; Vanka, K.; Sen Gupta, S. *Inorg. Chem*. **2015**, *54*, 6112.
59. Singh, K. K.; Sen Gupta, S. *Chem. Commun*. **2017**, *53*, 5914.

Chapter II

Tuning the Reactivity of $Fe^{V}(O)$ towards C-H Bonds at Room Temperature: Effect of Water

2.1 Abstract

The presence of a $Fe^{V}(O)$ species has been postulated as the active intermediate for the oxidation of both C-H and C=C bonds in the Rieske dioxygenase family of enzymes. Understanding the reactivity of these high valent iron-oxo intermediates, especially in an aqueous medium, would provide a better understanding of these enzymatic reaction mechanisms. The formation of an $Fe^{V}(O)$ complex at room temperature in an aqueous-CH_3CN mixture that contains up to 90% water using NaOCl as the oxidant is reported here. The stability of $Fe^{V}(O)$ decreases with increasing water concentration. We show that the reactivity of $Fe^{V}(O)$ toward the oxidation of C-H bonds, such as those in toluene, can be tuned by varying the amount of water in the H_2O/CH_3CN mixture. Rate acceleration of up to 60 times is observed for the oxidation of toluene upon increasing the water concentration. The role of water in accelerating the rate of the reaction has been studied using kinetic measurements, isotope labeling experiments, and density functional theory (DFT) calculations. A kinetic isotope effect of ~13 was observed for the oxidation of toluene and d_8-toluene showing that C-H abstraction was involved in the rate-determining step. Activation parameters determined by using Eyring plots for toluene oxidation in H_2O/CH_3CN mixtures showed a gain in enthalpy with a concomitant loss in entropy. This points to the formation of a more-ordered transition state involving water molecules. To further understand the role of water, we performed a careful DFT study, concentrating mostly on the rate-determining hydrogen abstraction step. The DFT-optimized structure of the starting $Fe^{V}(O)$ and the transition state indicates that the rate enhancement is due to the transition state's favored stabilization over the reactant due to enhanced hydrogen bonding with water.

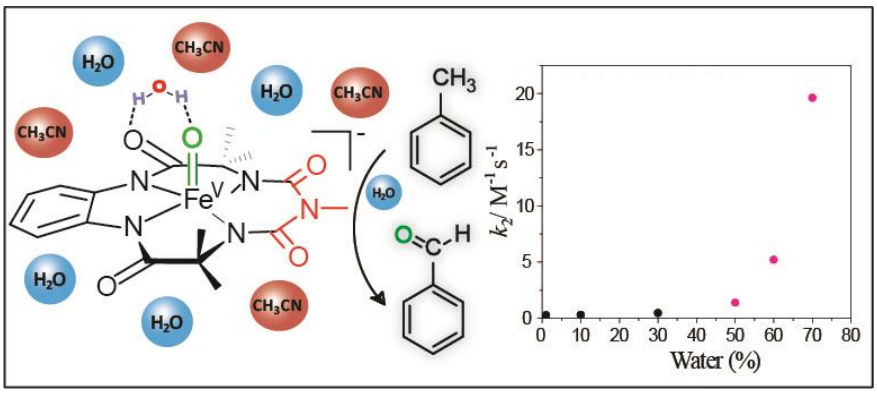

2.2 Introduction

Metalloenzymes use oxidants like O_2 and H_2O_2 to catalyze oxidation reactions that exhibit exquisite substrate specificity and selectivity and operate under mild conditions through inherently "green" processes.[1] Examples of such catalysts include cytochrome P450 and peroxidases enzymes that use an iron(IV)-oxo porphyrin radical cation (Cpd I) intermediate to catalyze the oxidation of various organic substrates, which are of vital importance for regulating drug metabolism, detoxification and biosynthesis.[2] Based on numerous experimental observations, such as stereo chemical scrambling, kinetic isotope effect as well as theoretical studies, rebound mechanism hypothesis has been proposed for the C-H bond hydroxylation reaction.[1-3] Shaik and others have proposed a two state reactivity for hydroxylation by Cpd I, where two different spin states, doublet (S=1/2) and quartet (S=3/2) displayed parallel but different barrier for H-atom abstraction step. Subsequently, the intermediate forms alcohol product by rebound in a barrier-free manner through doublet surface, while the quartet surface showed certain barrier to cross. Hydrogen atom abstraction from substrate RH is the rate determining step, in which reactant complex is connected to a hydroxo intermediate radical species by a transition structure. Subsequently, C-O bond formation takes place *via* a second transition state where quartet surface has significant barrier, but a negligible barrier has been observed through doublet surface.[4] These study of Cpd I and model complexes has been limited with bare Fe-oxo moiety[5] without taking into account of medium polarization and specific interaction with the amino acid group and water molecule of protein pocket. Theoretical and experimental studies showed that the proximal NH-S hydrogen bond affects the monooxygenase activity whereas the hydrogen bond in distal pocket stabilizes the Fe-Oxo moiety of Cpd I in chloro-peroxidase.[6] Another specific interaction of Cpd I with water has been demonstrated in $CytP450_{StaP}$ during the conversion of the chromopyrrolic acid to an antitumor derivative compound (Scheme 2.1).[7] A FeO-HOH bond (hydrogen bond) exists and plays an important role during the reaction towards the substrate.[8] Also, the detail theoretical study on $P450_{cam}$ described the role of crystal water molecule that is liberated during the conversion of Cpd 0 to Cpd I and act as a catalyst for hydrogen abstraction by forming hydrogen bond with the 'O' of Fe-oxo reactive intermediate.[9] As a consequence of hydrogen bonding, barrier for the transition state of hydrogen atom abstraction from the substrate (camphor) lowers down by 4-6 kcal mol^{-1}.

Scheme 2.1. The complex of $CytP450_{StaP}$ Cpd I with chromopyrolic acid.

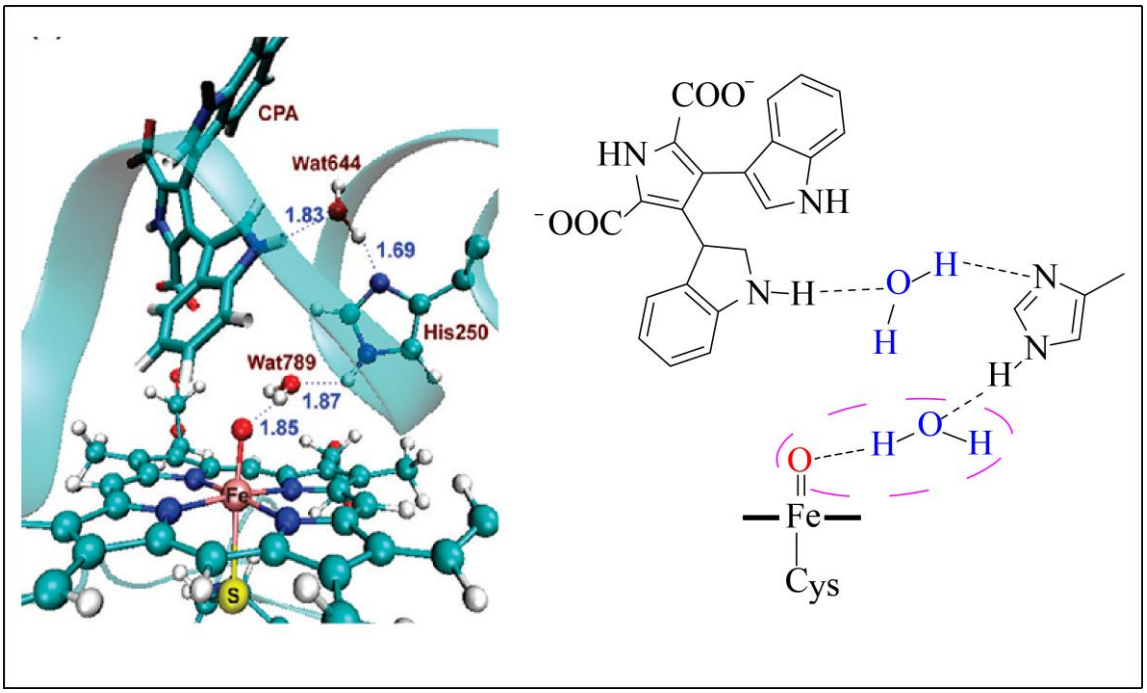

Because the iron monooxygenase reactions occur in water,[2(d)] it is important to understand the effect of water on the rate of reaction for the oxidation of C-H bonds by Fe-oxo. Water has been shown to play a critical role during oxidation of organic substrates in heme-containing enzymes such as cytochrome P450.[10] Although several models of $Fe^{IV}(O)$ intermediates have been synthesized, and their reactivity for oxidizing C-H bonds has been studied in detail[11] but very few studies have explored the synthesis and characterization of $Fe^{V}(O)$,[12] which is isoelectronic of $Fe^{IV}(O)$(porphyrin-radical-cation), due to a lack of their stability.[13] However, a study on the role of water during the reaction of Fe(O) towards oxidation of C-H bonds is rare. The availability of an $Fe^{V}(O)$ complex, that is both stable and reactive at ambient to physiological temperatures and study of role of solvent as a bulk medium as well as explicit role of water molecule would have the potential advance insight into enzymatic oxidation processes, especially oxidations of the C–H bonds of unactivated alkanes which are among the most difficult of all oxidation processes to carry out in a controlled fashion.

Recently, we reported for the first time the quantitative formation of a well-defined $Fe^{V}(O)$ complex at room temperature using biuret-modified Fe-TAML[14] and *m*CPBA in CH_3CN.[15] $Fe^{V}(O)$ was characterized by UV-vis, X-band electron paramagnetic resonance

(EPR), Mössbauer, and high-resolution mass spectrometry (HR-MS). It has also been shown to catalyze the oxidation of C-H bonds with the abstraction of the hydrogen atom being the rate-determining step. The formation of $Fe^{IV}(O)$ by Fe-TAML in water has been previously reported.[16] In this chapter, we verify the stability of $Fe^{V}(O)$ in H_2O/CH_3CN mixtures containing up to 90% water. The effect of water on the reactivity of $Fe^{V}(O)$ during C-H activation has also been studied both experimentally and theoretically. We also report that the rate of oxidation of toluene with $Fe^{V}(O)$ in an H_2O/CH_3CN mixture is enhanced up to 60-fold, likely attributable to preferential stabilization of the transition state during C-H abstraction due to hydrogen bonding with water molecules.

Scheme 2.2. Formation of $Fe^{V}(O)$ species in H_2O/CH_3CN mixture and its reaction towards toluene.

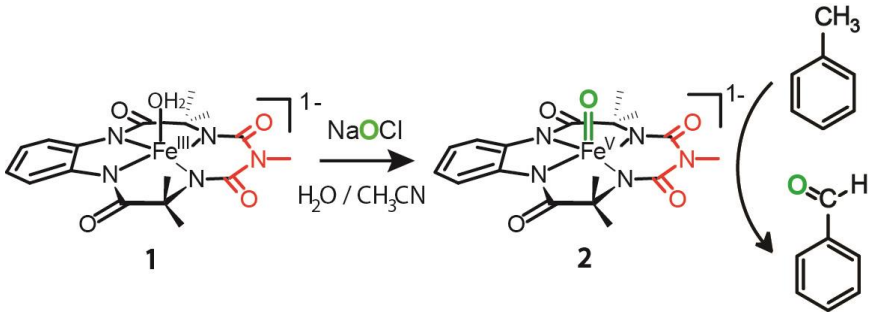

2.3 Experimental section

2.3.1 Materials

Biuret-amide-modified Fe-TAML (**1**) was synthesized as we have previously reported.[14] $^{57}FeCl_2$ was purchased from Trace Sciences International Corporation (Canada). Aqueous sodium hypochlorite (reagent grade, Aldrich, available chlorine 4.00 - 4.99 %) was used as received and quantified by iodiometry. Acetonitrile (HPLC grade, Aldrich) was used after passing through an activated neutral alumina column. D_2O (99.9 atom % D) was used as received (Aldrich). ^{18}O-enriched water (98%) was procured from the Shanghai Research Institute of Chemical Industry (China). Deionized water was used to make all of the stock solutions for the reaction and kinetic runs. Toluene (Aldrich, 99.8 %) was passed through activated neutral alumina and distilled prior to use. All reactions were carried out without any special precautions under atmospheric conditions unless otherwise specified.

2.3.2 General Instrumentation

X-band EPR spectra were recorded on a Bruker 300 spectrometer equipped with an Oxford ESR-910 liquid helium cryostat. For both instruments, the microwave frequency was calibrated with a frequency counter and the magnetic field with an NMR gaussmeter. Mössbauer spectra were recorded with two spectrometers using a Janis Research Super Vari-Temp Dewar. UV-vis spectral studies were carried out using an Agilent diode array 8453 spectrophotometer with an attached electrically controlled thermostat. Gas chromatography (GC) was performed on a PerkinElmer Arnel Clarus 500 instrument equipped with a hydrogen flame ionization detector; BP20 columns (polar) (12 m × 0.53 mm × 1 μm) were used helium as the carrier gas at a flow rate of 1 ml min^{-1}. GC-MS was performed on an Agilent 5977A mass selective detector interfaced with an Agilent 7890B gas chromatograph using an HP-5ms capillary column (30 m × 0.32 mm × 0.25 μm, J & W Scientific). HR-MS was performed in a Thermo Scientific Q-Exactive Orbitrap analyzer using an electronspray ionization source connected with a C18 column (150 m × 4.6 mm × 8 μm).

EPR Spectroscopy

The sample for EPR analysis was prepared by adding 10 μL of 40 mM NaOCl to 190 μL of 2 mM biuret-modified Fe-TAML (**1**) in an ice bath; the spectrum was taken at 21 K. The signal was quantified relative to a Cu-EDTA spin standard. A modulation frequency of 100 kHz was used for the EPR spectra. The EPR simulation software (*SpinCount*) was written by one of the authors.[17] The software diagonalizes the spin Hamiltonian (eq i), where **S** is the total spin of the complex (unless explicitly stated otherwise), and the parameters have the usual definitions. The quantitative simulation was a least-square fit of the experimental spectra generated with consideration for the intensity factor, which allows for the computation of simulated spectra at a specified sample concentration.

$$\boldsymbol{H}=\boldsymbol{\beta e}\mathbf{B}.\mathbf{g}.\mathbf{S}+\mathbf{S}.\mathbf{D}.\mathbf{S}+\mathbf{S}.\mathbf{A}.\mathbf{I} \quad \text{(i)}$$

Mössbauer Spectroscopy

^{57}Fe-enriched **1** was prepared following the procedure used for the synthesis of **1**; in this case, $^{57}FeCl_3$ was used in place of $^{56}FeCl_2$ (70% yield). The corresponding ^{57}Fe-enriched **2** (2 mM) was quantitatively prepared by reacting **1** with 2 equiv of NaOCl in an ice bath; spectra were recorded at 4.2 K. The isomer shift was reported relative to the Fe metal. Simulation of the Mössbauer spectra was calculated with least squares fitting using the program *SpinCount* and the standard spin Hamiltonian (eq ii).

$$\boldsymbol{H = \beta_e \mathbf{B}.\mathbf{g}.\mathbf{S} + \mathbf{S}.\mathbf{D}.\mathbf{S} + \mathbf{S}.\mathbf{A}.\mathbf{I} - g_n b_n \mathbf{B}.\mathbf{I} + \frac{eQV_{zz}}{12}[3I_z^2 - I(I+1) + \eta(I_x^2 - I_y^2)]} \quad \text{(ii)}$$

2.3.3 Preparation of $Fe^{V}(O)$ (2) in Different H_2O/CH_3CN Mixtures

NaOCl (1.1 equiv) was added to a 1×10^{-4} M solution of biuret-modified Fe-TAML (**1**) in different H_2O/CH_3CN mixtures (10, 30, 50, 70, and 90% water); and UV-vis spectra of $Fe^{V}(O)$ (**2**) were recorded at 25 °C.

2.3.4 Stability of $Fe^{V}(O)$ (2) in Different H_2O/CH_3CN Mixtures

The rate constant ($k_{5/4,3}$) (Table 1) for the spontaneous reduction of Fe^{V} to Fe^{IV}/Fe^{III} in H_2O/CH_3CN mixtures at 25 °C was measured by the initial rate approach. The quantitative formation of Fe^{V} was carried out by adding 1.1 equiv of NaOCl in solution to **1**. The rate of spontaneous reduction of Fe^{V} to Fe^{IV}/Fe^{III} was monitored by measuring the decrease in absorbance at 613 nm (λ_{max} for Fe^{V}). Linear correlation of the initial rate against [Fe^{V}] was found, which indicated the first-order dependency on Fe^{V} (i.e. rate = $k_{5/4,3}$[Fe^{V}]).

2.3.5 Reactivity of $Fe^{V}(O)$ (2) toward Toluene Oxidation

Kinetics were monitored in either kinetic mode or scanning spectral kinetics mode of the spectrophotometer using a 1.0 cm quartz cell at 375 nm (the isosbestic points of Fe^{IV} and Fe^{III} species) at 25.0 °C (Figure 2.1).[18] All of the kinetic experiments were carried out in H_2O/CH_3CN mixtures where the percentage of water present varied as required per experiment. During kinetic measurements, the concentration of the $Fe^{V}(O)$ complex (10^{-4} M) was kept constant while the substrate concentration was varied. A pseudo-first-order rate constant (k_{obs}) was calculated at the isosbestic wavelength by nonlinear curve fitting [$A_t = A_\alpha - (A_\alpha - A_o)e^{(-kobst)}$] and was in good agreement with the rate constant value (within

5% error). The resulting k_{obs} values correlated linearly with the substrate concentration to give the second-order rate constant k_2 (Table 2.1).

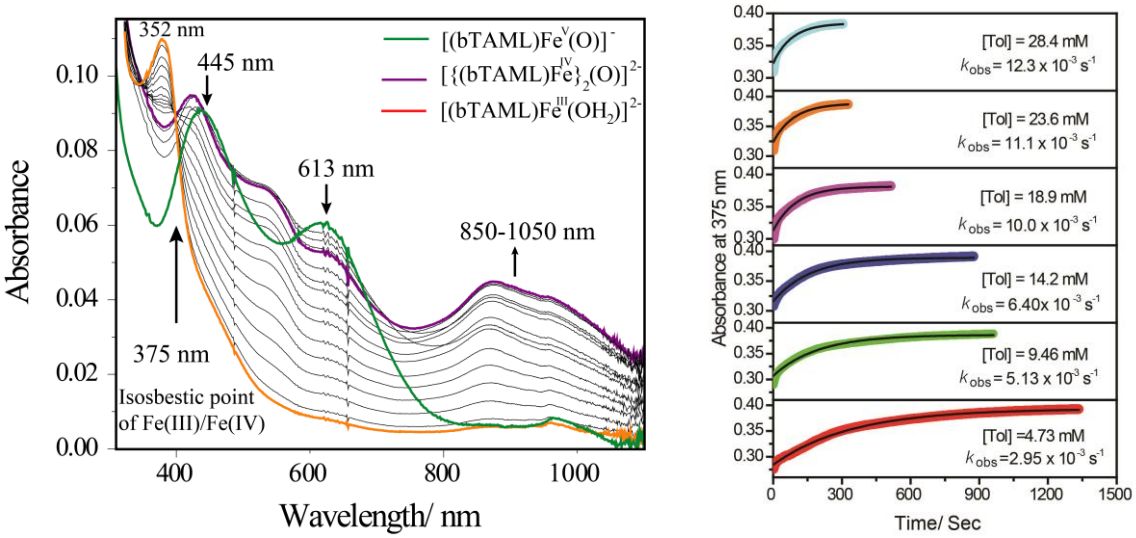

Figure 2.1. UV–vis spectral changes associated with the reaction of **2** with toluene to Fe^{IV} / Fe^{III} in 50% H_2O/CH_3CN mixture at 25 °C (in left). Kinetic traces for the reaction of **2** with toluene at various toluene concentrations in 30% H_2O/CH_3CN (in the right). The kinetic traces were fitted to the equation, $[(A_t = A_\alpha – (A_\alpha – A_o)e^{(-kobst)}]$ for obtaining k_{obs} values.

2.3.6 Product Quantification

Gas chromatography (GC) was used for product quantification. The excess substrate (100 μL, 1×10^{-1} M) was added to a freshly prepared 1 mL solution of **2** (generated by the reaction of **1** (1×10^{-4} M) and NaOCl (1.1×10^{-4} M)) at room temperature under an argon atmosphere. After completion of the reaction (determined by UV-vis spectroscopy), the internal standard bromobenzene was added, and the reaction mixture was immediately passed through an alumina column. Product (% yield) was quantified by GC using the calibration curve obtained with authentic benzaldehyde and bromobenzene.

2.3.7 Computational Methods

All of the minima and transition states reported in this study were fully optimized at the density functional theory (DFT) UB3LYP/6-31G*, LANL2DZ (Fe) level of theory[19] using the *Gaussian09* suite of quantum chemical programs.[20] The stationary points on the potential energy surface were characterized by evaluating the vibrational frequencies. The

transition states were characterized by a single imaginary frequency. The zero point vibrational energy corrections and thermal corrections were applied to the "bottom-of-the-well" values to obtain values for the Gibbs free energy at 298.15 K.

The experimental results suggest that the solvent plays a vital role in the rate-determining step, as the hydroxylation reaction of toluene by $[(bTAML)Fe^{V}(O)]^{-}$ is favored by increasing the polarity of the solvent. The electrostatic effect of the solvent dielectric on the reactive species was determined by full geometry optimizations at the UB3LYP/6-31G*, LANL2DZ (Fe) level of theory in the dielectric continuum of acetonitrile and water using the conductor-like polarizable continuum model (CPCM).[21] Charge stabilization through hydrogen-bonding interactions with explicitly added water molecules was studied by spotting the water-bound reactants, transition states, and intermediates in the gas phase for the rate-determining hydrogen abstraction step. This solvent model has recently been employed in several DFT studies.[22]

Recent literature suggests that improved treatment of hydrogen bond interactions could be achieved with the M06 functional.[23] Therefore, single point energies were calculated at the ROM062X/6-31G*, LANL2DZ (Fe) level of theory for the species involved in the rate-determining step (RDS) for UB3LYP-optimized structures. These energy values have better concurrence with the experimental findings. All of the values reported at the ROM062X/6-31G*, LANL2DZ (Fe) level of theory are single point energies. In order to fair comparison between UB3LYP and ROM062X energies, only the electronic energy values describing the effect of the solvent has been reported in this Article. All assessments on the role of the solvent are thus made on the basis of their relative electronic energy values.

All of the energies were calculated with respect to optimized structures with all of the reactants a finite distance from each other. This approach is purported to minimize errors in the computation of the translational entropy in determining the relative free energy values. Intermediates were optimized by keeping $Fe^{IV}(OH)$ and the toluene radical together in the relative vicinity of each other in one structure. The same strategy was employed for obtaining the optimized geometries of the final product. Such strategies have been employed in the recent past in other computational reports.[24]

2.4 Results and Discussion

2.4.1 Formation and Characterization of $[(bTAML)Fe^{V}(O)]^{-}$ complex in H_2O/CH_3CN Solvent Mixture

Water-soluble NaOCl (household bleach) was used as an oxidant for the formation of $Fe^{V}(O)$. NaOCl has been used as a co-oxidant for a variety of metal-catalyzed oxidation reactions, such as olefin epoxidation.[25] The addition of NaOCl to **1** showed the same UV-vis spectral features (Figure 2.2(A)) previously observed using *m*CPBA in organic media (with both 0.5 and 1.1 equiv of oxidant). The EPR and Mössbauer spectra (Figure 2.2 C and D, respectively) of this species determined by the addition of 1.1 equiv of NaOCl to **1** are similar to the spectra of the $Fe^{V}(O)$ species we reported previously.[15] The *g* tensors of the species observed in the X-band EPR spectra from our previous study were 1.983, 1.935, and 1.726 with *m*CPBA as the oxidant and are 1.977, 1.888, and 1.720 in the present work using NaOCl as the oxidant. Spin quantification of the observed signal indicated quantitative conversion of 1 to the $Fe^{V}(O)$ species. The Mössbauer spectra showed a single quadrupole doublet with an isomer shift of -0.45 mm/s and quadrupole splitting of 4.27 mm/s for the $Fe^{V}(O)$ species, which are within the error compared to the parameters of the species from *m*CPBA.[15]

We then proceeded to evaluate the formation of $Fe^{V}(O)$ in H_2O/CH_3CN mixtures through monitoring its characteristic spectra in UV-vis spectroscopy. It was observed that in H_2O/CH_3CN mixtures with 10, 30, 50, 70, and 90% water the spectral characteristics were identical to that of fully characterized $Fe^{V}(O)$ in acetonitrile medium (Figure 2.2 A and B). Formation of **2** in a 30:70 H_2O/CH_3CN mixture was also confirmed by HR-MS spectra (Figure 2.3). At 100% water the spectrum of $Fe^{V}(O)$ was not observed; instead, a violet species was observed whose UV-vis spectrum was similar to that of the µ-Oxo-Fe^{IV}dimer species.[15,18,26] The EPR spectrum of complex **2** in 50:50 H_2O/CH_3CN showed a species characteristic of the $S = ½$ species of $Fe^{V}(O)$.[27] The slight difference observed from the spectra in pure CH_3CN may be due to hydrogen bonding of water with the $Fe^{V}(O)$ complex, as has been proposed below.

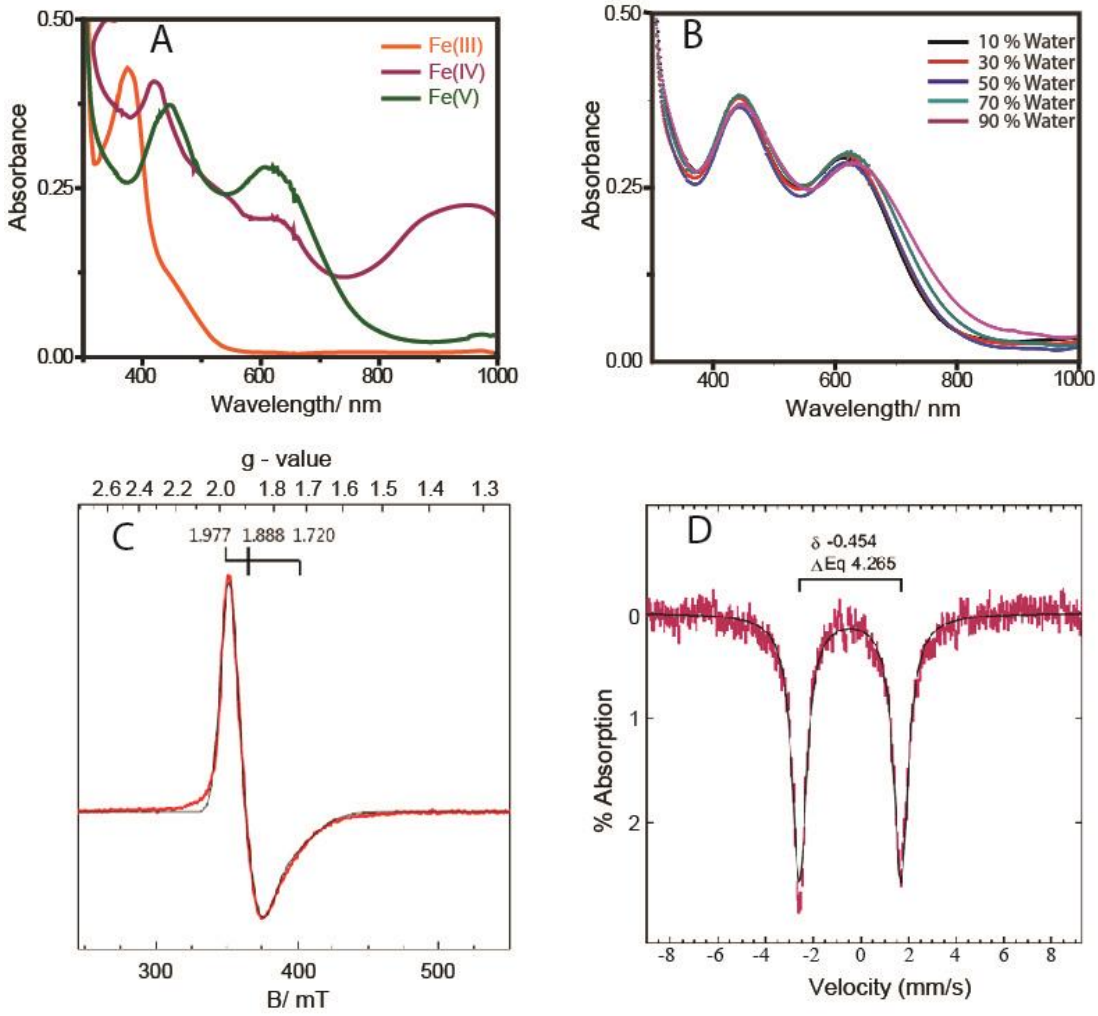

Figure 2.2. (A) UV−vis spectral changes of **1** (10^{-4} M) (orange) upon the addition of 0.5 equiv of NaOCl (5×10^{-5} M) in CH_3CN forming the μ-Oxo-Fe^{IV} dimer species (violet). The addition of another 0.5 equiv of NaOCl (5×10^{-5} M) to the preformed μ-Oxo-Fe^{IV}dimer species produces the spectrum of $Fe^{V}(O)$ (**2**, green). (B) UV-vis spectra of $Fe^{V}(O)$ in different H_2O/CH_3CN mixtures. (C) EPR spectra of $Fe^{V}(O)$ (**2**) in acetonitrile (2 mM) at 21 K. Black = experimental, red = simulated. (D) Mössbauer spectra of ^{57}Fe-enriched $[(bTAML)Fe^{V}(O)]^{-}$ (**2**) in acetonitrile (2 mM) at 4.2 K. The solid lines are spectral simulations.

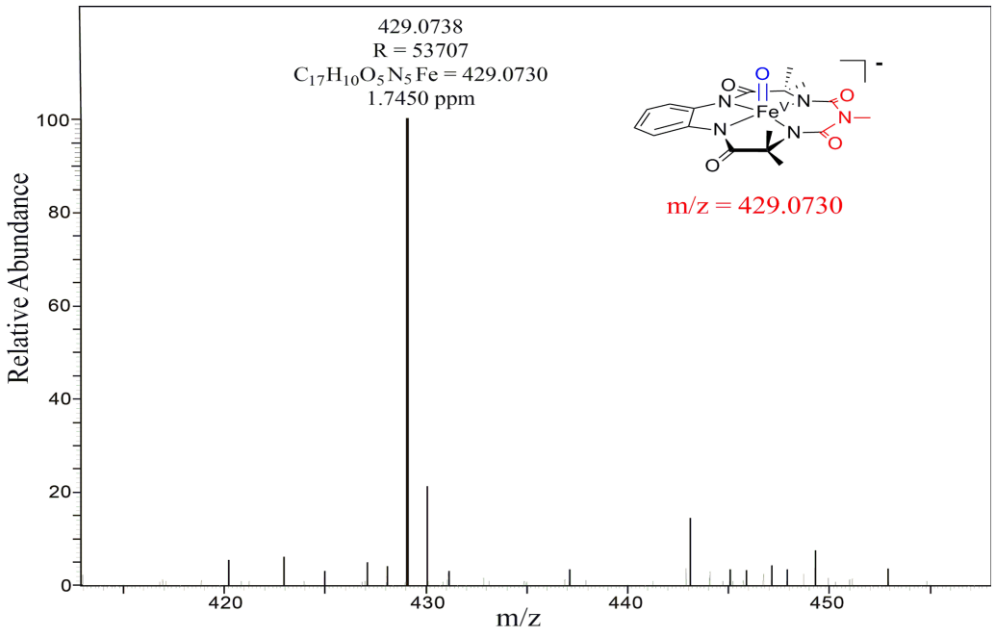

Figure 2.3. HR-MS of **2** in 30% H_2O/CH_3CN mixture. Calculated m/z of **2** is 429.0730.

2.4.2 Stability of $Fe^{V}(O)$ in Different H_2O/CH_3CN Mixtures

We then proceeded to evaluate the stability of the $Fe^{V}(O)$ complex as a function of increasing water concentration. The stability was measured by monitoring the spontaneous self-reduction of Fe^{V} to Fe^{IV}/Fe^{III} at room temperature using UV-vis spectroscopy at 613 nm (characteristic band of the $Fe^{V}(O)$ species). The initial rate of decay at 613 nm displayed the first-order dependency with respect to $Fe^{V}(O)$, and the first-order rate constant ($k_{5/4,3}$, s^{-1}) was determined from the slope of the fitted straight line (Figure 2.4(A), Table 2.1). It was observed that the stability of $Fe^{V}(O)$ decreased with increasing water concentration. At 90:10 H_2O/CH_3CN, the rate constant $k_{5/4,3}$ was 10-fold higher than that observed in 100% CH_3CN. This is likely due to the attack of water molecules on $Fe^{V}(O)$, as we have recently proposed while studying photochemical water oxidation using **1**.[27] However, the stability at 70:30 H_2O/CH_3CN was only 4 times lower than that in 100% CH_3CN, and the self-reduction was much slower than what we observed for toluene oxidation by $Fe^{V}(O)$ in 100% CH_3CN.[15] We, therefore, proceeded to evaluate the rate of toluene oxidation in H_2O/CH_3CN mixtures with the water concentration varied from <1 to 70% (Table 2.1).

Table 2.1. Stability and Reactivity of the $Fe^{V}(O)$ Intermediate for Toluene Oxidation in Various H_2O/CH_3CN mixtures

% of water in H_2O/CH_3CN mixture	stability ($k_{5/4,3}$/ s^{-1})	reactivity (k_2/ $M^{-1}s^{-1}$)	yield (% of benzaldehyde)
<1	2.4×10^{-5}	0.27	23
10	2.8×10^{-5}	0.31	21
30	3.1×10^{-5}	0.47	19
50	6.5×10^{-5}	1.4	20
60	7.6×10^{-5}	5.2	20
70	1.1×10^{-4}	19.6	20
90	3.2×10^{-4}	-	

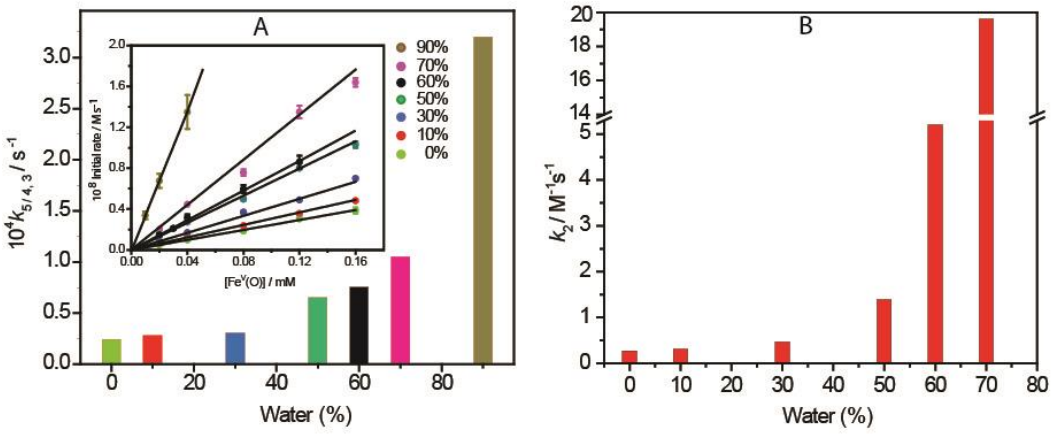

Figure 2.4. (A) First-order rate constant $k_{5/4,3}$ varies with water concentration. The inset shows initial rate *vs.* $[(bTAML)Fe^{V}(O)]^{-}$. (B) Second-order rate constant k_2 for toluene oxidation *vs.* the percentage of water content in the H_2O/CH_3CN mixture.

2.4.3 Reactivity of $Fe^{V}(O)$ in Different H_2O/CH_3CN Mixtures towards Toluene Oxidation

The ability of $Fe^{V}(O)$ to facilitate toluene oxidation was studied under pseudo-first-order conditions at the isosbestic points of Fe^{III} and Fe^{IV} interconversions (345 and 375 nm) at 25 °C, as has been shown before.[15] The reaction was studied for different H_2O/CH_3CN mixtures (10, 30, 50, 60, and 70% H_2O). The pseudo-first-order rate constant was determined by nonlinear curve fitting of the absorbance relative to time data using the equation $A_t = A_\alpha - (A_\alpha - A_o)e^{(-kobst)}$ and exhibited good agreement with rate constant values within ± 5% error. The k_{obs} correlated linearly with the toluene concentration (Figure 2.5) and the second-order rate constant k_2 ($M^{-1}s^{-1}$) was calculated from the slope of the straight line that passed through the origin. All the second order rate constant (k_2) values mentioned in this report are obtained by adopting the same methodology (Table 2.1, Figure 2.4(B)). At the end of the reaction, the parent Fe^{III} complex was quantitatively regenerated as was observed from the UV-vis spectra (peak at 356 nm; Figure 2.1(A)) and HR-MS (*m/z* = 413.0716; Appendix A1). After completion of the reaction, product identification was carried out by GC-MS (Figure 2.6) and HR-MS (Appendix A2). The results showed that benzaldehyde was formed, and the yield was quantified by GC to be 20-23% (theoretically, only 25% is expected because toluene oxidation to benzaldehyde is a four-electron process and 50% of $Fe^{V}(O)$ comproportionates with **1**). The UV-vis scanning kinetics study showed that the starting $Fe^{V}(O)$ species changed to the diamagnetic μ-Oxo-Fe^{IV}dimer species, which gradually regenerated parent Fe^{III} complex **1** (Figure 2.1(A)). In all of the different H_2O/CH_3CN composite mixtures (10 to 70%), the rate of toluene oxidation (k_{obs}) was much faster than the spontaneous reduction of $Fe^{V}(O)$. The variation in k_2 values indicated that the reactivity of $Fe^{V}(O)$ increased with water concentration. Initially, the rate enhancements were modest, but it increased significantly when the water concentration exceeded 50%. At 70% water k_2 was around 60-fold higher than that in 100% CH_3CN. Such an increase in the rate of oxidation of aromatic hydrocarbons by $Ru^{V}(O)$ has been previously reported by Meyer *et al.*.[28]

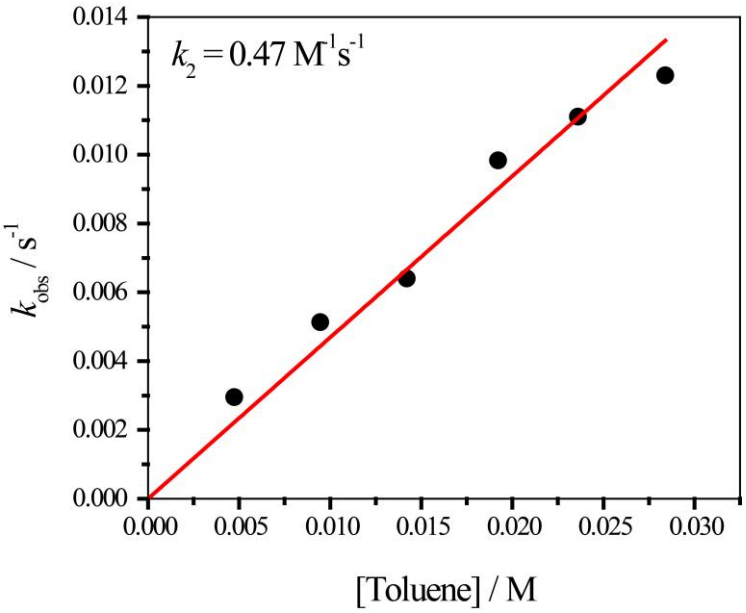

Figure 2.5. A Linear fit of toluene concentration [Toluene] against k_{obs} to determine second order rate constant (k_2).

2.4.4 Kinetic Isotope Effect (KIE) and Source of O-Atom (^{18}O-labelling) in Product Formation

The role of H_2O during C-H abstraction was then investigated. First, the direct role of water, such as its attack on the benzylic carbon of toluene to facilitate C-H bond cleavage, was investigated. Toluene oxidation was performed using a 50:50 $H_2{}^{18}O/CH_3CN$ mixture so that the direct attack of $H_2{}^{18}O$ on the benzylic carbon would lead to the exclusive formation of ^{18}O-benzaldehyde. However, the percentage of ^{18}O incorporation (calculated on the basis of the relative abundance of ^{16}O and ^{18}O in the product by GC-MS) was found to be only 20% (Figure 2.6). This ^{18}O incorporated product was likely the result of (a) exchange of $H_2{}^{18}O$ with product benzaldehyde via the formation of a gem-diol and (b) oxygen atom exchange between $Fe^{V}(O)$ (**2**) and $H_2{}^{18}O$ leading to the formation of some amounts of $Fe^{V}(^{18}O)$, which would lead to the incorporation of ^{18}O-benzaldehyde.[29] The absence of exclusive ^{18}O-benzaldehyde formation indicates that direct attack of water is unlikely. Next, the kinetics of C-H abstraction was studied in mixed H_2O/CH_3CN solvents to evaluate if they differed from the kinetics in pure CH_3CN that we have reported previously.[15] Kinetic isotope effects (KIE) of 13 and 9 for the oxidation of toluene/toluene-d_8 in 50:50 and 70:30 H_2O/CH_3CN (Figure 2.7), respectively, were observed. This value is similar to the value determined for pure CH_3CN (KIE of 9).[15] This observation suggests

that the rate-determining step in 50:50 H_2O/CH_3CN involves a C-H abstraction, as has been reported for pure CH_3CN.[15] Further, a similar rate enhancement was also observed with 2,3-dimethylbutane suggesting that this phenomenon was not limited to only toluene (Appendix A3). To further understand the role of water, the solvent kinetic isotope effect (SKIE) was evaluated with varying D_2O/CH_3CN mixtures as the solvent for toluene oxidation. A constant SKIE ($k_{H2O/CH3CN}/ k_{D2O/CH3CN}$) value of 1.4-1.5 was observed in 10, 30, 50, and 70% H_2O or D_2O (Table 2.2), indicating the likely involvement of hydrogen bonding in the transition state.

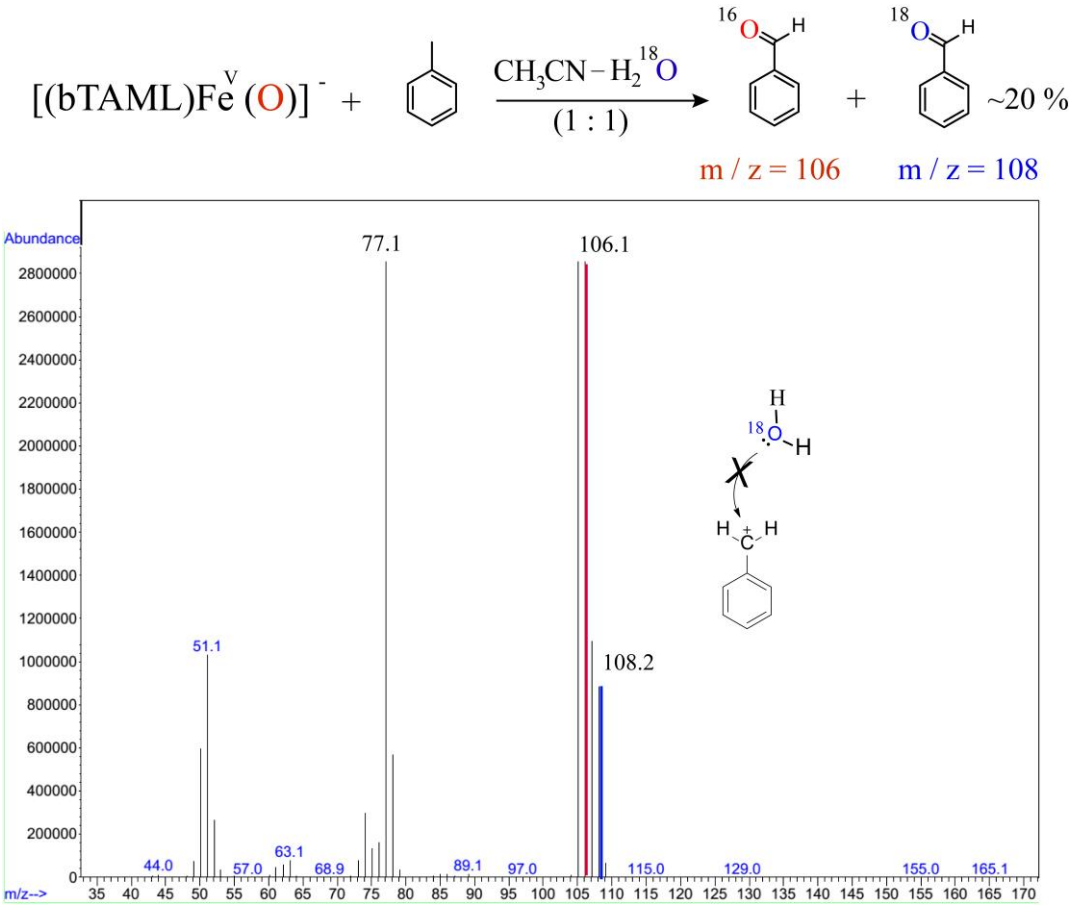

Figure 2.6. GC-MS trace for the product formed by reaction of **2** (10^{-4} M) with toluene (1000 equivalent) in 50% $H_2{}^{18}O/CH_3CN$ mixture.

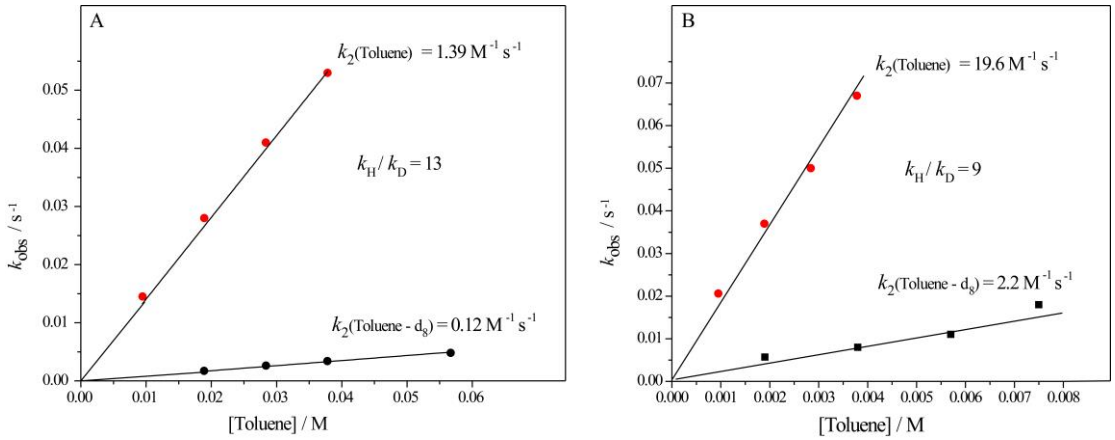

Figure 2.7. Plot of k_{obs} vs. [toluene] (red dots) and [d_8-toluene-] (black dots) showing pronounce KIE at 25 ^{o}C (A) in 50% H_2O/CH_3CN mixture; (B) in 70% H_2O/CH_3CN mixture.

Table 2.2. SKIE Value [$k_2(H_2O)$/ $k_2(D_2O)$] of $Fe^{V}(O)$ for Toluene Oxidation in Various Mixtures of H_2O and D_2O in CH_3CN

H_2O or D_2O (%)	k_2/ $M^{-1}s^{-1}$ (in H_2O)	k_2/ $M^{-1}s^{-1}$(in D_2O)	$k_2(H_2O)$/ $k_2(D_2O)$
10%	0.31	0.21	1.5
30%	0.47	0.33	1.4
50%	1.4	0.91	1.5
70%	19.6	14.0	1.4

2.4.5 Thermodynamic Parameters for Toluene Oxidation by $Fe^{V}(O)$

For a better understanding of the transition state, variable-temperature (283–300 K) kinetic measurements (Table 2.3(A)) were performed for toluene oxidation to determine the activation parameters (Table 2.3(B), Figure 2.8) on the basis of Eyring plots for the rate constants. According to the activation parameters for toluene oxidation in CH_3CN ($\Delta H^{\#}$ = 69.3 kJ mol^{-1}; $T\Delta S^{\#}$ = -7.6 kJ mol^{-1}; 300 K) and 70:30 H_2O/CH_3CN ($\Delta H^{\#}$ = 51.1 kJ mol^{-1}; $T\Delta S^{\#}$ = -14.7 kJ mol^{-1}; 300K), the 60-fold increase in the reaction rate is mainly controlled by the favorable activation enthalpy terms (a gain of 18 kJ mol^{-1} in $\Delta H^{\#}$). In contrast, the

contribution of the activation entropy terms (as loss of 7 kJ mol^{-1} in $\Delta S^{\#}$) to the transition states is negative upon the addition of water. Because the enthalpy gain is 3 times that of the entropic loss, a favorable $\Delta G^{\#}$ leads to rate acceleration upon the addition of water. The gain in enthalpy with a concomitant loss in entropy points to the formation of an ordered transition state involving water molecules. To more comprehensively understand the role of water in the reaction kinetics, we performed a careful density functional theory (DFT) study, concentrating mostly on the rate-determining hydrogen abstraction step.[30]

Table 2.3. (A) Rate constant (k_2) values for toluene oxidation in CH_3CN and in 70 % of H_2O/CH_3CN mixture at different temperature. (B) Thermodynamic parameters ($\Delta H^{\#}$, $\Delta S^{\#}$ & $\Delta G^{\#}$) values at 300 K for toluene oxidation in CH_3CN and in 70 % of H_2O/CH_3CN mixture in temperature range of 283-300 K.

A

Temperature (K)	k_2 (CH_3CN) ($M^{-1}s^{-1}$)	k_2 (70 % H_2O) ($M^{-1}s^{-1}$)
283	0.04	5.40
288	0.08	9.40
293	0.13	14.3
300	0.25	19.6

B

	$\Delta H^{\#}$ (kJ Mol^{-1})	$\Delta S^{\#}$ (J K^{-1})	$\Delta G^{\#}$ (kJ Mol^{-1})
CH_3CN (100 %)	69.3	-25.3	76.9
30 % CH_3CN - 70 % H_2O	51.1	-49.2	65.8

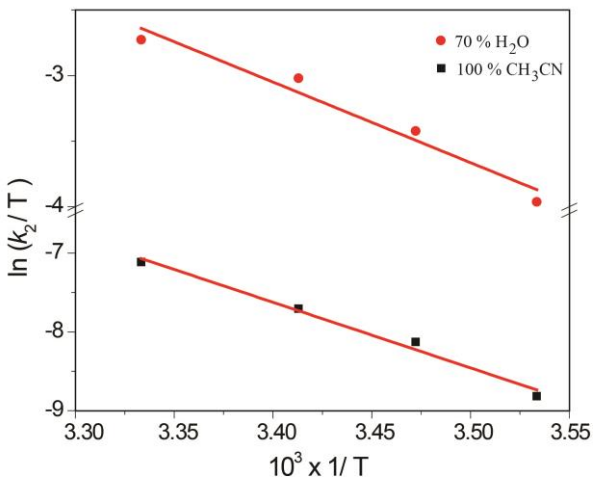

Figure 2.8. Plot of ln(k_2/ T) *vs.* 1/ T for toluene oxidation in 100 % CH_3CN and in 70:30 of H_2O/CH_3CN in the temperature range of 283–300 K.

2.4.6 Density Functional Theory (DFT) Studies for Toluene Hydroxylation by $Fe^{V}(O)$

All of the stationary points were fully optimized at the DFT-UB3LYP/6-31G*, LANL2DZ (Fe) level of theory.[19-21] The complete gas-phase energy profile clearly indicates that the intermediate with the quartet spin state is more stable than the doublet (Figure 2.9(A) and Table 2.4). This result is further confirmed by the separate optimization of the intermediate complex $[Fe^{IV}(OH)]^{-}$ in singlet and triplet spin states in both the gas phase and in an acetonitrile solvent. The triplet is stabilized by more than 15.0 kcal mol^{-1} compared to the singlet. The energy values are summarized in Table 2.5 of the supporting information. Because the reaction is favored by increasing the polarity (i.e., by increasing the relative concentration of water), we envisaged that water could affect the barrier through two separate mechanisms: by direct active participation in hydrogen abstraction (ruled out by the experimental kinetic isotope study) or by favored stabilization of the rate-determining transition state over that of the reactant.

Table 2.4. The relative gas phase reaction energies in kcal mol^{-1} at the UB3LYP/6-31G*, LANL2DZ (Fe) level of theory for toluene hydroxylation catalyzed by $Fe^{V}(O)$ (**2**).

	R	TS1	I	TS2	P
ΔE^{a}	0.0	17.2	4.1	11.2	-15.1
$\Delta(E+ZPE)^{a}$	0.0	13.1	1.9	9.5	-14.0
ΔG^{a}	0.0	15.2	1.9	11.8	-12.8
ΔE^{b}	0.0	32.8	1.3	4.1	-41.9
$\Delta(E+ZPE)^{b}$	0.0	28.8	-0.2	2.2	-39.7
ΔG^{b}	0.0	30.6	-1.4	2.0	-38.2
ΔE^{c}	0.0	17.2	4.3	7.1	-38.8
$\Delta(E+ZPE)^{c}$	0.0	13.1	2.0	4.3	-37.5
ΔG^{c}	0.0	15.2	0.1	3.5	-36.8

a. S = 1/2 spin state; b. S = 3/2 spin state; c. most favorable energy profile when the spin flip occurs at an intermediate state.

Table 2.5. The relative gas phase energies of the intermediate complex $Fe^{IV}(OH)$ in a singlet and triplet electronic states in kcal mol^{-1} at the UB3LYP/6-31G*, LANL2DZ (Fe) and ROM062X/6-31G*, LANL2DZ (Fe) level of theories. Values outside the parenthesis are in gas phase and inside the parenthesis are in solvent phase.

	ΔE (UB3LYP)	Δ(E+ZPE) (UB3LYP)	ΔG (UB3LYP)	ΔE (ROM062X)
S = 0	0.0 (0.0)	0.0 (0.0)	0.0 (0.0)	0.0 (0.0)
S = 1	-15.5 (-15.6)	-16.2 (-16.3)	-17.8 (-17.3)	-18.7 (-18.5)

Two possible means for the differential stabilization of the transition state and reactant RDS with increasing concentrations of water were investigated: (a) a bulk solvation effect (macrosolvation) through the solvent dielectric and (b) a solute-solvent interaction through hydrogen bonding interactions (micro solvation). Only a marginal decrease in the rate-determining barrier (RDB) was obtained by changing the dielectric of the medium (Table 2.6) from acetonitrile to pure water, which suggests that bulk solvation has a nominal effect on the rate enhancement with increasing water concentrations. On the other hand, micro solvation through the explicit consideration of one and two water molecules was found to be the primary reason for the decreased RDB (Figure 2.9(B) and Table 2.7). A clear decrease in the rate-determining barrier (by 9.3 kcal mol^{-1}) at the ROM062X level, which is known to provide better treatment of hydrogen bonds,[23] upon the inclusion of one explicit water molecule, and a further decrease of 2.8 kcal mol^{-1} upon inclusion of a second explicit water molecule corroborate the experimental findings.

Table 2.6. The relative reaction energies in kcal mol^{-1} for the rate determining step of toluene hydroxylation catalyzed by $Fe^{V}(O)$ (**2**) in dielectric continuum of acetonitrile and water at the CPCM/UB3LYP/6-31G*, LANL2DZ (Fe) and CPCM/ROM062X/6-31G*, LANL2DZ (Fe) level of theories.

	ΔE (UB3LYP)	Δ(E+ZPE) (UB3LYP)	ΔG (UB3LYP)	ΔE (ROM062X)
$^{2}R^{a}$	0.0	0.0	0.0	0.0
$^{2}TS1^{a}$	17.2	13.1	15.2	23.3

$^{4}I^{a}$	4.3	2.0	3.4	-5.3
$^{2}R^{b}$	0.0	0.0	0.0	0.0
$^{2}TS1^{b}$	13.8	9.9	11.7	18.7
$^{4}I^{b}$	1.1	-0.8	-0.9	-17.9
$^{2}R^{c}$	0.0	0.0	0.0	0.0
$^{2}TS1^{c}$	13.7	10.0	12.3	17.5
$^{4}I^{c}$	1.0	-0.9	-0.9	-18.0

a. gas phase; b. in the dielectric continuum of acetonitrile; c. in the dielectric continuum of water

Table 2.7. The relative gas phase reaction energies in kcal mol^{-1} for the rate determining step of toluene hydroxylation catalyzed by $Fe^{V}(O)$ (**2**) with explicitly added water molecules at the UB3LYP/6-31G*, LANL2DZ (Fe) and ROM062X/6-31G*, LANL2DZ (Fe) level of theories.

	ΔE (UB3LYP)	Δ(E+ZPE) (UB3LYP)	ΔG (UB3LYP)	ΔE (ROM062X)
$^{2}R^{a}$	0.0	0.0	0.0	0.0
$^{2}TS1^{a}$	17.2	13.1	15.2	23.3
$^{4}I^{a}$	4.3	2.0	3.4	-5.3
$^{2}R^{b}$	0.0	0.0	0.0	0.0
$^{2}TS1^{b}$	16.1	13.0	16.3	14.0
$^{4}I^{b}$	2.5	1.2	2.7	-21.9
$^{2}R^{c}$	0.0	0.0	0.0	0.0
$^{2}TS1^{c}$	15.4	12.6	15.1	11.2
$^{4}I^{c}$	0.9	0.1	0.2	-24.6

a. With no explicit water; b. with one explicit water; c. with two explicit water molecules

Our calculations show that water is capable of making a hydrogen bond with the oxo group of the $Fe^{V}(O)$ complex. At the same time, the $Fe^{V}(O)$ complex exhibits other hydrophilic hydrogen bonding interactive sites, as well those that can compete with the oxo group. However, the increasing concentration of water enhances the possibility of oxo-water interactions. It also increases the chance of having more water in the active site of the $Fe^{V}(O)$ complex. Careful examination of the water-bound reactant structures implies that the Fe-O bond length increases with an increase in the number of water molecules hydrogen bonded to the oxo group in the active site of $Fe^{V}(O)$ (**2**) (Table 2.8 and Appendix A4). An increase of 0.053 Å in the Fe-O bond length upon the inclusion of two explicit water molecules in the reactant structure suggests that the increasing concentration of water leads to a decrease in the Fe-O bond order of $Fe^{V}(O)$ (Table 2.8). This means that the bond dissociation energy of the Fe-O bond decreases. We also know that elongation of a chemical bond is associated with a decrease in the overlap of the involved orbitals, which usually causes weakening (and thus destabilization) of the chemical bond, and thus makes the bond (and eventually the molecule *via* that bond) more prone to dissociation upon chemical attack. On the other hand, we can see that the Fe-O bond is elongated upon consideration of explicit water molecules in the transition state structures as well. However, this elongation decreases upon the addition of additional explicit water molecules (0.12, 0.092, and 0.087 Å for zero, one, and two explicit water molecules, respectively, with respect to the corresponding reactants). The extent of elongation of the Fe-O bond in the transition state compared to that of the corresponding reactants can be directly correlated with the barrier according to the "extended activation strain model" proposed by Jong *et al*.[31] This model proposes that smaller deformation in the structure of the involved species results in less strain energy, which leads to a lower activation barrier. We should also note that the Fe-O bond in the equilibrium geometry of the reactant with two explicitly added water molecules is significantly longer than in the bare reactant, which causes the strain energy to increase to a lesser extent as this bond expands in the activated complex compared to that of the bare reactant without any explicit water included. Hence, the smaller difference between the transition state and reactant geometries, as well as the change that occurs when the Fe-O bond has been weakened significantly by solute-solvent interactions through hydrogen bonding upon the inclusion of explicit water molecules together leads to a smaller barrier and an enhanced rate of reaction. This indicates that the bond dissociation energy of the Fe-O bond should decrease. A theoretical study on a related $Fe^{III}(O)$ system by Borovik

et al. confirms that the bond dissociation energy of the Fe-O bond decreases upon the inclusion of hydrogen bonds from the solvent water.[32] Their study further supports the notion that the Fe-O bond length increases upon the inclusion of explicit water molecules. They have also shown that the increase in bond length is associated with a decrease in the percentage of the covalent character of the Fe-O bond. This suggests that the ionic character of the Fe-O bond in the transition state should be greater as the Fe-O bond becomes distended. This elongation is 0.12 Å in the structure without consideration of explicit water. The greater ionic character of the Fe-O bond explains the stronger hydrogen bonding with water in the transition state relative to that of the reactant.

Table 2.8. Fe-O distances (in Å) in water bound reactant, transition state and intermediate structures obtained by geometry optimization at the UB3LYP/6-31G*, LANL2DZ (Fe) level of theory.

	Gas phase	CH_3CN dielectric	Water dielectric	1 H_2O explicit	$2H_2O$ explicit	$3H_2O$ explicit
^{2}R	1.583	1.590	1.590	1.621	1.636	1.645
$^{2}TS1$	1.703	1.696	1.695	1.713	1.723	-
^{4}I	1.776	1.778	1.778	1.792	1.815	-

To understand the differential stabilization of water-bound reactants and transition states in more detail, we looked at the Mulliken population analysis[33] of all species involved in the RDS (Table 2.9). The oxo atom in Fe-O in the transition state having a greater negative charge than in the reactant indicates the possibility of a better electrostatic interaction (i.e. stronger hydrogen bond) with water in the transition state compared to that with the reactant. Consequently, the barrier decreases with an increasing number of hydrogen bonds, thereby providing an explanation for the effect of microsolvation on the activity of the $Fe^{V}(O)$ system.

Table 2.9. Mulliken population analysis of reactant, TS1 and intermediate with and without explicit water at UB3LYP/6-31gG*, LANL2DZ(Fe) level of theory.

		^{2}R	^{2}TS1	^{4}I
Without water	O_1	-0.42286	-0.54984	-0.71367
	Fe	0.767298	0.749967	0.766455
One explicit water	O_1	-0.50248	-0.67346	-0.74256
	Fe	0.724989	0.728948	0.771006
	H_1	0.463241	0.511496	0.45797
	O	-0.87027	-0.87519	-0.87547
	H	0.411398	0.41589	0.414554
Two explicit water	O_1	-0.559	-0.6607	-0.77745
	Fe	0.720593	0.760374	0.771028
	H_1	0.47157	0.464143	0.461174
	O	-0.85732	-0.87523	-0.86243
	H	0.400214	0.409659	0.416611
	H_1	0.478431	0.457258	0.459801
	O	-0.85603	-0.87664	-0.87335
	H	0.422106	0.414891	0.415717

O_1 : oxygen atom of Fe-O ; H_1 : Hydrogen atom of water molecule bonded with O_1 of Fe-O

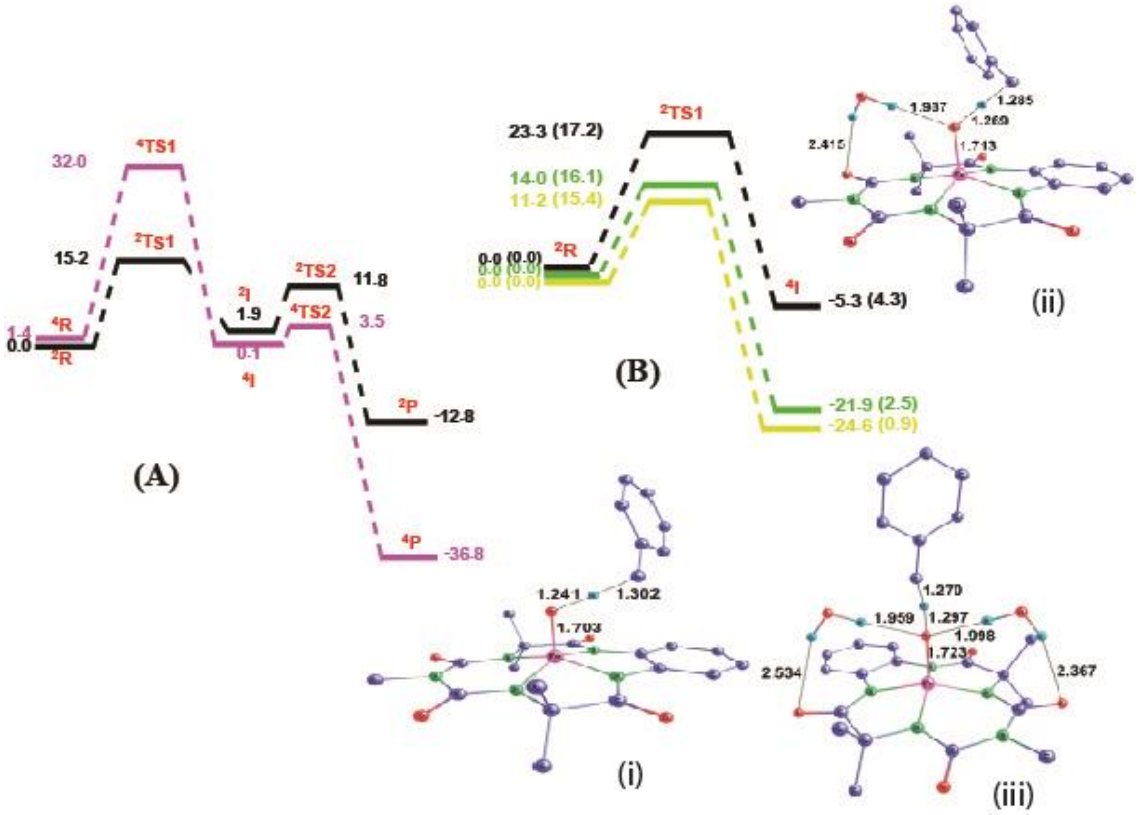

Figure 2.9. (A) Gas phase free energy profile for the hydroxylation of toluene by **2** at the UB3LYP/6-31G*, LANL2DZ (Fe) level of theory. Violet and black colors represent energy profiles at S = 3/2 and S = 1/2 spin states, respectively. All of the values are in kcal mol^{-1}; (B) Electronic energy profile for the rate-determining step of toluene hydroxylation catalyzed by **2**. All of the values correspond to gas-phase data. Values outside and inside the parentheses correspond to the ROM062X/6-31G*, LANL2DZ (Fe) and UB3LYP/6-31G*, LANL2DZ (Fe) levels of theory, respectively. Black, green, and yellow colors represent the energy profile with zero, one, and two explicitly added water molecules, respectively, (i, ii, and iii) UB3LYP optimized transition state structures for the hydrogen atom abstraction rate-determining step (RDS) with zero, one, and two explicitly added water molecules, respectively. Hydrogen atoms not involved in the reaction coordinate are removed for clarity. All of the values are in kcal mol^{-1}. All the atom-atom distances are in Å.

2.5 Conclusion

In summary, we have demonstrated for the first time the formation of a $Fe^{V}(O)$ complex in H_2O/CH_3CN mixtures. This complex was synthesized by the reaction of biuret-modified Fe-TAML (**1**) and NaOCl in H_2O/CH_3CN mixtures with up to 90% water. The stability of the $Fe^{V}(O)$ complex decreases with increasing water content. This complex is reasonably stable, allowing for studies on the rate of oxidation of C-H bonds. We show that for toluene oxidation in 70:30 H_2O/CH_3CN mixtures, the rate of toluene oxidation increases 60-fold. The increase in activity for $Fe^{V}(O)$ upon the addition of water is due to the preferential stabilization of the transition state by water during the C-H abstraction process. We believe that this study will help to elucidate the role of water molecules in the active site of Fe-based enzymes.

2.6 References

1. Costas, M.; Mehn, M. P.; Jensen, M. P.; Que, L. *Chem. Rev.* **2004**, *104*, 939. (b) Que, L.; Tolman, W. B. *Nature* **2008**, *455*, 333.
2. (a) Meunier, B.; de Visser, S. P.; Shaik, S. *Chem. Rev.* **2004**, *104*, 3947. (b) Ortiz de Montellano, P. R. *Chem. Rev.* **2009**, *110*, 932. (c) Rittle, J.; Green, M. T. *Science*. **2010**, *330*, 933. (e) Groves, J. T. *J. Inorg. Biochem*. **2006**, *100*, 434. (f) Guengerich, F. P. *Chem. Res. Toxicol*. **2008**, *21*, 70. (g) Shaik, S.; Kumar, D.; de Visser, S. P.; Altun, A.; Thiel, W. *Chem. Rev*. **2005**, *105*, 2279. (h) Denisov, I. G.; Makris, T. M.; Sligar, S. G.; Schlichting, I. *Chem. Rev*. **2005**, *105*, 2253.
3. (a) Gelb, M. H.; Heimbrook, D. C.; Malkonen, P.; Sligar, S. G. *Biochemistry* **1982**, *21*, 370. (b) Hjelmeland, L. M.; Aronow, L.; Trudell *J. Biochem. Biophys. Res. Commun*. **1977**, *76*, 541. (c) Groves, J. T.; McClusky, G. A. *J. Am. Chem. Soc*. **1976**, *98*, 859.
4. (a) Schöneboom, J. C.; Cohen, S.; Lin, H.; Shaik, S.; Thiel, W. *J. Am. Chem. Soc*. **2004**, *126*, 4017. (b) Ogliaro, F.; Harris, N.; Cohen, S.; Filatov, M.; de Visser, S. P.; Shaik, S. *J. Am. Chem. Soc*. **2000**, *122*, 8977. (c) Shaik, S.; Cohen, S.; de Visser, S. P.; Sharma, P. K.; Kumar, D.; Kozuch, S.; Ogliaro, F.; Danovich, D. *Eur. J. Inorg. Chem*. **2004**, *35*, 207.
5. (a) Green, M. T. *J. Am. Chem. Soc*. **1999**, *121*, 7939. (b) Harris, D. L.; Loew, G. H. *J. Am. Chem. Soc*. **1998**, *120*, 8941. (c) Antony, J.; Grodzicki, M.; Trautwein, A. X.

J. Phys. chem. A **1997**, *101*, 2692. (d) Ogliaro, F.; Harris, N.; Cohen, S.; Filatov, M.; de Visser, S. P.; Shaik, S. *J. Angew. chem. Int. Ed*. **2000**, *39*, 3855.

6. (a) Poulos, T. L. *J. Bioinorg. Chem*. **1996**, *1*, 356. (b) Sigman, J. A.; Pond, A. E.; Dawson, J. H.; Lu, Y. *Biochemistry* **1999**, *38*, 11122. (c) Suzuki, N.; Higuchi, T.; Urano, Y.; Kikuchi, K.; Uekusa, H.; Ohashi, Y.; Uchida, T.; Kitagawa, T.; Nagano, T. *J. Am. Chem. Soc*. **1999**, *121*, 11571. (d) Weiss, R.; Mandon, D.; Wolter, T.; Trautwein, A. X.; M_ther, M.; Bill, E.; Gold, A.; Jayaraj, K.; Terner, J. *J. Bioinorg. Chem*. **1996**, *1*, 377.
7. (a) Wang, Y.; Chen, H.; Makino, M.; Shiro, Y.; Nagano, S.; Asamizu, S.; Onaka, H.; Shaik, S. *J. Am. Chem. Soc*. **2009**, *131*, 6748. (b) Wang, Y.; Hirao, H.; Chen, H.; Onaka, H.; Nagano, S.; Shaik, S. *J. Am. Chem. Soc*. **2008**, *130*, 7170.
8. (a) Schlichting, I.; Berendzen, J.; Chu, K.; Stock, A. M.; Maves, S. A.; Benson, D. A.; Sweet, R. M.; Ringe, D.; Petsko, G. A.; Sligar, S. G. *Science* **2000**, *287*, 1615. (b) Sono, M.; Roach, M. P.; Coulter, E. D.; Dawson, J. H. *Chem. Rev*. **1996**, *96*, 2841. (c) Groves, J. T.; Hang, Y.-Z. In *Cytochrome P450, Structure, Mechanisms and Biochemistry*, 2nd ed.
9. (a) Ogliaro, F.; Cohen, S.; de Visser, S. P.; Shaik, S. *J. Am. Chem. Soc*. **2000**, *122*, 12892. (b) Altun, A.; Guallar, V.; Friesner, R. A.; Shaik, S.; Thiel, W. *J. Am. Chem. Soc*. **2006**, *128*, 3924. (c) Altun, A.; Shaik, S.; Thiel, W. *J. Comput. Chem*. **2006**, *27*, 1324.
10. Wang, Y.; Chen, H.; Makino, M.; Shiro, Y.; Nagano, S.; Asamizu, S.; Onaka, H.; Shaik, S. *J. Am. Chem. Soc*. **2009**, *131*, 6748.
11. (a) McDonald, A. R.; Que, L. *Coord. Chem. Rev.* **2013**, *257*, 414. (b) Nam, W.; Lee, Y.-M.; Fukuzumi, S. *Acc. Chem. Res.* **2014**, *47*, 1146. (c) Fukuzumi, S.; Morimoto, Y.; Kotani, H.; Naumov, P.; Lee, Y.-M.; Nam, W. *Nat. Chem.* **2010**, *2*, 756. (d) Que, L. *Acc. Chem. Res*. **2007**, *40*, 493. (e) Rohde, J.-U.; In, J.-H.; Lim, M. H.; Brennessel, W. W.; Bukowski, M. R.; Stubna, A.; Münck, E.; Nam W.; Que, L. *Science* **2003**, *299*, 1037. (f) Kaizer, J.; Klinker, E. J.; Oh, N. Y.; Rohde, J.-U.; Song, W. J.; Stubna, A.; Kim, J.; Münck, E.; Nam W.; Que, L. *J. Am. Chem. Soc.* **2003**, *126*, 472.
12. (a) de Oliveira, F. T.; Chanda, A.; Banerjee, D.; Shan, X.; Mondal, S.; Que, L.; Bominaar, E. L.; Münck E.; Collins, T. J. *Science* **2007**, *315*, 835. (b) Lyakin, O. Y.; Bryliakov, K. P.; Britovsek G. J. P.; Talsi, E. P. *J. Am. Chem. Soc.* **2009**, *131*,

10798. (c) McDonald, A. R.; Que, L. *Nat. Chem.* **2011**, *3*, 761. (d) Prat, I.; Mathieson, J. S.; Güell, M.; Ribas, X.; Luis, J. M.; Cronin L.; Costas, M. *Nat. Chem.* **2011**, *3*, 788.

13. (a) Chakrabarty, S.; Austin, R. N.; Deng, D.; Groves J. T.; Lipscomb, J. D. *J. Am. Chem. Soc.* **2007**, *129*, 3514. (b) Ferraro, D. J.; Gakhar L.; Ramaswamy, S. *Biochem. Biophys. Res. Commun.* **2005**, *338*, 175. (c) Krebs, C.; GalonicÌ Fujimori, D.; Walsh C. T.; Bollinger, J. M. *Acc. Chem. Res.* **2007**, *40*, 484. (d) Xue, G.; Wang, D.; De Hont, R.; Fiedler, A. T.; Shan, X.; Münck E.; Que, L. *Proc. Natl. Acad. Sci. U.S.A.* **2007**, *104*, 20713.
14. Panda, C.; Ghosh, M.; Panda, T.; Banerjee R.; Sen Gupta, S. *Chem. Commun.* **2011**, *47*, 8016.
15. Ghosh, M.; Singh, K. K.; Panda, C.; Weitz, A.; Hendrich, M. P.; Collins, T. J.; Dhar, B. B.; Sen Gupta, S. *J. Am. Chem. Soc.* **2014**, *136*, 9524.
16. Chanda, A.; Shan, X.; Chakrabarti, M.; Ellis, W. C.; Popescu, D. L.; Tiago de Oliveira, F.; Wang, D.; Que, L.; Collins, T. J.; Münck E.; Bominaar, E. L. *Inorg. Chem.* **2008**, *47*, 3669.
17. Golombek, A. P.; Hendrich, M. P. *J. Magn. Reson.* **2003**, *165*, 33.
18. Kundu, S.; Thompson, J. V. K.; Ryabov, A. D.; Collins, T. J. *J. Am. Chem. Soc.* **2011**, *133*, 18546.
19. (a) Perdew, J. P.; Chevary, S. H.; Vosko, K. A.; Jackson, K. A.; Pederson, M. R.; Singh, D. J.; Fiolhais, C. *Phys. Rev. B* **1992**, *46*, 6671. (b) Perdew, J. P.; Chevary, S. H.; Vosko, K.A.; Jackson, K. A.; Pederson, M. R.; Singh, D. J.; Fiolhais, C. *Phys. Rev. B* **1993**, *48*, 4978. (c) Perdew, J. P.; Burke, K.; Wang, Y. *Phys. Rev. B* **1996**, *54*, 16533. (d) Adamo, C.; Barone, V. *J. Chem. Phys.* **1998**, *108*, 664. (e) Becke, A. D. *J. Chem. Phys.* **1993**, *98*, 5648. (f) Lee, C.; Yang, W.; Parr, R. G. *Phys. Rev. B* **1988**, *37*, 785. (g) Roothan, C. C. J. *Rev. Mod. Phy.* **1960**, *36*, 179. (h) McWeeny R.; Dierksen, G. *J. Chem. Phys.* **1968**, *49*, 4852. (i) Pople, J. A.; Nesbet, R. K. *J. Chem. Phys.* **1954**, *22*, 571.
20. Frisch, M. J.; Trucks, G. W.; Schlegel, H. B.; Scuseria, G. E.; Robb, M. A.; Cheeseman, J. R.; Scalmani, G.; Barone, V.; Mennucci, B.; Petersson, G. A.; Nakatsuji, H.; Caricato, M.; Li, X.; Hratchian, H. P.; Izmaylov, A. F.; Bloino, J.; Zheng, G.; Sonnenberg, J. L.; Hada, M.; Ehara, M.; Toyota, K.; Fukuda, R.; Hasegawa, J.; Ishida, M.; Nakajima, T.; Honda, Y.; Kitao, O.; Nakai, H.; Vreven,

T.; Montgomery, J. A. Jr.; Peralta, J. E.; Ogliaro, F.; Bearpark, M.; Heyd, J. J.; Brothers, E.; Kudin, K. N.; Staroverov, V. N.; Kobayashi, R.; Normand, J.; Raghavachari, K.; Rendell, A.; Burant, J. C.; Iyengar, S. S.; Tomasi, J.; Cossi, M.; Rega, N.; Millam, J. M.; Klene, M.; Knox, J. E.; Cross, J. B.; Bakken, V.; Adamo, C.; Jaramillo, J.; Gomperts, R.; Stratmann, R. E.; Yazyev, O.; Austin, A. J.; Cammi, R.; Pomelli, C.; Ochterski, J. W.; Martin, R. L.; Morokuma, K.; Zakrzewski, V. G.; Voth, G. A.; Salvador, P.; Dannenberg, J. J.; Dapprich, S.; Daniels, A. D.; Farkas, Ö.; Foresman, J. B.; Ortiz, J. V.; Cioslowski, J.; Fox, D. J. Gaussian 09, revision B.01; Gaussian, Inc.: Wallingford, CT, **2009**.

21. (a) Barone, V.; Cossi, M. *J. Phys. Chem. A* **1998**, *102*, 1995. (b) Cossi, M.; Rega, N.; Scalmani, G.; Barone, V. *J. Comp. Chem.* **2003**, *24*, 669.
22. (a) Kong, S.; Evanseck, J. D. *J. Am. Chem. Soc*. **2000**, *122*, 10418. (b) Di Valentin, C.; Freccero, M.; Zanaletti, R.; Sarzi-Amad, M. *J. Am. Chem. Soc*. **2001**, *123*, 8366. (c) Chandrasekhar, J.; Shariffskul, S.; Jorgensen, W. L. *J. Phys. Chem. B* **2002**, *106*, 8087. (d) Domingo, L. R.; Andrés, J. *J. Org. Chem*. **2003**, *68*, 8662. (e) Freccero, M.; Di Valentin,C.; Sarzi-Amad, M. *J. Am. Chem. Soc*. **2003**, *125*, 3544. (f) Mujika,J. I.; Mercero, J. M.; Lopez, X. *J. Am. Chem. Soc*. **2005**, *127*, 4445. (g) Saettel, N. J.; Wiest, O. *Tetrahedron* **2006**, *62*, 6490 (h) Gordillo, R.; Dudding,T.; Anderson,C. D.; Houk, K. N. *Org. Lett*. **2007**, *9*, 501. (i) Shi, F.-Q.; Li, X.; Xia, Y.; Zhang, L.; Yu, Z.-X. *J. Am. Chem. Soc*. **2007**, *129*, 15503. (j) Patil, M. P.; Sunoj, R. B. *Chem. Eur. J*. **2008**, *14*, 10472.
23. (a) Zhao, Y.; Truhlar, D. G. *Theor. Chem. Acc.* **2008**, *120*, 215. (b) Zhao, Y.; Truhlar, D. G. *J. Phys. Chem. A* **2006**, *110*, 13126. (c) Zhao, Y.; Truhlar, D. G. *J. Chem. Phys.* **2006**, *125*, 194101.
24. (a) Kelly, E.; Seth, M.; Ziegler, T. *J. Phys. Chem. A* **2004**, *108*, 2167. (b) Yin, H.; Wang, D.; Valiev, M. *J. Phys. Chem. A* **2011**, *115*, 12047. (c) Williams, V. M.; Kong, J. R.; Ko, B. J.; Mantri, Y.; Brodbelt, J. S.; Baik, M.-H.; Krische, M. J. *J. Am. Chem. Soc.* **2009**, *131*, 16054. (d) Janse van Rensburg, W.; Grové, C. Steynberg, J. P.; Stark, K. B.; Huyser, J. J.; Steynberg, P. J. *Organometallics* **2004**, *23*, 1207. (e) Qi, Y.; Dong, Q.; Zhong, L.; Liu, Z.; Qiu, P.; Cheng, R.; He, X.; Vanderbilt, J.; Liu, B. *Organometallics* **2010**, *29*, 1588. (f) Bagno, A.; Kantlehner, W.; Kress, R.; Saielli, G.; Stoyanov, E. *J. Org. Chem.* **2006**, *71*, 9331. (g) Li, J.-N.; Pu, M.; Ma,

C.-C.; Tian, Y.; He, J.; Evans, D. G. *J. Mol. Catal. A* **2012**, *359*, 14. (h) Kumawat, J.; Gupta, V. K.; Vanka, K. *Eur. J. Inog. Chem*. **2014**, *29*, 5063.

25. (a) Meunier, B.; Guilmet, E.; De Carvalho, M. E.; Poilblanc, R. *J. Am. Chem. Soc.* **1984**, *106*, 6668. (b) Yoon, H.; Burrows, C. J. *J. Am. Chem. Soc.* **1988**, *110*, 4087.
26. Ghosh, A.; Tiago de Oliveira, F.; Yano, T.; Nishioka, T.; Beach, E. S.; Kinoshita, I.; Münck, E.; Ryabov, A. D.; Horwitz, C. P.; Collins, T. J. *J. Am. Chem. Soc*. **2005**, *127*, 2505.
27. Panda, C.; Debgupta, J.; Diaz Diaz, D.; Singh, K. K.; Sen Gupta S.; Dhar, B. B. *J. Am. Chem. Soc.* **2014**, *136*, 12273.
28. Thompson, M. S.; Meyer, T. J. *J. Am. Chem. Soc*. **1982**, *104*, 5070.
29. Seo, M. S.; In, J-H.; Kim, S. O.; Oh, N. Y.; Kim, J. H. J.; Que, L.; Nam, W. *Angew. Chem., Int. Ed.* **2004**, *43*, 2417.
30. Shaik, S.; Hirao, H.; Kumar, D. *Acc Chem. Res.* **2007**, *40*, 532.
31. Jong, G. T. de and Bickelhaupt, F. M. *Chem. Phys. Chem.* **2007**, *8*, 1170-1181.
32. Dey, A.; Hocking, R. K.; Larsen, P.; Borovik, A. S.; Hodgson, K. O.; Hedman, B.; Solomon, E. I. *J. Am. Chem. Soc*. **2006**, *128*, 9825.
33. Mulliken, R. S., *J. Chem. Phys.* **1955**, *23*, 1833.

Chapter III

On the Mechanism of Oxygen Atom Transfer from $Fe^{V}(O)$ to Olefins at Room Temperature

3.1 Abstract

In biological oxidations, the intermediate $Fe^{V}(O)(OH)$ has been proposed to be the active species for catalyzing the epoxidation of alkenes by non-heme iron complexes. However, no study has been reported yet that elucidates the mechanism of direct O-atom transfer during the reaction of $Fe^{V}(O)$ with alkenes to form the corresponding epoxide. For the first time, we study the mechanism of O-atom transfer to alkenes using the $Fe^{V}(O)$ complex of biuret-modified Fe-TAML at room temperature. The second-order rate constant (k_2) for the reaction of different alkenes with $Fe^{V}(O)$ was determined under single turnover conditions. An 8000-fold rate difference was found between electron-rich (4-methoxystyrene; k_2 = 216 $M^{-1}s^{-1}$) and electron-deficient (Methyl *trans*-cinnamate; k_2 = 0.03 $M^{-1}s^{-1}$) substrates. This rate difference indicates the electrophilic character of $Fe^{V}(O)$. The use of *cis*-stilbene as a mechanistic probe leads to the formation of both *cis*- and *trans*-stilbene epoxides (73:27). This suggests the formation of a radical intermediate, which would allow C-C bond rotation to yield both stereoisomers of stilbene-epoxide. Additionally, a Hammett ρ value of –0.56 was obtained for the *para*-substituted styrene derivatives. Detailed DFT calculations show that the reaction proceeds via a two-step process through a doublet spin surface. Finally, using biuret-modified Fe-TAML as the catalyst and NaOCl as the oxidant under catalytic conditions epoxide was formed with modest yields and turnover numbers.

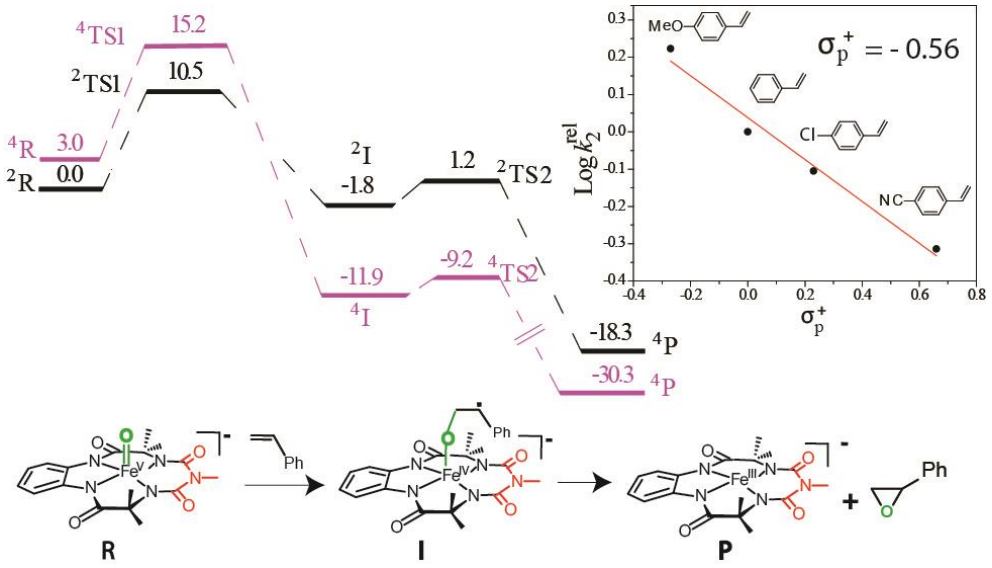

3.2 Introduction

The development of a biomimetic oxidation catalyst containing cheap, readily available, and nontoxic metals like Fe is being keenly pursued, but the development of Fe-based complexes that catalyze epoxidation of olefins with high selectivity using inexpensive and environmentally friendly terminal oxidants[1] remains a challenge. The key to such development lies in understanding the mechanism of biological and biomimetic oxidations, especially in identifying metal-based high valent iron-oxo intermediates and in mapping their reactivity with target substrates.[2] In biological systems, Fe-containing heme and non-heme centers have both been shown to catalyze epoxidation reaction. For heme-containing cytochrome P450, the well-established $Fe^{IV}(O)$-porphyrin$^{\cdot+}$ is the active oxidant.[3] Mechanistic exploration of the reactivity of alkenes with synthetic porphyrin complexes suggests the intermediacy of metallaoxetane (I), π-radical cation (II), carbocation (III), a carbon radical (IV), and oxene (V) species. A number of factors, such as oxidation potential of the alkene and the active oxidant, the steric and electronic structure of the reactants, and propensity of various substrates to undergo rearrangements, have been anticipated for the formation of such intermediates (I-V, Scheme 3.1(A)). The stereochemistry of the epoxide product, as well as analysis of other rearranged products, have been proven as a guiding tool to propose compounds I-V as reactive intermediates (Scheme 3.1(A)) for epoxidation with metal-oxo complexes. Theoretical investigations have also been performed to elucidate the epoxidation mechanism involving $Fe^{IV}(O)$-porphyrin-radical cation (Cpd I). A multistate reactivity has been proposed where different spin states (doublet, quartet, etc.) give different product distribution pattern. For instance, the calculation for the reaction of Cpd I with styrene showed state dependent product formation (Scheme 3.1(B)), as described below. (a) The low spin (doublet) pathway supports concerted oxene insertion mechanism with predominant epoxide product formation. (b) Reaction that proceeds through high spin (quartet) surface showed a finite barrier for ring-closure which gives a sufficiently long lifetime to undergo rearrangement leading to the formation of side products. However, in the case of the low barrier which is comparable to C-C bond rotation barrier, loss of stereochemistry in the epoxide product (*cis*-stilbene resulted in a mixture of *cis* and *trans*-epoxide) can be observed. (c) The high-spin pathway, where ring closure barrier is very high, can result in suicidal inactivation as well as aldehyde product formation.

Scheme 3.1. (A) Different type of Intermediates Suggested for the Reaction of Cpd I and Olefins, (B) Representative Example for Possible Product Distribution Pattern during the Reaction of Cpd I and Olefins (Theoretical Investigation for Spin State Dependency).

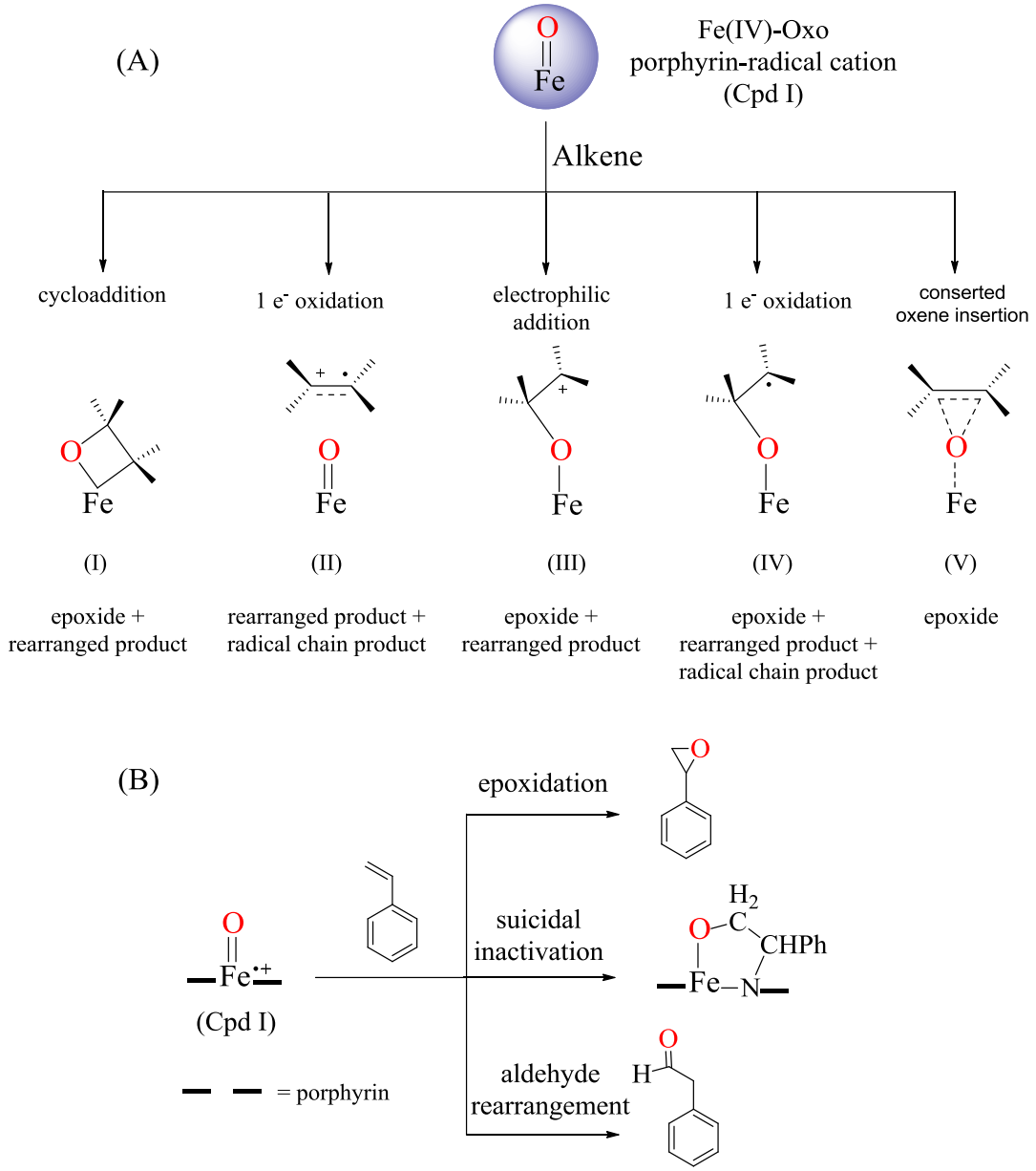

In non-heme enzymes, the reactive intermediate $Fe^{V}(O)(OH)$ has been proposed to catalyze both the epoxidation and the *cis*-dihydroxylation reaction.[4] These have been shown to be two closely related transformations in olefins oxidation by non-heme iron catalysts using H_2O_2 as the oxidant, and the product outcome can be controlled by addition of additives such as acetic acid (Scheme 3.2).[5] In contrast, the related $Fe^{IV}(O)$ has been shown

to be weakly active in catalyzing epoxidation reactions.[5c] Several non-heme Fe-based complexes catalyze the epoxidation (and related *cis*-dihydroxylation reaction) and can be divided into Class A catalysts, such as $[Fe(TPA)(OTf)_2]$, which preferentially carry out epoxidation of electron-rich olefins, and Class B catalysts, such as $[Fe(6\text{-}Me_3\text{-}TPA)(OTf)_2]$, which selectively perform epoxidation of electron-poor olefins like acrylate and fumarate more rapidly than electron-rich olefins.[6] The $Fe^{V}(O)$ intermediate has been proposed to be the active oxidant for Class A catalysts. In 2009, Talsi *et al.*[7a] reported the probable involvement of $Fe^{V}(O)$ during epoxidation by a non-heme iron catalyst at -70 °C by only EPR measurements (the amount was estimated to be around 15%). The epoxidation rate was estimated by the decay of this S=1/2 species in EPR measurements. However, no direct experiments have been reported yet that characterize the reactivity of $Fe^{V}(O)$ intermediate with olefins with varying electronic and steric properties. Given that epoxidation is a synthetically useful and mechanistically important process, such studies would shed light on the reactivity of non-heme iron complexes that catalyze epoxidation reaction.

Scheme 3.2. Proposed Mechanism for Oxidation of Olefins by Non-heme Iron Catalyst.

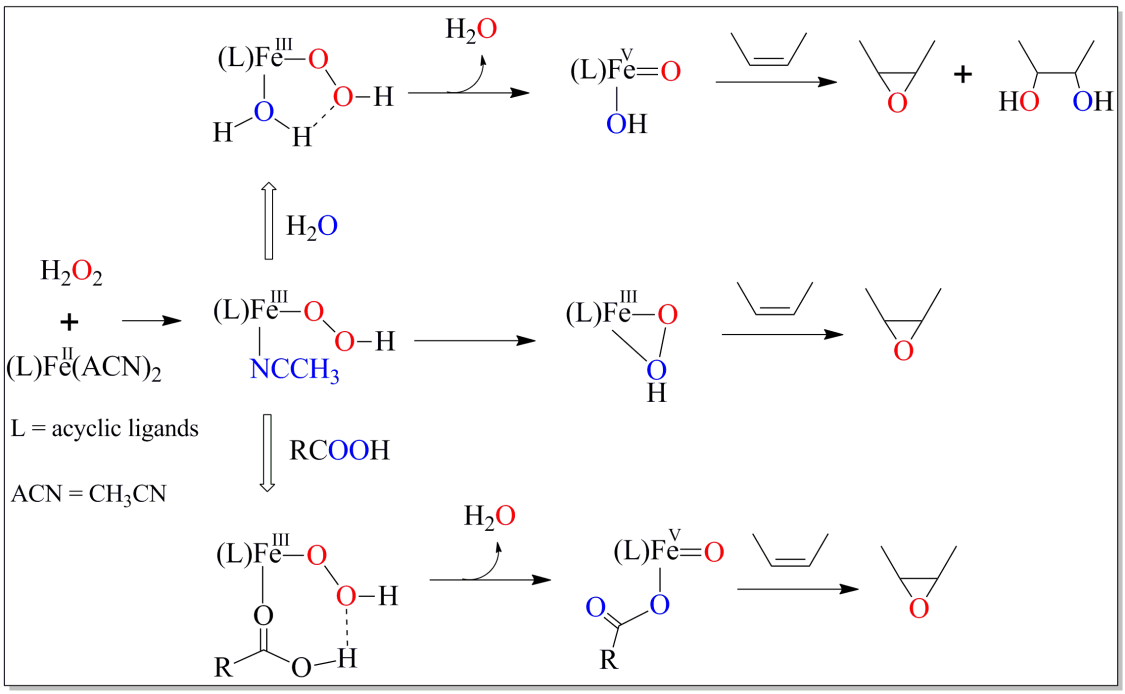

We have recently reported the stoichiometric formation of $[(bTAML)Fe^{V}(O)]^{-}$ complex **2** at room temperature (RT) with NaOCl/*m*-CPBA as an oxidant.[7b] The reactivity of this $Fe^{V}(O)$ for activation of C-H bonds and in photochemical water-oxidation has been

reported.[7b,8] In this work, we report the reactivity of $[(bTAML)Fe^{V}(O)]^{-}$ (**2**) with a wide variety of alkenes (Scheme 3.3). The second-order rate constants derived with alkenes with varying electronic properties indicate the $Fe^{V}(O)$ to be an electrophilic oxidant. Using a combination of experimental and theoretical studies (DFT), we propose a detailed mechanism of the epoxidation reaction.

Scheme 3.3. Catalytic Scheme for the Epoxidation of *cis*-Cyclooctene by $[(bTAML)Fe^{V}(O)]^{-}$.

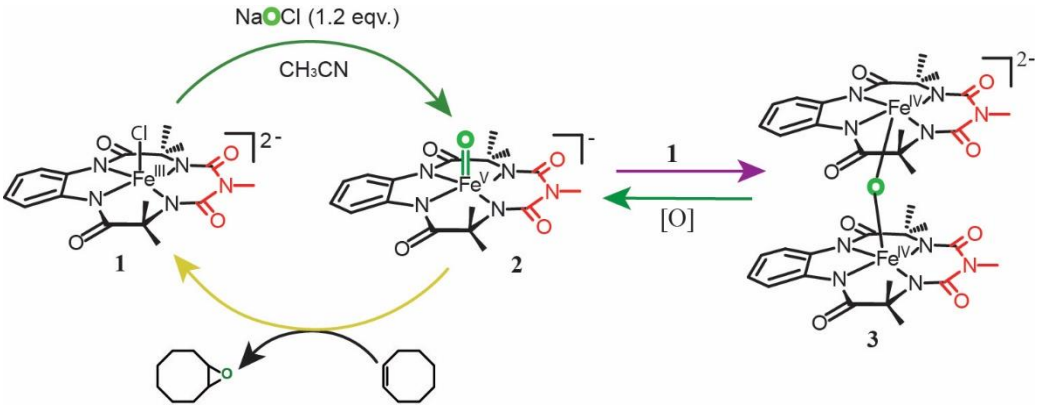

3.3 Experimental Section

3.3.1 Materials

Biuret-amide-modified Fe-TAML (**1**) was synthesized as reported by us before.[9a] Aqueous sodium hypochlorite (aq NaOCl) (reagent grade, Aldrich, available chlorine 4.00 - 4.99 %) was used as received and quantified by iodiometry. Acetonitrile (HPLC grade, Aldrich) was used after passing through an activated neutral alumina column. ^{18}O-enriched (98%) water was procured from Shanghai Research Institute of Chemical Industry, China. Deionized water was used to make all stock solutions of NaOCl for the reaction and the kinetic runs. Styrene, 4-chlororstyrene, 4-methoxystyrene, and *cis*-cyclooctene were purchased from Aldrich and distilled before use. *cis*-stilbene, *trans*-stilbene, norbornene, methyl *trans*-cinnamate, and KPF_6 were purchased from Aldrich and used as received. 4-Cyanostyrene was synthesized by the Wittig reaction,[9b] and purity were checked by GC. All reactions were carried out without any special precautions under atmospheric condition unless mentioned.

3.3.2 General Instrumentation

UV-vis spectral studies were carried out using an Agilent diode array 8453 spectrophotometer attached to an electrically controlled thermostat. Gas chromatography (GC) was performed on a PerkinElmer Arnel Clarus 500 instrument equipped with a hydrogen flame ionization detector and HP-5 (30 m × 0.32 mm × 0.25 μm) column. Helium was used as carrier gas at a flow rate of 30 mL min^{-1}. GC-MS were performed on an Agilent 5977A mass-selective detector interfaced with an Agilent 7890B GC in similar conditions using an HP-5-Ms capillary column (30 m × 0.32 mm × 0.25 μm, J & W Scientific). High-resolution mass spectrometry (HR-MS) was done in a Thermo Scientific Q-Exactive, using an electron spray ionization source and an Orbitrap as the analyzer and connected with a C18 column (150 m × 4.6 mm × 8 μm).

3.3.3 Second-Order Rate Constant (k_2) Determination for the Reaction of $Fe^{V}(O)$ with Alkenes

At least three kinetic runs were carried out for each experiment; mean values are reported here. The kinetics were monitored in either the kinetic mode of the spectrophotometer or the scanning spectral kinetics mode using a 1.0 cm quartz cell at 396 nm [Isosbestic points of Fe^{IV} species and Fe^{III}] at 25.0 °C.[7b,10] All kinetic experiments were carried out in CH_3CN. During kinetic measurements, $Fe^{V}(O)$ was prepared by using 1.1 equiv NaOCl, and substrate was added to it under pseudo-first-order condition (concentration of **2** was from 2×10^{-5} M to 1×10^{-4} M, depending upon reactivity of the substrate, and different alkenes concentrations were chosen according to the needs of the experiment, which was from 2×10^{-4} M to 1.8×10^{-1} M, see Figure 3.1). The pseudo-first-order rate constant (k_{obs}) was calculated at the isosbestic wavelength by nonlinear curve fitting [$A_t = A_\alpha - (A_\alpha - A_o)e^{(-kobst)}$] and had a good agreement in rate constant value within 10% error. Resulting k_{obs} values correlated linearly with substrate concentration to give second-order rate constant k_2 (Figure 3.1).

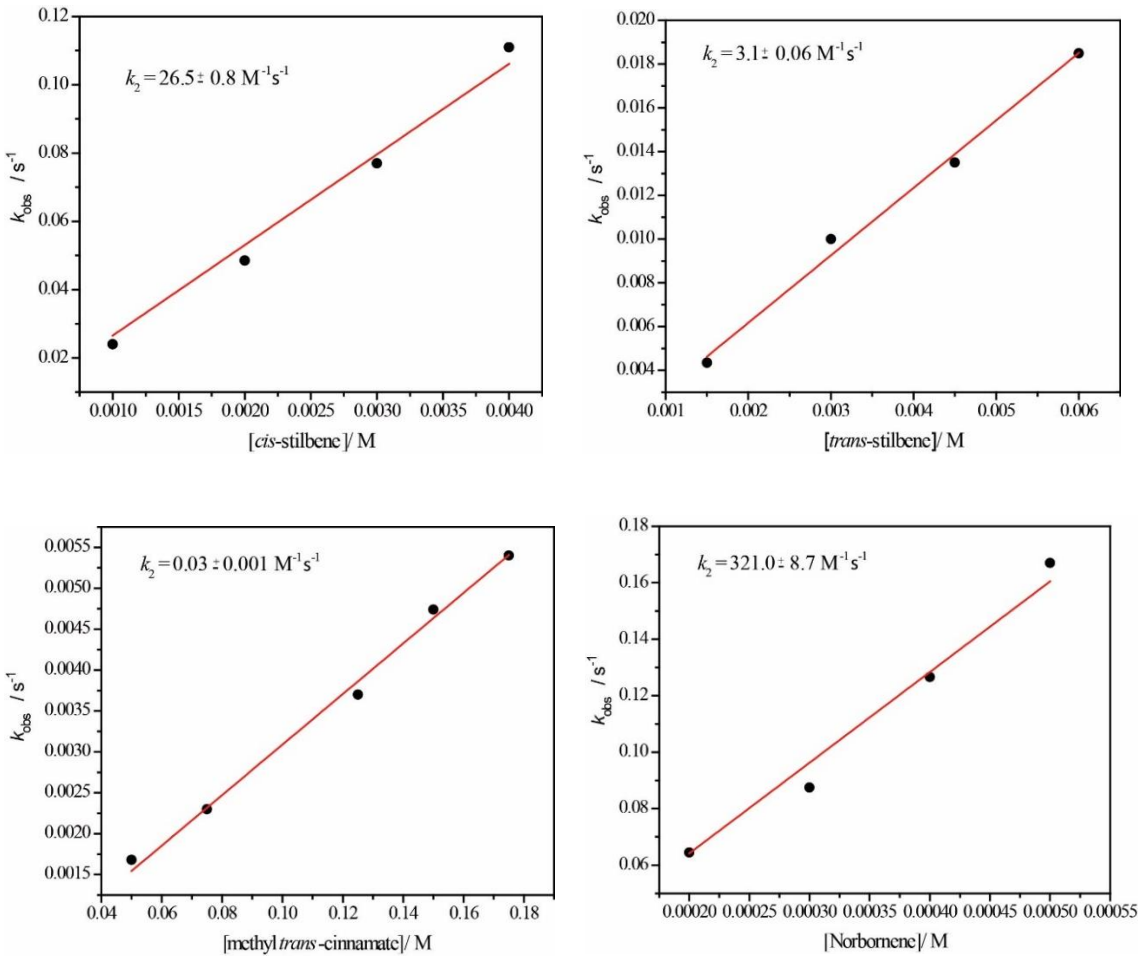

Figure 3.1. Plot of k_{obs} vs [substrate] for *cis*-stilbene, *trans*-stilbene, methyl *trans*-cinnamate, and norbornene). k_2 value determined for each substrate is the slope of the linear plot.

3.3.4 Single-Turnover Reaction of $Fe^{V}(O)$ with Alkenes

The excess substrate (50 µL, 10^{-1}M) was added to a freshly prepared 500 µL solution of **2** [generated by the reaction of **1** (2×10^{-4} M) and NaOCl (2.2×10^{-4} M)] at room temperature (RT). The reaction mixture was stirred for 20-70 min. After completion of the reaction (determined by UV-vis spectroscopy), the products (yield %) were quantified by GC using a calibration curve obtained with authentic epoxides of respective alkene (Table 3.1). The products were identified by GC-MS and NMR.

3.3.5 Cyclic Voltammetry (CV) Measurement

Cyclic voltammetry (CV) was carried out using a BioLogic potentiostat (Model VMP-3) in a conventional three-electrode electrochemical cell with glassy carbon as the working electrode, saturated calomel electrode (SCE) as a reference electrode, and platinum foil as a counter electrode. The measurements were carried out with a 0.25 mM solution of **2** in acetonitrile (prepared by addition of two equiv of NaOCl into complex **1**) with 10 mM KPF_6 as the supporting electrolyte in ice bath at temperature 0 °C (Figure 3.2). All peaks were independently calibrated with respect to an internal Ferrocene/Ferrocenium (Fc/Fc^{+}) redox couple under identical condition.

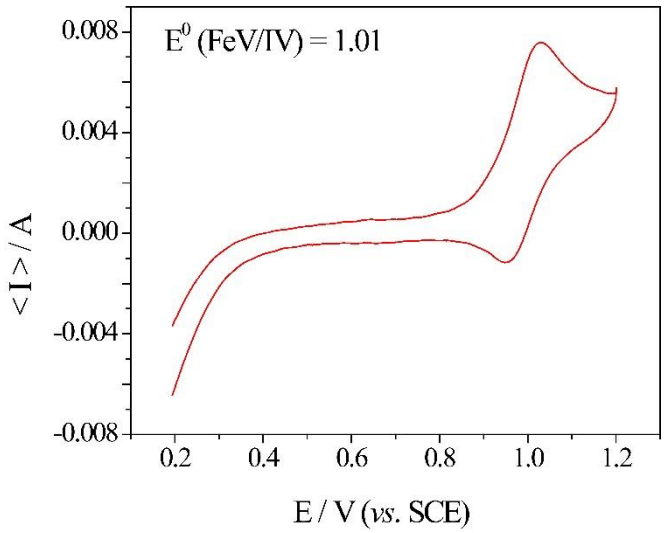

Figure 3.2. Cyclic voltammogram of complex 2, $Fe^{V}(O)$, in acetonitrile using glassy carbon as working electrode.$E_{1/2}$ ($Fe^{V/IV}$) = 1.01 V *vs*. SCE.

3.3.6 Catalytic Reaction of $Fe^{V}(O)$ with Alkenes

A 200 equiv amount (with respect to complex **1**) of aq NaOCl (at pH 11.4) was added to 1 mL of acetonitrile solution containing complex **1** (1×10^{-4} M – 1.5×10^{-4} M) and 67-100 equiv of substrate (with respect to complex **1**). The reaction was run with stirring for 10, 40, and 70 min for 4-methoxystyrene, stilbene (*cis* and *trans*), and methyl *trans*-cinnamate, respectively. At the end of the reaction, 2 ml of water was added to the reaction mixture, and product was extracted in dichloromethane (five times with 2 ml of dichloromethane each time). Collected organic phase solvent was evaporated by purging nitrogen gas, and the volume was adjusted to 500 µl for product quantification by GC.

3.3.7 ^{18}O Incorporation Experiment

To 200 µL of an acetonitrile solution of **1** (5×10^{-4} M), 1.2 equiv NaOCl was added, which leads to the formation of $Fe^{V}(O)$ (**2**). $H_2{}^{18}O$ (20 µL) was introduced into the solvent media of species **2,** and the solution was allowed to stand approximately 3 h at -22 °C. The HRMS showed 30% incorporation of ^{18}O, leading to the formation of $[(bTAML)Fe^{V}(^{18}O)]^{-}$ *m/z* 431.0763 (calculated *m/z* 431.0773). Into two separate sets of the same experiment, 50 µL of a solution of 10^{-1} M *cis*-cyclooctene and methyl *trans*-cinnamate substrate was added to the labeled $Fe^{V}(^{18}O)$ solution. HR-MS and GC-MS showed the ^{18}O labeled corresponding epoxides (Figure 3.3).

3.3.8 Computational Details

To carry out the mechanistic study, methods based on density functional theory (DFT) have been employed. All minima and transition states reported in this study were fully optimized at the UB3LYP/6-31G*, LANL2DZ (Fe) level of theory[11] using the Gaussian09 suite of quantum-chemical programs.[12] The stationary points on the potential energy surface were characterized by evaluating the vibrational frequencies. The zero-point vibrational energy corrections and thermal corrections were applied to the "bottom-of-the-well" values to obtain values for the Gibbs free energy at 298.15 K. The mechanism was derived considering styrene as the representative structure of its derivatives, such as para-substituted styrenes and stilbene. All energies were calculated with respect to the infinitely separated reactants. The products are also considered to be infinitely separated. All values provided in Figure 3 are electronic energies.

3.4 Results and Discussion

3.4.1 Kinetics of *cis*-Cyclooctene Epoxidation under Single-Turnover Condition

Compound **2** was prepared at 25 °C from the parent biuret-TAML activator, $[Et_4N]_2[(bTAML)Fe^{III}(Cl)]$ (**1**), in CH_3CN by adding equimolar (1.1 equiv) amounts of NaOCl, as reported before. The unprecedented high stability of **2** allowed us to perform extensive kinetic studies in single-turnover condition to ascertain the mechanism of epoxidation using UV-vis spectroscopy at RT (Scheme 3.3). Initial experiments showed that upon addition of *cis*-cyclooctene (2.5×10^{-3} M) to a preformed solution of **2** (4×10^{-5} M), the green color of the reaction mixture immediately changed to brown. A UV-vis

scanning kinetics study showed that the starting $Fe^{V}(O)$ species changed to the diamagnetic μ-Oxo-Fe^{IV} dimer species, which then slowly regenerated the parent Fe^{III} complex **1** (Figure 3.3(A), peak at 379 nm) quantitatively (for complete characterization of μ-Oxo-Fe^{IV} dimer species, please see ref 7b). The direct conversion of **2** to **1** was not observed in initial spectral scans since the rate of the comproportionation reaction (1.0×10^5 M^{-1} s^{-1}) between **1** and **2** (eq 2) was faster than the rate of epoxidation (29 M^{-1} s^{-1}; Table3.1, entry 8).

$$\mathbf{Fe^{V}(O)} + \mathbf{Alkene} \longrightarrow \mathbf{Products} + \mathbf{Fe^{III}} \qquad (1)$$

$$\mathbf{Fe^{V}(O)} + \mathbf{Fe^{III}} \xrightarrow{\mathbf{(1:1)}} \mathbf{Fe^{IV}}\!-\!\mathbf{O}\!-\!\mathbf{Fe^{IV}} \qquad (2)$$

The pseudo-first-order rate constant (k_{obs}) correlated linearly with [*cis*-cyclooctene] (Figure 3.3(B)), and the second-order rate constant k_2 (29 M^{-1} s^{-1}) was calculated from the slope of the straight line (Figure 3.3(C)). After completion of the reaction, product identification was carried out by GC-MS; the results showed that cyclooctene oxide was formed as the major product (~65%). It should be noted that the fast comproportionation between **1** and **2** would allow only 50% of **2** to react with alkenes and yield a maximum of only 50% yield epoxide (with respect to **2**). The higher yields of epoxide observed are due to the slow reaction of alkenes with the Fe^{IV} dimer (Figure 3.5) (separately discussed below). Less than 1% of *trans*-cyclooctane-1,2-diol was observed as a side product. Quantification of the epoxide was done by GC. Control experiments with only NaOCl in our experimental conditions showed no formation of cyclooctene oxide.

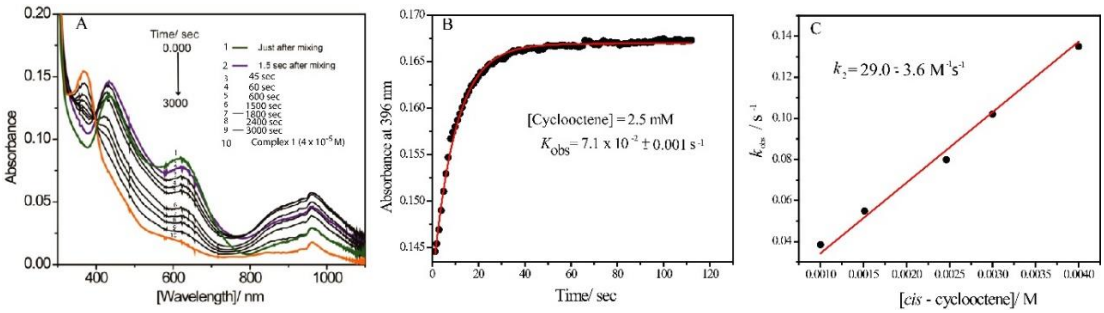

Figure 3.3. (A) UV–vis spectral changes upon reaction of **2** (4×10^{-5} M) with *cis*-cyclooctene (2.5×10^{-3} M); (B) absorbance *vs* time plot at 396 nm for reaction of **2** (4×10^{-5} M) with *cis*-cyclooctene (2.5×10^{-3} M) (●) indicates experimental data point; (red line) first-order fit according to the equation [$(A_t = A_\alpha - (A_\alpha - A_o)e^{(-kobst)}$]. The reaction was performed at RT in acetonitrile solvent under a nitrogen atmosphere. (C) Plot of k_{obs} vs

substrate concentration [*cis*-cyclooctene] to determine k_2 value from the slope of the linear plot.

3.4.2 Kinetics of the Epoxidation of Various Alkenes under Single-Turnover Conditions

To ascertain the mechanism of epoxidation, single-turnover experiments were performed by adding preformed **2** (from 2×10^{-5} to 1×10^{-4} M, depending upon the reactivity of the substrate) to various alkenes having varying electronic and steric properties under pseudo-first-order conditions (Table 3.1). After completion of the reaction, all products of these single-turnover reactions were identified by GC-MS and then quantified by GC (Appendix B1). GC-MS showed the exclusive formation of epoxide with moderate yields (>70%) for most alkenes. For the alkenes *trans*-stilbene, norbornene, and *cis*-cyclooctene, the side products formed were identified as benzaldehyde (<2%), *trans*-norbornane-2,3-diol (<1%), and *trans*-cyclooctane-1,2-diol (< 1%) respectively. When *cis*-stilbene was used as a substrate, in addition to the formation of *cis*-stilbene oxide (56%), considerable amounts of isomerized products, i.e., *trans*-stilbene oxide (21%), were observed (Table 3.1, entry 6). When *trans*-stilbene was used as the substrate, the *trans*-stilbene oxide was formed exclusively, and no *cis*-stilbene oxide was found (Table 3.1, entry 7). Additionally, stereochemical retention was also observed for the epoxidation of methyl *trans*-cinnamate. In all the reactions, the starting Fe^{III} complex (**1**) was quantitatively regenerated after the single-turnover reaction. To ascertain that the O-atom was incorporated into the alkene upon epoxidation from the $Fe^{V}(O)$, ^{18}O labeling experiments were performed. Epoxidation was carried out on two different alkenes (methyl *trans*-cinnamate, *cis*-cyclooctene) using a mixture of $Fe^{V}(^{16}O)$ and $Fe^{V}(^{18}O)$ (ratio of 68:32) (Figure 3.4(A)). The epoxides obtained after completion of the reaction showed ~30% incorporation of ^{18}O into the epoxide, which confirmed that oxygen incorporated into the epoxide was transferred from $Fe^{V}(O)$ (Figure 3.4(B)).

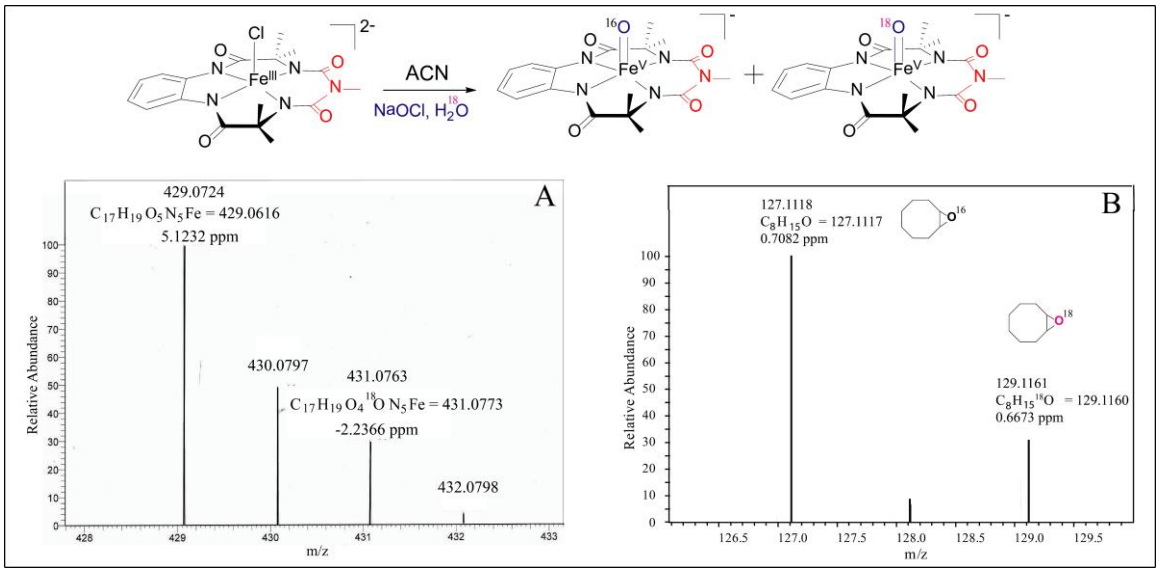

Figure 3.4. (A) HR-MS of **2** in CH_3CN after 3 hrs incubation in H_2O^{18} at -22 °C. Calculated m/z of **2** after ^{18}O incorporation = 431.0763. (B) The HR-MS spectra of *cis*-cyclooctene epoxide product obtained after reaction with *cis*-cyclooctene and ^{18}O labeled complex **2** in CH_3CN.

The kinetics of the reaction was then studied to determine the second-order rate constant k_2, as described above. The k_2 values obtained for all of the different alkenes show that the rates of epoxidation of electron-rich substrates were much faster than those of the electron-deficient ones. For example, the k_2 value for 4-methoxystyrene (Table 3.1, entry 1) was determined to be 216 M^{-1} s^{-1}, while that of methyl *trans*-cinnamate (Table 3.1, entry 9) was 0.03 M^{-1} s^{-1}. This 8000-fold rate difference between electron-rich and electron-deficient substrates indicates that $Fe^{V}(O)$ has electrophilic character, reminiscent of non-heme epoxidation catalysts that have been discussed before. The reactivity of the disubstituted alkenes (e.g., cyclooctene, *cis*-stilbene) is much slower than expected, possibly due to the steric-crowding of the disubstituted alkenes. The effect of electron-donation and -withdrawing groups on alkenes was explored in more detail by using a series of substituted styrenes. Kinetic studies revealed that styrene with a para-substituted electron-donating group was more reactive than styrene having a para-substituted electron-withdrawing group (Table 3.1). For example, k_2 for the epoxidation of *p*-cyanostyrene was determined to be ~3 times slower than the rate of *p*-methoxystyrene. We were unable to determine the exact k_2 value of *p*-nitro styrene since its strong UV absorption in the 300-400 nm region interfered with the $Fe^{III/IV}$ isosbestic point (Appendix B2).

Table 3.1. Epoxidation of Different Alkenes by $Fe^{V}(O)$[a] at RT in CH_3CN Solvent under Air.

Entry	Substrates[b]	Products	time / min	k_2/ $M^{-1}s^{-1}$	%Yields[c]
1	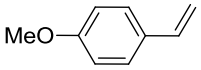	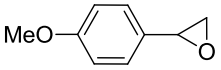	20	216.0 ± 3.2	74 ± 6
2	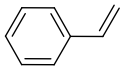	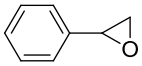	50	148 ± 8.1	71 ± 6
3	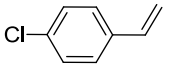	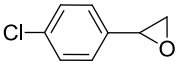	50	116 ± 4.6	70 ± 6
4	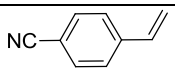	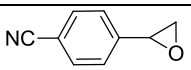	50	72.0 ± 3.7	62 ± 5
5	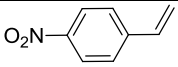	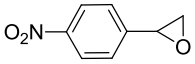	50	n.d.	66 ± 5
6	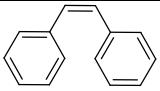	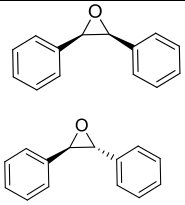	50	26.5 ± 0.8	77 ± 4, (73:27)
7	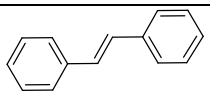	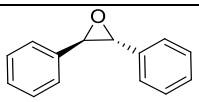	50	3.1 ± 0.06	81 ± 4
8		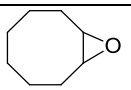	30	29.0 ± 3.6	65 ± 5
9	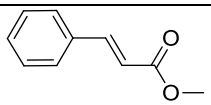	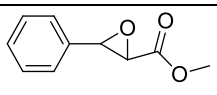	70	0.03 ± 0.001	86 ± 6
10		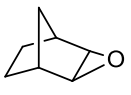	20	321.0 ± 8.7	78 ± 7

[a] Concentration of $Fe^{V}(O)$ used to obtain k_2 values was 2×10^{-5} M (for entries 1 and 10), 4×10^{-5} M (for entries 2-4 and 8), and 1×10^{-4} M (for entries 6,7, and 9). For a yield of epoxides under single-turnover conditions, the concentration of $Fe^{V}(O)$ was 2×10^{-4} M. [b]

Concentration variation of substrates used to obtain k_2 was in the range of 10-100 equiv (for entries 1-4, 6-8, and 10) and 500-1750 equiv (for entry 9) with respect to $Fe^{V}(O)$. For obtaining single-turnover yields, the substrate concentration used was 1×10^{-2} M. [c] Yields of epoxides are with respect to $Fe^{V}(O)$.

3.4.3 Reactivity of μ-Oxo-Fe^{IV} Dimer

The >50% yield of epoxide formation observed in the single-turnover experiments is unlikely because the fast comproportionation between **1** and **2** would only allow 50% of **2** to react with alkenes and yield a maximum of only 50% epoxide (with respect to **2**). The higher yields of epoxide observed are due to the slow reaction of alkenes with the μ-Oxo-Fe^{IV} dimer, which was investigated in the reaction of 4-methoxystyrene and *cis*-cyclooctene with μ-Oxo-Fe^{IV} dimer (Table 3.2). The μ-Oxo-Fe^{IV} dimer was synthesized by addition of 0.5 equiv of NaOCl in complex **1**, which has characteristic UV-vis spectra similar to the previously reported μ-Oxo-Fe^{IV} dimer (which is formed upon equimolar amounts of **1** in **2**; characterized by ^{1}H NMR and EPR).[7b,10] The μ-Oxo-Fe^{IV} dimer species reacts with alkenes to form a corresponding epoxide. For example, in the reaction of a μ-Oxo-Fe^{IV} dimer with 4-methoxystyrene, *cis*-cyclooctene and styrene corresponding epoxide were observed with a rate of reaction more than 50-fold slower than the corresponding reaction with $Fe^{V}(O)$, **2**. Although we do not have any conclusive evidence of the mechanism of this reaction, we believe that the μ-Oxo-Fe^{IV} dimer disproportionates into $Fe^{V}(O)$ (**2**) and Fe^{III} complex (**1),** after which the $Fe^{V}(O)$ reacts with alkenes to form the epoxide product (Figure 3.5). Two scenarios are possible: (1) binding of alkene to the μ-Oxo-Fe^{IV} dimer leads to the disproportionation reaction, after which the $Fe^{V}(O)$ reacts, or (2) the μ-Oxo-Fe^{IV} dimer exists in equilibrium with the $Fe^{V}(O)$ and Fe^{III} complex. The reaction of the alkene with $Fe^{V}(O)$ leads to more disproportionation of the dimer, leading to the formation of more $Fe^{V}(O)$, which reacts with the alkene until all of it is converted to the starting Fe(III) complex. If the first hypothesis is correct, a saturation in the k_{obs} values of the reaction of the μ-Oxo-Fe^{IV} dimer with the substrate should be observed at high substrate concentration. However, no saturation was observed for the k_{obs} with styrene/methoxystyrene with up to 750 equiv of the substrate, implying that the substrate-mediated disproportionation was probably not occurring. Further, the reaction of a μ-Oxo-Fe^{IV} dimer with 4-methoxystyrene in the presence of different amounts of parental Fe^{III} complex **1** showed a reduction in

reaction rates with increasing amounts of **1** into the reaction mixture. The plot of reaction rate vs amount of Fe^{III} (**1**) in reaction mixture shows a good fit with the kinetic model

$$Rate = \frac{k_1 k_2[\mu - Oxo - Fe^{IV} dimer][substrate]}{k_{-1}\,[Fe^{III}] + k_2\,[substrate]}$$

Using a k_2 value of 216 $M^{-1}\,s^{-1}$ (as earlier determined for methoxystyrene under single-turnover conditions), the k_1 and k_{-1} was determined to be 100 and 24196, respectively (Figure 3.5(C)).

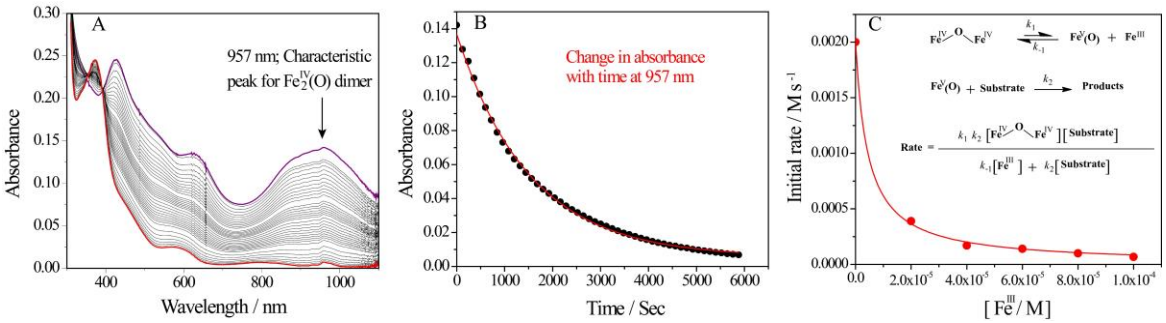

Figure 3.5. (A) UV–vis spectral changes upon reaction of µ-Oxo-Fe^{IV}dimer (2×10^{-5} M) with *cis*-cyclooctene (4×10^{-3} M); (B) the absorbance *vs* time plot at 957 nm for reaction of µ-Oxo-Fe^{IV}dimer (2×10^{-5} M) with *cis*-cyclooctene (4×10^{-3} M); (● indicates experimental data point; the red line is the first-order fit according to the equation [$(A_t = A_\alpha - (A_\alpha - A_o)e^{(-kobst)}$]. The reaction was performed at RT in acetonitrile solvent under inert condition. (C) The plot of initial rate *vs* concentration of Fe^{III}, complex **1**, added for the reaction of µ-Oxo-Fe^{IV}dimer (2×10^{-5} M) with 4-methoxy styrene (5×10^{-4} M). k_1 (100) and k_{-2} (24196) were obtained by non-linear curve fit according to the equation obtained from proposed reaction scheme of µ-Oxo-Fe^{IV}dimer in presence alkene.

Table 3.2. Epoxidation of Alkenes by μ-Oxo-Fe^{IV} dimer[a] at RT in CH_3CN Solvent under Air.

Substrates[b]	Products	k_2/ $M^{-1}s^{-1}$
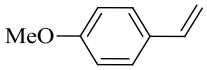	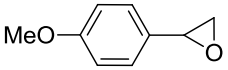	4.4 ± 0.2
	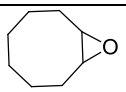	0.2 ± 0.01
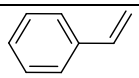	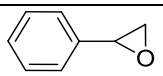	0.8 ± 0.02

[a] Concentration of μ-Oxo-Fe^{IV}dimer was 1×10^{-5} M for reaction with 4-methoxystyrene and 2×10^{-5} M for reaction with *cis*-cyclooctene and styrene. [b] Concentration of substrates was in the range from 2.5×10^{-4} M to 4×10^{-3} M.

3.4.4 Investigations on the Different Possible Pathways for the Epoxidation of C=C Bond Involving $Fe^{V}(O)$ Species

Three possible mechanisms for initial attack of "O" into the alkene during the epoxidation reaction have been proposed:

(1) the transfer of oxygen into the alkene by a concerted process (Scheme 3.4, path C), as is known for the epoxidation of alkenes by the enzyme cytochrome P450,[2a,3a,13]

(2) generation of the acyclic carbocation radical through one-electron transfer [14] (Scheme 3.4, path B), and

(3) radical intermediate formation via electrophilic attack of $Fe^{V}(O)$ upon alkene with concomitant C-O bond formation[15] (Scheme 3.4, path A).

Understanding the pathway is important since the product selectivity during the epoxidation reaction depends upon the mechanism through which the reaction proceeds. For example, both the second and the third pathways have been observed for synthetic Fe-porphyrin complexes as well as Mn-Salen complexes.[16] Also, it has been shown that the reaction pathway between 2 and 3 can be manipulated by varying the axial ligands in synthetic iron porphyrins.[17] The other possibility for the catalytic reaction is the axial coordination of the

second equivalent of NaOCl to the $Fe^{V}(O)$, resulting in the formation of $Fe^{V}(O)OCl$, as observed in Fe-porphyrins. We exclude this possibility since the addition of excess NaOCl to complex **2** does not show any change in the UV-vis spectra of the starting $Fe^{V}(O)$. All possible pathways are schematically shown below (Scheme 3.4).

Scheme 3.4. Detailed Mechanistic Scheme for the Epoxidation of Alkenes by $[(bTAML)Fe^{V}(O)]^{-}$.

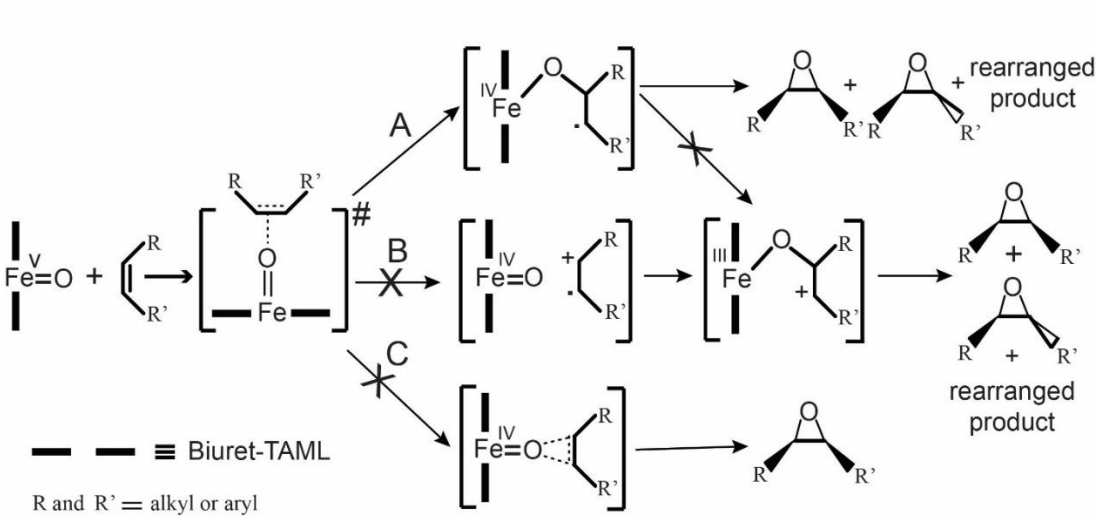

Epoxidation by Pathway C. To probe experimentally if the epoxidation reactions by $Fe^{V}(O)$ occurs via pathway C, the substrate *cis*-stilbene was used as a mechanistic probe, as has been shown by Bruice et al. in the case of electron-deficient cytochrome P-450 model complexes (e.g., *meso*-tetrakis(2,6-dichlorophenyl)porphinato-oxo-iron(IV), $[(C_{l8}TPP^{+\cdot})$-$Fe^{lV}(O)]$.[14b,18] If *cis*-stilbene leads to the exclusive formation of *cis*-stilbene oxide, it indicates the predominance of a concerted mechanism. In contrast, if a mixture of both *cis*- and *trans*-configured epoxide is observed, it would point to the formation of a radical intermediate that would allow C-C bond rotation to give the stereoisomers. In the epoxidation of *cis*-stilbene with $Fe^{V}(O)$, the formation of both *cis*- and *trans*-stilbene epoxide is observed (ratio 73:27); hence, the pathways via a concerted mechanism looks unlikely (Path C in Scheme 3.4). Further, DFT calculations discussed below also show that the epoxidation of styrene by $Fe^{V}(O)$ complexes are indeed nonconcerted processes.

Epoxidation via Pathway A and B. The loss of stereochemistry during the epoxidation of *cis*-stilbene can be explained by invoking the formation of a radical intermediate (Scheme 3.4, Path A or B). To distinguish between pathway A and pathway

B, we looked carefully at the rates of epoxidation with variously substituted alkenes. It has been shown that for epoxidation reactions operating via pathway B, i.e., the rate-determining step (RDS) being one-electron oxidation, the second-order rate constants vary linearly with the ionization potential (IP) of alkenes.[19] In our study of alkene epoxidation by $Fe^{V}(O)$, the plot of k_2 *vs* IP of alkenes does not show any linearity (Figure 3.6).

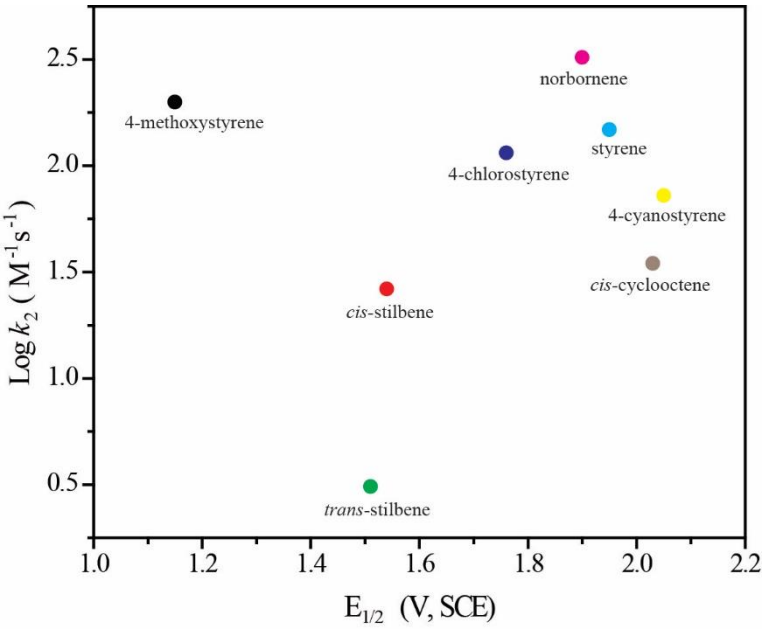

Figure 3.6. Plot of the log of the second-order rate constant (k_2) for the epoxidation with $Fe^{V}(O)$ (**2**) *vs* the $E_{1/2}$ for 1e oxidation of the alkenes.[25] The alkenes are color coded: styrene (cyan), 4-methoxystyrene (black), 4-chlorostyrene (blue), 4-cyanostyrene (yellow), *cis*-cyclooctene (brown), *cis*-stilbene (red), *trans*-stilbene (green), norbornene (magenta).

DFT studies also point to the fact that pathway B is not followed during the epoxidation process. The calculations show that the epoxidation of styrene by $Fe^{V}(O)$ complexes **2** is indeed a nonconcerted process, with the C-O bond formation being the rate-determining step (Figure 3.8 and Table 3.4), followed by a very low barrier ring-closing step. This corresponds to pathway A in Scheme 3.4. The existing literature on analogous systems suggests similar observations, which were further supported by DFT studies.[3c,18,20] For investigating pathway B (see Scheme 3.4), we looked at the correlation diagram of the ionization potential of the substrates versus the experimentally measured second-order rate constants (Figure 3.6). No correlation between the ionization potential and the rate of reaction was obtained, which indicates that one-electron oxidation of the styrene coupled with the one-electron reduction of the monoanionic $Fe^{V}(O)$ complex is unlikely. This is in

contrast to the epoxidation catalyzed by Mn and Cr porphyrin catalysts, in which the second-order rate constants strongly correlated to the $E_{1/2}$ of the substrates.[18,19] Thermodynamic analysis of the epoxidation of olefins by **2** precludes the involvement of the one-electron reduced $Fe^{IV}(O)$ as the active species during the O-atom transfer leading to the formation of the C-O bond. First, the free energy of activation during the epoxidation reaction was determined from the second-order rate constants. This was compared to the standard free energies required for the formation of a one-electron-oxidized alkene, i.e., $Fe^{V}(O)$ + alkene $\rightleftharpoons$ $Fe^{IV}(O)$ + alkene$^{\bullet+}$ (The redox potential of Fe^{V}/Fe^{IV} was determined by performing cyclic voltammetry experiments with chemically synthesized $Fe^{V}(O)$; see the Experiment Section). The analysis shows that, for several alkenes, the free energy of the one-electron oxidation of alkenes by $Fe^{V}(O)$ exceeds that of the free energy of the transition state during the epoxidation of alkenes by $Fe^{V}(O)$ (Table 3.3), thereby precluding the role of $Fe^{IV}(O)$ as the active species during C-O bond formation.

Table 3.3. Calculated Values of the Free Energy of Formation of the Transition State (ΔG^{a}) and Standard Free Energy (ΔG^{o}) for the One-Electron Transfer in the Transition State during the Reaction of $Fe^{V}(O)$ with Alkene at Temperature 25^{o}C in Acetonitrile[a].

Substrate	Log k_2 (M^{-1} s^{-1})	ΔG^{a} (kJ mol^{-1})	$E_{1/2}$ (V, SCE)	ΔG^{o} (kJ mol^{-1})
Norbornene	2.51	47.5	1.90	85.9
Styrene	2.17	49.5	1.95	90.7
4-chlorostyrene	2.06	50.1	1.76	72.4
4-cyanostyrene	1.86	51.3	2.05	100.3
cis-cyclooctene	1.54	53.1	2.03	98.4

[a]ΔG^{a} = - RT ln (k_2h/ kT); ΔG^{o} = - nF(P_1-P_2), where; n=1, P_1 = $E_{1/2}$ (V, SCE) of substrates oxidation, P_2 = $E_{1/2}$ (V, SCE) of $Fe^{V}(O)$ reduction = 1.01, F = 96485 C mol^{-1}, T = 298 K, R = 8.314 J K^{-1} mol^{-1}, k = 1.38 x 10^{-23} J K^{-1}, h = 6.6 x 10^{-34} J s.

To investigate this further, a geometry optimization of the cationic styrene and the dianionic $Fe^{IV}(O)$ complex was performed in the solvent phase, using the conductor like polarization continuum model (CPCM) method[21] and with acetonitrile (dielectric constant, ε = 35.688) as the solvent. The free energy difference between the obtained ionic species and the rate-determining transition state (RDTS) of Pathway A (in this case, also optimized with solvent corrections for the purpose of comparison) was calculated to be 13.0 kcal/mol

(Appendix B3). The calculated free energy of the reaction leading to the formation of the ionic intermediates in pathway B was endergonic by 34.4 kcal/mol (Appendix B3), which further indicates its unlikelihood.

To understand the effect of the electronic environment associated with the substituent on styrene, different para-substituted styrene derivatives with electron-donating substituents displayed enhanced second-order rate constant (k_2) values when compared to electron-withdrawing para substituents (Table 3.1). The k_2^{rel} ($k_2^{rel} = k_2^{X}/k_2^{H}$) value for styrene and its analog was used for linear free energy correlation analysis (Figure 3.7), and a Hammett ρ value of –0.56 was obtained. The relatively small value of ρ indicated the buildup of partial positive charge on the olefinic carbon in the transition state. However, previous studies showed that the rate-limiting carbocation formations *via* electrophilic additions to substituted styrenes are associated with much more negative ρ values [i.e., -3.58 (hydration) and -4.8 (bromination)].[22] When the barrier heights for pathway A obtained from the DFT calculations were compared for styrene and *p*-chlorostyrene, it was seen that the barrier height for the *p*-chlorostyrene case was higher by 1.9 kcal/mol than for styrene (10.5 kcal/mol for styrene and 12.4 kcal/mol for *p*-chlorostyrene; Table 3.4 and Appendix B4). This observation indicates that pathway A most likely represents the actual epoxidation mechanism, and therefore, the direction of the flow of electrons inside the styrene substrates during the reaction occurs from the phenyl ring to the CH2=CH- group. To further investigate the effect of the solvent and the Hammett-type behavior of the styrene derivatives on the rate determining barriers (RDB), the RDB were calculated using the conductor polarized continuum model (CPCM) in acetonitrile (ε = 35.688) for 4-methoxystyrene, styrene, and 4-chlorostyrene substrates. The obtained result followed the experimental trend, i.e., the barriers are obtained in the following order: 4-chlorostyrene (12.7 kcal/mol) > styrene (9.2 kcal/mol) > 4-methoxystyrene (8.8 kcal/mol) (Appendix B5).

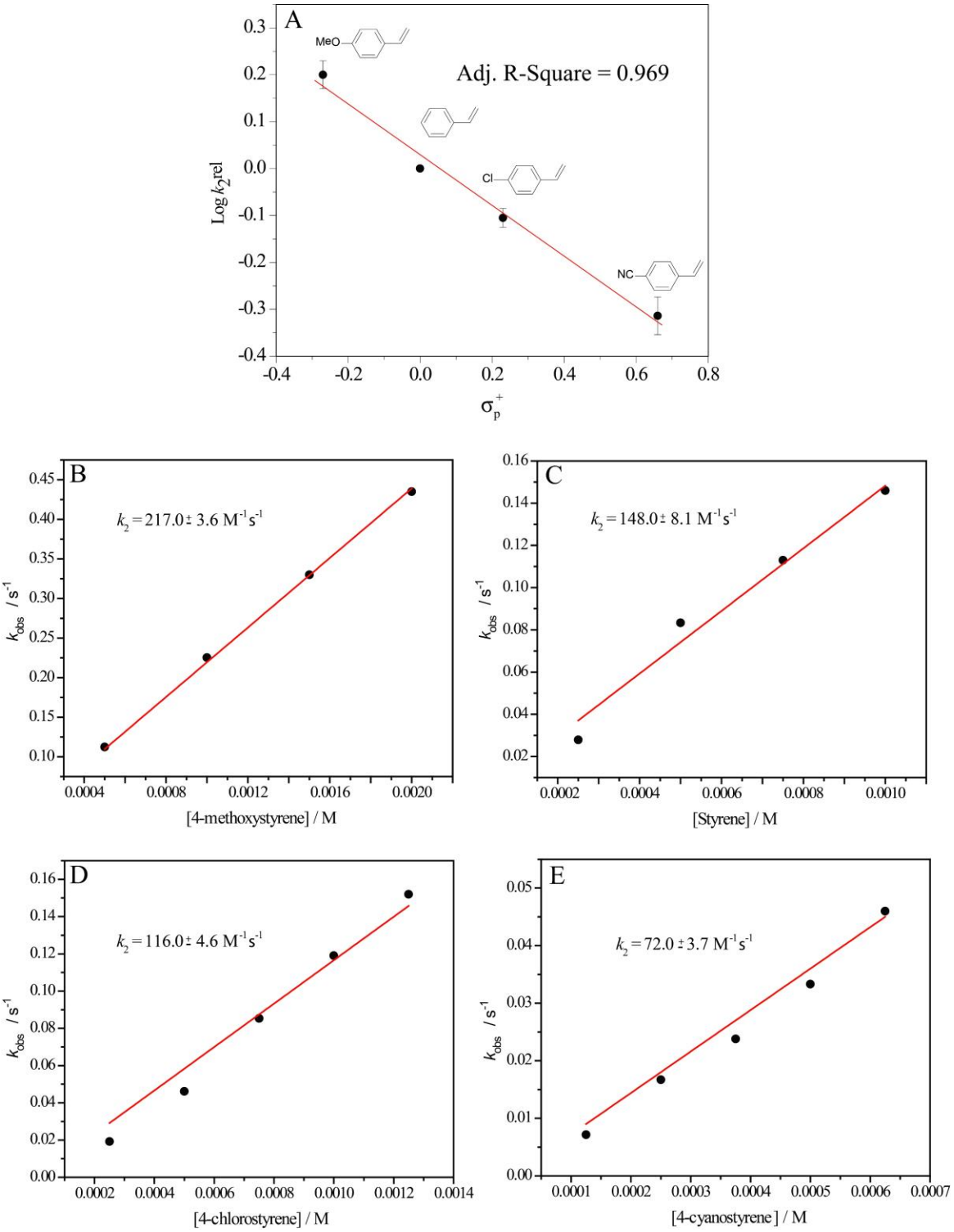

Figure 3.7. (A) Hammett plots of log k_2^{rel} against *para*- σ^+ for the epoxidation of styrene and its *para*-substituted derivatives by $Fe^{V}(O)$ at RT in CH_3CN. Hammett value ρ is -0.56; $k_2^{rel} = k_2^X/k_2^H$, (k_2^X and k_2^H are second-order rate constants for *para*-substituted styrene and styrene, respectively). (B), (C), (D), and (E) are plots of k_{obs} *vs* substrate concentration for

4-methoxystyrene, styrene, 4-chlorostyrene, and 4-cyanostyrene, respectively. The k_2 value determined for each substrate is the slope of the linear plot.

3.4.5 Mechanistic Insite by Density Functional Theory (DFT)

Understanding the *α* and *β* Pathway during Styrene Epoxidation. Depending upon the mode of attack on the oxo group by the substrate styrene, two possible pathways for epoxidation are possible for pathway A: the *α* pathway and the *β* pathway (Figures 3.8(A) and 3.8(B)). The *α* pathway entails the approach of the *α* carbon of styrene onto the oxo group of the catalyst, whereas the *β* pathway involves the attack of the *β* carbon onto the catalyst. The complete energy profile suggests that the *β* attack is energetically more favorable (see Figure 3.8(B)). The reactive species formed by the *β* attack is more stable due to the extended conjugation of the phenyl ring.

For the *β* pathway, there are again two possibilities that need to be investigated: the reaction could occur on the doublet surface or on the quartet surface. As Figure 3.8 indicates, the reactant $Fe^{V}(O)$ complex is more stable as a doublet than a quartet by 3.0 kcal/mol (Appendix B6). This suggests that the species would exist predominantly in the doublet state, a result that is supported by the experimental observations (the EPR of $Fe^{V}(O)$ shows resonances characteristic of $S = 1/2$ species).[7b] At the intermediate stage, after the crossing of the first barrier, the calculations show that the quartet adduct structure is more stable than the doublet by 10.2 kcal/mol (Table 3.4). While this suggests a thermodynamic incentive for the system to convert from the doublet to the quartet at the intermediate stage, the barrier for the subsequent reaction is only 3.0 kcal/mol on the doublet surface, which indicates that the reaction would most likely proceed in the forward direction on the doublet surface. It has been observed in the past that while the spin-flip barrier is expected to be low, it is unlikely that the spin-flip would compete with the forward reaction process for reactions having forward barriers less than 5.0 kcal/mol.[23] Hence, the reaction would proceed to its end on the doublet surface and lead to the formation of the doublet product ($S = 1/2$). Subsequent to this, with no further reaction occurring, this kinetically obtained product can convert to the quartet product ($S = 3/2$), which is 12.0 kcal/mol lower in energy (see Table 3.4 and Figure 3.8(B)). Hence, the calculations predict a reaction occurring on the doublet surface and leading to the formation of a final quartet product: a result that matches the experimental observation that the final product is a quartet.

Table 3.4. The gas phase relative reaction energies in kcal/mol at the UB3LYP/6-31G*, LANL2DZ (Fe) level of theory for styrene epoxidation catalyzed by $[(bTAML)Fe^{V}(O)]^{-}$.

	R	TS1	I	TS2	P
ΔE^{a}	0.0 (0.0)	10.5	-1.8	1.2	-18.3
$\Delta(E+ZPE)^{a}$	0.0 (0.0)	10.3	-1.4	1.6	-17.9
ΔG^{a}	0.0 (0.0)	22.1	9.8	13.2	-17.9
ΔE^{b}	0.0 (0.0)	12.2	-14.9	-12.2	-30.3
$\Delta(E+ZPE)^{b}$	0.0 (0.0)	12.7	-13.4	-11.2	-31.4
ΔG^{b}	0.0 (0.0)	25.4	-2.1	0.6	-31.0
ΔE^{c}	0.0 (0.0)	14.5	10.5	15.4	-18.3
$\Delta(E+ZPE)^{c}$	0.0 (0.0)	14.1	10.1	15.0	-17.9
ΔG^{c}	0.0 (0.0)	26.2	22.2	27.4	-17.9
ΔE^{d}	0.0 (0.0)	16.6	-0.3	1.4	-30.3
$\Delta(E+ZPE)^{d}$	0.0 (0.0)	16.6	-0.2	1.2	-31.4
ΔG^{d}	0.0 (0.0)	28.8	11.7	14.0	-31.0

a. S=1/2 spin state, β-attack; b. S=3/2 spin state, β-attack; c. S=1/2 spin state, α-attack; d. S=3/2, α-attack.

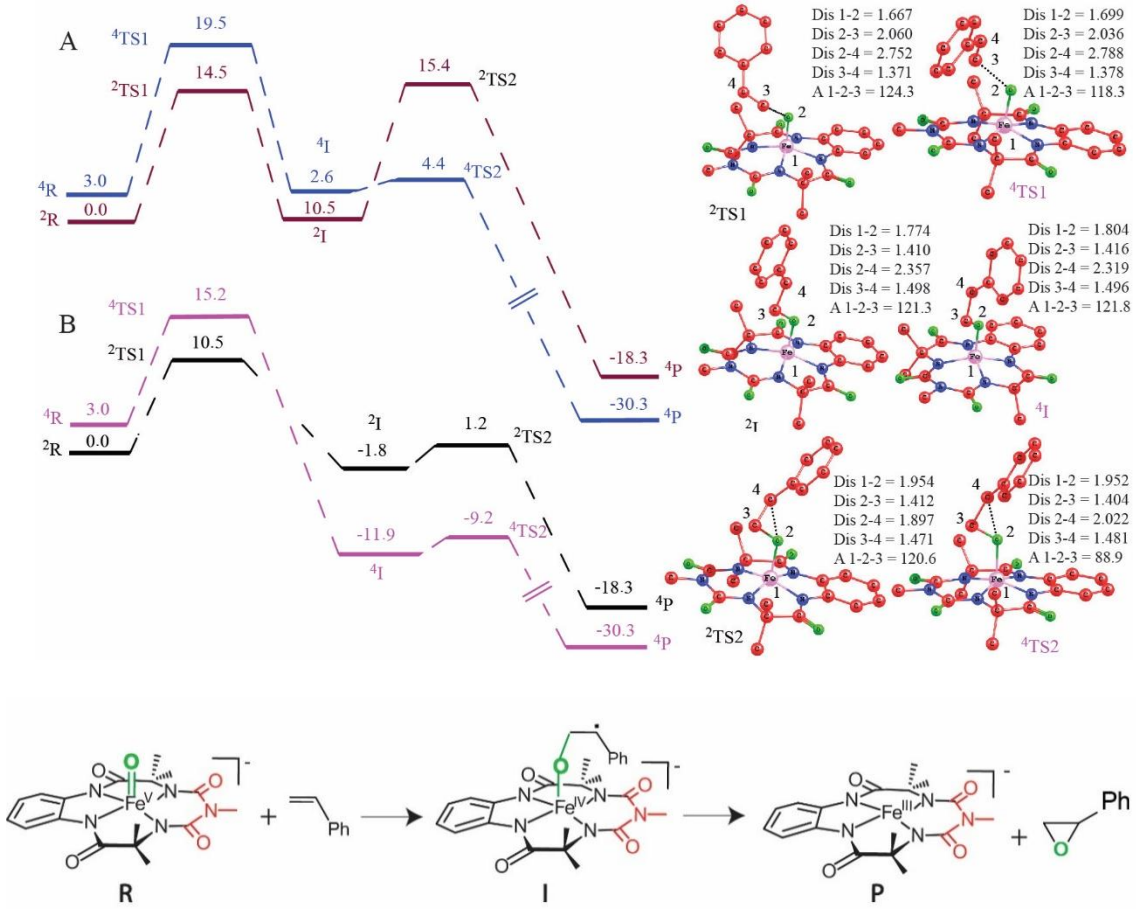

Figure 3.8. Gas-phase energy profile with optimized geometries of the intermediates and transition states for the epoxidation of styrene by **2** at the UB3LYP/6-31G*, LANL2DZ (Fe) level of theory from doublet and quartet surfaces for (A) α pathway; (B) β pathway (Dis and A denote distance and angles, respectively; superscripts 2 and 4 represent geometries in the doublet and quartet spin states).

3.4.6 Molecular Mechanism of Epoxidation by $Fe^{V}(O)$

Figure 3.9 shows the frontier orbitals obtained from the DFT calculations for the styrene substrate. As mentioned in the previous section, the reaction would occur on the doublet surface, with the quartet finally being obtained as the thermodynamic product at the end of the reaction. Parts R and I of Figure 3.9 show the MOs corresponding to the reactant and the intermediate Fe complexes on the doublet surface. The HOMO in the intermediate doublet geometry is seen to be localized on the styrene. Part P shows the MOs obtained for the kinetic doublet product as well as for the thermodynamic quartet product. As also indicated in Appendix B7, the energy of the HOMO in the quartet structure is 3.9

kcal/mol lower than the energy of the HOMO in the doublet. According to the "HOMO rule," the more stable of two structures of a given species is the one whose HOMO is at a lower energy.[24] This explains why the quartet structure is more stable than the doublet and, therefore, why the final product of the reaction is a quartet.

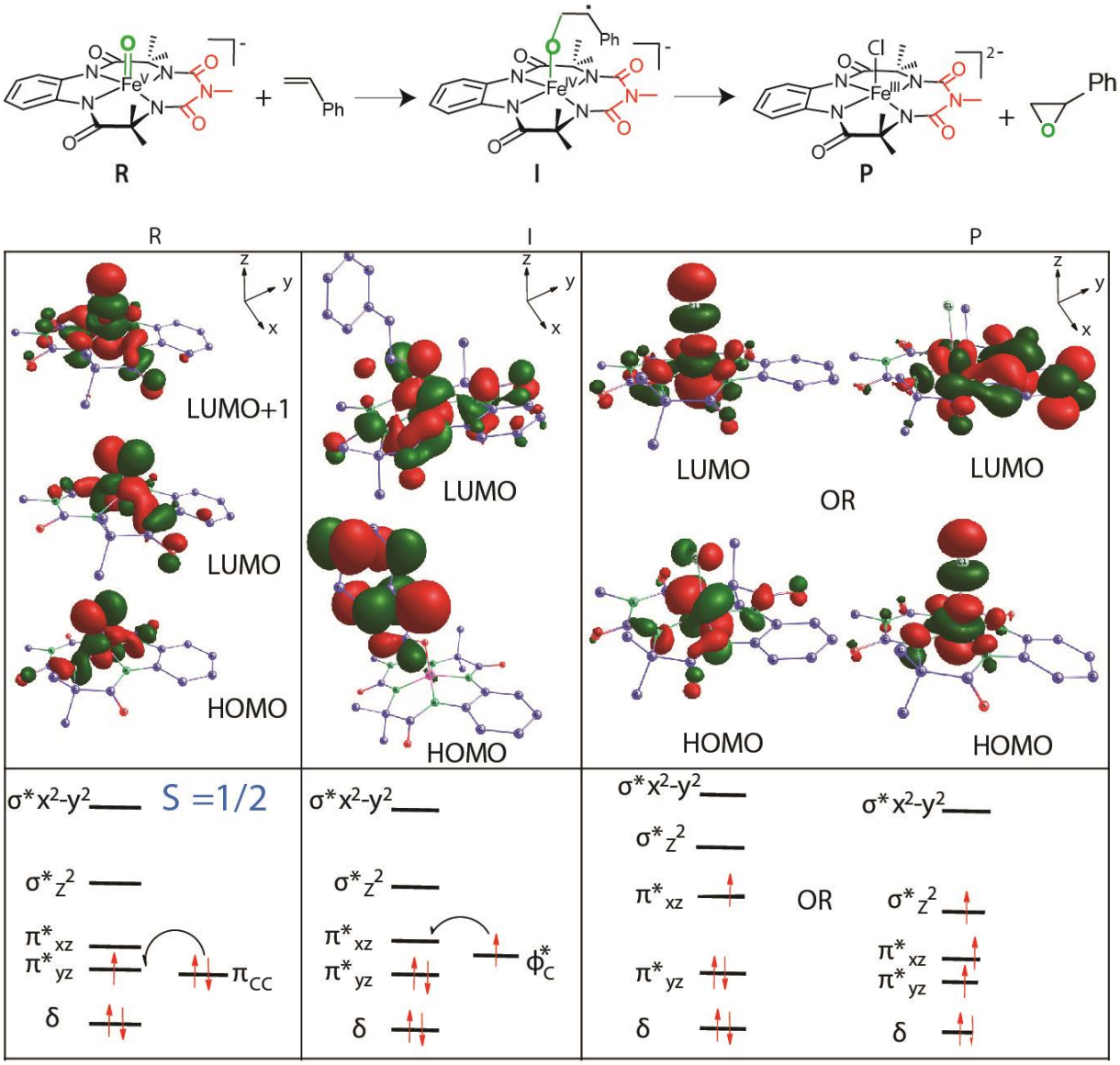

Figure 3.9. Molecular orbital pictures of the HOMO and LUMO of reactant, intermediate, and product, and orbital occupancy for styrene epoxidation by $Fe^{V}(O)$ at the ROB3LYP/6-31G*, LANL2DZ (Fe) level of theory in the gas phase.

3.4.7 Catalytic Activity

Quantitative regeneration of Fe^{III} (**1**) after the single-turnover reaction gave us an opportunity to study the epoxidation reaction in the catalytic condition. The catalytic epoxidation at RT in CH_3CN under air was performed with excess NaOCl (adjusted to pH 11.4). Different olefins (such as 4-methoxystyrene, methyl *trans*-cinnamate, and *trans*-stilbene) were used for the catalytic condition. To optimize reaction conditions, the influence of catalyst concentration was studied in the epoxidation of *cis*-stilbene, *trans*-stilbene, and methyl *trans*-cinnamate in the presence of catalyst **1**. It was observed that the increase in catalyst loading (1-1.5 %) leads to faster conversion and greater formation of epoxide due to the increase in the reaction rate (Appendix B8). When the catalyst loading was < 1%, less conversion was observed. If the reactions were performed under exclusion of dioxygen, the conversion and yield of epoxide were unaffected; this indicates that molecular oxygen did not have any role in the formation of epoxide. The products formed under optimized reaction conditions are shown in Table 3.5. Under our reaction condition, side products included *trans*-diol and aldehydes, but the amounts were less than 5 % of the epoxide. $PhCH_2C(O)Ph$ was also identified as a side product during the epoxidation of the *cis*/*trans*-stilbene reactions. In the case of 4-methoxystyrene, the increase in reaction time leads to increased conversion of an alkene, but with reduced yield of epoxide. Several unidentified side products were observed during this reaction.

Table 3.5. Summary of the Catalytic Epoxidation[a] of Different Alkenes by **1** at RT in CH_3CN under Air

Alkene	**Conversion (%)**	**Yield[c] (%)/ Epoxide (Reaction time)**
4-methoxy styrene [a]	74	79 (10 min)
cis-stilbene[b]	97	86 (40 min)
trans-stilbene[a]	99	89 (40 min)
methyl *trans*-cinnamate[b]	95	90 (70 min)

[a]Catalyst **1** (1×10^{-4} M):NaOCl (2×10^{-2} M):Substrates (1×10^{-2} M) = 1: 200:100). [b]Catalyst **1** (1.5×10^{-4} M):NaOCl (3×10^{-2} M):Substrates (1×10^{-2} M) = 1.5:300:67).[c] Yield of epoxides is with respect to alkenes consumed during the reaction (5% error).

4.4.8 Proposed Catalytic Cycle

Scheme 3.5. Proposed Catalytic Cycle for Epoxidation with Complex **1** and NaOCl

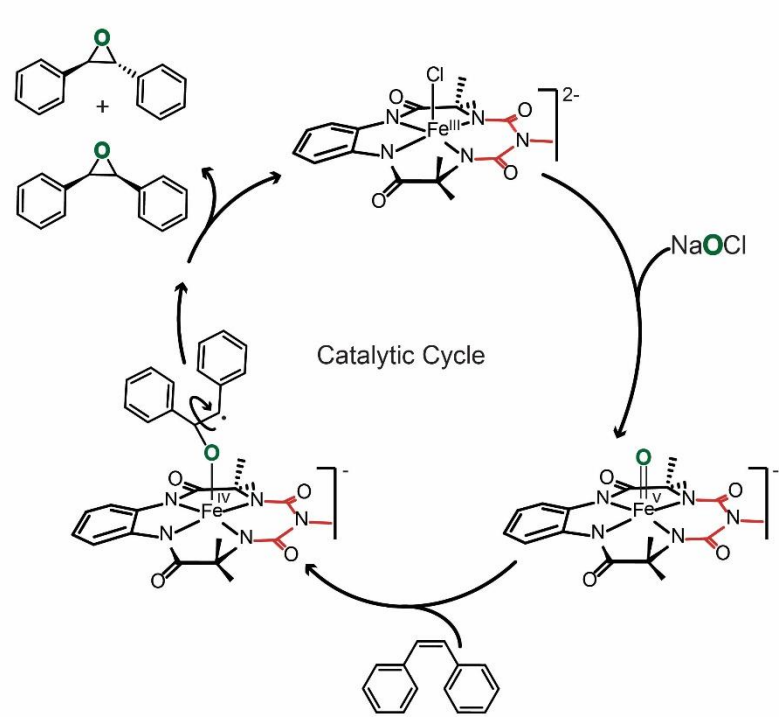

4.5 Conclusion

A mechanism has been proposed for the epoxidation of olefins by $Fe^{V}(O)$ (see Scheme 3.5). Using a combination of experiments and theoretical calculations, we show that the epoxidation proceeds via generation of a radical intermediate through an electrophilic attack on the alkene (Scheme 3.4, path A). This is followed by a very fast (low-barrier) ring-closing step. There is an 8000-fold rate difference between electron-rich and electron-deficient substrates, which indicates the electrophilic character of $Fe^{V}(O)$ and is reminiscent of Class A Fe-based epoxidation catalysts. DFT calculations suggest that the reaction proceeds via a two-step process and that both involve a doublet spin surface. We also show that the epoxidation can be carried out in a catalytic manner with modest yields and turnover numbers. Currently, we are studying the deactivation pathways of the catalytic reaction to try to develop more robust catalytic systems.

3.6 References

1. Lane, B. S.; Burgess, K. *Chem. Rev*. **2003**, *103*, 2457. (b) Que, L. Jr. *Acc. Chem. Res*. **2007**, *40*, 493.
2. (a) Ostović, D.; Bruice, T. C. *Acc. Chem. Res*. **1992**, *25*, 314. (b) Stephenson, N. A.; Bell, A. T. *J. Am. Chem. Soc*. **2005**, *127*, 8635. (c) Traylor, T. G.; Miksztal, A. R. *J. Am. Chem. Soc*. **1989**, *111*, 7443. (d) Que, L., Jr.; Tolman, W. B. *Nature* **2008**, *455*, 333.
3. (a) Fruetel, J. A.; Collins, J. R.; Camper, D. L.; Loew, G. H.; Ortiz de Montellano, P. R. *J. Am. Chem. Soc*. **1992**, *114*, 6987. (b) Vaz, A. D. N.; McGinnity, D. F.; Coon, M. J. *Proc. Natl. Acad. Sci. USA*. **1998**, *95*, 3555. (c) Kumar, D. de Visser, S. P.; Shaik, S. *Chem. Eur. J*. **2005**, *11*, 2825. (d) Groves, J. T.; Myers, R. S. *J. Am. Chem. Soc*. **1983**, *105*, 5791. (e) Song, W. J.; Ryu, Y. O.; Song, R.; Nam, W. *J. Biol. Inorg. Chem*. **2005**, *10*, 294. (f) Fusii, H. *Coord. Chem. Rev*. **2002**, *226*, 51.
4. (a) Moelands, M. A. H.; Nijsse, S.; Folkertsma, E.; de Bruin, B.; Lutz, M.; Spek, A. L.; Klein Gebbink, R. J. M. *Inorg. Chem*. **2013**, *52*, 7394. (b) Tiwa T.; Nakada M. *J. Am. Chem. Soc*. **2012**, *134*, 13538. (c) Feng, Y.; England, J.; Que, L., Jr. *Acs. Catal*. **2011**, *1*, 1035. (d) Krebs, C.; Fujimori, D. G.; Wals, C. T.; Bollinger, J. M. *Acc. Chem. Res*. **2007**, *40*, 484.
5. (a) Mas-Ballesté, R.; Que, L., Jr. *J. Am. Chem. Soc*. **2007**, *129*, 15964. (b) Ye, W.; Ho, D. M.; Friedle, S.; Palluccio, T. D.; Rybak-Akimova, E. V. *Inorg. Chem*. **2012**, *51*, 5006. (c) Suh, Y.; Seo, M. S.; Kim, K. M.; Kim, Y. S.; Jang, H. G.; Tosha, T.; Kitagawa, T.; Kim, J.; Nam, W. *J. Inorg. Biochem.*. **2006**, *100*, 627.
6. (a) Fujita, M.; Costas, M.; Que, L., Jr. *J. Am. Chem. Soc*. **2003**, *125*, 9912. (b) Chen, K.; Costas, M.; Kim, J.; Tipton, A. K.; Que, L., Jr. *J. Am. Chem. Soc*. **2002**, *124*, 3026.
7. (a) Lyakin, O. Y.; Bryliakov, K. P.; Britovsek, G. J. P.; Talsi, E. P. *J. Am. Chem. Soc*. **2009**, *131*, 10798. (b) Ghosh, M.; Singh, K. K.; Panda, C.; Weitz, A.; Hendrich, M. P.; Collins, T. J.; Dhar, B. B.; Sen Gupta, S. *J. Am. Chem. Soc.* **2014**, *136*, 9524.
8. (a) Panda, C.; Debgupta, J.; Diaz Diaz, D.; Singh, K. K.; Sen Gupta S.; Dhar, B. B. *J. Am. Chem. Soc.* **2014**, 136, 12273. (b) Singh, K. K.; Tiwari, k. M.; Ghosh, M.; Panda, C.; Weitz, A.; Hendrich, M. P.; Dhar, B. B.; Sen Gupta, S. *Inorg. Chem.* **2015**, *54*, 1535.

9. (a) Panda, C.; Ghosh, M.; Panda, T.; Banerjee R.; Sen Gupta, S. *Chem. Commun.* **2011**, *47*, 8016. (b) Wittig, G; Schoellkopf, U. *Org. Synth. Coll. Vol.* **1973**, *5*, 751. Procedure: Methyltriphenylphosphonium bromide (1.1 eq) was dissolved in dry tetrahydrofurane (25 ml) under inert condition and to it n-butyl lithium (1.2 eq) was added drop wise. It formed yellow color solution. Then after 1 hour stirring of reaction solution at 0 ^{o}C, 4-cyanobenzaldehyde (1 gm) was added. Reaction was stirred overnight then solvent was evaporated by rotary evaporator. Crude product was adsorbed over silica and compound was separated by column chromatography.
10. Kundu, S.; Thompson, J. V. K.; Ryabov, A. D.; Collins, T. J. *J. Am. Chem. Soc.* **2011**, *133*, 18546.
11. (a) Perdew, J. P.; Chevary, S. H.; Vosko, K. A.; Jackson, K. A.; Pederson, M. R.; Singh, D. J.; Fiolhais, C. *Phys. Rev. B* **1992**, *46*, 6671. (b) Perdew, J. P.; Chevary, S. H.; Vosko, K.A.; Jackson, K. A.; Pederson, M. R.; Singh, D. J.; Fiolhais, C. *Phys. Rev. B* **1993**, *48*, 4978. (c) Perdew, J. P.; Burke, K.; Wang, Y. *Phys. Rev. B* **1996**, *54*, 16533. (d) Adamo, C.; Barone, V. *J. Chem. Phys.* **1998**, *108*, 664. (e) Becke, A. D. *J. Chem. Phys.* **1993**, *98*, 5648. (f) Lee, C.; Yang, W.; Parr, R. G. *Phys. Rev. B* **1988**, *37*, 785. (g) Roothan, C. C. J. *Rev. Mod. Phy.* **1951**, *23*, 69. (h) McWeeny R.; Dierksen, G. *J. Chem. Phys.* **1968**, *49*, 4852. (i) Pople, J. A.; Nesbet, R. K. *J. Chem. Phys.* **1954**, *22*, 571.
12. Frisch, M. J.; Trucks, G. W.; Schlegel, H. B.; Scuseria, G. E.; Robb, M. A.; Cheeseman, J. R.; Scalmani, G.; Barone, V.; Mennucci, B.; Petersson, G. A.; Nakatsuji, H.; Caricato, M.; Li, X.; Hratchian, H. P.; Izmaylov, A. F.; Bloino, J.; Zheng, G.; Sonnenberg, J. L.; Hada, M.; Ehara, M.; Toyota, K.; Fukuda, R.; Hasegawa, J.; Ishida, M.; Nakajima, T.; Honda, Y.; Kitao, O.; Nakai, H.; Vreven, T.; Montgomery, J. A. Jr.; Peralta, J. E.; Ogliaro, F.; Bearpark, M.; Heyd, J. J.; Brothers, E.; Kudin, K. N.; Staroverov, V. N.; Kobayashi, R.; Normand, J.; Raghavachari, K.; Rendell, A.; Burant, J. C.; Iyengar, S. S.; Tomasi, J.; Cossi, M.; Rega, N.; Millam, J. M.; Klene, M.; Knox, J. E.; Cross, J. B.; Bakken, V.; Adamo, C.; Jaramillo, J.; Gomperts, R.; Stratmann, R. E.; Yazyev, O.; Austin, A. J.; Cammi, R.; Pomelli, C.; Ochterski, J. W.; Martin, R. L.; Morokuma, K.; Zakrzewski, V. G.; Voth, G. A.; Salvador, P.; Dannenberg, J. J.; Dapprich, S.; Daniels, A. D.; Farkas, Ö.; Foresman, J. B.; Ortiz, J. V.; Cioslowski, J.; Fox, D. J. Gaussian 09, revision B.01; Gaussian, Inc.: Wallingford, CT, **2009**.

13. Groves, J. T.; Watanabe, Y. *J. Am. Chem. Soc*. **1986**, *108*, 507.
14. (a) Collman, J. P.; Kodadek, T.; Brauman, J. I. *J. Am. Chem. Soc*. **1986**, *108*, 2588. (b) Castellino, A. J.; Bruice, T. C. *J. Am. Chem. Soc*. **1988**, *110*, 158.
15. (a) Groves, J. T.; Kruper, W. J.; Jr.; Haushalter, R. C. *J. Am. Chem. Soc*. **1980**, *102*, 6375. (b) Guengerich, F. P.; Macdonald, T. L. *Acc. Chem. Res*. **1984**, *17*, 9. (c) Castellino, A. J.; Bruice, T. C. *J. Am. Chem. Soc*. **1988**, *110*, 1313.
16. (a) Srinivasan, K.; Michaud, P.; Kochi, J. K. *J. Am. Chem. Soc*. **1986**, *108*, 2309. (b) Yoon, H.; Burrows, C. J. *J. Am. Chem. Soc*. **1988**, *110*, 4087. (c) Zhang, W.; Loebach, J. L.; Wilson, S. R.; Jacobsen, E. N. *J. Am. Chem. Soc*. **1990**, *112*, 2801.
17. (a) Cussó, O.; Garcia-Bosch, I.; Ribas, X.; Lloret-Fillol, J.; Costas, M. *J. Am. Chem. Soc*. **2013**, *135*, 14871. (b) Nam, W.; Lim, M. H.; Oh, S.- Y.; Lee, J. H.; Lee, H. J. Woo, S. K.; Kim, C.; Shin, W. *Angew. Chem. Int. Ed*. **2000**, *39*, 3646. (c) Nam, W.; Lee, H. J.; Oh, S.- Y.; Kim, C.; Jang, H. G. *J. Inorg. Biochem.*. **2000**, *80*, 219.
18. Arasasingham, R. D.; He, G.- X.; Bruice, T. C. *J. Am. Chem. Soc*. **1993**, *115*, 7985.
19. Garrison, J. M.; Ostović, D.; Bruice, T. C. *J. Am. Chem. Soc*. **1989**, *111*, 4960.
20. (a) Meunier, B.; Guilmet, E.; Carvalho, M.- E. De; Poilblanc, R. *J. Am. Chem. Soc*. **1984**, *106*, 6668. (b) Shaik, S.; Hirao, H.; Kumar, D. *Acc. Chem. Res*. **2007**, *40*, 532. (c) Kumar, D.; Karamzadeh, B.; Sastry, G. N.; de Visser, S. P. *J. Am. Chem. Soc*. **2010**, *132*, 7656.
21. (a) Barone, V.; Cossi, M. *J. Phys. Chem. A* **1998**, *102*, 1995. (b) Cossi, M.; Rega, N.; Scalmani, G.; Barone, V. *J. Comp. Chem.* **2003**, *24*, 669.
22. (a) Schubert, W. M.; Keeffe, J. R. *J. Am. Chem. Soc*. **1972**, *94*, 559. (b) Yates, K.; MacDonald, R. S.; Shapiro, S. A. *J. Org. Chem*. **1973**, 38, 2460.
23. (a) Cho, K.- B.; Shaik, S.; Naam, W. *J. Phys. Chem. Lett*. **2012**, *3*, 2851. (b) Kwon, E.; Cho, K.- B.; Hong, S.; Naam, W. *Chem. Commun*. **2014**, *50*, 5572.
24. Jean, Y.; *Molecular Orbitals of Transition Metal Complexes*. Oxford University Press Inc., New York. **2005**. Page 61.
25. (a) Pysh, E. **S.;** Yang, **N.** C. *J. Am. Chem. Soc.* **1963**, *85***,** 2124. (b) Loveland, J. W.; Dimeler, G. R. *Anal. Chem.* **1961**, *33*, 1196. (c) Neikman, W. C.; Dimeler, G. R.; Desmond, M. M. *J. Electrochem. Soc.* **1964,** *111*, 1190.

Chapter IV

Reductive Activation of O_2 by a Bioinspired Fe-Complex for Catalytic Epoxidation Reactions

4.1 Abstract

Use of molecular oxygen (O_2) by enzymes is vital for many processes in biological systems. Some of these enzymes are known for an O_2 carrier or its storage while others do biochemical transformation. Hence, the understanding of O_2 activation for various chemical reactions is important. The dioxygen activation by cytochrome P450 is accomplished by using NADP (coenzyme) as an exogenous electron source. In a similar approach, many synthetic model complexes are known to activate O_2 using sacrificial reductant (hydride, H_2/Pt, ascorbic acid, *etc*.). However, the additional use of chemical as a sacrificial reductant is avoidable for the synthetic use of O_2 as an oxygen atom source. Therefore, development of metal complexes for oxidation reactions without the use of sacrificial reductant is desirable. Aerobic epoxidation of olefins catalyzed by iron complexes without the use of sacrificial coreductant is unknown. We report the reductive activation of O_2 by a bioinspired $[(bTAML)Fe^{III}(H_2O)]^-$ (**1**) complex to catalyze the epoxidation of alkenes with TONs of up to 80. Due to the low redox potential of metal center in $[(bTAML)Fe^{III}(H_2O)]^-$ complex, Fe^{III} itself can act as an electron source to reduce the O_2 molecule, and both the oxygen atom get transferred to the substrate. The $[(bTAML)Fe^{III}(H_2O)]^-$ complex serve as a mimic of the dioxygenase enzymes, which is very uncommon in model systems. Spectroscopic and kinetic evidence indicates the involvement of $Fe^{V}(O)$ as the active oxidant during the reaction. Mechanistic studies using UV-vis and EPR spectroscopy showed Fe-O_2 adduct formation upon O_2 interaction with the iron center.

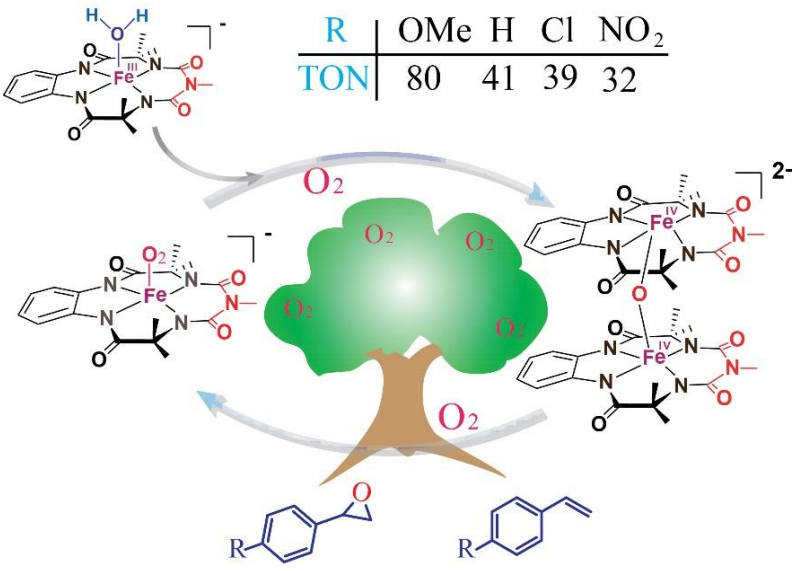

4.2 Introduction

Interaction of oxygen molecule with the metal center in metalloenzymes is central to several biological processes.[1] For example, Hemoglobin (Hb) transports oxygen from lungs to tissues and myoglobin (Mb) stores oxygen in muscle cells which is used for the energy production.[2] In contrast, P450 cytochrome monooxygenases do reductive activation of oxygen and transfer the oxygen atom into various organic molecules (Figure 4.1).[3] Hence, the study of iron-oxygen interaction, as well as activation of molecular oxygen (O_2) for organic transformation by model complexes, is required for more insight into the structural and functional understanding of enzymes.

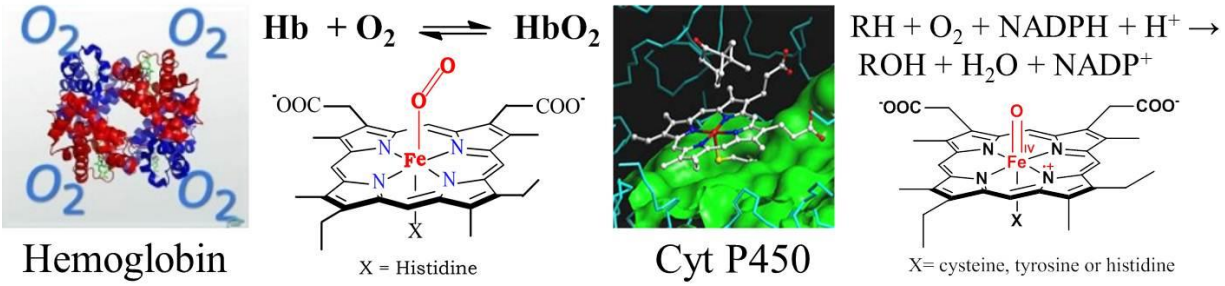

Figure 4.1. Examples of iron-containing metalloenzymes and intermediates during their biological function, Hemoglobin (in left)[2] and Cytochrome P450 (in right).[3]

Among organic transformations, epoxides represent an extremely important class of chemicals both to synthetic chemists and chemical industries. Traditionally, epoxides are synthesized by intramolecular etherification of intermediate chlorohydrins formed by the reaction of alkenes with hypochlorous acid or by the reaction of peracids with alkenes. Safety and environmental concerns have led to the development of catalytic epoxidation methods using alkyl hydroperoxides and hydrogen peroxide.[4] The major limitations of peroxide based oxidants are their sensitive nature towards self-decomposition and the subsequent catalysis of a radical-chain reaction at higher concentrations. A more efficient and greener approach would be catalytic oxygen atom transfer from dioxygen to alkenes, resulting in the formation of epoxides as is observed in monooxygenases such as cytochrome P450. The stoichiometry of this reaction requires two electrons from an exogenous source which is typically a coenzyme.[3] Thus, most functional mimics of cytochrome P450 which catalyze epoxide formation have employed reduced oxygen species such as peroxides as terminal oxidants.[5] Epoxide formation *via* reductive activation of dioxygen by metal complexes has been reported, but each requires the consumption of

at least stoichiometric amounts of a reducing agent (hydride, H_2/Pt, ascorbic acid, *etc*.).[6] Even the use of inexpensive electron and proton sources is unsatisfactory for the large scale synthesis of epoxides. It is, however, possible to conceive dioxygenase activity for metal complexes, especially with the cheap and environmentally friendly metal Fe, for oxidation reactions, without the use of a sacrificial reductant as shown below (Scheme 4.1).

Scheme 4.1. Use of O_2 by Dioxygenases in Oxygen Atom Transfer Reaction.

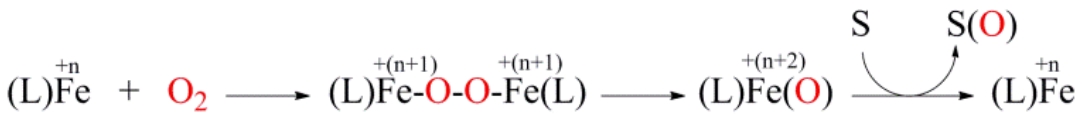

S = substrate; L = ligand

Few such efforts have been reported in the literature for iron-heme,[7] iron-nonheme[8], and Fe-TAML[9] complexes. Electron withdrawing substituted porphyrin complexes have been shown to be an active catalyst for the hydroxylation of light alkanes by O_2 under mild conditions (1 atmosphere O_2, 25 $^{\circ}$C).[7(b)] However, mechanistic studies indicate a radical-chain autoxidation pathway which results in poor selectivity.[10] A mononuclear non-heme iron complex, $[Fe^{II}(TMC)(CF_3SO_3)_2]$ (TMC = 1,4,8,11-tetramethyl-1,4,8,11-tetraazacyclotetradecane), activates dioxygen for the catalytic aerobic oxidation of triphenyl phosphine, thioanisole and benzyl alcohol.[11] Fe-TAMLs have also been shown to activate O_2 to form the corresponding room temperature stable $[\{(TAML)Fe^{IV}\}_2$-μ-Oxo$]^{2-}$ dimer (TAML = tetraamido macrocyclic ligand). This dimer was reactive at elevated temperatures, but its reactivity was only limited to oxidation of benzyl alcohol.[9] However, due to the inability of these complexes to form a reactive high valent mononuclear iron-oxo complex by reductive activation of O_2, they remained catalytically inactive for reactions such as the epoxidation of alkenes to epoxides. It should, however, be noted that such aerobic epoxidation of olefins using a ruthenium porphyrin complex, $Ru^{IV}(TMP)(O)_2$ {TMP = 5, 10, 15, 20-(tetramesityl)porphyrin}, without any coreductant was reported in 1985 (Figure 4.2(A)).[12] Subsequently, epoxidation with other ruthenium complexes and a ruthenium substituted polyoxometalate, $\{[WZnRu_2(OH)(H_2O)](ZnW_9O_{34})_2\}^{11-}$ has also been observed (Figure 4.2(B)).[13] However, this epoxidation reaction was stoichiometric in nature and not catalytic. This limitation was due to the complete inhibition of O_2 binding to the ruthenium active center by alkene coordination. Although in a biomimetic approach a plethora of model iron complexes have been generated to activate molecular oxygen, none

of them have been proved as a potential epoxidation catalyst where molecular oxygen can be used as a terminal oxidant without the use of a coreductant.[14]

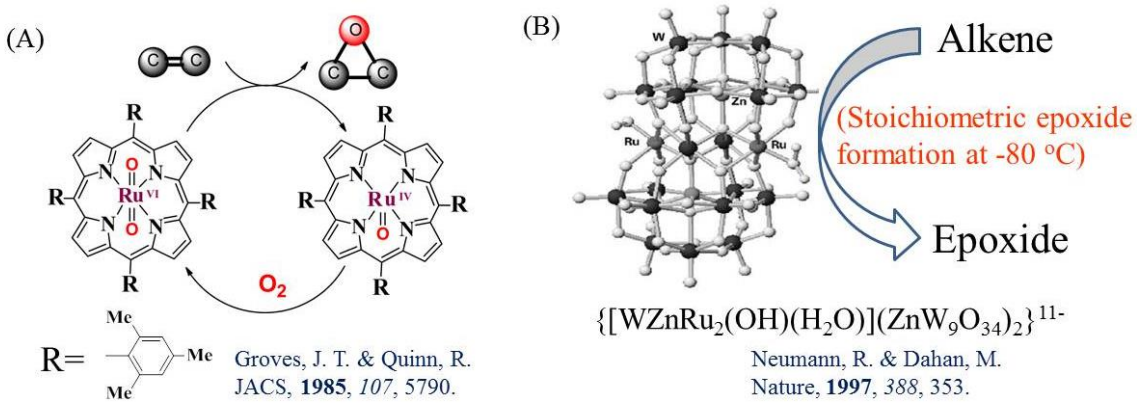

Figure. 4.2. Example for aerobic epoxidation without use of coreductant (A) $Ru^{IV}(TMP)(O)_2$ {TMP = 5, 10, 15, 20-(tetramesityl)porphyrin};[12] (B) Ruthenium substituted polyoxometalate, $\{[WZnRu_2(OH)(H_2O)](ZnW_9O_{34})_2\}^{11-}$.[13]

We have recently shown that Fe complexes of biuret-modified TAML (bTAML) can be transformed into the corresponding $[\{(bTAML)Fe^{IV}\}_2$-μ-Oxo$]^{2-}$ dimer (**2**) by reaction with 0.5 equiv. of NaOCl. Dimer **2** is a competent oxidant for both epoxidation of alkenes and hydroxylation of alkanes unlike the prototype Fe-TAML reported earlier by Collins.[15] Mechanistic studies indicate that dimer (**2**) exists in equilibrium with the starting $[(bTAML)Fe^{III}]^-$ complex and $[(bTAML)Fe^{V}(O)]^-$ complex (**3**), which upon reaction with alkenes and alkanes results in the quantitative regeneration of the starting Fe^{III} complex (**1**) at the end of the reaction.[15(b),15(d)] Since such μ-Oxo-Fe^{IV}_2 dimers can also be quantitatively generated from the reaction of Fe^{III}-TAML and O_2; we hypothesized that catalytic epoxidation of alkenes could be performed only with complex **1** and O_2 as is shown in Scheme 4.2. In this work, for the first time, we report the catalytic epoxidation of alkenes by a Fe complex using O_2 as the oxidant in the absence of any added sacrificial reductant (Scheme 4.2).

Scheme 4.2. Aerobic Catalytic Epoxidation with **1**.

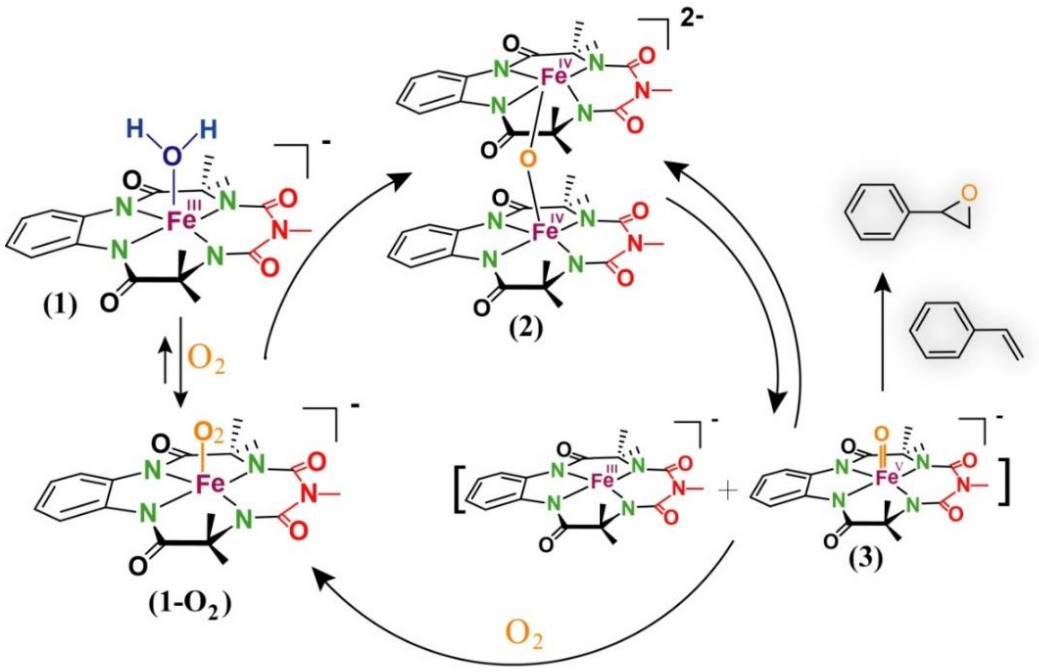

4.3 Experimental Section

4.3.1 Materials

An axially ligated aqua complex $[PPh_4][(bTAML)Fe^{III}(OH_2)]$ (**1**) was synthesized by metathesis reaction of $[Li][(bTAML)Fe^{III}(OH_2)]$ with excess amount of PPh_4Cl in water.[15(a)] Dichloromethane (DCM) and 1, 2-dichlorobenzene (DCB) were purified and dried according to the published procedure.[19] Styrene, 4-chlororstyrene, 4-methoxystyrene, 4-nitrostyrene were purchased from Aldrich and distilled before use. *cis*-stilbene, *trans*-stilbene, norbornene and methyl *trans*-cinnamate were purchased from Aldrich and used as received. All other solvents and reagents were purchased from Aldrich or other commercial sources and were used as received, unless otherwise noted. 98% ^{18}O enriched water ($H_2{}^{18}O$) was procured from Shanghai Research Institute of Chemical Industry, China. $^{18}O_2$ was received from Icon (Isotopes) Services Inc.

4.3.2 General Instrumentation

UV-vis spectral studies were carried out using Agilent diode array 8453 spectrophotometer attached to an electrically controlled thermostat. GC-MS was performed on a Thermo Scientific ISQ QD Mass Spectrometer attached with Thermo Scientific TRACE 1300 gas chromatograph using an HP-5ms capillary column (30 m × 0.25 mm ×

0.25 μm, J&W Scientific) with helium as the carrier gas. HR-MS was performed in a Thermo Scientific Q-Exactive Orbitrap analyzer using an electrospray ionization source connected with a C18 column (150 m × 4.6 mm × 8.0 μm). X-band EPR spectra was recorded on Bruker EMX EPR spectrometer equipped with a liquid nitrogen cryostat.

4.3.3 Electron Paramagnetic Resonance (EPR) Measurements

Solution of complex **1** (8.0 mM) was prepared in degassed dichloromethane (DCM) and in aerated DCM. X-band EPR measurement was performed at 100 K temperature. A modulation frequency of 100 kHz was used for the EPR spectral measurements.

4.3.4 Catalytic Reaction of Complex 1 with Alkenes under Oxygen Pressure

Complex **1** (0.25 mM) was dissolved in 5 mL dry DCM in a 20 ml reactor and 40 mM of substrate was added to the solution. Reactor was tightly closed and O_2 gas pressure (5 bar or as per need of experiment (10 bar, 20 bar)) was inserted through inlet of the reactor. Inlet was closed and reaction solution was stirred for 20 h under oxygen pressure. After end of the reaction, the product was identified and quantified by GC-MS. Calibration curve for all epoxides were obtained from corresponding authentic epoxides for product quantification. Similar reaction conditions were used for all the substrates.

4.3.5 Catalytic Reaction of Complex 1 with Alkenes at Atmospheric Pressure and at Different Temperature

The reaction condition used was similar for all the alkenes that are described below. Compound **1** (0.25 mM) was dissolved in 1,2-dichlorobenzene (5 ml) and 40 mM of styrene was added to the solution. Three sets of reaction mixture were stirred at different temperatures of 25 ˚C, 50 ˚C, and 70 ˚C and turnover number (TON) of styrene oxide product (quantified by GC-MS) was monitored with time (Figure 4.3). Faster completion of reaction was observed when temperature of the reaction mixture was increased. However, an optimal temperature of 50 ˚C was used for all substrates. Due to insolubility of catalyst **1** in 1, 2-dichlorobenzene at 25 ˚C, a minimum amount of dichloromethane (300 μL) was added for proper solubility of complex.

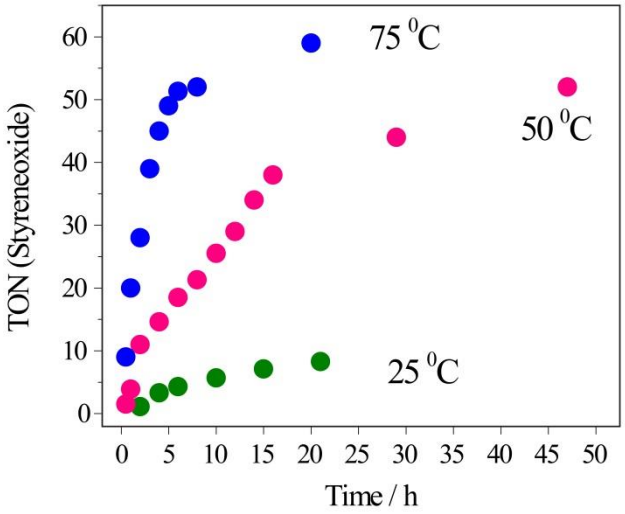

Figure 4.3. TON of styrene oxide trace with time at different temperature; 25 ˚C (green), 50 ˚C (red), and 70 ˚C (blue).

4.3.6 Reaction of Complex 1 with Thioanisole and Styrene in the Presence of $^{18}O_2$

To a solution of complex **1** (0.25 mM) in dry and oxygen free dichloromethane (DCM) was added thioanisole (40 mM), and subsequently the solution was purged with $^{18}O_2$. After 10 minute of the reaction, product was analyzed with GC-MS. Similar procedure was adopted for the reaction with styrene (reaction time 60 minute).

4.3.7 Reaction of $[PPh_4][(bTAML)Fe^{III}(H_2O)]$ with Styrene in the Presence of $H_2{}^{18}O$ in Air

To a solution of complex **1** (0.25 mM) in dichloromethane (DCM) was added styrene (40 mM) and 50 µL $H_2{}^{18}O$. After 60 minute of reaction, the product was analyzed with GC-MS.

4.3.8 Synthesis of Complex $[Et_4N][(bTAML)Fe^{IV}(Cl)]$

To a solution of $[Et_4N]_2[(bTAML)Fe^{III}(Cl)]$ (20 mg) in DCM, was added 10 equivalent of ceric ammonium nitrate (CAN) and the solution was stirred for 5 min. The solution was filtered through cotton and the solvent was evaporated by argon purging. The complex was then dissolved in minimum amount of acetone and subsequently stored at -20 ˚C for crystallization using slow diffusion method (diethyl ether as the co-solvent). Deep violet colored crystals were obtained which was confirmed as an $Et_4N[(bTAML)Fe^{IV}(Cl)]$ complex by single crystal X-ray diffraction measurement (Appendix C5). UV-vis

spectroscopic measurement showed absorbance at wavelength 543 (ε = ~ 5000 cm^{-1} M^{-1}) nm and 857 nm (broad) (Figure 4.4). This Fe^{IV} species is X-band EPR silent due to *S*=1 spin state.

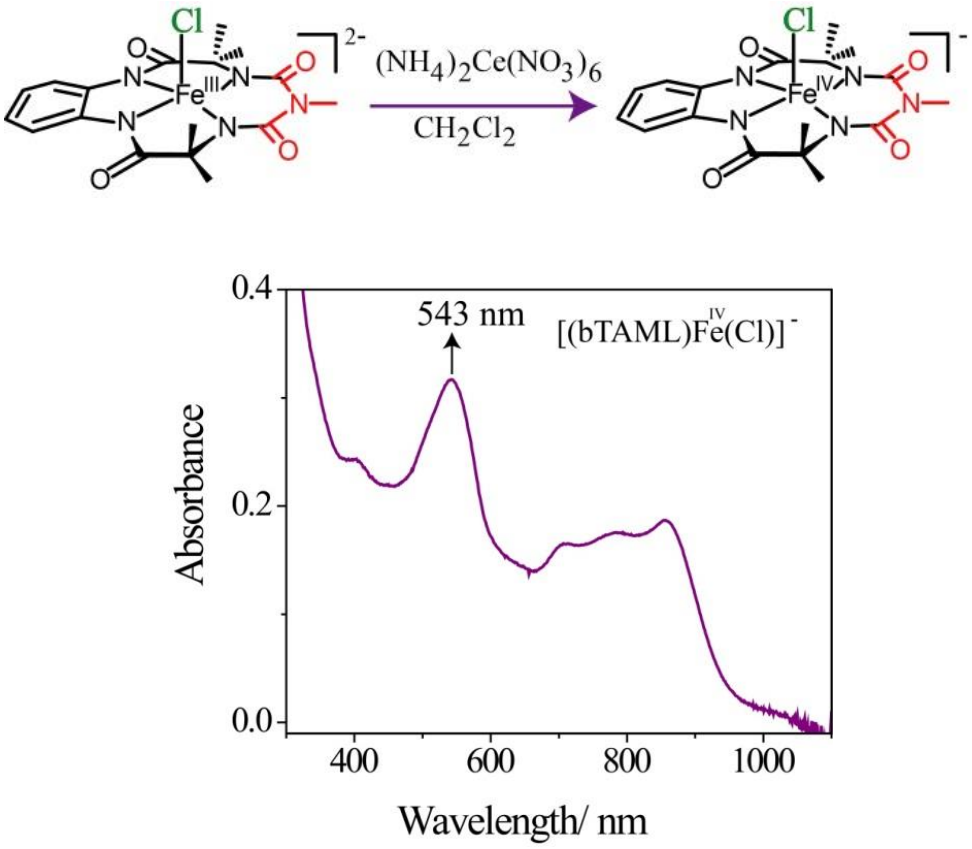

Figure 4.4. UV-vis spectrum of complex $[(bTAML)Fe^{IV}(Cl)]^-$ in dichloromethane formed by the reaction of $[(bTAML)Fe^{III}(Cl)]^{2-}$ with $(NH_4)_2Ce(NO_3)_6$ at room temperature (RT, 25 ˚C).

4.3.9 Synthesis of Complex $[(bTAML)Fe^{III}(superoxide)]^{2-}$

To a solution of the complex $[(bTAML)Fe^{III}(Cl)]^{2-}$ (4×10^{-5} M) in DCM, was added excess solid KO_2 at -40 ˚C in presence of 18-Crown-6. UV-vis spectrum showed generation of a new peak at 490 nm (Figure 4.5). This new species was assigned as an $[(bTAML)Fe^{III}(superoxide)]^{2-}$ complex due to its similarity with a recently reported $[(TAML)Fe^{III}(superoxide)]^{2-}$ complex with similar TAML ligand framework.[20]

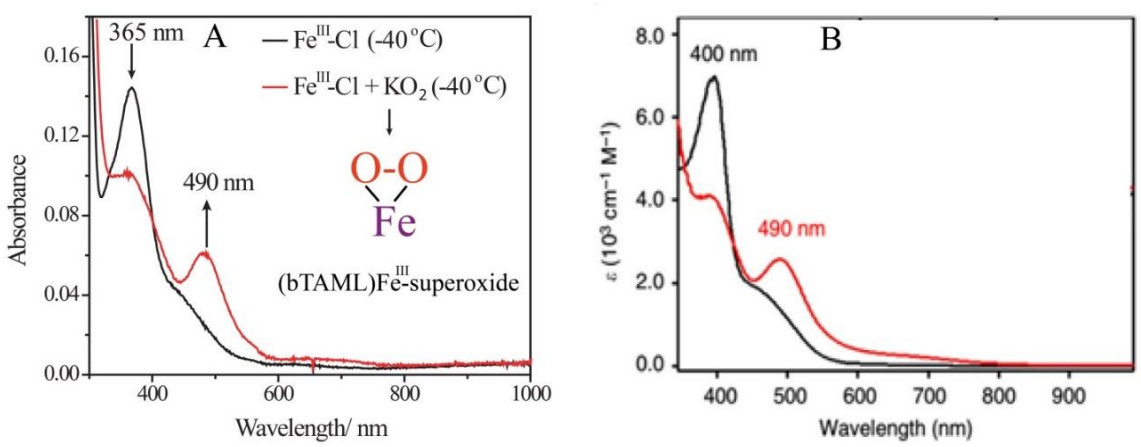

Figure 4.5. (A) UV-vis spectra of $[(bTAML)Fe^{III}(Cl)]^{2-}$ (black line) and $[(bTAML)Fe^{III}(O_2^{\cdot-})]^{2-}$ (red line) in DCM at -40 ˚C. (B) UV-vis spectra of $[(TAML)Fe^{III}(Cl)]^{2-}$ (black line) and $[(TAML)Fe^{III}(O_2^{\cdot-})]^{2-}$ (red line).[20]

4.3.10 Computational Details

For the structural comparison between $[\{(TAML)Fe^{IV}\}_2\text{-}\mu\text{-}oxo]^{2-}$ and $[\{(bTAML)Fe^{IV}\}_2\text{-}\mu\text{-}oxo]^{2-}$ complexes and energy values of complex, methods based on density functional theory (DFT) have been employed. Structures were fully optimized at the B3LYP/6-31G*, LANL2DZ (Fe) level of theory[21] using the Gaussian09 suite of quantum-chemical programs.[22] The stationary points on the potential energy surface were characterized by evaluating the vibrational frequencies. The zero-point vibrational energy corrections and thermal corrections were applied to the "bottom-of-the-well" values to obtain values for the Gibbs free energy at 298.15 K.

4.4 Results and Discussion

4.4.1 UV-vis Spectroscopic Observations for μ-Oxo-$(Fe^{IV})_2$ Dimer (2) Formation Using O_2 and Complex 1

We first investigated the reductive activation of O_2 by $[(bTAML)Fe^{III}(H_2O)]^-$ (**1**) using UV-vis spectroscopy. When solid complex **1** was added to dichloromethane (DCM; CH_2Cl_2) in the air, a reddish colored solution was observed which displayed an absorbance at 412 nm wavelength. Over time (~10 min) the color of the solution changed to dark brown and new spectral features having a broad peak between 850 and1050 nm were observed (Figure 4.6(B)). This solution having dark brown color has been previously characterized as dimer **2** using ^{1}H NMR and EPR.[15(b)] Dimer **2** has also been independently synthesized

earlier by the comproportionation reaction of $[(bTAML)Fe^{III}(Cl)]^{2-}$ and $[(bTAML)Fe^{V}(O)]^{-}$.[15(b)] Since the O-atom in dimer **2** was derived from molecular oxygen (shown earlier for related Fe-TAMLs and other iron complexes[9,16]), we hypothesized that the reddish color solution observed upon dissolution of solid **1** in DCM in air was likely a dioxygen adduct of (bTAML)Fe (**1-O₂**). To test this hypothesis, the reddish colored solution having a UV-vis spectral feature at 412 nm was freshly prepared and purged with argon (Ar) for 15 minutes. It was observed that the spectral feature of 412 nm disappeared and a new peak at 375 nm appeared, which remained unchanged over several hours of rigorous exclusion of O_2 (Figure 4.6(A)). A solution having an absorption maximum at 375 nm was also independently prepared by addition of **1** in DCM with rigorous exclusion of air. Upon exposing this solution to air, the spectral features changed, first with the appearance of a peak at 412 nm which then subsequently formed dimer **2** as shown below (Figure 4.6). Hence, the reactivity of **1** with O_2 to form the dimer complex **2** quantitatively was similar to what has been previously reported for Fe-heme and Fe-TAML. However, unlike other systems, this dimer with the bTAML ligand has been shown to be reactive with alkenes to form the corresponding epoxide under single turnover conditions, and the parent Fe^{III} complex (**1**) is quantitatively generated at the end of the reaction.[15(d)] We, therefore, attempted the catalytic epoxidation of alkenes with **1** as the catalyst and O_2 as the terminal oxidant without the use of any sacrificial reductant.

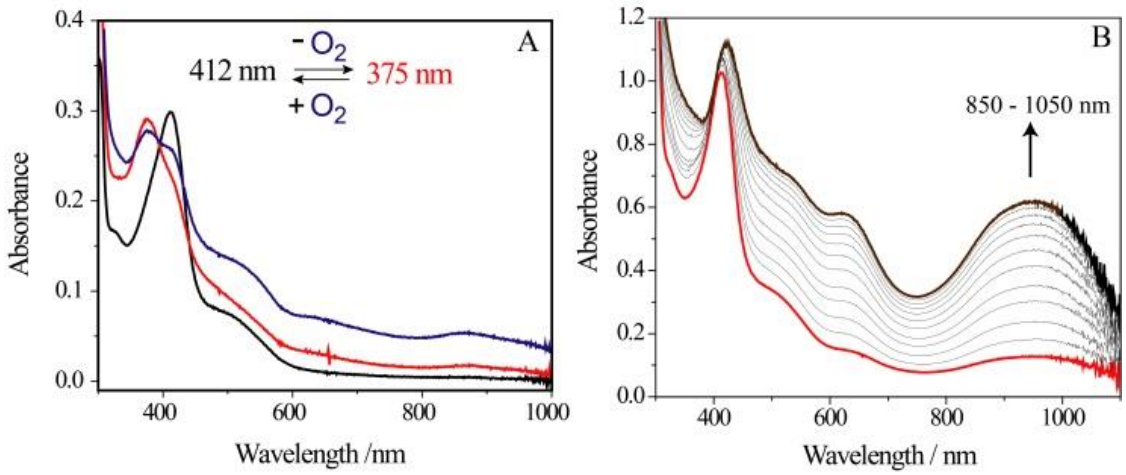

Figure 4.6. (A) UV–vis spectral changes for reversible O_2 binding with complex **1** in DCM at room temperature (25 °C) and (B) the UV-vis spectral scan for the formation of dimer complex **2** by the reaction of complex **1** (3×10^{-4} M) in DCM with air (10 min reaction time, 25 °C and atmospheric pressure).

4.4.2 Product Analysis After Reaction of 1 with Alkenes Using O_2

To a solution of styrene (40 mM, 1 equiv.) complex **1** (0.006 equiv.; 0.25 mM) in 5 mL DCM was added, and the reaction mixture was stirred at room temperature (RT, 25 °C) in the air for 20 hours. At the end of the reaction, analysis of the product showed the formation of styrene oxide (2 mM, TON 8, TON = turnover number; moles of the product divided by moles of catalyst **1**). We attempted to increase the product yield by carrying out the reaction at 5 bar O_2 pressure *via* increasing the reaction rate. A five-fold increase in the formation of styrene oxide (10 mM, TON 40) was observed at 5 bar O_2 pressure. Upon further increasing the O_2 pressure to 10 bars and 20 bars, a decrease in the TON (34 and 26, respectively) was observed (Appendix C1). Although high selectivity towards the formation of styrene oxide was observed (<10% side products), moderate yields of styrene oxide obtained led us to investigate the fate of the catalyst at the end of the reaction. It was observed that the color of the reaction mixture turned purple after completion of the reaction and the UV-vis spectrum of this spent reaction mixture showed the formation of a monomeric Fe^{IV} complex reminiscent of $[(bTAML)Fe^{IV}(Cl)]^-$ which has been independently synthesized by us (Figure 4.4). Analysis of the spent reaction mixture by UV-vis spectroscopy and HR-MS showed the presence of the $[(bTAML)Fe^{IV}(Cl)]^-$ complex (Figure 4.7). We hypothesized that this monomeric $[(bTAML)Fe^{IV}(Cl)]^-$ complex was formed from either the reaction of $Fe^{V}(O)$ (**3**) (which exists in equilibrium with the dimer complex **2**) with DCM (Figure 4.8) or by a radical chain reaction, where Cl radicals can react with complex **1**. Thus, a likely inactivation pathway of the catalyst during the epoxidation reaction is DCM solvent mediated.

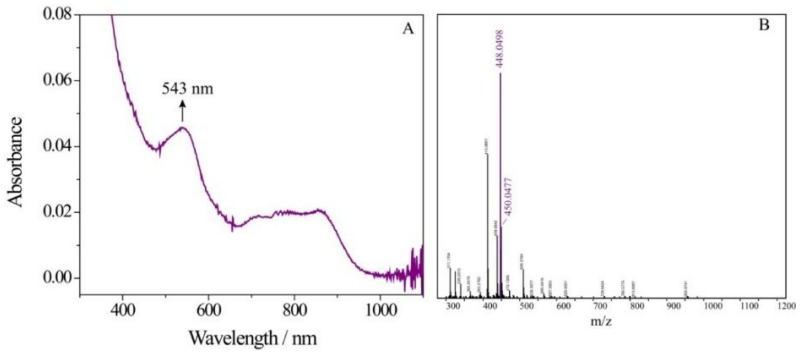

Figure 4.7. (A) UV-vis spectra of the reaction mixture after completion of the reaction with complex **1** and styrene at 5 bar O_2 pressure. The UV-vis observed is similar to the $[(bTAML)Fe^{IV}(Cl)]^-$ complex. (B) HR-MS of the reaction mixture after completion of the reaction with complex **1** and styrene at 5 bar O_2 pressure. Calculated m/z of $[(bTAML)Fe^{IV}(Cl)]^-$ is 448.0475. Observed m/z 448.0498.

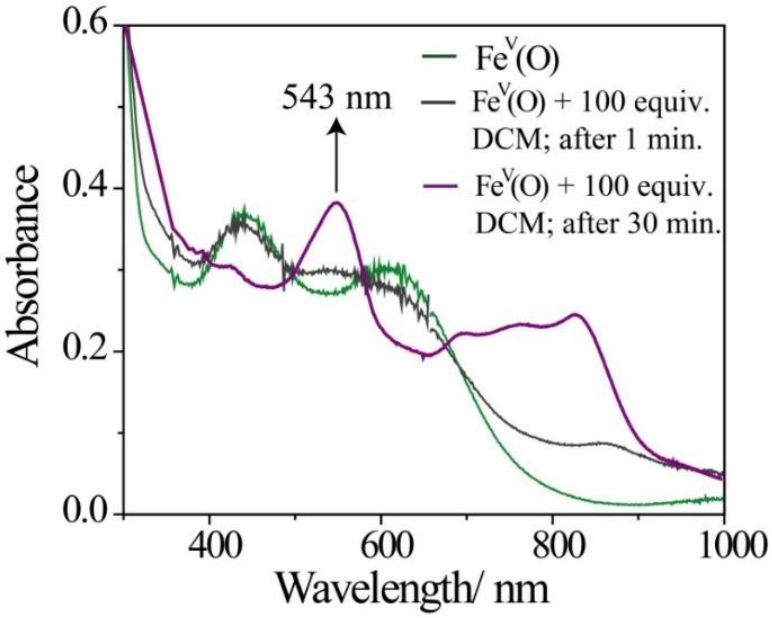

Figure 4.8. UV-vis spectral change for the reaction of $[(bTAML)Fe^{V}(O)]^{-}$ (1×10^{-4} M) with 100 equiv. of CH_2Cl_2 in acetonitrile. Monomeric $[(bTAML)Fe^{IV}(Cl)]^{-}$ was formed at the end of the reaction.

In order to avoid the catalyst deactivation reaction described above, we investigated the use of 1, 2-dichlorobenzene (DCB) as an alternative solvent. DCB is unreactive towards $Fe^{V}(O)$, and also has the necessary properties of hydrophobicity required for O_2 activation. Since complex **1** was fairly insoluble in 1, 2-dichlorobenzene at room temperature (25 °C), an elevated temperature of 50 °C was used to increase its solubility during the reaction (Figure 4.3). Using DCB as the solvent at 50 °C under atmospheric pressure of air, epoxidation of styrene resulted in styrene oxide with moderate yields (10 mM, TON 41). For the electron-rich alkene 4-methoxystyrene, the amount of epoxide obtained doubled to 20 mM (TON: 80; Table 4.1, entry 1) while with an electron deficient alkene like methyl *trans*-cinnamate, a very small yield of the epoxide product was obtained (TON: 0.4; Table 4.1, entry 8). The selectivity of the catalyst towards oxidation of the C=C bond over the C-H bond was observed in the case of norbornene. This is in line with what was observed for the reactions of norbornene with $Fe^{V}(O)$.[15(d)] A low yield of the epoxide product was obtained with *trans*-stilbene (TON = 2.4; Table 4.1, entry 7) in comparison to *cis*-stilbene (TON = 12; Table 4.1, entry 6). The most probable reason for the reduced yield of epoxide with *trans*-stilbene is its sterically bulky nature which hinders the approach of the iron-oxo intermediate towards the C=C bond.

Table 4.1. Epoxidation of Different Alkenes by Complex **1** and O_2 in DCB at 50 °C.

Entry	Substrate	Product	TON	Other products	TON
1.	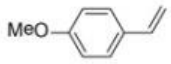	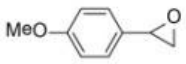	80 (5)	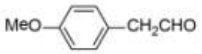	Trace
				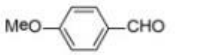	3.9
2.	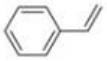	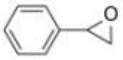	41 (3)	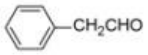	1.6
				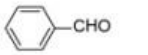	1.9
3.		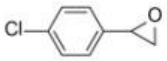	39 (3)	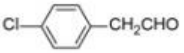	3.9
				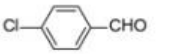	2.1
4.	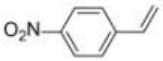		32 (3)	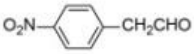	2.9
5.			29 (3)		0.9
6.		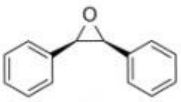	09 (1)	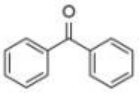	0.9
		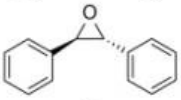	03 (0.2)	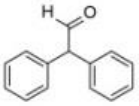	1.1
7.	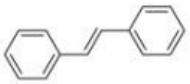	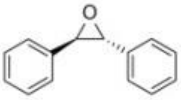	2.4 (0.2)	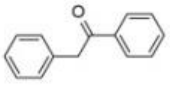	0.6
8.	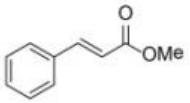	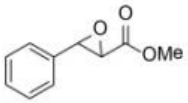	0.4 (0.1)		

Reaction conditions: Complex **1** (0.25 mM), substrate (40 mM), air (atmospheric pressure), temperature 50 °C, 20 hours; TON = moles of product/moles of catalyst **1**; values in parentheses represent the possible error (±) in TON determination.

4.4.3 Hammett Plot

In order to understand the effect of the electronic environment associated with the substituent on styrene, different *para*-substituted styrene derivatives were studied, and an enhanced rate of epoxide formation was obtained for electron donating substituents compared to electron withdrawing *para* substituents. A relatively small Hammett ρ value of –0.87 was obtained for styrene and its *para*-substituted analog (Figure 4.9), indicating the electrophilic nature of the terminal oxidant. In the case of *cis*-stilbene, a mixture of both *cis* and *trans* configured epoxides was observed which points to the formation of a radical

intermediate where it would allow C-C bond rotation to yield the stereoisomers. Such an isomerization was also observed for the epoxidation of *cis*-stilbene with $Fe^{V}(O)$.[15(d)] All these observations indicate the involvement of a high valent electrophilic iron-oxo intermediate reminiscent of $Fe^{V}(O)$.

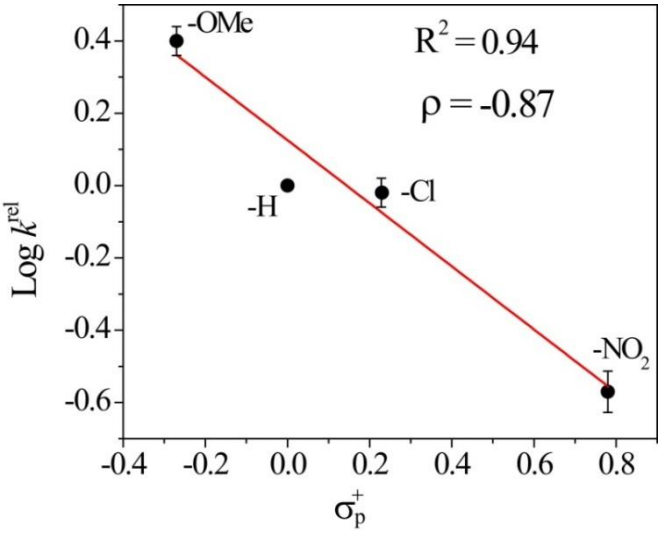

Figure 4.9. Hammett plots of logk^{rel} against *para*- σ^+ for the epoxidation of styrene and its *para*-substituted derivatives obtained from the reaction of complex **1** in DCB at 50 °C. Hammett value ρ is -0.87; $k^{rel} = k^X/k^H$, where k^X and k^H are concentration of epoxide product for *para*- substituted styrene and concentration of epoxide product for styrene respectively.

4.4.4 ^{18}O Labelling Experiments

To convincingly demonstrate that the O-atom present in the epoxide resulted from O_2, epoxidation reactions were carried out with $^{18}O_2$. Incorporation of ~35% of labeled ^{18}O was observed in the product styrene oxide (Figure 4.10). The low incorporation of the ^{18}O atom is due to the exchange of the O-atom of $Fe^{V}(^{18}O)$ with the $H_2{}^{16}O$ present in the reaction mixture, and this is aided by the long reaction times required for the reaction of styrene with **2**. As a consequence, the remaining 65% styrene oxide showed the incorporation of ^{16}O. In fact, when $^{18}O_2$ was used for the sulfoxidation reaction of thioanisole, where the reaction rates are much faster, ~70% incorporation of labeled ^{18}O was observed in the product (Figure 4.11). Analogous observations have been reported in related systems.[17,11,9(a)] We also carried out the reaction of styrene with **1** in the presence of small amounts of $H_2{}^{18}O$ under atmospheric air. Here ~45% of labeled ^{18}O was incorporated in the product (Figure 4.12). As a control, the reaction of complex **1** and styrene in an O_2 free environment with

$H_2{}^{18}O$ in DCM showed no product formation over a period of 20 h. These results clearly indicate molecular dioxygen as the O-atom source and the operation of an electrophilic high-valent iron-oxo as the active intermediate for the epoxidation reaction.

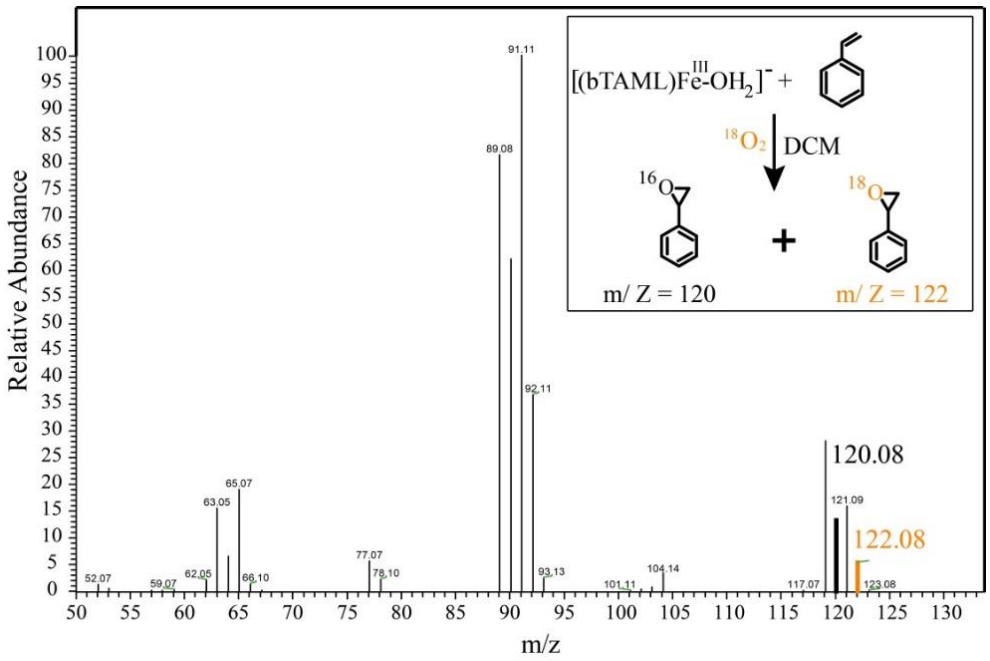

Figure 4.10. GC-MS spectra of the product after 60 min. of reaction with complex **1** and styrene in the presence of $^{18}O_2$.

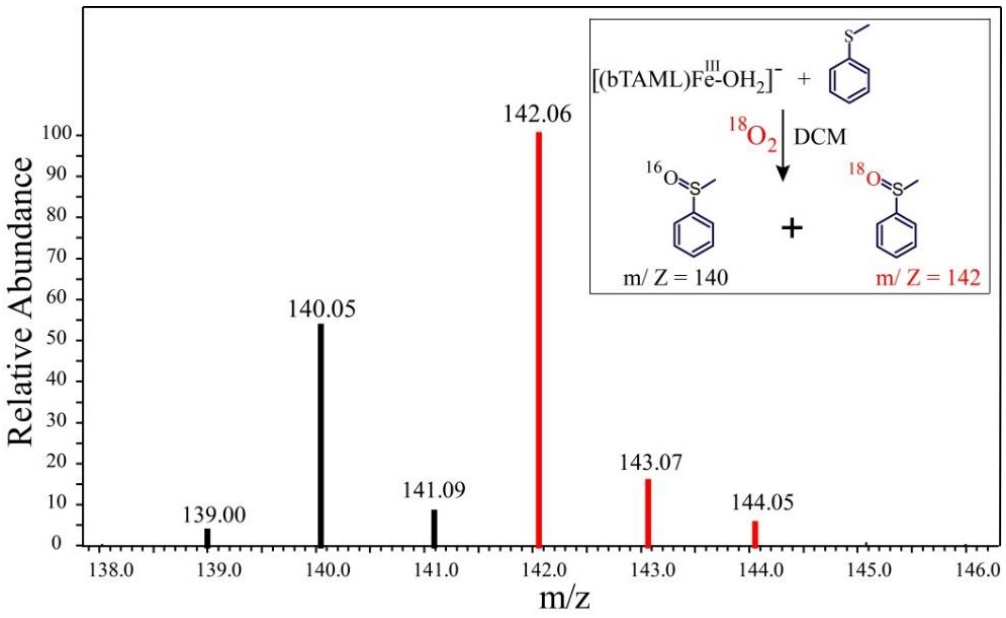

Figure 4.11. GC-MS spectra of the product after 10 min. of reaction with complex **1** and thioanisole in the presence of $^{18}O_2$.

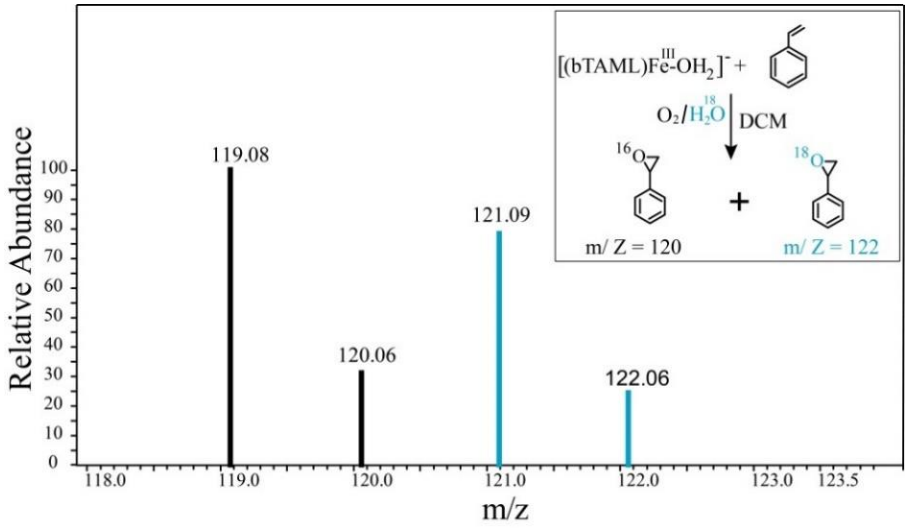

Figure 4.12. GC-MS spectra of the product after 60 min. of reaction with complex **1** and styrene in the presence of $H_2{}^{18}O$ and air ($^{16}O_2$).

4.4.5 Fate of the Catalyst

The progress of the reaction in DCB was similar to what was observed in DCM. The reaction of complex **1** with O_2 in DCB resulted in the formation of dimer complex **2**. However, at the end of the reaction, no purple solution of inactive [(bTAML)Fe^{IV}(Cl)]$^-$ complex was observed. Instead, a yellow precipitate was observed which was isolated by filtration. This precipitate was insoluble in DCM or any non-coordinating solvent, but it was solubilized upon the addition of a coordinating additive (acetonitrile, methanol, *etc.*). The UV-vis and HR-MS spectra of the acetonitrile solution of precipitate were identical to those the solution of the (bTAML)Fe^{III} complex in acetonitrile (Appendix C2 and Appendix C3). This indicates that no chemical change in the complex took place during the reaction and the structure of the complex remained intact. The likely reason for precipitation could be an aggregation of the (bTAML)Fe^{III} complex *via* binding of a ligand amide O-atom to the electrophilic Fe^{III} center in the absence of a coordinating ligand. When acetonitrile was removed from this solution, the remaining solid was reused to catalyze aerobic epoxidation in DCB.

4.4.6 Mechanistic Investigations for O_2 Interaction with Iron Center of Complex 1

In monooxygenases (e.g. cytochrome P450), two electrons are from NAD(P)H are donated to the Fe-O_2 adduct to generate the Fe^{IV}(O)porphyrin$^{\cdot+}$ reactive intermediate.[3] While one oxygen atom of O_2 is transferred to the substrate via Fe^{IV}(O)porphyrin$^{\cdot+}$, the

other oxygen atom is reduced to water. Unlike cytochrome P450, complex $[(bTAML)Fe^{III}(H_2O)]^-$ serve as a dioxygenase. The low redox potential ($E^\circ(Fe^{IV/III})$ = 0.85 *vs* NHE)[23] of complex $[(bTAML)Fe^{III}(H_2O)]^-$ acts as an electron source to reduce the oxygen molecule. Here, we propose that upon solubilizing **1** in a hydrophobic and non-coordinating solvent such as DCB, the axial H_2O is replaced by O_2. This was indicated by our UV-vis studies (Figure 4.6) and supported by literature reports on related complexes.[9] The Fe-O_2 adduct reacts with a second molecule of the iron complex to form a peroxo-bridged iron dimer, $Fe^{IV}OOFe^{IV}$ (which remains undetected). The subsequent homolytic cleavage of the O-O bond in $Fe^{IV}OOFe^{IV}$ results in the formation of putative $Fe^{V}(O)$ which immediately comproportionates with the parental Fe^{III} complex to form the dimer complex **2** (Scheme 4.3). Kinetic studies on the formation of $Fe^{IV}OFe^{IV}$ from Fe-O_2 indicate a second-order dependency on the catalyst concentration which partly supports this mechanism (Figure 4.13). This proposal is based on available literature where it has been demonstrated that Fe^{II} porphyrins and other iron complexes form μ-Oxo-Fe^{III} dimers by autoxidation.[16(a),24]

Scheme 4.3. Proposed Mechanism for the Formation of **2** by Reaction of Complex **1** and O_2.

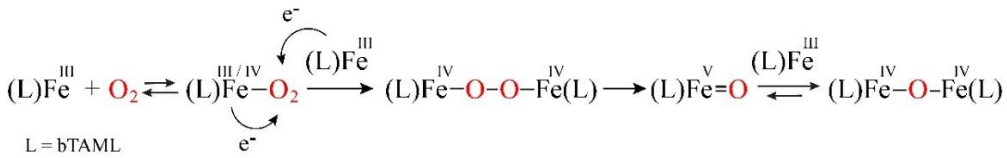

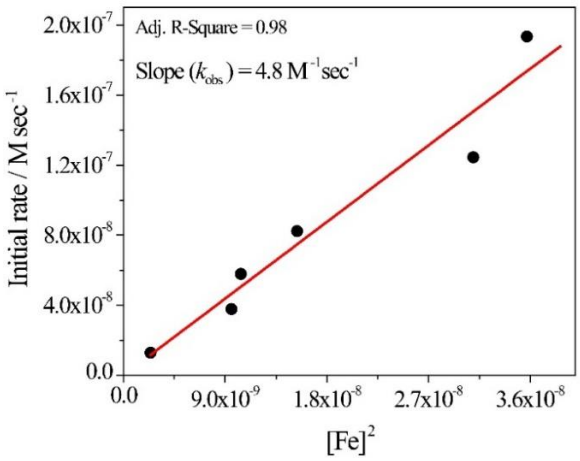

Figure 4.13. Plot of initial rate *vs* square of complex **1** concentration. k_{obs} were obtained by linear fit according to the equation: rate = k_{obs}[catalyst]^2. The reaction was performed under air in dichloromethane at 25 ˚C.

4.4.7 EPR Spectroscopic Observations

In order to identify the intermediates formed prior to the dimer formation; temperature of the complex solution was lowered down to the -40 °C. Interestingly, it was observed that the absorbance at 412 nm for the proposed iron-O_2 adduct shifted to the 365 nm upon lowering the temperature (Figure 4.14(A)). At this temperature, the species formed was stable and did not convert into the dimer complex (up to 9 h in the presence of O_2 balloon). Upon increasing the temperature of this solution from -40 °C to 25 °C, this proposed Fe-O_2 adduct converted to the dimer **2** and two isosbestic points were observed in the UV-vis during this conversion (Figure 4.14(B)). The EPR measurement of the solution at 100 K exhibited the presence of *S*=1/2 spin species (Figure 4.16). In a separate observation, complex $[(bTAML)Fe^{IV}(Cl)]^-$ (*S*=1; X-band EPR silent) (see experimental section) upon reaction with potassium superoxide (KO_2) in DCM at -40 °C, showed a similar UV-vis spectra with absorbance at 360 nm (Figure 4.15(A)) as well as *S*=1/2 spin EPR signal ($g_{x,y}$ = 2.15 and g_z = 2.03) (Figure 4.15(B)). The species formed was converted into a dimer (**2**) upon increasing temperature from -40 °C to 25 °C which is in agreement with the above discussion and observations for Fe^{III}-O_2 adduct formation upon reaction of complex **1** and O_2 prior to dimer formation. This Fe-O_2 adduct could be best described as $[(bTAML)Fe^{III}(O_2)]^-$ or $[(bTAML)Fe^{IV}(O_2^{\cdot-})]^-$ and further characterization by Raman and Mossbauer are required to distinguish between these two species. The speculation for the formation of $[(bTAML)Fe^{III}(superoxide)]^{2-}$ (Figure 4.5(A)) due to excess use of KO_2 has been negated by comparative analysis of UV-vis and EPR spectra with related $[(TAML)Fe^{III}(superoxide)]^{2-}$ complex (Figure 4.5(B)).

In addition, the UV-vis spectra shift from 412 nm to 365 nm at a lower temperature, correspond to iron-O_2 adduct, albeit in a different spin state of the complex $[(bTAML)Fe^{III}(O_2)]^-$. DFT calculations show a very small relative energy difference of 0.68 kcal mol^{-1} between sextet (*S*=5/2) $[(bTAML)Fe^{III}(O_2)]^-$ and doublet (*S*=1/2) $[(bTAML)Fe^{III}(O_2)]^-$ complex (Appendix C4). This supports the possible existence of two spin states which could be interconverted with changes in temperature. Further, the X-band EPR of a solution of complex **1** formed in DCM in air (measured at 100 K) showed signals which could be assigned to a mixture of two species with *S*=1/2 (g = 2.2, 2.1 and 1.9) and *S*=3/2 (g = 4.3) spin (Figure 4.16(B)). We propose that the species having *S*=1/2 spin represents the Fe-O_2 intermediate in which the Fe^{III} center is anti-ferromagnetically coupled to *S*=1 of O_2 (alternatively, Fe^{IV}-O_2 is also possible). The signal at g = 4.3 represents the

starting S=3/2 Fe^{III} complex (Figure 4.16(A)) that is left over due to incomplete formation of Fe-O_2. At higher complex concentration, the reaction of O_2 with complex **1** is not quantitative, and this leaves unreacted Fe^{III} having S=3/2 spin.

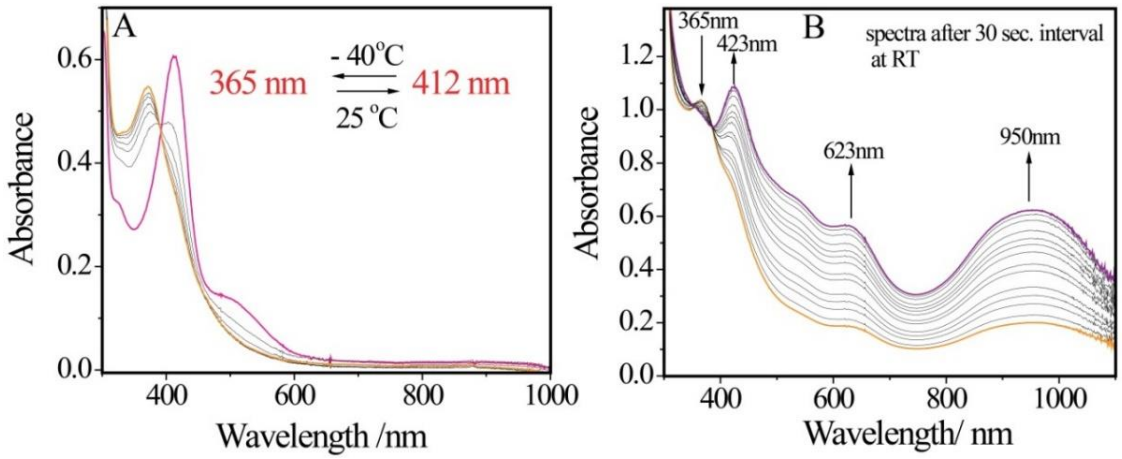

Figure 4.14. (A) UV–vis spectral changes upon lowering the temperature from 25 °C to -40 °C for complex Fe-O_2 (**1**) in DCM. (B) UV-vis spectral scan for dimer (**2**) formations upon increasing temperature from -40 °C to 25 °C.

$$[(bTAML)Fe^{IV}\text{-}Cl]^- + KO_2 \longrightarrow [(bTAML)Fe^{III}\text{-}Cl]^{2-} \xrightarrow{KO_2} [(bTAML)Fe^{III}\text{-}O^{\cdot-}]^{2-} \quad \text{(i)}$$

$$[(bTAML)Fe^{IV}\text{-}Cl]^- + KO_2 \longrightarrow [(bTAML)Fe^{III/IV}\text{-}O_2]^- \longrightarrow [\{(bTAML)Fe^{IV}\}_2\text{-}Oxo]^{2-} \quad \text{(ii)}$$

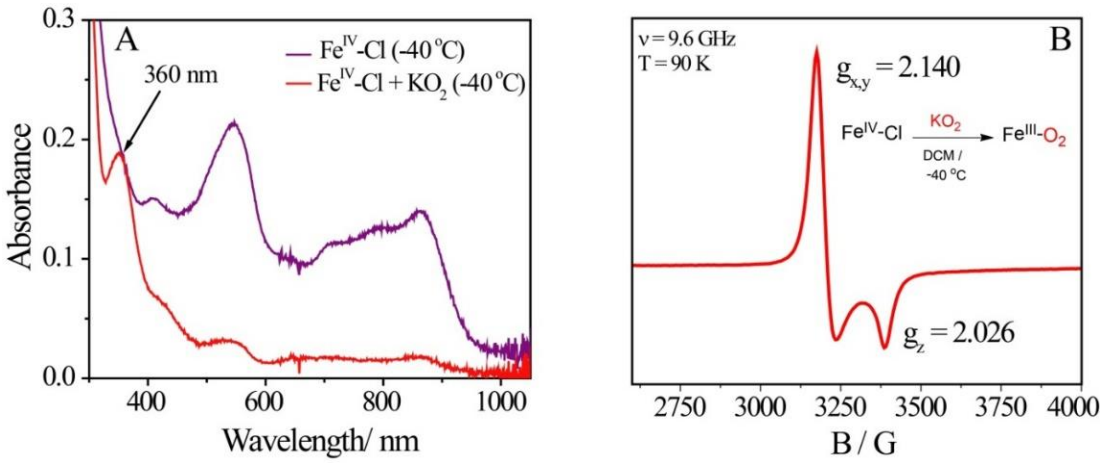

Figure 4.15. (A) UV–vis spectral changes of Fe^{IV}-Cl complex (5×10^{-5}M) upon reductive binding of superoxide (excess KO_2) in DCM; (B) X-band EPR signal of resulting solution Fe^{III}-O_2 adduct after reaction of Fe^{IV}-Cl and KO_2; at 100 K, in DCM.

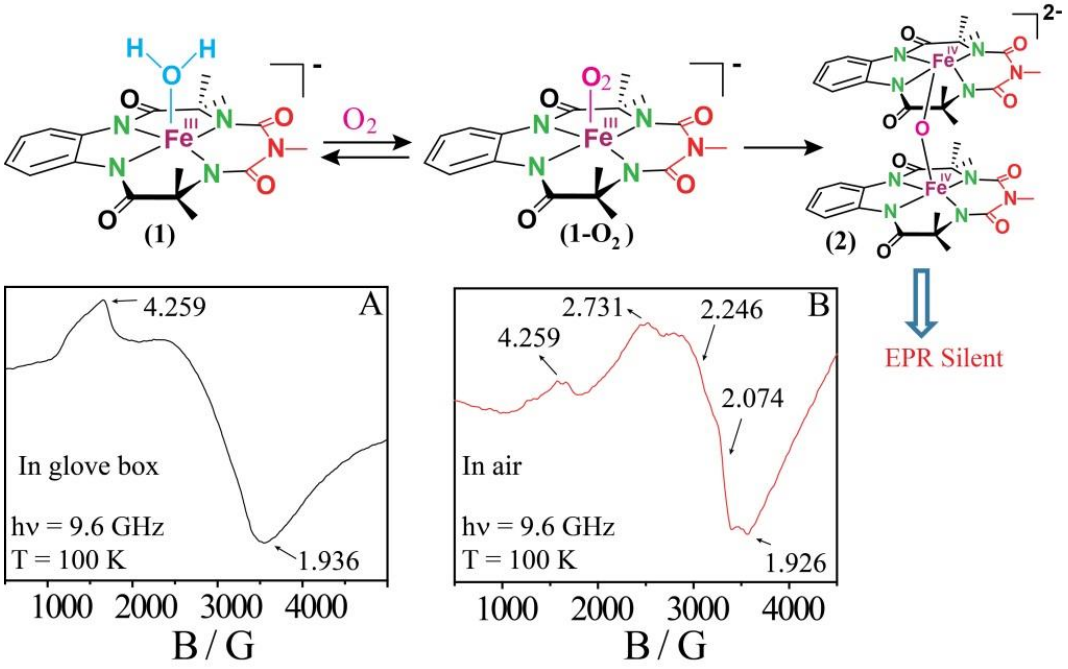

Figure 4.16. (A) X-band EPR of complex **1** (8.0 mM) in degassed dichloromethane (DCM) at 100 K; (B) X-band EPR of complex **1** (8.0 mM) in oxygenated DCM at 100 K.

4.4.8 Reason for the Reactivity of [{(bTAML)Fe^{IV}}$_2$-μ-oxo]$^{2-}$ Dimer

Unlike previous reports with iron-heme and Fe-TAML complexes, this iron(IV) dimer **2** has limited stability in the presence of substrates such as alkenes or alkanes, since it exists in equilibrium with the Fe^{V}(O) and Fe^{III} complex. The iron-dimer complex of bTAML ligand environment shows reactivity toward alkenes, but such reaction is not known for TAML ligand system. In view to understanding the structural difference between bTAML and TAML based iron dimer complexes we used DFT as an alternative tool (procurement of [{(bTAML)Fe^{IV}}$_2$-μ-oxo]$^{2-}$ dimer crystal was unsuccessful). To validate the DFT method, [{(TAML)Fe^{IV}}$_2$-μ-oxo]$^{2-}$ dimer complex was optimized (B3LYP, 6-31G*) by taking the coordinates from reported crystal structure data.[9(a)] The different bond lengths and angles of the optimized structure were very close to the reported crystal structure. For example, the distance between FeO…H (2.398 Å) from DFT optimized structure (Figure 4.17(A)) shows a minor change from the crystal structure (2.319 Å). Hence, DFT optimized structure of these systems could be a close comparison with obtained crystal structure. bTAML differs from TAML by only substitution of the CMe_2 moiety with an NMe group. Crystal structure of [{(TAML)Fe^{IV}}$_2$-μ-oxo]$^{2-}$ dimer indicates for H-bonding between O atom of Fe-oxo moiety and H atom of –CMe_2 group (where O and H distance is 2.32 Å; *see reference 9(a)*). Whereas, DFT optimized structure of

[{(bTAML)Fe^{IV}}$_2$-μ-oxo]$^{2-}$ dimer (B3LYP, 6-31G*) shows the presence of H atom of N-Me group far away from the Fe-oxo moiety (4.92 Å) (Figure 4.17(B)). Therefore, we hypothesized that hydrogen bonding could give extra stability to the TAML based dimer complex, unlike bTAML based dimer complex. Furthermore, the steric due to the –CMe_2 group in TAML can also hinder the approach of substrates towards Fe-oxo moiety for the reaction. Therefore, unlike [{(bTAML)Fe^{IV}}$_2$-μ-oxo]$^{2-}$, [{(TAML)Fe^{IV}}$_2$-μ-oxo]$^{2-}$ is more stable and not known for reactions towards hydrocarbon oxidation.

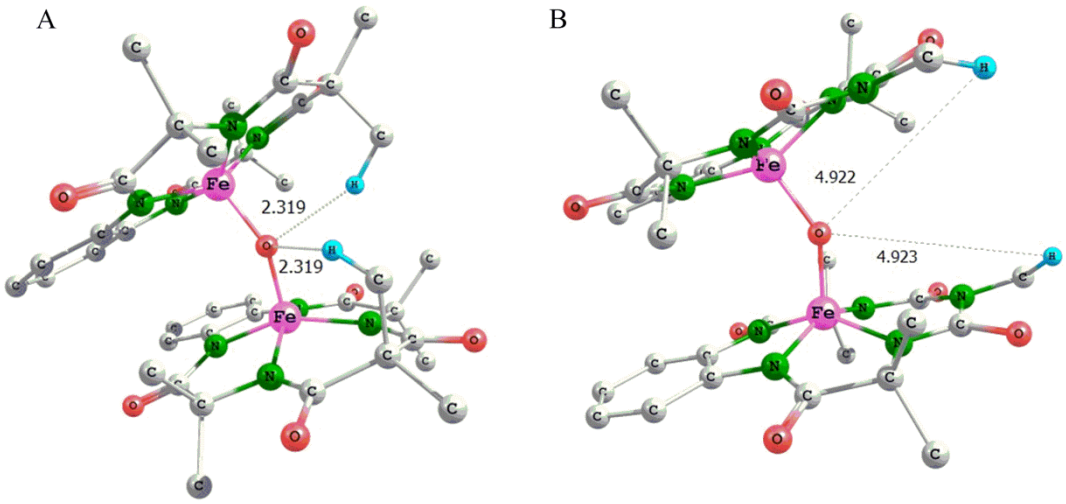

[{(TAML)Fe^{IV}}$_2$-μ-oxo]$^{2-}$ Dimer (Crystal structure)

[{(bTAML)Fe^{IV}}$_2$-μ-oxo]$^{2-}$ Dimer (DFT Optimized structure)

Figure 4.17. At the B3LYP/6-31G*, LANL2DZ (Fe) level of theory, gas-phase optimized geometries of (A) [{(TAML)Fe^{IV}}$_2$-μ-oxo]$^{2-}$, [9(a)] and (B) [{(bTAML)Fe^{IV}}$_2$-μ-oxo]$^{2-}$.

4.4.9 Evidence for the Involvement of Fe^{V}(O) Species in the Epoxidation Reaction

Kinetic evidence for the reaction of dimer [{(bTAML)Fe^{IV}}$_2$-μ-oxo]$^{2-}$ with alkenes indicates the existence of the Fe^{V}(O) and Fe^{III} complex upon disproportionation of [{(bTAML)Fe^{IV}}$_2$-μ-oxo]$^{2-}$ complex.[15(d)]. In addition, when this dimer was incubated with a nitro-substituted [(NO_2-bTAML)Fe^{III}(Cl)]$^{2-}$ complex,[18] scrambling of the O-atom from **2** was observed by high-resolution mass spectrometry (HR-MS) analysis (Figure 4.18) which substantiates our hypothesis for the existence of Fe^{V}(O). Upon addition of an alkene, Fe^{V}(O) reacts with the alkene to form an epoxide and regenerates the starting Fe^{III} complex, which again reacts with another O_2 molecule to start the cycle once again. This catalytic cycle continues until the catalyst precipitates out from the solution. We believe that complex **1** functions like a dioxygenase, where both the O-atoms of the O_2 molecule are utilized for

oxidation of the substrate. Such an atom-economical use of O_2 is clearly superior to monooxygenases where one O-atom inserts into the organic substrate while the other O-atom is reduced to H_2O in the presence of a coreductant.

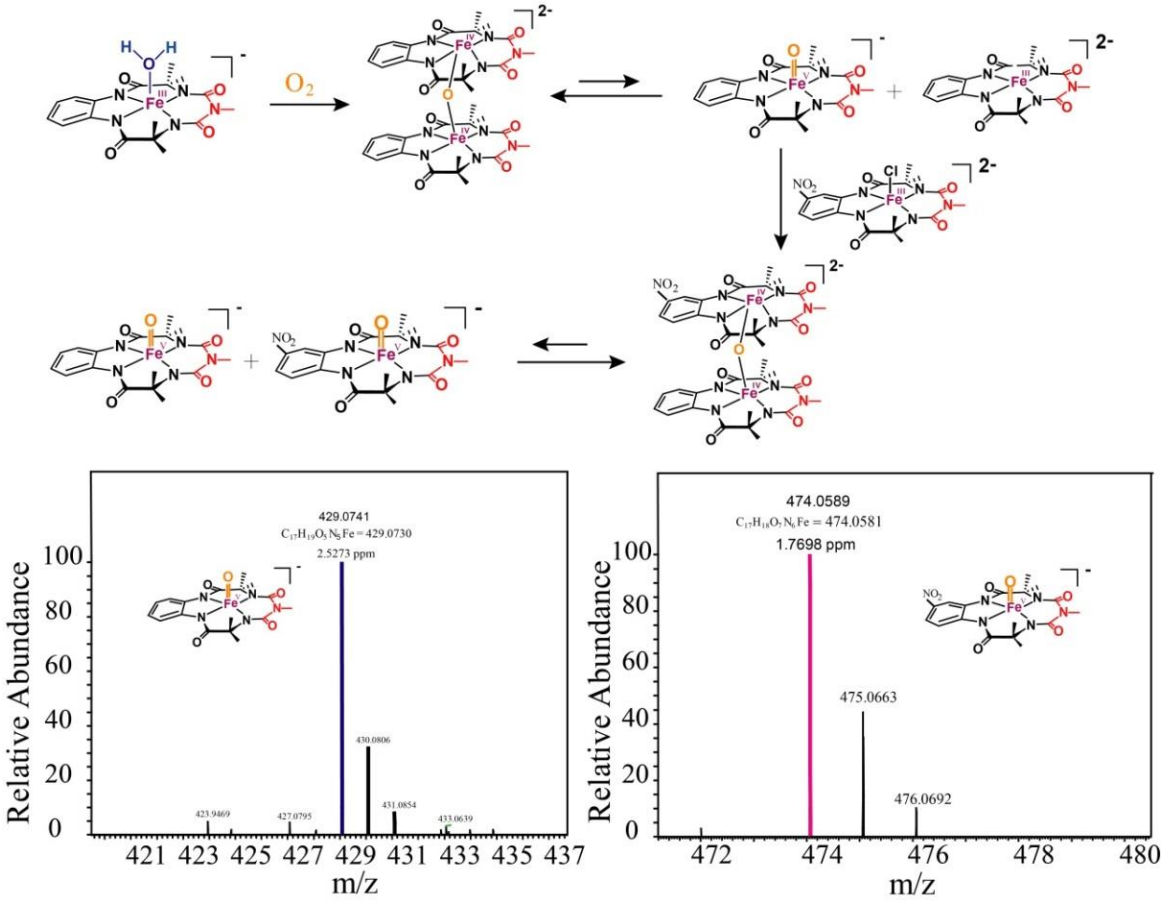

Figure 4.18. HR-MS of $[(bTAML)Fe^{V}(O)]^{-}$ and $[(NO_2\text{-}bTAML)Fe^{V}(O)]^{-}$ complexes which are formed after incubation of $[\{(bTAML)Fe^{IV}\}_2\text{-}\mu\text{-}oxo]^{2-}$ dimer (**2**) solution with a nitro-substituted complex, $[(NO_2\text{-}bTAML)Fe^{III}(Cl)]^{2-}$. Calculated m/z of $[(bTAML)Fe^{V}(O)]^{-}$ and $[(NO_2\text{-}bTAML)Fe^{V}(O)]^{-}$ is 429.0730 and 474.0581 respectively.

Note: The mass spectrum of $[\{(bTAML)Fe^{IV}\}_2\text{-}\mu\text{-}oxo]^{2-}$ display two peaks corresponding to the mass of $[(bTAML)Fe^{III}]^{-}$ and $[(bTAML)Fe^{V}(O)]^{-}$. Hence, the presence of mass corresponding to $[(NO_2\text{-}bTAML)Fe^{V}(O)]^{-}$ after incubation of $[\{(bTAML)Fe^{IV}\}_2\text{-}\mu\text{-}oxo]^{2-}$ dimer (**2**) solution with a nitro-substituted $[(NO_2\text{-}bTAML)Fe^{III}(Cl)]^{2-}$ complex is probably indicative of the presence of scrambled dimer.

4.5 Conclusion

In summary, a monomeric Fe^{III}-bTAML complex **1** is competent to activate molecular dioxygen (O_2) to generate a dimeric complex **2** which is reactive towards alkenes. The catalytic use of O_2 by a monomeric iron-complex towards the epoxidation reaction without the use of any coreductant is unprecedented. The above investigations indicate the involvement of a high valent $Fe^{V}(O)$ species during the reaction of complex **1** and O_2 with alkenes, although we are currently unable to spectroscopically observe this intermediate under the reaction conditions. Further investigations for understanding the binding of O_2 with the monomeric iron(III) center and the sequential steps for the formation of the dimer are being carried out in our laboratory.

4.6 References

1. Ortiz de Montellano, P. R. *Cytochrome P-450: Structure, Mechanism, and Biochemistry*, Plenum New York **1986**. (b) Rosenzweig, A. C.; Frederick, C. A.; Lippard, S. J.; Nordlund, P. *Nature* **1993**, *366*, 537. (c) Lee, S. –K.; Fox, B. G.; Froland, W. A.; Lipscomb, J. D.; Münck, E. *J. Am. Chem. Soc.* **1993**, *115*, 6450. (d) Lee, S. –K.; Nesheim, J. C.; Lipscomb, J. D. *J. Biol. Chem*. **1993**, *268*, 21569. (e) Liu, K. E. *J. Am. Chem. Soc*. **1994**, *116*, 7465. (f) Feig, A. L.; Lippard, S. J. *Chem. Rev*. **1994**, *94*, 759. (g) Que, L., Jr.; True, A. E. *Prog. Inorg. Chem*. **1990**, *38*, 97. (h) Sánchez-Ferrer, A.; Rodríguez-López, J. N.; García-Cánovas, F.; García-Carmona, F. *Biochim. Biophys. Acta* **1995**, *1*, 1247. (i) Nordlund, P.; Sjöberg, B. –M.; Eklund, H. *Nature* **1990**, *345*, 593. (j) Bollinger, J. M., Jr. *J. Am. Chem. Soc*. **1994**, *116*, 8024.
2. (a) Pauling, L. *Standford Med. Bull* **1948**, *6*, 2015. (b) Pauling, L. *Nature* **1964**, *203*, 182. (c) Grifith, J. S. *Proc. Roy. Soc. Ser. A* **1956**, *235*, 23. (d) Weiss, J. J. *Nature* **1964**, *202*, 83. (e) Phillips, S. E. V. *Nature* **1978**, *273*, 247.
3. (a) Costas, M.; Mehn, M. P.; Jensen, M. P.; Que, L., Jr. *Chem. Rev*. **2004**, *104*, 939. (b) Que, L., Jr.; Tolman, W. B. *Nature* **2008**, *455*, 333. (c) Meunier, B.; de Visser, S. P.; Shaik, S. *Chem. Rev*. **2004**, *104*, 3947. (d) Poulos, T. L. *Chem. Rev*. **2014**, *114*, 3919. (e) Smith, L. J.; Kahraman, A.; Thornton, J. M. *Proteins: Struct. Funct. Genet*. **2010**, *78*, 2349. (f) Ortiz de Montellano, P. R. *Chem. Rev*. **2010**, *110*, 932.

4. (a) Jørgensen, K. A. *Chem. Rev*. **1989**, *89*, 431. (b) Lane, B. S.; Burgess, K. *Chem. Rev*. **2003**, *103*, 2457.
5. (a) Groves, J. T.; Nemo, T. E.; Myers, R. S. *J. Am. Chem. Soc*. **1979**, *101*, 1032. (b) Mas-Balleste, R.; Que, L., Jr. *J. Am. Chem. Soc*. **2007**, *129*, 15964. (c) de Oliveira, F. T.; Chanda, A.; Banerjee, D.; Shan, X.; Mondal, S.; Que, L., Jr.; Bominaar, E. L.; Münck, E.; Collins, T. J. *Science* **2007**, *315*, 835.
6. (a) Tabushi, I.; Yazaki, A. *J. Am. Chem. Soc*. **1981**, *103*, 7371. (b) Mansuy, D.; Fontecave M.; Bartoli, J.-F. *J. Chem. Soc., Chem. Commun*. **1983**, *6*, 253. (c) Battioni, P.; Bartoli, J. F.; Leduc, P.; Fontecave, M.; Mansuy, D. *J. Chem. Soc., Chem. Commun*. **1987**, 791.
7. (a) Evans, S.; Smith, J. R. L. *J. Chem. Soc., Perkin Trans* **2000**, *2*, 1541. (b) Lyons, J. E.; Ellis, P. E.; Myers, H. K. *J. Catal*. **1995**, *155*, 59. (c) Che, C.-M.; Lo, V. K.-Y.; Zhou, C.-Y.; Huang, J.-S. *Chem. Soc. Rev*. **2011**, *40*, 1950.
8. (a) Lee, Y.-M.; Hong, S.; Morimoto, Y.; Shin, W.; Fukuzumi, S.; Nam, W. *J. Am. Chem. Soc.* **2010**, *132*, 10668. (b) He, Y.; Goldsmith, C. R. *Chem. Commun*. **2012**, *48*, 10532. (c) Sheet, D.; Paine, T. K. *Chem. Sci.* **2016**, *7*, 5322. (d) Sahu, S.; Goldberg, D. P. *J. Am. Chem. Soc.* **2016**, *138*, 11410.
9. (a) Ghosh, A.; de Oliveira, F. T.; Yano, T.; Nishioka, T.; Beach, E. S.; Kinoshita, I.; Münck, Ryabov, E. A. D.; Horwitz, C. P.; Collins, T. J. *J. Am. Chem. Soc.* **2005**, *127*, 2505. (b) Tang, L. L.; Gunderson, W. A.; Weitz, A. C.; Hendrich, M. P.; Ryabov, A. D.; Collins, T. J. *J. Am. Chem. Soc*. **2015**, *137*, 9704.
10. (a) Ellis, P. E., Jr.; Lyons, J. E. *Coord. Chem. Rev*. **1990**, *105*, 181. (b) Grinstaff, M. W.; Hill, M. G.; Labinger, J. A.; Gray, H. B. *Science* **1994**, *264*, 1311.
11. Kim, S. O.; Sastri, C. V.; Seo, M. S.; Kim, J.; Nam, W. *J. Am. Chem. Soc.* **2005**, *127*, 4178.
12. Groves, J. T.; Watanabe, Y. *J. Am. Chem. Soc*. **1986**, *108*, 7834.
13. (a) Leising, R. A.; Takeuchi, K. J. *Inorg. Chem*. **1987**, *26*, 4391. (b) Goldstein, A. S.; Beer, R. H.; Drago, R. S. *J. Am. Chem. Soc*. **1994**, *116*, 2424. (c) Neumann, R.; Dahan, M. *Nature* **1997**, *388*, 353.
14. (a) Momenteau, M.; Reed, C. A. *Chem. Rev*. **1994**, *94*, 659. (b) Kitajima, N.; Tamura, N.; Amagai, H.; Fukui, H.; Moro-oka, Y.; Mizutani, Y.; Kitagawa, T.; Mathur, R.; Heerwegh, K.; Reed, C. A.; Randall, C. R.; Que, L., Jr.; Tatsumi, K. *J. Am. Chem. Soc.* **1994**, *116*, 9071. (c) Ookubo, T.; Sugimoto, H.; Nagayama, T.; Masuda, H.; Sato, T.; Tanaka, K.; Maeda, Y.; Okawa, H.; Hayashi, Y.; Uehara, A.;

Suzuki, M. *J. Am. Chem. Soc*. **1996**, *118*, 701. (d) Dong, Y.; Yan, S.; Young, V. G., Jr.; Que, L., Jr. *Angew. Chem. Int. Ed. Engl.* **1996**, *35*, 618. (e) Thibon, A.; England, J.; Martinho, M.; Young, V. G., Jr.; Frisch, J. R.; Guillot, R.; Girerd, J.-J.; Münck, E.; Que, L., Jr.; Banse, F. *Angew. Chem. Int. Ed.* **2008**, *47*, 7064. (f) Nam, W.; *Acc. Chem. Res*. **2015**, *48*, 2415. (g) Chatterjee, S.; Paine, T. K. *Angew. Chem. Int. Ed.* **2015**, *54*, 9338.

15. (a) Panda, C.; Ghosh, M.; Panda, T.; Banerjee, R.; Sen Gupta, S. *Chem. Commun.* **2011**, *47*, 8016. (b) Ghosh, M.; Singh, K. K.; Panda, C.; Weitz, A.; Hendrich, M. P.; Collins, T. J.; Dhar, B. B.; Sen Gupta, S. *J. Am. Chem. Soc.* **2014**, *136*, 9524. (c) Singh, K. K.; Tiwari, M. k.; Ghosh, M.; Panda, C.; Weitz, A.; Hendrich, M. P.; Dhar, B. B.; Vanka, K.; Sen Gupta, S. *Inorg. Chem.* **2015**, *54*, 1535. (d) Singh, K. K.; Tiwari, M. k.; Dhar, B. B.; Vanka, K.; Sen Gupta, S. *Inorg. Chem*. **2015**, *54*, 6112.
16. (a) Chin, D.-H.; Mar, G. N. L.; Balch, A. L. *J. Am. Chem. Soc*. **1980**, *102*, 4344. (b) Dong, Y.; Ménage, S.; Brennan, B. A.; Elgren, T. E.; Jang, H. G.; Pearce, L. L.; Que, L., Jr. *J. Am. Chem. Soc.* **1993**, *115*, 1851. (c) Guo, C.; Peng, Q.; Liu, Q.; Jiang, G. *J. Mol. Cat. A: Chem.* **2003**, *192*, 295. (d) Rosenthal, J.; Luckett, T. D.; Hodgkiss, J. M.; Nocera, D. G. *J. Am. Chem. Soc.* **2006**, *128*, 6546. (e) Harischandra, D. N.; Lowery, G.; Zhang, R.; Newcomb, M. *Org. Lett*. **2009**, *11*, 2089.
17. Seo, M. S.; In, J.-H.; Kim, S. O.; Oh, N. Y.; Hong, J.; Kim, J.; Que, L., Jr.; Nam, W. *Angew. Chem. Int. Ed*. **2004**, *43*, 2417.
18. *For synthesis of [(NO_2-bTAML)Fe^{III}(Cl)]$^-$ see* Panda, C.; Debgupta, J.; Diaz Diaz, D.; Singh, K. K.; Sen Gupta, S.; Dhar, B. B. *J. Am. Chem. Soc.* **2014**, *136*, 12273.
19. Kadish, K. M.; Anderson, J. E. *Pure & Appl. Chem*. **1887**, *59*, 703.
20. Hong, S.; Sutherlin, K. D.; Park, J.; Kwon, E.; Siegler, M. A.; Solomon, E. I.; Nam, W. *Nat. Commun*. **2014**, *5*, 5440.
21. (a) Perdew, J. P.; Chevary, S. H.; Vosko, K. A.; Jackson, K. A.; Pederson, M. R.; Singh, D. J.; Fiolhais, C. *Phys. Rev. B* **1992**, *46*, 6671. (b) Perdew, J. P.; Chevary, S. H.; Vosko, K.A.; Jackson, K. A.; Pederson, M. R.; Singh, D. J.; Fiolhais, C. *Phys. Rev. B* **1993**, *48*, 4978. (c) Perdew, J. P.; Burke, K.; Wang, Y. *Phys. Rev. B* **1996**, *54*, 16533. (d) Adamo, C.; Barone, V. *J. Chem. Phys*. **1998**, *108*, 664. (e) Becke, A. D. *J. Chem. Phys.* **1993**, *98*, 5648. (f) Lee, C.; Yang, W.; Parr, R. G. *Phys. Rev. B* **1988**, *37*, 785. (g) Roothan, C. C. J. *Rev. Mod. Phy*. **1951**, *23*, 69. (h) McWeeny R.;

Dierksen, G. *J. Chem. Phys.* **1968**, *49*, 4852. (i) Pople, J. A.; Nesbet, R. K. *J. Chem. Phys.* **1954**, *22*, 571.

22. Frisch, M. J.; Trucks, G. W.; Schlegel, H. B.; Scuseria, G. E.; Robb, M. A.; Cheeseman, J. R.; Scalmani, G.; Barone, V.; Mennucci, B.; Petersson, G. A.; Nakatsuji, H.; Caricato, M.; Li, X.; Hratchian, H. P.; Izmaylov, A. F.; Bloino, J.; Zheng, G.; Sonnenberg, J. L.; Hada, M.; Ehara, M.; Toyota, K.; Fukuda, R.; Hasegawa, J.; Ishida, M.; Nakajima, T.; Honda, Y.; Kitao, O.; Nakai, H.; Vreven, T.; Montgomery, J. A. Jr.; Peralta, J. E.; Ogliaro, F.; Bearpark, M.; Heyd, J. J.; Brothers, E.; Kudin, K. N.; Staroverov, V. N.; Kobayashi, R.; Normand, J.; Raghavachari, K.; Rendell, A.; Burant, J. C.; Iyengar, S. S.; Tomasi, J.; Cossi, M.; Rega, N.; Millam, J. M.; Klene, M.; Knox, J. E.; Cross, J. B.; Bakken, V.; Adamo, C.; Jaramillo, J.; Gomperts, R.; Stratmann, R. E.; Yazyev, O.; Austin, A. J.; Cammi, R.; Pomelli, C.; Ochterski, J. W.; Martin, R. L.; Morokuma, K.; Zakrzewski, V. G.; Voth, G. A.; Salvador, P.; Dannenberg, J. J.; Dapprich, S.; Daniels, A. D.; Farkas, Ö.; Foresman, J. B.; Ortiz, J. V.; Cioslowski, J.; Fox, D. J. Gaussian 09, revision B.01; Gaussian, Inc.: Wallingford, CT, **2009**.
23. Pattanayak, S.; Chowdhury, D. R.; Garai, B.; Singh, K. K.; Paul, A.; Dhar, B. B.; Gupta, S. S. *Chem. Eur. J*. **2017**, *23*, 3414.
24. (a) Cohen, I. A.; Caughey, W. S. *Biochemistry* **1968**, *7*, 636. (b) Balch, A. L.; Chan, Y.-W.; Cheng, R.-J.; Mar, G. N. L.; Latos-Grazynski, L.; Renner, M. *J. Am. Chem. Soc*. **1984**, *106*, 7779.

Chapter V

Valence Tautomerization in High-Valent $Fe^{V}(O)$-bTAML Complex: Effect of Acid on Secondary Coordination Sphere

5.1 Abstract

Cytochrome P450 generates $Fe^{IV}(O)$-radical-cation during their catalytic cycle of substrate oxidation. The non-innocent nature of the active center is due to the π-extended delocalization in porphyrin ring. Electronic redistribution between ligand and iron center causes $Fe^{IV}(O)$-radical-cation formation which is valence tautomer of $Fe^{V}(O)$. The versatility of this species in selective hydroxylation makes it highly significant. Hence, which species between $Fe^{IV}(O)$-radical-cation and isoelectronic $Fe^{V}(O)$ would be more favorable towards oxidation of hydrocarbons are essential to understand, in view of their utility in chemical reactions. We report, formation of a mononuclear [(H-bTAML•+)$Fe^{IV}(O)$] by reaction of [(bTAML)$Fe^{V}(O)]^{-}$ complex with Lewis acid ($B(C_6F_5)_3$) in acetonitrile at -40 ˚C. The X-band EPR measurement displayed the presence of S=1/2 spin species. The signal near g = 2 showed hyperfine splitting of g_x and g_y tensor, which is indicative of nuclear spin coupling with nitrogen nucleus and an unpaired electron on the ligand moiety. HR-MS spectrum of the generated species displayed a mass peak at m/z = 430.0808, whose mass and isotope distribution pattern supported for the (bTAML)Fe(O)(H)-radical cation species (calculated m/z = 430.0815). Upon titration of this new species with ferrocene, required two equivalents of ferrocene for complete reduction into the complex (bTAML)Fe^{III}. This indicates that this new species formed represents complex isoelectronic to Fe^{V}. Further, DFT calculations suggested for the addition of H^{+} in ligand moiety due to the higher nucleophilicity of the carbonyl oxygen than that of the oxygen of the $Fe^{V}(O)$. These observations from UV-vis, EPR, and HR-MS spectroscopy led us to postulate that addition of H^{+} into [(bTAML)$Fe^{V}(O)]^{-}$ leads to the formation of [(H-bTAML•+)$Fe^{IV}(O)$] complex. The reactivity of the [(H-bTAML•+)$Fe^{IV}(O)$] complex is compared to that of the [(bTAML)$Fe^{V}(O)]^{-}$ in hydrogen atom transfer reaction using 9,10-dihydroanthacene (DHA) as substrate. Reaction of DHA with [(H-bTAML•+)$Fe^{IV}(O)$] (k_2 = 0.24 M^{-1} s^{-1}) showed ~720 fold slower reaction rate than the reaction rate of its isoelectronic complex [(bTAML)$Fe^{V}(O)]^{-}$ (k_2 = 173 M^{-1} s^{-1}). The presence of kinetic isotope effect (KIE) for both the species in reaction with deuterated 9,10-dihydroanthacene confirms that hydrogen atom abstraction is the rate determining step.

5.2 Introduction

Cytochrome P450 has been widely studied for its pivotal role in oxidative transformation in many vital biological processes.[1] For the C-H bond hydroxylation mediated by Cytochrome P450, $Fe^{IV}(O)$-porphyrin radical cation (Compound I) (considered as a valence tautomer of $Fe^{V}(O)$-porphyrin), or $Fe^{IV}(O)$-porphyrin (Compound II) has been found to be the active intermediate.[1(a),2] This redox non-innocent behavior in the active intermediates in these metal-containing enzymes have been attributed to the π-extended delocalization in porphyrin, phthalocyanine, and corroles ligands. Synthetic heme-based iron-oxo and manganese-oxo complexes have contributed significantly towards understanding and correlating the electronic structure and reactivity of these high valent metal-oxo chemistry in a biological system.[3] Some of these synthetic metal-oxo complexes are known to display valence tautomerization by electronic redistribution between ligand and metal upon activation. Previous studies using porphyrin, corroles, and porphyrinoids systems reveal that manipulation of the donor ability of axial or equatorial ligand can drive the generation of valence tautomers.[4] For example, substitution of axial ClO_4 with strong π-donor OMe ligand results in the conversion of $Fe^{III}(TMP^{\bullet+})(ClO_4)_2$ (TMP = 5,10,15,20-tetramesityl porphyrinato) to its valance tautomer $Fe^{IV}(TMP)(OMe)_2$.[5] Similarly, $Fe^{IV}(TPFC)(Cl)$ (TPFC = 5,10,15-tris-(pentaflurophenyl)corrolato generates a valence tautomer $Fe^{III}(TPFC^{\bullet+})(Cl)$ upon axial substitution of Cl with the weaker donor ClO_4 ligand.[6] Moreover, valence tautomerization in high valent Fe-Oxo complexes has attracted more attention because of its wide efficacy in the enzymatic system.

Although the use of $Fe^{IV}(O)$ and $Fe^{V}(O)$ complexes for the study of hydrogen atom transfer (HAT), oxygen atom transfer (OAT) and electron transfer (ET) reactions have exploded in the past few years,[3,7] the comparative study of their valence tautomers are very few. In a very recent report, a metastable $Mn^{IV}(O)(TBP_8Cz^{\bullet+})$ (TBP_8Cz = octakis(p-tert-butylphenyl) corrolazinato)$^{3-}$) was generated by treatment of the corresponding $Mn^{V}(O)(TBP_8Cz)$ complex with acid.[8] Similarly, complex $(tpfc)Mn^{V}(O)$ showed that an isoelectronic $(tpfc^{\bullet+})Mn^{IV}(OH)$ species was formed by the protonation of terminal oxo upon addition of Brønsted acids.[9] However, the comparison of the electronic structure and reactivity of a pair between Fe(V)-Oxo and its valence tautomer Fe^{IV}-Oxo-radical cation has not been reported till date.

The only example of a $Fe^{V}(O)$ that has been fully spectroscopically characterized is $[(TAML)Fe^{V}(O)]^{-}$ (TAML = tetraamido macrocyclic ligands) complex.[10] The density

functional theory (DFT) study on Fe-TAML complexes suggests for the possibility of ligand-based oxidation which can generate (TAML)$Fe^{IV}(O)$-radical cation and (TAML)$Fe^{V}(O)$-radical cation,[10,11] although the only experimental evidence for ligand-based oxidation of TAML is that of a (TAML)Fe^{III}-radical cation.[12] Subsequently, we have reported the generation of a $Fe^{V}(O)$ complex at room temperature, based on a fifth generation TAML ligand (bTAML biuret-tetraamide macrocycle ligand).[13] Later, the detailed mechanistic study for HAT and OAT reactions using $[(bTAML)Fe^{V}(O)]^{-}$ has been demonstrated.[14] Recently, this complex was shown to form $[(bTAML)Fe^{IV}(O)]^{2-}$ complex at pH 12, and its reactivity towards benzyl alcohol was shown to be 2500-fold slower than its one electron oxidized congener $[(bTAML)Fe^{V}(O)]^{-}$.[15] Since the occurrence of ligand oxidation in TAML systems has been shown before, we attempted the synthesis of $Fe^{IV}(O)$radical-cation which is a valance tautomer of the corresponding $Fe^{V}(O)$ complex. In this study, we have demonstrated the use of acid on $[(bTAML)Fe^{V}(O)]^{-}$ complex which leads to the formation of the isoelectronic $[(H\text{-}bTAML^{\bullet+})Fe^{IV}(O)]$ species (Scheme 5.1). Further, a study of the comparative HAT and OAT have been carried out to determine the factors that are crucial for controlling their reactivity.

Scheme 5.1. Synthesis of complex **[**$(H\text{-}bTAML^{\bullet+})Fe^{IV}(O)]$.

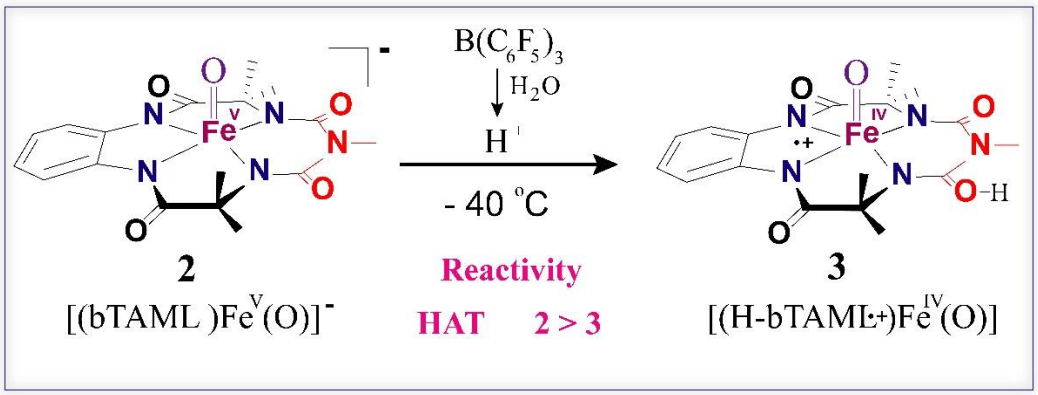

5.3 Experimental Section

5.3.1 Materials

An axially ligated aqua complex $[PPh_4][(bTAML)Fe^{III}\text{-}OH_2]$ (**1**) was synthesized by metathesis reaction of $[Li][(bTAML)Fe^{III}\text{-}OH_2]$ with an excess amount of PPh_4Cl in water.[16] Acetonitrile (LCMS grade, Aldrich) was used as received. *meta*-chloroperbenzoic acid (*m*CPBA, Aldrich) was purified by a reported method. 9,10-dihroanthacene, Tris-

(pentafluorophenyl)borane, Tris(4-bromophenyl)aminiumyl hexachlorideoantimonate (Magic blue), Trifluoromethanesulfonic acid, and Ferrocene, Tetraphenylphosphonium chloride were purchased from Aldrich and used as received. Deuterated 9,10-dihydroanthracene (DHA-d_4) was synthesized by following the literature method and purity was checked by GC-MS. All other solvents and reagents were purchased from commercial sources and were used as received unless otherwise noted.

5.3.2 General Instrumentation

UV-vis spectral studies were carried out using Agilent diode array 8453 spectrophotometer attached to an electrically controlled thermostat. GC-MS was performed on a Thermo Scientific ISQ QD Mass Spectrometer attached with Thermo Scientific TRACE 1300 gas chromatograph using an HP-5ms capillary column (30 m × 0.25 mm × 0.25 μm, J&W Scientific) with helium as a carrier gas. HR-MS was performed in a Thermo Scientific Q-Exactive Orbitrap analyzer using an electrospray ionization source connected with a C18 column (150 m × 4.6 mm × 8.0 μm). EPR spectra were recorded on Bruker EMX EPR spectrometer equipped with a liquid nitrogen cryostat.

5.3.3 Synthesis of Complex $[(bTAML)Fe^{V}(O)]^{-}$ (2)

$[(bTAML)Fe^{V}(O)]^{-}$ was prepared by reaction of $[(bTAML)Fe^{III}(OH_2)]^{-}$ complex (5×10^{-5} M) and 1.2 equiv mCPBA in acetonitrile as reported before.[13] UV-vis spectral change confirmed the formation of $Fe^{V}(O)$ species.

5.3.4 Synthesis of Complex $[(H\text{-}bTAML^{\bullet+})Fe^{IV}(O)]$ (3)

Complex $[(H\text{-}bTAML^{\bullet+})Fe^{IV}(O)]$ was prepared in situ by reacting $[(bTAML)Fe^{V}(O)]^{-}$ (5×10^{-5} M) with 3 equiv of $B(C_6F_5)_3$ in acetonitrile at -40 °C, resulted in a color change from green to gray. UV-vis spectroscopic measurement showed a spectral shift from 445 nm to 500 nm and 613 nm to 630 nm with the appearance of a broad peak at an absorbance of 865 nm wavelength.

5.3.5 Electron Paramagnetic Resonance (EPR) Measurements

Solution of complex $[(H\text{-}bTAML^{\bullet+})Fe^{IV}(O)]$ (2.0 mM) was prepared in acetonitrile. X-band EPR measurement was performed at 100 K temperature. A modulation

frequency of 100 kHz was used for the EPR spectral measurements. Bruker EMX EPR spectrometer.

5.3.6 Kinetic Measurements for Reaction of $[(bTAML)Fe^{V}(O)]^{-}$ with 9,10-Dihydroanthacene

At least three kinetic runs were carried out for each experiment; mean values are reported here. The kinetics were monitored in the scanning spectral kinetics mode of the spectrophotometer using a 1.0 cm quartz cell. All kinetic experiments were carried out in CH_3CN. Under pseudo-first-order condition, the substrate (9,10-Dihydroanthacene) was added into the freshly prepared $Fe^{V}(O)$ complex at -40 ˚C. The pseudo-first-order rate constant (k_{obs}) was calculated at 857 nm wavelength (generation of Fe^{IV}) by nonlinear curve fitting [$A_t = A_\alpha - (A_\alpha - A_o)e^{(-kobst)}$] and had a good agreement with rate constant value within 10% error (Figure 5.1). Resulting k_{obs} values correlated linearly with substrate concentration to give second-order rate constant k_2.

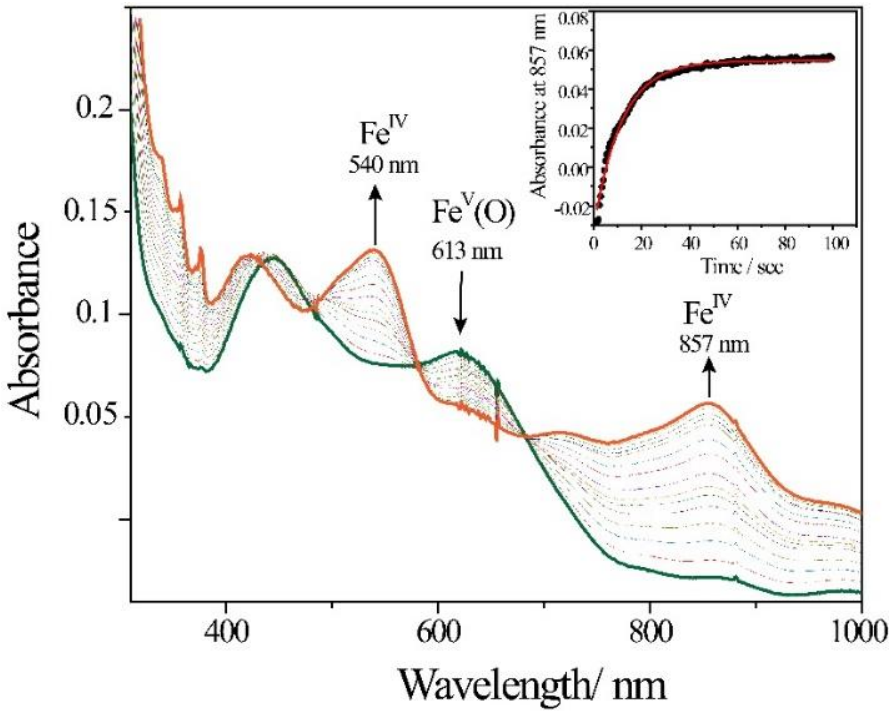

Figure 5.1. (A) UV–vis spectral changes upon reaction of $Fe^{V}(O)$ (4×10^{-5} M) with 9,10-dihydroanthracene (5×10^{-4} M); (inset) Absorbance *vs.* time plot at 857 nm (● indicates experimental data point; the red line is the first order fit according to the equation [$(A_t = A_\alpha - (A_\alpha - A_o)e^{(-k_{obs}t)}$]. The reaction was performed in acetonitrile solvent at -40 ˚C.

5.3.7 Kinetic Measurements for Reaction of [(H-bTAML•+)$Fe^{IV}(O)$] with 9,10-Dihydroanthacene

Before the addition of substrate, $Fe^{IV}(O)$-radical cation was prepared by adding three equiv of $B(C_6F_5)_3$ into the $Fe^{V}(O)$ at -40 °C. Under pseudo-first-order condition, the substrate (9,10-Dihydroanthacene) was added into a freshly prepared $Fe^{IV}(O)$-radical cation (**3**) at -40 °C. Initial reaction rates were determined from the absorbance decay at 630 nm because the rate of change of absorbance at 630 nm is related to the change in concentration of **3** (Figure 5.2(A)). During the initial reaction the change of absorbance at 630 nm are linear, and thus the rate of change of absorbance can be calculated from the slopes of the straight lines. The k_{obs} have been computed by a linear fit of initial rates with substrate concentration (Figure 5.2(B)). Further, second-order rate constant (k_2) can be obtained by dividing resulting k_{obs} values with a concentration of **3**.

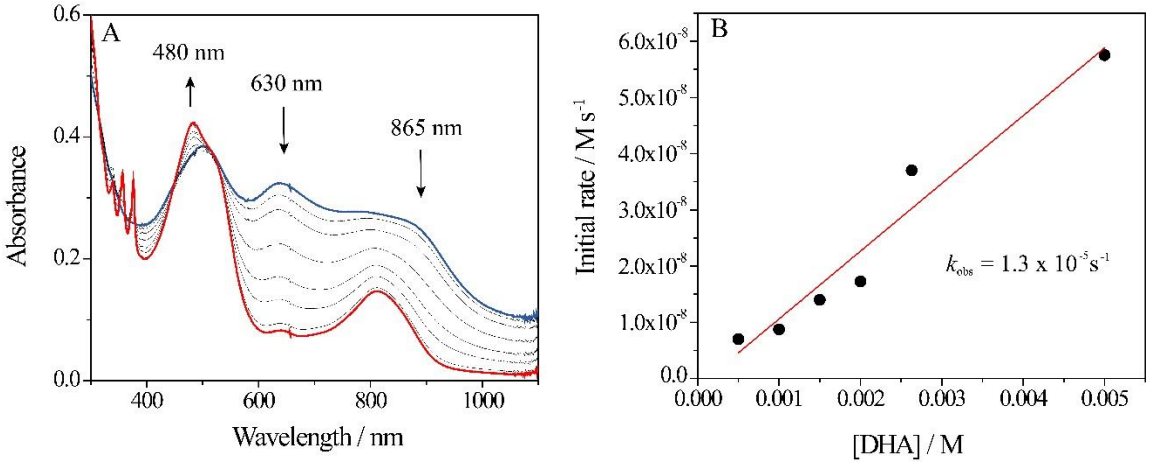

Figure 5.2. (A) UV–vis spectral changes with time upon reaction of [(H-bTAML•+)$Fe^{IV}(O)$] (5.5×10^{-5} M) and DHA (5.5×10^{-4} M); (B) the initial rare (at 630 nm) *vs* [DHA] plot for reaction of [(H-bTAML•+)$Fe^{IV}(O)$] (5.5×10^{-5} M) with DHA (5.5×10^{-4} - 5.5×10^{-3} M); (● indicates experimental data point; the red line is the linear fit according to the equation k_{obs} = initial rate / [DHA]. The reaction was performed at -40 °C in acetonitrile solvent.

5.4 Results and Discussion

5.4.1 Formation and Characterization of [(H-bTAML•+)Fe^{IV}(O)] (3) Complex

The addition of Lewis acid ($B(C_6F_5)_3$) to a solution of complex **2** in acetonitrile at -40 °C resulted in the formation of a new species, which exhibited a red-shifted absorption band at 500 nm, 630 nm and a broad peak between 750-950 nm. Formation of this new species above 0 °C was transient and hence unstable. Upon titration of this new species with ferrocene, complete reduction leading to the formation of the two electrons reduced complex (bTAML)Fe^{III}, required two equivalents of ferrocene. This indicates that this new species formed represents complex isoelectronic to Fe^{V}. The X-band EPR (100 K) measurement displayed the presence of *S*=1/2 spin species and the EPR spectra obtained was different in nature for that of the *S*=1/2 (bTAML)Fe^{V}(O) complex. The signal near g = 2 showed hyperfine splitting of g_x and g_y tensor, which is indicative of nuclear spin coupling with nitrogen nucleus and an unpaired electron on the ligand moiety. Therefore, this species was assigned as (bTAML•+)Fe^{V}(X) complex which was formed due to the intramolecular electronic redistribution (valence tautomerization) between Fe and bTAML ligand moiety of (bTAML)Fe^{V}(O) complex. Further, the HR-MS spectrum of solution displayed a mass peak at m/z = 430.0808, (Appendix D1) whose mass and isotope distribution pattern supported for the **2**-H species (calculated m/z = 430.0815). Hence, the new species was proposed as an either (H-bTAML•+)Fe^{IV}(O) or (bTAML•+)Fe^{IV}(OH) as a consequence of protonation at oxygen of carbonyl group in bTAML ligand or terminal oxo of Fe(O), respectively. DFT calculations on **2** indicate that the nucleophilicity of the carbonyl oxygen to be higher than that of the oxygen of the Fe^{V}(O) (Mulliken charge on oxygen atom in Fe=O is -0.42 and in C=O is -0.50 & -0.55). A similar observation has been reported for (TAML)Mn^{V}(O) complex, where Sc^{3+} was proposed to bind with the carbonyl oxygen of TAML ligand. On similar lines, the possibility exists for the binding of $B(C_6F_5)_3$ to the carbonyl oxygen in the TAML framework leading to the valance tautomerism. However, it is also possible that $B(C_6F_5)_3$ reacts with the residual water of solvent to generate H^+ which then protonates the carbonyl oxygen of ligand moiety leading to the formation of the valence tautomer [(H-bTAML•+)Fe^{IV}(O)], **3** (Figure 5.3). To distinguish between both this pathway, titration of Fe^{V}(O) (**2**) with the Bronsted acid (CF_3COOH and $HClO_4$) was carried out and the observations we similar to that obtained with $B(C_6F_5)_3$. These observations from UV-vis, EPR, and HR-MS spectral leads us to postulate that addition of H^+ onto **2** leads to

the formation of **3**. However, it should be noted that Mössbauer and Resonance Raman spectroscopy has to be carried out to conclusively assign the oxidation state and nature of the Fe-O bond.

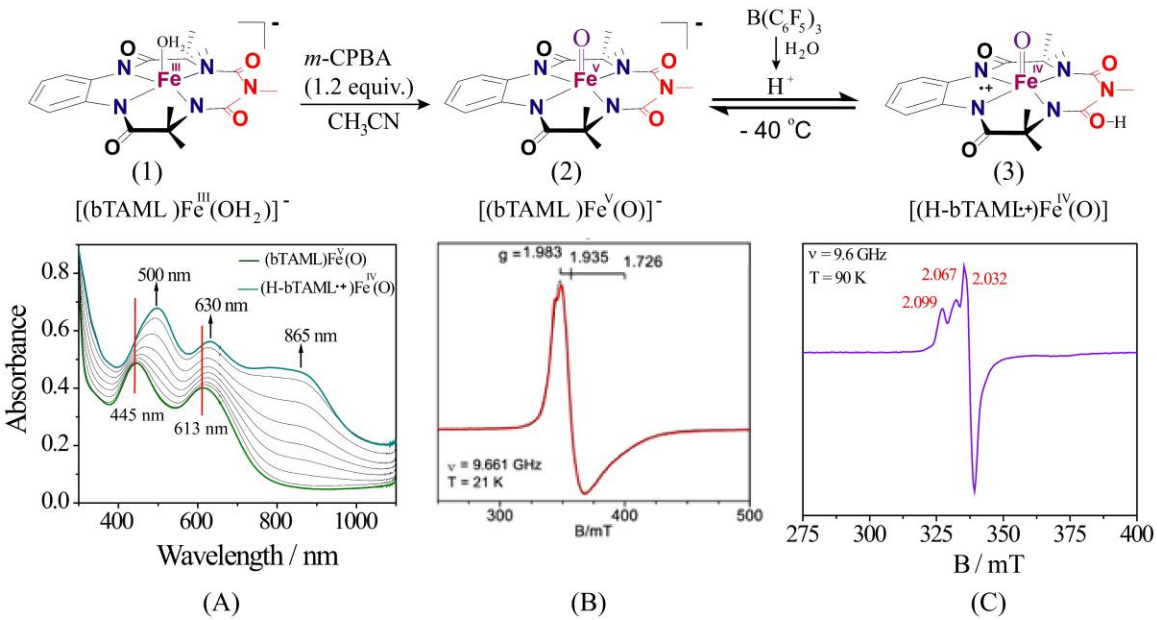

Figure 5.3. (A) UV–vis spectral changes for the formation of **3** upon addition of 3 equiv of $B(C_6F_5)_3$ to **2** (1.0×10^{-4} M) at -40 ˚C in acetonitrile; (B) X-band EPR of complex **2** (2.0 mM) at 100 K;[13] (C) X-band EPR of complex **3** (2.0 mM) in acetonitrile at 100 K.

5.4.2 Comparative Reactivity of Complex 2 and 3 for Hydrogen Atom Transfer (HAT) Reaction

Reaction kinetics of complex **2** and **3** for HAT was performed using 9,10-dihydroanthracene (DHA) as a substrate under pseudo-first-order condition. Fe^{V}(O) (**2**) was chemically synthesized from precursor Fe(III) complex and *m*CPBA (1:1). To this solution in CH_3CN at -40 °C was added DHA under pseudo-first order conditions. A decrease in the characteristic Fe^{V}(O) peak at 613 was observed with the concomitant increase in the peak at 857 nm (Fe^{IV} species). The kinetics was monitored by measuring the increase in the absorbance of the Fe^{IV} species at 857 nm over the whole course of the reaction. The pseudo first-order rate constant (k_{obs}) was calculated at 857 nm by non-linear curve fitting [$A_t = A_\alpha - (A_\alpha - A_o)e(-^{kobst})$] and had a good agreement in rate constant value within 10% error. Resulting k_{obs} values correlated linearly with substrate concentration to give a second order rate constant (k_2) 173±15 $M^{-1}s^{-1}$. By using deuterated 9,10-dihydroanthacene (DHA-d_4) as the substrate, kinetic isotope effect (KIE) k_H/k_D was determined to be 5.2. The presence of

KIE confirms that hydrogen atom transfer is the rate determining step. The addition of DHA to the solution of **2** resulted in the oxidation product anthracene (42 % yield) and anthrone (4 % yield). Formation of anthracene as a predominant product is in contrast to the previous report for $[(TAML)Fe^{V}(O)]^{-}$, where anthrone was shown as a major product and an alternative mechanism was proposed rather than the rate-limiting hydrogen atom transfer . The product yield for the reaction of **2** and DHA exhibited consumption of two equivalent of catalyst for the generation of one molecule of anthracene which is due to the non-rebound mechanism. The reaction of the complex **3** with DHA displayed reaction rate (k_2) of 0.24 $M^{-1}s^{-1}$ which is ~720 fold slower reactivity than its isoelectronic complex **2**. Again, the presence of kinetic isotope effect (k_H/k_D ~30) for the reaction of **3** using DHA-d_4 as substrate supports for the hydrogen atom abstraction as the rate determining step as was observed with **2**. However, the yield of the product anthracene was observed to be 95 % upon reaction of DHA and **3**, which is twofold higher than the amount of the product formed with **2**.

Scheme 5.2 Comparative Reaction Profile for Complex **2** and **3**.

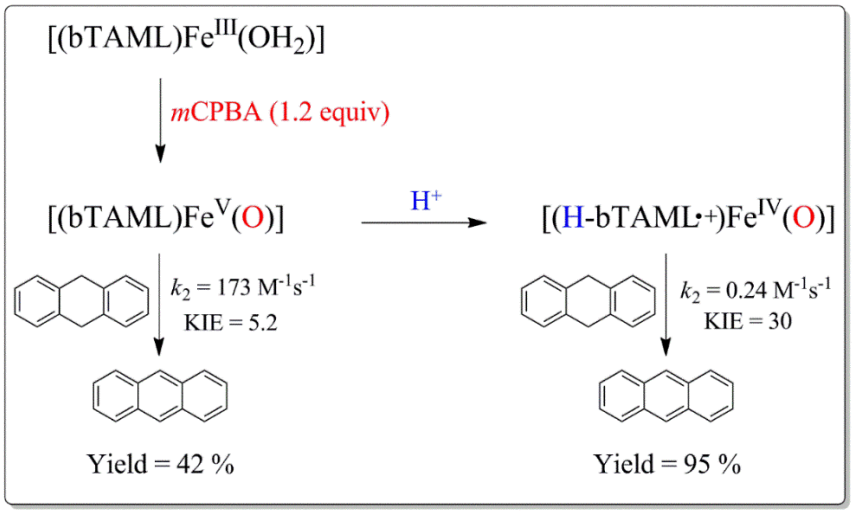

The reaction of complex **2** with DHA generated a Fe^{IV} species which immediately converted to Fe^{III} at room temperature. We believe that the Fe^{IV} species formed to be a mixture of $[(bTAML)Fe^{IV}(OH)]^{-}$ and $[\{(TAML)Fe^{IV}\}_2\text{-}\mu\text{-}Oxo]^{2-}$ dimer formed due to the non-rebound hydrogen atom abstraction and condensation reaction of Fe^{IV}-OH, respectively. To support this argument, a separately synthesized $[(bTAM)Fe^{IV}(Cl)]^{-}$ complex was titrated with NaOH solution where axial Cl was substituted by OH through ligand metathesis and subsequently, transformed into the $[\{(TAML)Fe^{IV}\}_2\text{-}\mu\text{-}Oxo]^{2-}$ dimer by a condensation reaction (Figure 5.4).

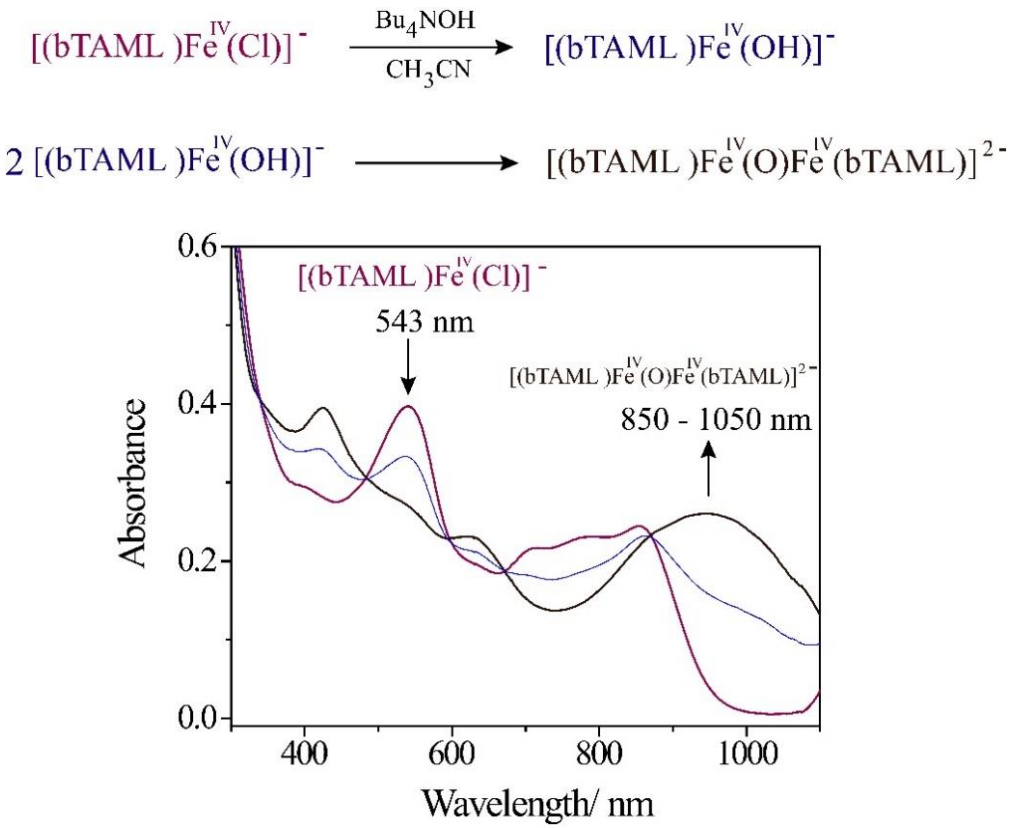

Figure 5.4. UV-vis spectral change for axial ligand substitution in complex $[(bTAML)Fe^{IV}(Cl)]^{-}$ upon titration with NaOH at 25 ˚C in acetonitrile.

Unlike complex **2**, in the case of complex **3**, a metastable Fe^{IV} complex was generated which is stable for few days at room temperature. This metastable complex was EPR silent and converted into Fe^{III} by the addition of one equivalent of ferrocene solution. We propose that, for **3**, hydrogen atom transfer from substrate to **3** leading to the formation of Fe^{IV}-OH via a common non-rebound pathway. This transient Fe^{IV}-OH then gets protonated in the presence of H^{+} and results in the formation of a stable Fe^{IV}-OH_2 complex (Figure 5.5(A)). In fact, the UV-vis spectra of this Fe^{IV} species exactly matched to the UV-vis spectra of a compound formed via one-electron oxidation of Fe^{III}-OH_2 complex with a one-electron oxidant tris(4-bromophenyl)aminiumyl hexachloridoantimonate (magic blue) (Figure 5.5(B)). This speculation can be correlated with the literature where the formation of the Fe^{IV}-OH_2 complex has been demonstrated by DFT as a thermodynamically favorable step for a related Fe-TAML complex.

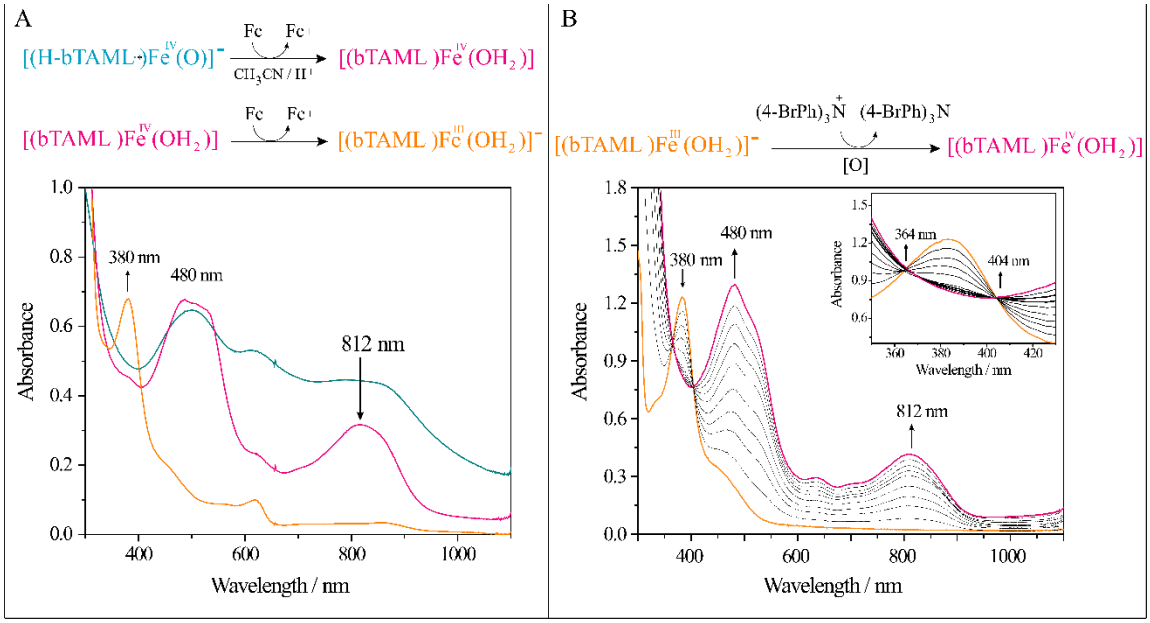

Figure 5.5. (A) UV-vis spectral change upon redox titration of complex **3** (1.5×10^{-4} M) (green): after addition of 1 equiv ferrocene (red), after addition of 2 equiv ferrocene (orange). (B) UV-vis spectral scan for 1 electron oxidation of $[(bTAML)Fe^{III}(OH_2)]^-$ (**1**) (3.0×10^{-4} M) (orange spectrum) with oxidant tris(4-bromophenyl)aminiumyl hexachlorideoantimonate (magic blue) (1 equiv) to form a proposed $[(bTAML)Fe^{IV}(OH_2)]$ complex at -40 ˚C in acetonitrile.

Oxygen atom transfer reaction was also observed for both the complex **2** and **3**. A reaction of thioanisole (PhSMe) resulted into sulfoxide (PhSOMe) product with complex **2** as well as **3**. The kinetic trace of reaction could not permit us to determine the rate of reaction due to the very fast reaction.

5.5 Conclusion

In summary, $[(H\text{-}bTAML^{\bullet+})Fe^{IV}(O)]$ (an isoelectronic of Fe^{V}) was synthesized by addition of Lewis acid to the $[(bTAML)Fe^{V}(O)]^-$. Protonation in secondary coordination sphere causes radical cation formation in bTAML ligand moiety of its $Fe^{V}(O)$ complex. This is the first example of non-heme $Fe^{IV}(O)$-radical cation as a valence tautomer of $Fe^{V}(O)$ with same ligand frame. The comparative reactivity study on hydrogen atom transfer reaction with DHA showed very significant rate difference between both the species (rate of reaction with DHA for $Fe^{V}(O)$ is greater than $Fe^{IV}(O)$-radical cation). Contrary, in a recent report, comparative kinetic studies showed an enhanced HAT reaction rate and inhibition of OAT reaction by $Mn^{IV}(O)(TBP_8Cz^{\bullet+})$ than isoelectronic

$Mn^{V}(O)(TBP_8Cz)$ species. This difference in the rate of HAT and OAT reactions was attributed to the comparatively higher reduction potential of $Mn^{IV}(O)(TBP_8Cz^{\bullet+})$ and low electrophilicity of its terminal oxo group, respectively.[8] However, an enhanced rate of OAT reaction has been displayed by the addition of Lewis acid into Mn-Oxo complexes of TAML,[7(j)] cyclam and N4Py ligand systems.[17] Therefore, further investigation of electron transfer (ET), HAT, and OAT reactions using this pair of valence tautomers ($[(bTAML)Fe^{V}(O)]^{-}$ and $[(H\text{-}bTAML^{\bullet+})Fe^{IV}(O)]$) are under progress in a separate study in our laboratory.

5.6 References

1. (a) Meunier, B.; de Visser, S. P.; Shaik, S. *Chem. Rev.* **2004**, *104*, 3947. (b) Groves, J. T. *J. Inorg. Biochem*. **2006**, *100*, 434. (c) Guengerich, F. P. *Chem. Res. Toxicol*. **2008**, *21*, 70. (d) Denisov, I. G.; Makris, T. M.; Sligar, S. G.; Schlichting, I. *Chem. Rev*. **2005**, *105*, 2253. (e) Czernuszewicz, R. S.; Mody, V.; Czader, A.; Galezowski, M.; Gryko, D. T. *J. Am. Chem. Soc*. **2009**, *131*, 14214. (f) Ostovic, D.; Bruice, T. C. *Acc. Chem. Res*. **1992**, *25*, 314. (g) Nam, W. *Acc. Chem. Res*. **2007**, *40*, 522. (h) Shaik, S.; Hirao, H.; Kumar, D. *Acc. Chem. Res*. **2007**, *40*, 532. (i) Franke, A.; Hessenauer-Ilicheva, N.; Meyer, D.; Stochel, G.; Woggon, W.-D.; van Eldik, R. *J. Am. Chem. Soc*. **2006**, *128*, 13611. (j) Zhang, R.; Newcomb, M. *Acc. Chem. Res*. **2008**, *41*, 468. (l) Coelho, P. S..; Brustad, E. M.; Kannan, A.; Arnold, F. H. *Science* **2013**, *339*, 307.
2. (a) Rittle, J.; Green, M. T. *Science*. **2010**, *330*, 933. (b) Ortiz de Montellano, P. R. *Chem. Rev.* **2010**, *110*, 932. (c) Hersleth, H.-P.; Ryde, U.; Rydberg, P.; Görbitz, C. H.; Andersson, K. K. *J. Inorg. Biochem*. **2006**, *100*, 460. (d) Behan, R. K.; Green, M. T. *J. Inorg. Biochem*. **2006**, *100*, 448. (e) Andersson, L. A.; D, J. H. *Struct. Bonding (Berlin, Ger.)* **1990**, *64*, 1. (f) Chance, B.; Powers, L.; Ching, Y.; Poulos, T.; Schonbaum, G. R.; Yamazaki, I.; Paul, K. G. *Arch. Biochem. Biophys*. **1984**, *235*, 596. (g) Penner-Hahn, J. E.; Smith Eble, K.; McMurry, T. J.; Renner, M.; Balch, A. L.; Groves, J. T.; Dawson, J. H.; Hodgson, K. O. *J. Am. Chem. Soc*. **1986**, *108*, 7819. (h) MacBeth, C. E.; Gupta, R.; Mitchell-Koch, K. R.; Young, V. G.; Lushington, G. H.; Thompson, W. H.; Hendrich, M. P.; Borovik, A. S. *J. Am. Chem. Soc*. **2004**, *126*, 2556. (i) Gupta, R.; Taguchi, T.; Borovik, A. S.; Hendrich, M. P. *Inorg. Chem*. **2013**, *52*, 12568.
3. (a) Groves, J. T.; Nemo, T. E.; Myers, R. S. *J. Am. Chem. Soc*. **1979**, *101*, 1032. (b) Mas-Balleste, R.; Que, L., Jr. *J. Am. Chem. Soc*. **2007**, *129*, 15964. (c) de Oliveira, F. T.; Chanda, A.; Banerjee, D.; Shan, X.; Mondal, S.; Que, L., Jr.; Bominaar, E. L.; Münck, E.; Collins, T. J. *Science* **2007**, *315*, 835. (d) Ostović, D.; Bruice, T. C. *Acc.*

Chem. Res. **1992**, *25*, 314. (e) Stephenson, N. A.; Bell, A. T. *J. Am. Chem. Soc*. **2005**, *127*, 8635. (f) Traylor, T. G.; Miksztal, A. R. *J. Am. Chem. Soc*. **1989**, *111*, 7443. (g) Que, L., Jr.; Tolman, W. B. *Nature* **2008**, *455*, 333.

4. (a) Buisson, G.; Deronzeir, A.; Duée, E.; Gans, P.; Marchon, J.-C.; Regnard, J.-R. *J. Am. Chem. Soc*. **1982**, *104*, 6793. (b) Das, P. K.; Samanta, S.; McQuarters, A. B.; Lehnert, N.; Dey, A. *Proc. Natl. Acad. Sci. USA* **2016**, *113*, 6611. (c) Goff, H. M.; Phillippi, M. A. *J. Am. Chem. Soc*. **1983**, *105*, 7567. (d) Spreer, L. O.; Maliyackel, A. C.; Holbrook, S.; Otvos, J. W.; Calvin, M. *J. Am. Chem. Soc*. **1986**, *108*, 1949.
5. Groves, J. T.; Quinn, R.; McMurry, T. J.; Lang, G.;Boso, B. *J. Chem. Soc. Chem., Commun*. **1984**, 1455.
6. Pan, Z.; Harischandra, D. N.; Newcomb, M. *J. Inorg. Biochem*. **2009**, *103*, 174.
7. (a) Green, M. T. *J. Am. Chem. Soc*. **1999**, *121*, 7939. (b) Harris, D. L.; Loew, G. H. *J. Am. Chem. Soc*. **1998**, *120*, 8941. (c) Antony, J.; Grodzicki, M.; Trautwein, A. X. *J. Phys. chem. A* **1997**, *101*, 2692. (d) Ogliaro, F.; Harris, N.; Cohen, S.; Filatov, M.; de Visser, S. P.; Shaik, S. J. *Angew. chem. Int. Ed*. **2000**, *39*, 3855. (e) Grapperhaus, C. A.; Mienert, B.; Bill, E.; Weyhermu¨ller, T.; Wieghardt, K. *Inorg. Chem*. **2000**, *39*, 5306. (f) Rohde, J.-U.; In, J.-H.; Lim, M. H.; Brennessel, W. W.; Bukowski, M. R.; Stubna, A.; Nam, W.; Que, L., Jr. *Science* **2003**, *299*, 1037. (g) Lim, M. H.; Rohde, J.-U.; Stubna, A.; Bukowski, M. R.; Costas, M.; Ho, R. Y. N.; Munck, E.; Nam, W.; Que, L., Jr. *Proc. Natl. Acad. Sci. USA* **2003** , *100*, 3665. (h) Fukuzumi, S.; Morimoto, Y.; Kotani, H.; Naumov, P. e.; Lee, Y.-M.; Nam, W. *Nat. Chem.* **2010**, *2*, 756. (i) Que, L. *Acc. Chem. Res.* **2007**, *40*, 493. (j) Kim, S.; Cho, K.-B.; Lee, Y.-M.; Chen, J.; Fukuzumi, S.; Nam, W. *J. Am. Chem. Soc*. **2016**, *138*, 10654.
8. (a) Leeladee, P.; Baglia, R. A.; Prokop-Prigge, K. A.; Latifi, R.; de Visser, S. P.; Goldberg, D. P. *J. Am. Chem. Soc*. **2012**, *134*, 10397. (b) Zaragoza, J. P. T.; Baglia, R. A.; Siegler, M. A.; Golberg, D. P. *J. Am. Chem. Soc*. **2015**, *137*, 6531. (c) Bagalia, R. A.; Prokop-Prigge, K. A.; Neu, H. M.; Siegler, M. A.; Goldberg, D. P. *J. Am. Chem. Soc*. **2015**, *137*, 10874. (d) Baglia, R. A.; Crest, C. M.; Yang, T.; Leeladee, P.; Goldberg, D. P. *Inorg. Chem*. **2016**, *55*, 10800.
9. Bougher, C. J.; Liu, S.; Hicks, S. D.; Abu-Omar, M. M. *J. Am. Chem. Soc*. **2015**, *137*, 14481.
10. de Oliveira, F. T.; Chanda, A.; Banerjee, D.; Shan, X.; Mondal, S.; Que, L., Jr.; Bominaar, E. L.; Münck, E.; Collins, T. J. *Science* **2007**, *315*, 835.

11. (a) Kwon, E.; Cho, K.-B.; Hong, S.; Nam, W. *Chem. Commun*. **2014**, *50*, 5572. (b) Ertem, M. Z.; Gagliardi, L.; Cramer, C. *J. Chem. Sci*. **2012**, *3*, 1293. (c) Liao, R.-Z.; Li, X.-C.; Siegbahn, P. E. M. Eur. *J. Inorg. Chem*. **2014**, 728.
12. (a) Bartos, M. J.; Gordon-Wylie, S. W.; Fox, B. G.; James Wright, L.; Weintraub, S. T.; Kauffmann, K. E.; Münck, E.; Kostka, K. L.; Uffelman, E. S.; Richard, C. E. F.; Noon, K. R.; Collins, T. J. *Coord. Chem. Rev*. **1998**, *174*, 361. (b) Bartos, M. J.; Kidwell, C.; Kauffmann, K. E.; Gordon-Wylie, S. W.; Collins, T. J.; Clark, G. C.; Münck, E.; Weintraub, S. T. *Angew. Chem. Int. Ed. Engl*. **1995**, *34*, 1216.
13. Ghosh, M.; Singh, K. K.; Panda, C.; Weitz, A.; Hendrich, M. P.; Collins, T. J.; Dhar, B. B.; Sen Gupta, S. *J. Am. Chem. Soc.* **2014**, *136*, 9524.
14. (a) Singh, K. K.; Tiwari, M. k.; Ghosh, M.; Panda, C.; Weitz, A.; Hendrich, M. P.; Dhar, B. B.; Vanka, K.; Sen Gupta, S. *Inorg. Chem.* **2015**, *54*, 1535. (b) Singh, K. K.; Tiwari, M. k.; Dhar, B. B.; Vanka, K.; Sen Gupta, S. *Inorg. Chem*. **2015**, *54*, 6112. (c) Singh, K. K.; Sen Gupta, S. *Chem. Commun*. **2017**, *53*, 5914. (d) Ghosh, M.; Nikhil, Y. L. K.; Dhar, B. B.; Sen Gupta, S. *Inorg. Chem.* **2015,** *54*, 11792. (e) Panda, C.; Debgupta, J.; Díaz, D. D.; Singh, K. K.; Sen Gupta, S.; Dhar, B. B. *J. Am. Chem. Soc.* **2014,** *136*, 12273.
15. Pattanayak, S.; Jasniewski, A. J.; Rana, A.; Draksharapu, A.; Singh, K. K.; Weitz, A.; Hendrich, M.; Que, L., Jr.; Dey, A.; Sen Gupta, S. *Inorg. Chem*. **2017**, 56, 6352.
16. Panda, C.; Ghosh, M.; Panda, T.; Banerjee, R.; Sen Gupta, S. *Chem. Comm.* **2011**, *47*, 8016.
17. (a) Chen, J.; Lee, Y.-M.; Davis, K. M.; Wu, X.; Seo, M. S.; Cho, K.-B.; Yoon, H.; Park, Y. J.; Fukuzumi, S.; Pushkar, Y. N.; Nam, W. *J. Am. Chem. Soc*. **2013**, *135*, 6388. (b) Yoon, H.; Lee, Y.-M.; Wu, X.; Cho, K.-B.; Sarangi, R.; Nam, W.; Fukuzumi, S. *J. Am. Chem. Soc*. **2013**, *135*, 9186. (c) Chen, J.; Yoon, H.; Lee, Y.-M.; Seo, M. S.; Sarangi, R.; Fukuzumi, S.; Nam, W. *Chem. Sci.* **2015**, *6*, 3624. (d) Jung, J.; Kim, S.; Lee, Y.-M.; Nam, W.; Fukuzumi, S. *Angew. Chem., Int. Ed*. **2016**, *55*, 7450.

Chapter VI

Conclusion and Future Perspective

6.1. Conclusion

High-valent iron-oxo species have been identified as a key reactive intermediate in the catalytic cycle of various biological reactions by heme and non-heme enzymes using H_2O_2 and O_2. For example, methane monooxygenase generates $Fe^{IV}{}_2(\mu\text{-}O)_2$ intermediate to catalyze methane hydroxylation reaction, whereas $Fe^{IV}(O)$-radical cation and $Fe^{V}(O)(OH)$ species are known to mediate unactivated C-H and C=C bonds oxidation by Cytochrome P450 and Rieske dioxygenase, respectively. Their highly selective nature towards substrate (hydrocarbons) oxidation in the presence of various C-H and C=C bonds of protein motifs around the active site of enzymes, creates tremendous interest of research. However, limited stability of these enzymes (gets denatured upon heating or chemical changes) and the relatively low productivities (preparation, purification, and storage are time-consuming) are important features which hinder the commercial application. Hence, an approach perused by many chemists is to mimic enzymes both structurally and functionally to understand the mechanism of the various enzymatic reactions. Understanding of such mechanisms may lead to a new insight in bio-catalysis and drug design as well as the development of new approaches for industrial catalysis.

Over the years, several $Fe^{IV}(O)$ complexes have been generated with various ligand frame. For example, $Fe^{IV}(O)$ complexes of the pentadentate N_5 ligands N_4Py and Bn-tpen displayed room temperature stability and ability to hydroxylate strong C-H bonds such as cyclohexane (C-H bond strength of 99.3 kcal/mol). The mechanistic investigations on the C-H bond hydroxylation using porphyrin complexes and synthetic non-heme $Fe^{IV}(O)$ complexes reveals about the various factors which affect their reactivity. Such factors primarily include redox potential of the metal center and basicity of the Fe-oxo. Furthermore, the selectivity for the product formation was observed to be guided by the spin state and rebound or non-rebound pathway during the progress of the reaction. Effect of the axial ligand on the reactivity of these complexes has also been studied. However, the direct role of the $Fe^{V}(O)$ complex, which is isoelectronic to the (porphyrin)$Fe^{IV}(O)$-radical-cation (Cpd 1), in O-atom transfer reaction into the C-H and C=C bonds are unexplored. The paucity for the generation of $Fe^{V}(O)$ complexes is due to their unstable nature. Among very few examples, Fe-TAML is the first complex to generate spectroscopically characterized $Fe^{V}(O)$ species at -40 ˚C. However, instability of (TAML)$Fe^{V}(O)$ complex above -40 ˚C hampers its reactivity as well as its utility in mechanistic studies. Latter, we generated a fully spectroscopically characterized $[(bTAML)Fe^{V}(O)]^{-}$ complex at room

temperature using biuret-tetraamido macrocyclic ligand (bTAML; a modified TAML moiety). Further, this $Fe^{V}(O)$ species was demonstrated for the unactivated C-H bond hydroxylation reaction.

This thesis comprises of the detail mechanistic investigations on the O-atom transfer reactions for C-H bond hydroxylation and C=C bond epoxidation using $Fe^{V}(O)$ species as a terminal oxidant. Inspired by the enzymatic systems, we have successfully generated $Fe^{V}(O)$ complex in aqueous media. Further, the role of water on the reactivity of $Fe^{V}(O)$ during C-H bond hydroxylation has been described. After that, we elucidated the mechanism of direct O-atom transfer in the course of the reaction of $Fe^{V}(O)$ with alkenes to form the corresponding epoxide. The mechanism of each step of the reaction was evaluated using various spectroscopic and kinetic methods. Then, we used $[(bTAML)Fe^{III}(H_2O)]^-$ complex for the reductive activation of O_2 where molecular O_2 has been shown as an oxygen source for catalytic epoxidation reaction without the use of any sacrificial reductant. Latter, the effect of Lewis acid on $Fe^{V}(O)$ complex has been demonstrated. The redox non-innocent nature of the ligand of $[(bTAML)Fe^{V}(O)]^-$ complex has been observed to generate $Fe^{IV}(O)$-radical-cation in the presence of Lewis acid. The reactivity difference in hydrogen atom transfer from C-H bond of DHA has been studied using these two tautomers, $Fe^{V}(O)$ and $Fe^{IV}(O)$-radical cation. The key achievement of this thesis work entitled "Investigations on the Oxygen Atom Transfer Reaction Mediated through a Bio-Inspired $Fe^{V}(O)$ Complex" can be summarized as follows:

Chapter I:

- This chapter provides an overview of the existing literature on the importance of high-valent Fe-oxo intermediate in bio-inspired oxidations reactions.
- It describes the mechanism of various metal catalyzed C-H bond hydroxylation and C=C bond epoxidation reaction.
- A brief outline of synthetic heme and non-heme ligand systems which generate $Fe^{IV}(O)$ and $Fe^{V}(O)$ complexes.

Chapter II:

- We demonstrated for the first time the formation of a $Fe^{V}(O)$ complex in CH_3CN/H_2O mixture up to 90% water.

- It showed that the reactivity of $Fe^{V}(O)$ toward the oxidation of C-H bonds, such as those in toluene, can be tuned by varying the amount of water in the H_2O/CH_3CN mixture.
- The rate of the reaction of $Fe^{V}(O)$ for toluene oxidation has been shown to enhance by 60 fold in 70% water than pure organic solvent (acetonitrile).
- The role of water in accelerating the rate of the reaction has been studied using kinetic measurements, isotope labeling experiments, and density functional theory (DFT) calculations.
- A kinetic isotope effect of ~13 was observed for the oxidation of toluene and d_8-toluene showing that C-H abstraction was involved in the rate-determining step.
- Activation parameters determined by using Eyring plots for toluene oxidation in H_2O/CH_3CN mixtures. It showed a gain in enthalpy with a concomitant loss in entropy, which points to the formation of a more-ordered transition state involving water molecules. Hence, the increase in activity of $Fe^{V}(O)$ upon addition of water molecule is due to the preferential stabilization of the transition state.
- This study would help to elucidate the role of the water molecule in the active site of the Fe-based enzyme.

Chapter III:

- For the first time, we investigate the mechanism of O-atom transfer to alkenes using the $Fe^{V}(O)$ complex of biuret-modified Fe-TAML at room temperature.
- The second-order rate constant (k_2) for the reaction of different alkenes with $Fe^{V}(O)$ was determined under single turnover conditions. An 8000-fold rate difference was found between electron-rich (4-methoxystyrene; k_2 = 216 $M^{-1}s^{-1}$) and electron-deficient (Methyl *trans*-cinnamate; k_2 = 0.03 $M^{-1}s^{-1}$) substrates indicates the electrophilic character of $Fe^{V}(O)$.
- The use of *cis*-stilbene as a mechanistic probe leads to the formation of both *cis*- and *trans*-stilbene epoxides (73:27). This suggests the formation of a radical intermediate, which would allow C-C bond rotation to yield both stereoisomers of stilbene-epoxide.
- Detailed DFT calculations showed that the reaction proceeds via a two-step process through a doublet spin surface. Formation of epoxidation proceeds via generation of the radical intermediate through an electrophilic attack on alkene followed by a fast ring closing step.

- Finally, using biuret-modified Fe-TAML as the catalyst and NaOCl as the oxidant under catalytic conditions epoxide was formed with modest yields and turnover numbers.

Chapter IV:

- We report the reductive activation of O_2 by a bioinspired $[(bTAML)Fe^{III}(H_2O)]^-$ complex to catalyze the epoxidation of alkenes with TONs of up to 80.
- Due to the low redox potential of metal center in $[(bTAML)Fe^{III}(OH_2)]^-$ complex, Fe^{III} itself can act as an electron source to reduce the O_2 molecule, and both the oxygen atom get transferred to the substrate, as reminiscent of dioxygenase enzymes.
- Spectroscopic and kinetic evidence indicates the involvement of $Fe^V(O)$ as the active oxidant during the reaction. Mechanistic studies using UV-vis and EPR spectroscopy showed Fe-O_2 adduct formation upon O_2 interaction with the iron center.

Chapter V:

- We reported, formation of a mononuclear $Fe^{IV}(O)$-radical-cation by reaction of $[(bTAML)Fe^V(O)]^-$ complex with Lewis acid ($B(C_6F_5)_3$) in acetonitrile at -40 ˚C.
- UV-vis, EPR, and HR-MS spectral observations lead us to postulate that addition of H^+ into $[(bTAML)Fe^V(O)]^-$ leads to the formation of valence tautomer $[(H\text{-}bTAML^{\bullet+})Fe^{IV}(O)]$ complex.
- The reactivity of the $[(H\text{-}bTAML^{\bullet+})Fe^{IV}(O)]$ complex is compared to that of the $[(bTAML)Fe^V(O)]^-$ in hydrogen atom transfer reaction using 9,10-dihydroanthacene (DHA) as substrate. Reaction of DHA with $[(H\text{-}bTAML^{\bullet+})Fe^{IV}(O)]$ (k_2 = 0.24 M^{-1} s^{-1}) showed ~720 fold slower reaction rate than the reaction rate of its isoelectronic complex $[(bTAML)Fe^V(O)]^-$ (k_2 = 173 M^{-1} s^{-1}).

6.2 Future Perspective

Due to vital importance of high-valent iron-oxo complexes such as $Fe^{IV}(O)$, $Fe^V(O)$ and $Fe^{IV}(O)$-radical cation in several reactions of biological processes, the mechanistic understanding of direct role of $Fe^V(O)$ in hydrocarbons (alkane and alkene) oxidation (hydroxylation and epoxidation) demonstrated in this thesis would have

enormous applicative significance. Based on these findings, a rational approach can be adopted towards synthesis of a model complex for selective oxidation.

Understanding of this work led us to propose a Fe(III) complex based on modified TAML ligand frame (Figure 6.1). We believe, this new ligand framework would have the right electronics to stabilize the high-valent iron-oxo intermediate, as well as the bulky phenyl group, can disfavor the dimerization of catalyst during the reaction, which has been proven as the main drawback of many catalysts.

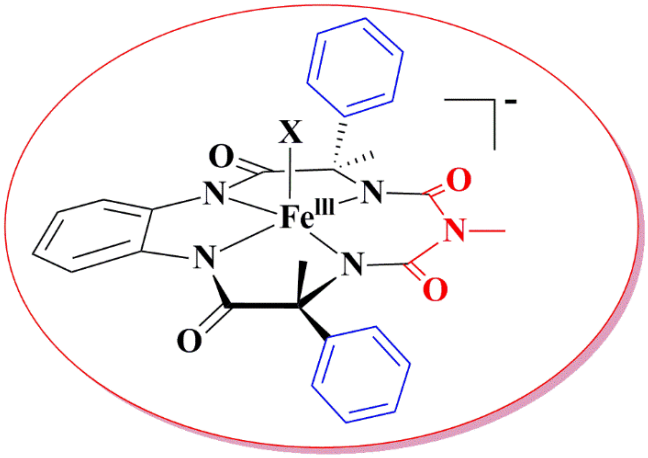

Figure 6.1. Proposed bTAML modified Fe^{III} complex.

The noticeable feature of the above-proposed complex could be:

1. The generation of chiral center in ligand frame due to the substitution of a methyl group by phenyl.

2. Formation of $Fe^{V}(O)$ can be envisioned due to the presence of tetra anionic nitrogen group as σ- donor to the iron center similar to TAML and bTAML.[1,2]

3. Extension in the application for asymmetric epoxidation and enantioselective hydroxylation reaction could be a primary achieving goal owing to the chiral center in ligand frame.

4. Phenyl substitution is expected to increase the steric in the ligand moiety. We believe this would inhibit comproportionation reactions to generate μ-oxo-$(Fe^{IV})_2$ as has been shown before for porphyrin analogs.[3-7]

6.3 References

1. (a) de Oliveira, F. T.; Chanda, A.; Banerjee, D.; Shan, X.; Mondal, S.; Que, L.; Bominaar, E. L.; Münck E.; Collins, T. J. *Science* **2007**, *315*, 835. (b) Kundu, S.; Thompson, J. V. K.; Ryabov, A. D.; Collins, T. J. *J. Am. Chem. Soc.* **2011**, *133*, 18546.
2. (a) Panda, C.; Ghosh, M.; Panda, T.; Banerjee R.; Sen Gupta, S. *Chem. Commun.* **2011**, *47*, 8016. (b) Ghosh, M.; Singh, K. K.; Panda, C.; Weitz, A.; Hendrich, M. P.; Collins, T. J.; Dhar, B. B.; Sen Gupta, S. *J. Am. Chem. Soc.* **2014**, *136*, 9524.
3. Meunier, B., *Chem. Rev.* **1992,** 92, 1411.
4. Chang, C. K.; Kuo, M.-S., *J. Am. Chem. Soc.* **1979,** 101, 3413.
5. Chang, C. K.; Ebina, F., *Chem. Comm.* **1981**, 778.
6. Ghosh, A.; Ryabov, A. D.; Mayer, S. M.; Horner, D. C.; Prasuhn, D. E.; Sen Gupta, S.; Vuocolo, L.; Culver, C.; Hendrich, M. P.; Rickard, C. E. F.; Norman, R. E.; Horwitz, C. P.; Collins, T. J., *J. Am.Chem. Soc.* **2003,** 125, 12378.
7. Nam, W., *Acc. Chem. Res.* **2007,** 40, 522.

Appendix A

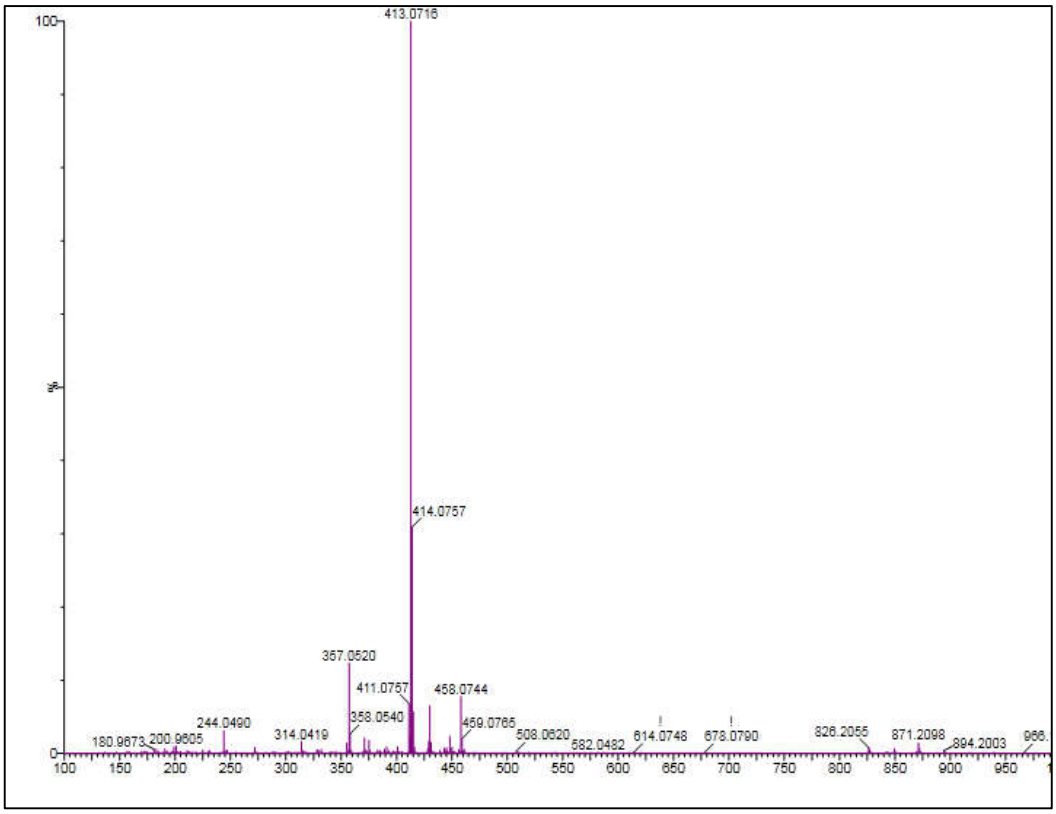

Appendix A1. HR-MS of **1** in 30% H_2O-CH_3CN mixture after completion of reaction. Calculated m/z of 1 is 413.0716.

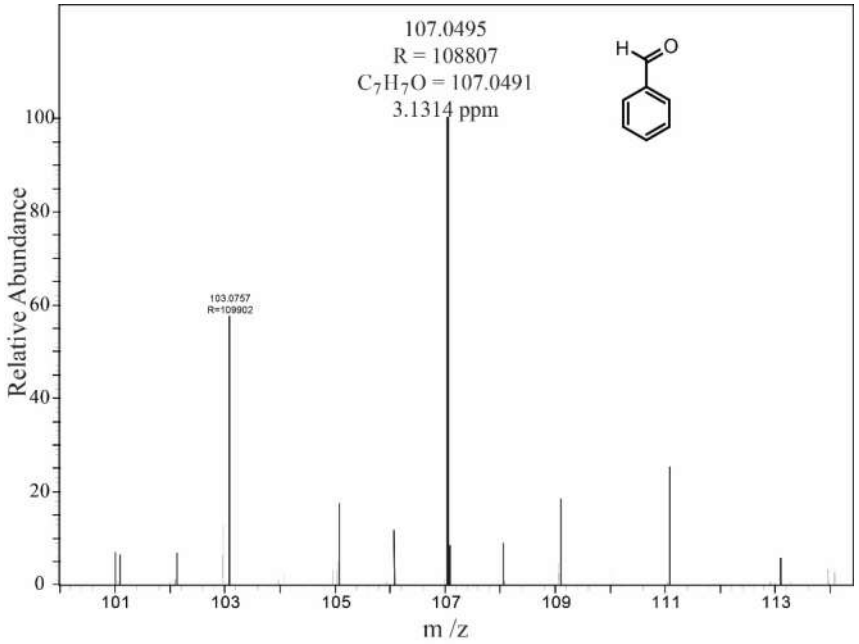

Appendix A2. The HR-MS spectra of benzaldehyde obtained after reaction with Toluene (1000 equiv) and **2** (10^{-4} M) in 30 % H_2O-CH_3CN mixture.

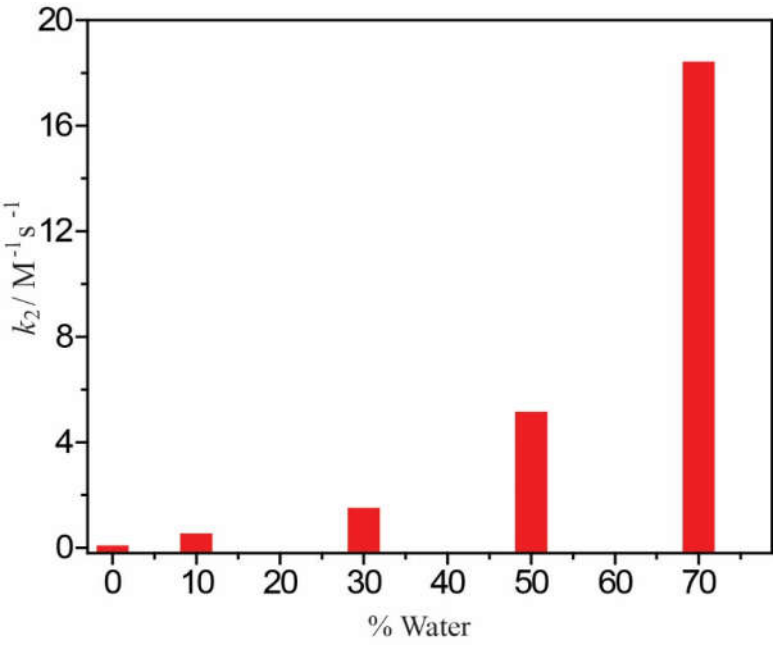

Appendix A3. Second order rate constant (k_2) for 2,3-Dimethylbutane oxidation vs. % of water content in H_2O-CH_3CN mixture.

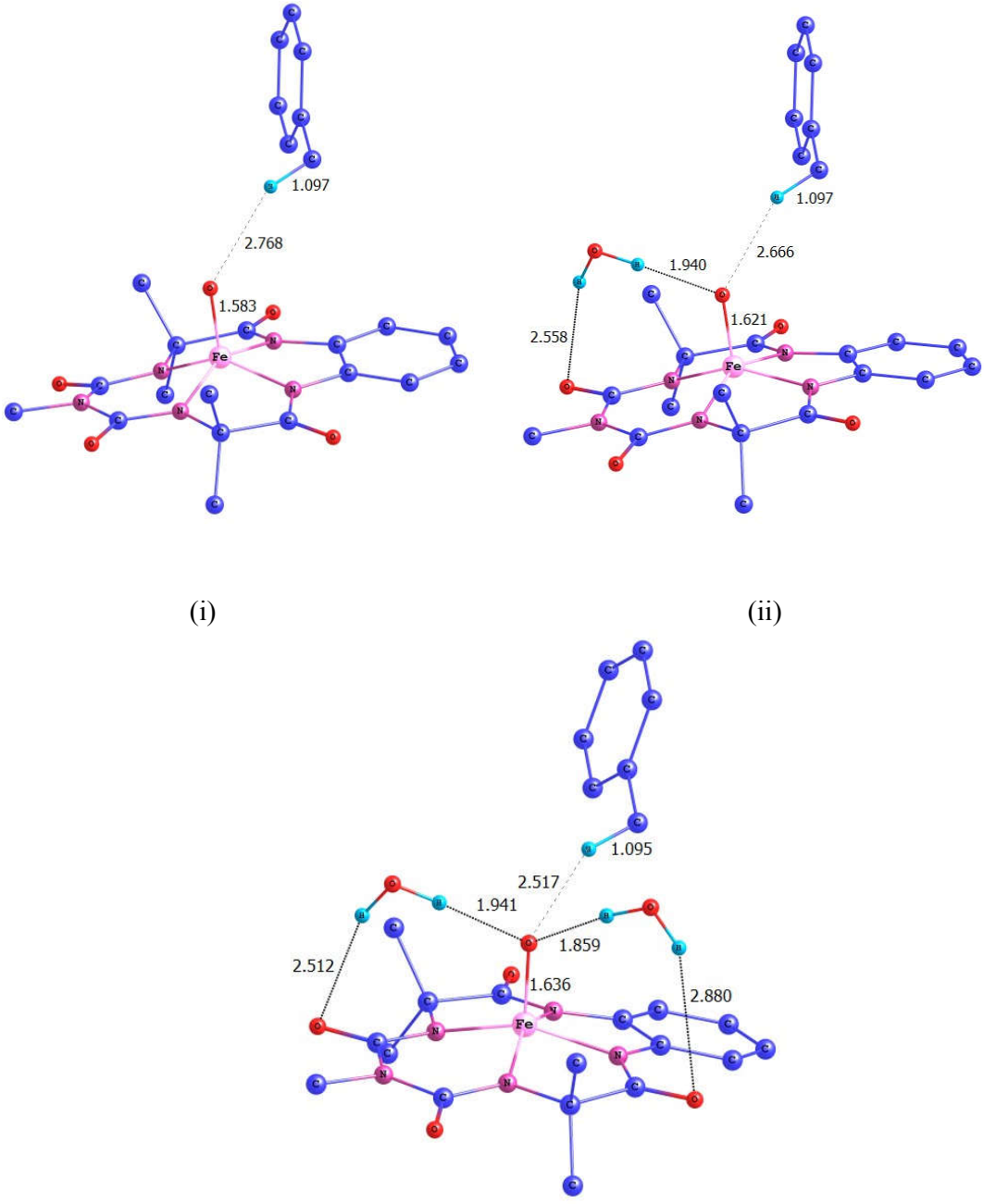

(i) (ii)

(iii)

Appendix A4. (i), (ii), and (iii) are UB3LYP optimized reactant structures with none, one and two explicitly added water molecules respectively; all the atom-atom distances are in Å.

XYZ coordinates of all the stationary points obtained by full optimization at UB3LYP/6-31G*, LANL2DZ (Fe) level of theory

Doublet Reactant, gas

C	1.843327	3.824391	1.768575
C	0.792962	4.590627	1.253422
C	-0.321119	3.981495	0.671598
C	-0.367923	2.582455	0.598324
C	0.700621	1.805653	1.114309
C	1.806660	2.429763	1.707882
N	-1.401465	1.785519	0.082106
Fe	-1.012675	-0.009849	-0.136211
N	-0.947947	-1.615742	0.757325
C	-1.775348	-2.687895	0.494310
N	-2.889976	-2.519778	-0.337485
C	-3.610522	-3.764698	-0.620823
N	0.448114	0.443327	0.990212
C	1.084352	-0.568662	1.627342
O	2.134775	-0.485523	2.272530
C	-2.599627	2.237500	-0.422382
O	-2.918192	3.420156	-0.516880
C	-3.520993	1.101406	-0.886628
C	-4.866175	1.292376	-0.151686
N	-2.859720	-0.165784	-0.526846
C	-3.523474	-1.320352	-0.764439
O	-4.634751	-1.403778	-1.305972
C	-3.698797	1.250295	-2.415145
C	0.317541	-1.898062	1.493386
C	1.226656	-2.877337	0.719743
C	0.047976	-2.392695	2.930572
O	-0.311168	-0.181609	-1.544283
O	-1.555082	-3.819867	0.941609
H	2.410711	0.269946	-1.759079
H	-2.738162	1.106384	-2.922181
H	-4.070448	2.254533	-2.644469
H	-4.404585	0.499153	-2.773859
H	-5.598235	0.570984	-0.514637
H	-5.221883	2.313176	-0.320835
H	-4.729688	1.147030	0.926610
H	-1.144581	4.559742	0.276990
H	0.837578	5.676159	1.302521
H	-4.359844	-3.543716	-1.376424
H	1.375761	-2.524849	-0.307218
H	2.201743	-2.918316	1.215406
H	0.780058	-3.871994	0.693475
H	-0.395406	-3.387886	2.912803
H	0.995368	-2.406359	3.477810
H	-0.636455	-1.706126	3.442710
H	2.600574	1.817536	2.114710
H	2.702370	4.314722	2.220878
H	-4.099194	-4.150730	0.280956
H	-2.905258	-4.520405	-0.971503
C	3.301845	0.909357	-1.736209
H	3.119818	1.663024	-0.961250
C	4.557489	0.118239	-1.450550
H	3.367479	1.424427	-2.701041
C	5.571888	-0.004063	-2.409399
C	6.731507	-0.738817	-2.148076
C	6.896718	-1.367352	-0.913621
C	5.892878	-1.252923	0.052565
C	4.736259	-0.518430	-0.210719
H	5.450185	0.483436	-3.374959
H	7.504058	-0.818060	-2.910188
H	7.797230	-1.940680	-0.705172
H	6.008931	-1.737893	1.019074
H	3.965503	-0.438636	0.553044

Quartet Reactant, gas

C	2.049807	3.494912	2.187521
C	1.145550	4.390652	1.567554
C	0.053897	3.928347	0.854627
C	-0.159462	2.533191	0.746581
C	0.769347	1.613568	1.382203
C	1.874863	2.124409	2.102735
N	-1.182214	1.895186	0.110446
Fe	-1.034922	-0.005376	0.012156
N	-1.043747	-1.725752	0.714591
C	-1.936311	-2.701427	0.383267
N	-3.089416	-2.335559	-0.362246
C	-3.940418	-3.485071	-0.689528
N	0.418888	0.306404	1.209932
C	1.016892	-0.825880	1.717233
O	2.074134	-0.853301	2.347065
C	-2.293844	2.438401	-0.502255
O	-2.505818	3.638521	-0.655262
C	-3.298131	1.356893	-0.983385
C	-4.668728	1.738222	-0.381534
N	-2.824450	0.030780	-0.505817
C	-3.585136	-1.065902	-0.781600
O	-4.680878	-1.024236	-1.360880
C	-3.330807	1.424993	-2.527320
C	0.201650	-2.113734	1.425742
C	1.087683	-3.034037	0.557158
C	-0.092045	-2.761455	2.797862
O	-0.194430	-0.130486	-1.394214
O	-1.818233	-3.896711	0.690758
H	2.215053	0.388785	-1.617031
H	-2.352724	1.143111	-2.931808
H	-3.569256	2.444460	-2.849416
H	-4.085370	0.732272	-2.904853
H	-5.439314	1.068590	-0.762268
H	-4.902327	2.775038	-0.641934
H	-4.636800	1.653801	0.711696
H	-0.648200	4.597753	0.375349
H	1.314388	5.461439	1.652451

H	-4.745175	-3.127918	-1.325860
H	1.278398	-2.561334	-0.412196
H	2.044899	-3.210746	1.058716
H	0.573842	-3.983366	0.395242
H	-0.599966	-3.714631	2.652139
H	0.847895	-2.910119	3.338434
H	-0.737576	-2.105363	3.394540
H	2.556893	1.426858	2.570772
H	2.899102	3.891508	2.738580
H	-4.350497	-3.933671	0.2217
H	-3.348692	-4.250576	-1.197355
C	3.134966	0.983640	-1.681767
H	3.071838	1.744845	-0.893902
C	4.376317	0.137561	-1.519260
H	3.131216	1.501105	-2.647449
C	5.342916	0.063066	-2.531024
C	6.493760	-0.714975	-2.379346
C	6.699203	-1.437094	-1.203569
C	5.742905	-1.373532	-0.185906
C	4.595182	-0.595907	-0.341006
H	5.189692	0.622806	-3.451780
H	7.227646	-0.755733	-3.181622
H	7.592465	-2.045377	-1.080919
H	5.888069	-1.934555	0.734378
H	3.860507	-0.559938	0.460280

Doublet TS1, gas

C	-1.761687	2.857357	-1.806679
C	-0.989492	1.744625	-1.446193
C	-1.332745	0.449480	-1.926660
C	-2.445727	0.283658	-2.762863
C	-3.206751	1.403631	-3.113624
C	-2.868654	2.675260	-2.641812
N	0.147670	1.718974	-0.629361
C	0.839039	2.793839	-0.141568
O	0.512782	3.975081	-0.264855
N	-0.445823	-0.529084	-1.475605
C	-0.373869	-1.830010	-1.881341
O	-1.145209	-2.391103	-2.661277
Fe	0.741385	0.017576	-0.119345
N	1.617071	-1.582227	-0.477108
C	2.762018	-2.008382	0.136289
N	3.491220	-1.085590	0.921591
C	4.652485	-1.679759	1.591193
O	-0.136142	-0.281188	1.309760
N	2.278428	0.911622	0.470704
C	2.128011	2.379801	0.603298
C	3.288059	3.144404	-0.071361
C	3.372862	0.326187	1.030716
O	4.265472	0.945456	1.627542
C	1.963515	2.811780	2.077733
C	0.833073	-2.570116	-1.259087
C	0.267469	-3.690821	-0.358997
C	1.644255	-3.157585	-2.433940
O	3.201832	-3.163724	0.060893
C	-2.237264	1.075070	1.759560
C	-3.337554	0.133134	1.977329
C	-3.624535	-0.368635	3.264336
C	-4.659539	-1.277373	3.465445
C	-5.430308	-1.714244	2.383169
C	-5.152983	-1.235230	1.098391
C	-4.120031	-0.324825	0.894804
H	-1.174024	0.377588	1.479283
H	1.155860	2.238389	2.547038
H	1.709442	3.876275	2.118195
H	2.889968	2.627386	2.624133
H	4.217568	2.971013	0.470932
H	3.048922	4.212063	-0.087475
H	3.411474	2.801994	-1.105752
H	-1.477093	3.834704	-1.439955
H	-3.468456	3.537452	-2.924771
H	5.045368	-0.944158	2.288077
H	-0.286346	-3.255576	0.480513
H	-0.418148	-4.311249	-0.945755
H	1.082980	-4.302216	0.031210
H	2.448284	-3.790880	-2.059055
H	0.969626	-3.734881	-3.073399
H	2.079426	-2.348556	-3.032899
H	-2.681831	-0.706833	-3.129296
H	-4.069642	1.277649	-3.764054
H	5.429325	-1.951028	0.866819
H	4.344745	-2.590672	2.107574
H	-2.323479	1.705880	0.874363
H	-1.905197	1.624717	2.643056
H	-3.023735	-0.033204	4.106593
H	-4.866763	-1.648147	4.466497
H	-6.237290	-2.425959	2.539033
H	-5.743389	-1.575977	0.251603
H	-3.901322	0.037727	-0.106415

Quartet TS1, gas

C	1.380694	3.334801	1.507970
C	0.737723	2.110311	1.265090
C	1.094890	0.952118	2.021306
C	2.087889	1.039926	3.010631
C	2.718353	2.267498	3.237832
C	2.368604	3.401766	2.495944
N	-0.279127	1.845130	0.343045
C	-0.969367	2.761986	-0.411814
O	-0.709564	3.967166	-0.492429
N	0.336685	-0.162953	1.664802
C	0.290779	-1.369946	2.308562
O	1.006309	-1.713271	3.256864
Fe	-0.725124	0.031812	0.109856
N	-1.553643	-1.533423	0.697847
C	-2.623641	-2.149147	0.100513
N	-3.344859	-1.416042	-0.881565
C	-4.438663	-2.140409	-1.536115
O	0.367051	-0.430583	-1.146549
N	-2.240103	0.699190	-0.766810

C	-2.154542	2.122607	-1.175986
C	-3.410759	2.926295	-0.781945
C	-3.267149	-0.048819	-1.265988
O	-4.139930	0.377821	-2.043141
C	-1.859198	2.261756	-2.683608
C	-0.795767	-2.304813	1.719957
C	-0.062824	-3.503747	1.084545
C	-1.677147	-2.751124	2.902945
O	-2.983735	-3.310451	0.361111
C	2.621585	0.870346	-1.518121
C	3.588282	-0.145903	-1.811888
C	3.835773	-0.573163	-3.145167
C	4.754789	-1.579461	-3.421690
C	5.458531	-2.204288	-2.382135
C	5.224889	-1.805714	-1.057725
C	4.309144	-0.799160	-0.773921
H	1.432782	0.169052	-1.279036
H	-0.981877	1.655405	-2.952911
H	-1.648796	3.316206	-2.914108
H	-2.724246	1.916727	-3.263163
H	-4.270011	2.595585	-1.375054
H	-3.214338	3.993810	-0.953612
H	-3.634516	2.780753	0.285533
H	1.092271	4.205842	0.923040
H	2.872116	4.353284	2.682550
H	-4.384902	-1.982951	-2.620389
H	0.538850	-3.167672	0.227010
H	0.606816	-3.950912	1.833446
H	-0.792575	-4.247877	0.743288
H	-2.385558	-3.521271	2.580868
H	-1.023924	-3.138272	3.697087
H	-2.238517	-1.893233	3.303307
H	2.338082	0.148952	3.583671
H	3.493994	2.334876	4.004425
H	-5.416552	-1.770952	-1.192319
H	-4.333427	-3.198208	-1.281496
H	2.782273	1.508963	-0.645768
H	2.438269	1.643370	-2.269044
H	3.286191	-0.095039	-3.959745
H	4.926672	-1.885748	-4.456465
H	6.176968	-2.996720	-2.601201
H	5.762130	-2.291672	-0.240041
H	4.124146	-0.500460	0.260643

Doublet Intermediate, gas

C	3.173106	1.501703	-2.969441
C	3.287726	0.120305	-3.159555
C	2.349555	-0.757330	-2.606575
C	1.286428	-0.234100	-1.857129
C	1.162561	1.173700	-1.674980
C	2.115327	2.038554	-2.231353
N	0.244639	-0.936347	-1.239833
Fe	-0.847037	0.074749	-0.102257
N	-2.169098	1.309412	0.311893
C	-3.344978	1.038470	0.952411
N	-3.722628	-0.322621	1.091853
C	-4.969081	-0.556132	1.828345
N	0.027560	1.511217	-0.936041
C	-0.445609	2.763457	-0.659247
O	0.070839	3.826332	-1.005283
C	-0.025050	-2.273830	-1.324889
O	0.691915	-3.121892	-1.860974
C	-1.378377	-2.645205	-0.672782
C	-2.243520	-3.264850	-1.793849
N	-1.984277	-1.403477	-0.135976
C	-3.188627	-1.493665	0.496852
O	-3.849798	-2.536670	0.599621
C	-1.092200	-3.680031	0.436895
C	-1.762578	2.729154	0.155114
C	-1.470590	3.392346	1.519615
C	-2.798251	3.544638	-0.648701
O	0.038893	-0.073712	1.425722
O	-4.095076	1.906405	1.418637
H	0.924619	-0.429389	1.217921
H	-0.512810	-3.216063	1.243450
H	-0.509961	-4.506674	0.016882
H	-2.030770	-4.053513	0.849150
H	-3.190011	-3.614985	-1.380932
H	-1.697509	-4.095605	-2.251755
H	-2.448880	-2.515557	-2.567575
H	2.414183	-1.827971	-2.751613
H	4.111429	-0.281223	-3.745772
H	-4.857044	-1.448170	2.445455
H	-0.749560	2.789566	2.082626
H	-1.043124	4.386740	1.353053
H	-2.393081	3.475538	2.097125
H	-3.719391	3.654892	-0.076589
H	-2.372379	4.525897	-0.878683
H	-3.026186	3.037184	-1.593940
H	2.001535	3.104694	-2.085852
H	3.911073	2.171640	-3.405364
H	-5.809547	-0.722915	1.143704
H	-5.169096	0.323468	2.434717
C	2.759740	-2.117669	1.231872
H	2.530994	-2.274554	0.183017
C	3.708676	-1.163888	1.651627
H	2.260103	-2.757402	1.953107
C	4.043303	-1.007560	3.030760
C	4.982215	-0.073190	3.438931
C	5.624375	0.746138	2.498206
C	5.308542	0.616554	1.137507
C	4.373479	-0.315668	0.714374
H	3.543077	-1.636585	3.763372
H	5.218120	0.027760	4.495801
H	6.355500	1.481852	2.822917
H	5.793091	1.257090	0.404916
H	4.123985	-0.401576	-0.339570

Quartet Intermediate, gas

C	2.722007	2.278252	3.231280

C	2.372461	3.410703	2.486288
C	1.384984	3.341358	1.497642
C	0.742461	2.116150	1.257472
C	1.098544	0.960082	2.018238
C	2.092197	1.049505	3.006862
N	-0.274329	1.848848	0.335204
Fe	-0.732538	0.035795	0.118170
N	-1.554155	-1.533963	0.702471
C	-2.622260	-2.150671	0.106802
N	-3.343759	-1.417479	-0.877180
C	-4.438221	-2.143117	-1.529289
N	0.339602	-0.156461	1.664636
C	0.294103	-1.362436	2.311726
O	1.009097	-1.703966	3.261145
C	-0.965902	2.763707	-0.419220
O	-0.709159	3.969902	-0.503209
C	-2.153167	2.121784	-1.180439
C	-3.409057	2.926477	-0.788460
N	-2.241720	0.699351	-0.766895
C	-3.267434	-0.051116	-1.265170
O	-4.140062	0.373702	-2.043670
C	-1.858651	2.256335	-2.688684
C	-0.793484	-2.300114	1.725530
C	-0.060491	-3.501208	1.093686
C	-1.674380	-2.742620	2.910639
O	0.354703	-0.464537	-1.167408
O	-2.984451	-3.311087	0.369620
H	1.243691	0.032771	-1.212973
H	-0.981365	1.648909	-2.956487
H	-1.648746	3.310023	-2.922907
H	-2.723865	1.908376	-3.266505
H	-4.268242	2.594665	-1.380977
H	-3.211859	3.993518	-0.961367
H	-3.633527	2.782503	0.279189
H	1.095070	4.211136	0.911665
H	2.874230	4.363108	2.672858
H	-4.386009	-1.987241	-2.613954
H	0.540357	-3.166634	0.235329
H	0.609180	-3.946490	1.843629
H	-0.791253	-4.245388	0.755312
H	-2.382644	-3.513647	2.591153
H	-1.020532	-3.126545	3.705917
H	-2.235308	-1.883146	3.307747
H	2.341114	0.160494	3.583267
H	3.496286	2.348830	3.999025
H	-5.415979	-1.773986	-1.184876
H	-4.332189	-3.200388	-1.272902
C	2.683720	0.905124	-1.530960
H	2.643285	1.345357	-0.532915
C	3.598628	-0.140027	-1.814526
H	2.249295	1.485075	-2.346885
C	3.836938	-0.580275	-3.149364
C	4.752827	-1.587957	-3.420786
C	5.457991	-2.208598	-2.378104
C	5.224563	-1.807400	-1.053272
C	4.313192	-0.799037	-0.770960
H	3.286906	-0.103559	-3.964195
H	4.922388	-1.901207	-4.453720
H	6.175851	-3.002028	-2.594912
H	5.760387	-2.293937	-0.235114
H	4.129559	-0.494812	0.262117

Doublet TS2, gas

C	0.539152	2.245535	1.166426
C	-0.506994	2.765943	0.345993
C	-0.602355	4.146412	0.124221
C	0.338909	4.998400	0.708728
C	1.368649	4.488377	1.505680
C	1.478665	3.114606	1.739591
N	-1.346747	1.761403	-0.143724
C	-2.518352	1.911226	-0.830355
O	-3.014087	2.976555	-1.202797
N	0.461169	0.857562	1.307470
C	1.279362	0.038355	2.021915
O	2.298874	0.371547	2.637350
Fe	-0.735530	0.013403	0.119144
N	-0.350634	-1.543281	1.071064
C	-1.004740	-2.736370	0.967856
N	-2.075759	-2.827093	0.037462
C	-2.608735	-4.182427	-0.134662
O	0.390860	-0.117085	-1.317394
C	2.171142	0.986474	-1.887405
C	3.295241	0.114513	-1.849710
C	4.045432	-0.064138	-0.653767
C	5.145307	-0.911630	-0.627222
C	5.537214	-1.609578	-1.777998
C	4.806598	-1.453874	-2.963986
C	3.704382	-0.610547	-3.002474
N	-2.421431	-0.520195	-0.465908
C	-3.219951	0.555156	-1.106334
C	-4.635771	0.661642	-0.499754
C	-2.871645	-1.803752	-0.551939
O	-3.920652	-2.145807	-1.115531
C	-3.287974	0.380371	-2.639330
C	0.772141	-1.429175	2.038546
C	1.949345	-2.354937	1.677034
C	0.301832	-1.691244	3.489504
O	-0.703156	-3.758408	1.600427
H	0.765802	-1.015322	-1.276027
H	-2.276105	0.289513	-3.051173
H	-3.767750	1.258799	-3.083368
H	-3.853767	-0.519816	-2.886597
H	-5.220287	-0.224212	-0.749630
H	-5.121987	1.561758	-0.888066
H	-4.570651	0.747187	0.591653
H	-1.409738	4.521963	-0.490965
H	0.265797	6.070191	0.536967
H	-3.096561	-4.238371	-1.105839
H	2.280635	-2.174608	0.647534
H	2.792177	-2.142437	2.341914
H	1.646038	-3.398507	1.773631

H	-0.013474	-2.729737	3.598474
H	1.123865	-1.473215	4.179058
H	-0.541462	-1.035115	3.735066
H	2.264323	2.701374	2.359082
H	2.094975	5.163973	1.952542
H	-3.346388	-4.429197	0.639596
H	-1.785453	-4.890989	-0.060245
H	1.981426	1.667701	-1.068986
H	1.694067	1.214585	-2.832868
H	3.139783	-0.491240	-3.924569
H	5.103124	-1.995680	-3.859250
H	6.398450	-2.272103	-1.749614
H	5.699916	-1.037406	0.299166
H	3.734999	0.453222	0.250425

Quartet TS2, gas

C	2.125551	-2.090559	0.451534
C	2.610356	-1.495015	-0.751446
C	3.518481	-2.190135	-1.562591
C	3.933420	-3.466871	-1.178477
C	3.455524	-4.052316	-0.000025
C	2.553025	-3.373847	0.821425
N	2.089600	-0.214449	-0.952945
C	2.463944	0.700673	-1.898778
O	3.281126	0.519532	-2.802327
N	1.253472	-1.247664	1.142501
C	0.686528	-1.452425	2.368910
O	0.816894	-2.453263	3.075726
Fe	0.679508	0.263142	0.183950
N	-0.102023	0.807107	1.791420
C	-0.734306	1.993415	2.011651
N	-0.692726	2.969364	0.977287
C	-1.487590	4.169608	1.257112
O	-0.795129	-0.360677	-0.720364
C	-2.063530	-1.857969	-2.079905
C	-3.433796	-1.679907	-1.784230
C	-4.065906	-2.411660	-0.737369
C	-5.411819	-2.234163	-0.452296
C	-6.182251	-1.325512	-1.192557
C	-5.582426	-0.591578	-2.226094
C	-4.237147	-0.760724	-2.519302
N	0.897424	1.990214	-0.507945
C	1.750572	2.065978	-1.718783
C	2.863506	3.126087	-1.569008
C	0.180017	3.087281	-0.144825
O	0.214768	4.177897	-0.733136
C	0.918247	2.317856	-2.995196
C	-0.165721	-0.243311	2.837978
C	-1.608722	-0.749139	3.050750
C	0.451479	0.231283	4.172331
O	-1.370522	2.270416	3.038627
H	-1.550462	0.165403	-0.402600
H	0.124753	1.566020	-3.078268
H	1.567245	2.238536	-3.873490
H	0.464768	3.309841	-2.953425
H	2.426899	4.124680	-1.534028
H	3.554662	3.041121	-2.413324
H	3.424497	2.951897	-0.643001
H	3.882773	-1.717253	-2.465239
H	4.637192	-4.009356	-1.806232
H	-1.700094	4.667022	0.313083
H	-2.036826	-1.079560	2.096660
H	-1.598849	-1.601371	3.737869
H	-2.226801	0.053125	3.458429
H	-0.159397	1.021397	4.609776
H	0.518228	-0.621346	4.855168
H	1.463068	0.618606	4.001795
H	2.179718	-3.805630	1.740957
H	3.789428	-5.048007	0.284300
H	-0.947848	4.870288	1.906952
H	-2.402737	3.870085	1.765738
H	-1.473072	-2.607557	-1.569976
H	-1.601456	-1.346991	-2.915025
H	-3.774965	-0.185634	-3.318061
H	-6.173721	0.117708	-2.800350
H	-7.235437	-1.187168	-0.963198
H	-5.870142	-2.801436	0.354143
H	-3.470565	-3.111651	-0.156646

Doublet Product, gas

C	0.878762	2.723188	-0.452310
C	0.221637	2.667069	0.817159
C	-0.254406	3.845130	1.407464
C	-0.077455	5.065445	0.747479
C	0.570893	5.120706	-0.489291
C	1.054128	3.956039	-1.093500
N	0.151739	1.365639	1.343274
C	-0.225192	0.980054	2.595656
O	-0.681558	1.707166	3.482990
N	1.297839	1.463768	-0.908919
C	2.168276	1.179153	-1.922775
O	2.660574	1.984458	-2.716183
Fe	0.734611	0.026506	0.152083
N	1.865263	-1.032031	-0.860563
C	2.006242	-2.384214	-0.720615
N	1.328275	-3.022885	0.360078
C	1.486420	-4.481362	0.359275
O	-1.160175	-0.525706	-0.491858
C	-2.165617	0.472824	-0.768151
C	-3.488160	-0.158387	-1.136619
C	-3.541922	-1.221683	-2.049532
C	-4.766830	-1.782746	-2.408116
C	-5.954767	-1.285400	-1.863948
C	-5.909336	-0.228809	-0.953674
C	-4.680821	0.326842	-0.588439
N	0.413944	-1.192576	1.586187
C	0.011392	-0.541545	2.861039
C	1.127132	-0.620472	3.927984
C	0.801076	-2.491208	1.588674
O	0.688631	-3.269589	2.548874

C	-1.296857	-1.138054	3.417908
C	2.522029	-0.339279	-1.999693
C	2.007848	-0.854967	-3.361749
C	4.058482	-0.450806	-1.924834
O	2.673553	-3.101190	-1.480297
H	-1.382755	-1.039463	0.312913
H	-2.098564	-1.080641	2.667550
H	-1.618849	-0.567152	4.294133
H	-1.141989	-2.186215	3.679719
H	1.306251	-1.661654	4.202600
H	0.831847	-0.044980	4.811140
H	2.056401	-0.194125	3.531334
H	-0.735959	3.784819	2.375331
H	-0.446754	5.978862	1.209383
H	0.737213	-4.904720	1.025016
H	0.913898	-0.785458	-3.406706
H	2.425355	-0.236273	-4.162811
H	2.299288	-1.897338	-3.500710
H	4.363966	-1.489849	-2.059161
H	4.505136	0.179442	-2.699938
H	4.413942	-0.101256	-0.948066
H	1.572230	3.978840	-2.044008
H	0.704746	6.076691	-0.991407
H	2.479806	-4.785011	0.712438
H	1.364119	-4.848309	-0.659859
H	-1.749744	1.047802	-1.600187
H	-2.269651	1.148561	0.086425
H	-4.646502	1.143745	0.128945
H	-6.827528	0.158288	-0.519052
H	-6.909213	-1.723646	-2.144931
H	-4.795252	-2.609128	-3.113867
H	-2.616662	-1.610619	-2.465355

Quartet Product, gas

C	0.450993	2.828488	-0.329818
C	-0.126348	2.618153	0.959689
C	-0.753687	3.675951	1.625706
C	-0.809469	4.935433	1.016253
C	-0.243669	5.141798	-0.242854
C	0.390141	4.094238	-0.922156
N	0.033241	1.295614	1.419668
C	-0.281356	0.779494	2.642181
O	-0.872597	1.359125	3.557242
N	1.047573	1.667687	-0.859034
C	1.823227	1.547756	-1.976689
O	2.058150	2.431837	-2.803345
Fe	0.815838	0.133516	0.176288
N	2.012693	-0.707882	-0.974097
C	2.461305	-1.988515	-0.873136
N	2.042475	-2.758503	0.262329
C	2.520829	-4.145855	0.277665
O	-1.179487	-0.705713	-0.682215
C	-2.339559	0.142891	-0.707980
C	-3.602182	-0.618842	-1.048448
C	-3.593778	-1.607350	-2.042804
C	-4.764461	-2.290797	-2.370466
C	-5.961139	-1.992421	-1.712539
C	-5.977685	-1.010783	-0.720541
C	-4.802661	-0.332920	-0.387812
N	0.808921	-1.150406	1.535320
C	0.211228	-0.692105	2.818988
C	1.250296	-0.662581	3.962029
C	1.405321	-2.376832	1.478304
O	1.398028	-3.205953	2.399924
C	-1.004625	-1.550158	3.222960
C	2.433908	0.120211	-2.136786
C	1.904561	-0.454656	-3.467821
C	3.965783	0.300393	-2.195718
O	3.191866	-2.542603	-1.707048
H	-1.281679	-1.368268	0.024808
H	-1.747559	-1.572550	2.412913
H	-1.485475	-1.113766	4.103915
H	-0.686218	-2.573083	3.431357
H	1.584792	-1.675329	4.191948
H	0.802496	-0.202120	4.848281
H	2.118557	-0.063305	3.662149
H	-1.177546	3.497323	2.606019
H	-1.298647	5.757152	1.535304
H	1.731612	-4.795993	0.658663
H	0.817845	-0.592586	-3.413134
H	2.124982	0.245440	-4.280246
H	2.371892	-1.420608	-3.668143
H	4.448435	-0.656124	-2.401137
H	4.213517	1.024921	-2.977594
H	4.337473	0.685114	-1.238045
H	0.842651	4.236589	-1.895389
H	-0.291369	6.124817	-0.706910
H	3.393307	-4.261620	0.932262
H	2.797080	-4.414779	-0.738480
H	-2.110215	0.890055	-1.473880
H	-2.447839	0.673200	0.245014
H	-4.815402	0.423357	0.394049
H	-6.901792	-0.778571	-0.196935
H	-6.873061	-2.526347	-1.968346
H	-4.743431	-3.057753	-3.140834
H	-2.660060	-1.841652	-2.546120

Doublet Reactant, CPCM CH_3CN

C	1.747627	3.902365	1.707446
C	0.683850	4.642140	1.177207
C	-0.416692	4.003685	0.603416
C	-0.438619	2.601446	0.550472
C	0.640817	1.851539	1.086733
C	1.734537	2.507061	1.671187
N	-1.452531	1.777646	0.038908
Fe	-1.027573	-0.014585	-0.143214
N	-0.924475	-1.618648	0.753992
C	-1.720210	-2.711341	0.483212
N	-2.815735	-2.574013	-0.379258
C	-3.493717	-3.838100	-0.700003

N	0.409964	0.481575	0.990431
C	1.046136	-0.504144	1.670112
O	2.069113	-0.376707	2.351879
C	-2.671277	2.192695	-0.446732
O	-3.016430	3.368305	-0.549077
C	-3.576831	1.033864	-0.879551
C	-4.900400	1.189576	-0.097400
N	-2.868894	-0.216237	-0.539378
C	-3.499731	-1.391116	-0.765133
O	-4.623044	-1.508256	-1.278265
C	-3.809375	1.178740	-2.400969
C	0.323827	-1.856449	1.536416
C	1.286186	-2.819844	0.808174
C	0.019590	-2.335614	2.972073
O	-0.309881	-0.169012	-1.553324
O	-1.480355	-3.835011	0.943345
H	2.571765	0.360315	-1.931872
H	-2.863632	1.074357	-2.944522
H	-4.226972	2.166884	-2.617401
H	-4.500566	0.407141	-2.742497
H	-5.625605	0.448143	-0.431711
H	-5.298716	2.195070	-0.260633
H	-4.725611	1.055856	0.976541
H	-1.243803	4.566856	0.195857
H	0.710549	5.727857	1.206781
H	-4.149650	-3.660988	-1.547830
H	1.473112	-2.473918	-0.214805
H	2.240164	-2.839485	1.343675
H	0.867793	-3.825834	0.772110
H	-0.399104	-3.341067	2.958318
H	0.947835	-2.328115	3.550475
H	-0.694001	-1.658870	3.456165
H	2.543117	1.922564	2.088331
H	2.596571	4.415501	2.150803
H	-4.088994	-4.198722	0.146334
H	-2.745399	-4.591865	-0.943059
C	3.455975	0.992161	-1.774768
H	3.210075	1.680510	-0.957732
C	4.678521	0.163632	-1.449216
H	3.605624	1.583283	-2.684225
C	5.711316	0.000985	-2.382967
C	6.835626	-0.775906	-2.087704
C	6.946101	-1.405313	-0.846240
C	5.924029	-1.249545	0.095510
C	4.802878	-0.472559	-0.202950
H	5.635140	0.489586	-3.351970
H	7.624534	-0.885785	-2.827610
H	7.819527	-2.008390	-0.612623
H	6.001675	-1.732020	1.066769
H	4.016957	-0.356210	0.540625

Doublet TS1, CPCM CH_3CN

C	-1.831926	2.783506	-1.848234
C	-1.024962	1.695249	-1.489663
C	-1.328223	0.392096	-1.971843
C	-2.435161	0.194050	-2.808308
C	-3.230874	1.289471	-3.159249
C	-2.932172	2.570329	-2.684901
N	0.113641	1.703849	-0.668009
C	0.788199	2.794522	-0.200436
O	0.457020	3.971234	-0.370586
N	-0.411472	-0.563036	-1.515601
C	-0.275486	-1.848825	-1.938563
O	-1.003442	-2.426696	-2.752740
Fe	0.726352	0.019796	-0.130003
N	1.655665	-1.567128	-0.457477
C	2.787138	-1.963348	0.192533
N	3.426472	-1.033984	1.049011
C	4.559660	-1.578095	1.809919
O	-0.174588	-0.293540	1.272876
N	2.231851	0.948775	0.493643
C	2.066498	2.419841	0.580489
C	3.234185	3.172678	-0.094104
C	3.308478	0.379524	1.096862
O	4.193118	1.009704	1.698125
C	1.867579	2.896422	2.036901
C	0.942793	-2.557873	-1.304097
C	0.401152	-3.741822	-0.473492
C	1.820529	-3.054704	-2.473718
O	3.281743	-3.097577	0.098941
C	-2.264405	1.096497	1.795996
C	-3.340733	0.129924	2.025757
C	-3.553467	-0.429884	3.305393
C	-4.562225	-1.365472	3.515317
C	-5.377248	-1.770088	2.450860
C	-5.175621	-1.231450	1.173851
C	-4.167678	-0.295680	0.961254
H	-1.228104	0.437128	1.482755
H	1.043311	2.348414	2.507262
H	1.622960	3.963316	2.042613
H	2.778131	2.728161	2.613829
H	4.155268	3.021448	0.468470
H	2.997482	4.239609	-0.137815
H	3.380372	2.809097	-1.118167
H	-1.586748	3.770509	-1.480198
H	-3.558165	3.413207	-2.965375
H	4.687237	-0.985539	2.713420
H	-0.209342	-3.375913	0.360048
H	-0.226086	-4.374373	-1.109426
H	1.227389	-4.331488	-0.074100
H	2.649843	-3.653606	-2.098201
H	1.206761	-3.654552	-3.151715
H	2.223526	-2.203344	-3.035114
H	-2.651017	-0.800315	-3.175620
H	-4.089304	1.137501	-3.808165
H	5.491496	-1.539854	1.232768
H	4.345489	-2.615621	2.056597
H	-2.396152	1.744210	0.927553
H	-1.924590	1.638654	2.681643
H	-2.922929	-0.114681	4.132987
H	-4.718176	-1.780034	4.507291

H	-6.164633	-2.500177	2.615385
H	-5.808411	-1.542213	0.347237
H	-4.010829	0.120207	-0.030926

Quartet Intermediate, CPCM CH_3CN

C	3.367530	0.394816	-3.147479
C	3.310412	-1.001450	-3.065866
C	2.265448	-1.635060	-2.387359
C	1.268399	-0.853473	-1.787134
C	1.323465	0.566854	-1.874565
C	2.380508	1.186870	-2.555875
N	0.145226	-1.293124	-1.071113
Fe	-0.776297	0.037548	-0.136256
N	-1.931401	1.487151	0.039800
C	-3.110035	1.480254	0.725367
N	-3.603334	0.235340	1.189452
C	-4.813189	0.332151	2.018163
N	0.239636	1.175515	-1.231886
C	-0.093356	2.498679	-1.228953
O	0.531418	3.403583	-1.789022
C	-0.332526	-2.570804	-0.976749
O	0.213303	-3.578009	-1.433391
C	-1.688885	-2.648998	-0.239407
C	-2.684218	-3.303624	-1.224116
N	-2.096357	-1.265723	0.113138
C	-3.268400	-1.082587	0.780870
O	-4.057832	-1.994323	1.072492
C	-1.482316	-3.534493	1.009075
C	-1.397993	2.784371	-0.448380
C	-1.037366	3.738247	0.711647
C	-2.365871	3.462886	-1.443398
O	0.108366	0.075796	1.405699
O	-3.771195	2.496555	0.986955
H	0.868008	-0.537684	1.333870
H	-0.779007	-3.060665	1.703250
H	-1.067863	-4.500419	0.704297
H	-2.432578	-3.689890	1.521384
H	-3.643745	-3.468349	-0.734151
H	-2.275952	-4.258096	-1.568807
H	-2.837503	-2.657199	-2.096194
H	2.206964	-2.713311	-2.323656
H	4.083828	-1.604180	-3.534196
H	-4.885820	-0.564773	2.628896
H	-0.353396	3.247709	1.413243
H	-0.540353	4.626492	0.309598
H	-1.939132	4.036537	1.247858
H	-3.275503	3.776820	-0.931636
H	-1.872989	4.332206	-1.887994
H	-2.633258	2.768123	-2.248400
H	2.409778	2.266312	-2.618993
H	4.186506	0.873114	-3.677974
H	-5.718902	0.414598	1.405381
H	-4.736892	1.218882	2.644246
C	2.652930	-1.973885	1.730910
H	2.535004	-2.376815	0.729874
C	3.516652	-0.887815	1.982158
H	2.146092	-2.484092	2.544457
C	3.716075	-0.390838	3.306554
C	4.564395	0.679401	3.547765
C	5.246842	1.298721	2.488302
C	5.068704	0.828450	1.177414
C	4.223695	-0.241532	0.921784
H	3.189712	-0.867763	4.129572
H	4.701584	1.040223	4.563643
H	5.909616	2.137035	2.682194
H	5.596433	1.305156	0.355620
H	4.088825	-0.601979	-0.094698

Doublet Reactant, CPCM water

C	1.747963	3.900236	1.712322
C	0.685564	4.640937	1.180290
C	-0.414245	4.003431	0.604320
C	-0.436932	2.601119	0.550594
C	0.641045	1.850224	1.088951
C	1.734049	2.505033	1.675750
N	-1.450317	1.778364	0.037079
Fe	-1.026977	-0.014705	-0.142846
N	-0.924465	-1.619864	0.753053
C	-1.720773	-2.711842	0.481862
N	-2.816239	-2.573148	-0.380621
C	-3.495127	-3.836570	-0.702433
N	0.409204	0.480529	0.992654
C	1.044882	-0.505911	1.672135
O	2.067506	-0.378882	2.354433
C	-2.668777	2.193991	-0.448898
O	-3.012852	3.369810	-0.552455
C	-3.575377	1.035497	-0.880499
C	-4.898277	1.192697	-0.097460
N	-2.868093	-0.215028	-0.539967
C	-3.499760	-1.389619	-0.765285
O	-4.623569	-1.505933	-1.277601
C	-3.808920	1.179712	-2.401812
C	0.322563	-1.858066	1.537290
C	1.285795	-2.821695	0.810499
C	0.016140	-2.337211	2.972516
O	-0.307733	-0.168447	-1.552737
O	-1.481726	-3.836030	0.941270
H	2.572529	0.365626	-1.936083
H	-2.863665	1.074620	-2.946081
H	-4.226180	2.167934	-2.618478
H	-4.500812	0.408407	-2.742541
H	-5.624200	0.451446	-0.430582
H	-5.296244	2.198219	-0.261326
H	-4.722824	1.059853	0.976477
H	-1.240105	4.567354	0.195274
H	0.713066	5.726604	1.210128
H	-4.149493	-3.658973	-1.551363
H	1.474621	-2.475741	-0.212124
H	2.238870	-2.841943	1.347569
H	0.867081	-3.827509	0.773569

H	-0.403410	-3.342296	2.958041
H	0.943591	-2.330888	3.552197
H	-0.697452	-1.659970	3.455906
H	2.541533	1.920070	2.094320
H	2.596401	4.412751	2.157308
H	-4.092209	-4.196572	0.142892
H	-2.747206	-4.591047	-0.944360
C	3.457238	0.996178	-1.776419
H	3.211072	1.683369	-0.958481
C	4.678249	0.165413	-1.450681
H	3.608928	1.588759	-2.684574
C	5.710816	0.000897	-2.384380
C	6.833584	-0.778209	-2.089059
C	6.942727	-1.407976	-0.847634
C	5.920895	-1.250337	0.094073
C	4.801278	-0.471128	-0.204470
H	5.635742	0.489789	-3.353311
H	7.622373	-0.889500	-2.828858
H	7.814985	-2.012710	-0.614001
H	5.997613	-1.733010	1.065303
H	4.015567	-0.353217	0.539097

Doublet TS1, CPCM water

C	4.159640	-0.122754	0.965429
C	3.296885	-0.537443	2.005681
C	3.539169	-0.054956	3.311651
C	4.609474	0.796033	3.569777
C	5.458620	1.191533	2.528559
C	5.229367	0.728363	1.226914
C	2.157120	-1.414423	1.728806
O	0.130490	0.111816	1.342388
Fe	-0.738080	0.022581	-0.110943
N	-2.129157	-1.191242	0.241156
C	-3.284523	-0.899611	0.892889
O	-4.111903	-1.744085	1.272334
N	0.078168	-1.417292	-0.979116
C	-0.459050	-2.655849	-0.780157
C	-1.803629	-2.613592	-0.022233
C	-1.626989	-3.427253	1.278470
C	1.220906	-1.093190	-1.728961
C	2.163975	-1.972484	-2.277757
C	3.239017	-1.451686	-3.005760
C	3.376848	-0.072041	-3.187066
C	2.444228	0.816667	-2.643134
C	1.362755	0.310176	-1.910356
N	0.327546	1.026360	-1.297074
C	0.039077	2.348229	-1.434215
C	-1.256615	2.753255	-0.694885
C	-2.186787	3.390194	-1.750201
O	0.031289	-3.720976	-1.166169
O	0.694297	3.172335	-2.081209
N	-1.846903	1.523290	-0.106676
C	-3.021437	1.630847	0.579272
O	-3.642010	2.694238	0.733858
N	-3.558294	0.465013	1.175517
C	-4.756416	0.697811	1.993480
C	-2.847380	-3.276169	-0.950067
C	-0.861482	3.780691	0.388563
H	1.161434	-0.671304	1.470417
H	-0.903495	-2.938641	1.940797
H	-1.252239	-4.425991	1.034320
H	-2.580029	-3.513106	1.801860
H	-3.809534	-3.345890	-0.442544
H	-2.502404	-4.276494	-1.227517
H	-2.971407	-2.686215	-1.865860
H	2.042024	-3.037975	-2.137846
H	3.970624	-2.131806	-3.433696
H	-4.869083	-0.135132	2.683486
H	-0.210911	3.317264	1.139236
H	-0.314880	4.606314	-0.077859
H	-1.752430	4.166951	0.885305
H	-3.080451	3.793609	-1.274618
H	-1.648564	4.190488	-2.266149
H	-2.487440	2.641977	-2.493201
H	2.536512	1.885549	-2.782033
H	4.216411	0.319298	-3.755457
H	-5.661169	0.769627	1.377846
H	-4.632163	1.632966	2.536149
H	2.242332	-2.020382	0.825692
H	1.785623	-1.982144	2.585377
H	2.881975	-0.363746	4.120742
H	4.787226	1.151393	4.580842
H	6.294323	1.855489	2.730604
H	5.889322	1.031203	0.418807
H	3.984993	-0.484051	-0.044624

Quartet Intermediate, CPCM water

C	3.368440	0.390539	-3.148562
C	3.310962	-1.005646	-3.065454
C	2.265728	-1.638272	-2.386498
C	1.268711	-0.855817	-1.787342
C	1.324186	0.564394	-1.876210
C	2.381524	1.183446	-2.557963
N	0.145334	-1.294421	-1.070898
Fe	-0.775094	0.037349	-0.136730
N	-1.929844	1.487590	0.038485
C	-3.108026	1.481629	0.724751
N	-3.600775	0.237393	1.191254
C	-4.809732	0.335271	2.021260
N	0.240453	1.173982	-1.234093
C	-0.092530	2.497120	-1.232808
O	0.532074	3.401235	-1.794437
C	-0.333656	-2.571659	-0.976517
O	0.210819	-3.579207	-1.434014
C	-1.689567	-2.648855	-0.238336
C	-2.686115	-3.302457	-1.222511
N	-2.095658	-1.265241	0.114565
C	-3.267098	-1.080957	0.782922
O	-4.057054	-1.991953	1.075536
C	-1.482908	-3.534768	1.009845

C	-1.396811	2.784056	-0.452138
C	-1.035716	3.740071	0.705994
C	-2.365240	3.460739	-1.447864
O	0.110470	0.076840	1.404860
O	-3.769158	2.498279	0.985241
H	0.867834	-0.539745	1.334751
H	-0.778482	-3.061986	1.703595
H	-1.069798	-4.501109	0.704601
H	-2.432888	-3.689363	1.522905
H	-3.645480	-3.466449	-0.731991
H	-2.279041	-4.257308	-1.567528
H	-2.839407	-2.655860	-2.094458
H	2.207224	-2.716441	-2.321605
H	4.084370	-1.609020	-3.532916
H	-4.881494	-0.560648	2.633574
H	-0.351118	3.251145	1.408113
H	-0.539264	4.627797	0.302144
H	-1.937166	4.039146	1.242275
H	-3.274625	3.775545	-0.936212
H	-1.872792	4.329395	-1.894213
H	-2.633023	2.764593	-2.251534
H	2.411282	2.262802	-2.622232
H	4.187657	0.868039	-3.679359
H	-5.716228	0.416586	1.409509
H	-4.732808	1.222893	2.645982
C	2.651087	-1.973651	1.735285
H	2.535620	-2.378978	0.734915
C	3.513839	-0.886606	1.985786
H	2.143502	-2.482796	2.549036
C	3.710501	-0.386639	3.309489
C	4.557812	0.684589	3.549934
C	5.241925	1.301953	2.490378
C	5.066578	0.828684	1.180167
C	4.222574	-0.242299	0.925318
H	3.183025	-0.862164	4.132599
H	4.693046	1.047612	4.565276
H	5.904007	2.140929	2.683700
H	5.595871	1.303706	0.358409
H	4.090034	-0.605265	-0.090586

Doublet Reactant, 1 explicit H_2O, gas

C	0.742349	1.874595	1.163979
C	-0.222621	2.699236	0.475260
C	-0.085034	4.106017	0.495207
C	0.987577	4.668772	1.166316
C	1.928635	3.862668	1.844823
C	1.811786	2.482126	1.860212
N	-1.239662	1.967746	-0.074368
C	-2.401723	2.438762	-0.648910
O	-2.632617	3.613667	-0.919145
N	0.431968	0.541602	1.104315
C	1.045677	-0.496204	1.768502
O	2.095248	-0.408318	2.404299
Fe	-1.023034	0.086594	-0.021609
N	-0.982419	-1.534494	0.894918
C	-1.838331	-2.566098	0.649654
N	-3.074613	-2.291433	0.025992
C	-3.898661	-3.490104	-0.175323
O	-0.266424	-0.201265	-1.426412
N	-2.853951	0.049865	-0.377610
C	-3.418958	1.311375	-0.923441
C	-4.725026	1.733842	-0.212718
C	-3.629976	-1.071625	-0.444490
O	-4.781892	-1.083712	-0.898576
C	-3.616575	1.226403	-2.453148
C	0.273742	-1.825390	1.633443
C	1.203526	-2.825797	0.907050
C	-0.026379	-2.309767	3.069630
O	-1.598610	-3.749804	0.939764
C	3.239105	0.800078	-1.725228
C	4.527459	0.077924	-1.405742
C	4.750149	-0.458095	-0.126387
C	5.937621	-1.126722	0.171514
C	6.931060	-1.273792	-0.800833
C	6.722955	-0.745717	-2.075151
C	5.531972	-0.076988	-2.370114
O	-0.295283	-3.010881	-2.205614
H	2.366695	0.137461	-1.668545
H	-2.682638	0.914194	-2.932830
H	-3.903798	2.209013	-2.842233
H	-4.394736	0.496122	-2.681543
H	-5.525591	1.035623	-0.452978
H	-4.993462	2.745483	-0.531947
H	-4.577972	1.741093	0.874306
H	-0.816787	4.706381	-0.028159
H	1.111127	5.748976	1.164640
H	-4.840661	-3.170350	-0.611392
H	1.292740	-2.573988	-0.153864
H	2.196483	-2.791037	1.366652
H	0.797823	-3.835035	0.987775
H	-0.532592	-3.275427	3.031127
H	0.910805	-2.402122	3.627116
H	-0.671100	-1.590377	3.588540
H	2.522138	1.851566	2.377271
H	2.764677	4.332279	2.357180
H	-4.065072	-3.995679	0.779442
H	-3.386774	-4.189574	-0.842773
H	3.056109	1.615870	-1.015347
H	3.263322	1.229876	-2.732539
H	5.376343	0.330237	-3.367268
H	7.486139	-0.853402	-2.843068
H	7.855857	-1.796156	-0.566711
H	6.085889	-1.535612	1.168334
H	3.986447	-0.353242	0.641060
H	-0.292231	-2.055632	-1.993240
H	-0.544899	-3.431475	-1.369044

Doublet TS1, 1 explicit H_2O, gas

C	4.131772	0.119869	-0.399913
C	3.454154	0.212809	-1.635798

C	3.962824	-0.516504	-2.731614
C	5.112254	-1.290060	-2.605698
C	5.778773	-1.360687	-1.378048
C	5.281057	-0.655373	-0.277354
C	2.241349	1.024272	-1.770560
O	0.104979	-0.291589	-1.328810
Fe	-0.793778	0.085899	0.079127
N	-2.554053	-0.347974	-0.343381
C	-3.094707	-1.604223	-0.338615
O	-4.208970	-1.872723	-0.804592
N	-1.345307	1.863025	-0.191671
C	-2.543252	2.056928	-0.817873
C	-3.333510	0.739699	-0.988550
C	-3.503096	0.495657	-2.503786
C	-0.458761	2.844803	0.254877
C	-0.511011	4.224756	0.016175
C	0.464917	5.049752	0.581186
C	1.483517	4.514305	1.374882
C	1.551239	3.139617	1.620405
C	0.579277	2.299202	1.060078
N	0.464751	0.908799	1.195026
C	1.202273	0.095052	2.008893
C	0.692867	-1.363594	2.015160
C	0.326206	-1.703184	3.477030
O	-2.996302	3.136568	-1.199272
O	2.170928	0.446763	2.686885
N	-0.512906	-1.416750	1.153056
C	-1.118869	-2.618664	0.954791
O	-0.679266	-3.701316	1.378544
N	-2.319411	-2.656432	0.213785
C	-2.851880	-4.012309	0.033564
C	-4.699412	0.964351	-0.302891
C	1.856623	-2.258911	1.531586
H	1.207799	0.319482	-1.474912
H	-2.526836	0.312429	-2.966878
H	-3.946940	1.385185	-2.962818
H	-4.144284	-0.371028	-2.673050
H	-5.360211	0.117140	-0.484463
H	-5.141442	1.884488	-0.696666
H	-4.562246	1.082282	0.778785
H	-1.313556	4.620809	-0.591863
H	0.425978	6.121319	0.398299
H	-3.765786	-3.930912	-0.548094
H	2.021351	-2.143195	0.456269
H	2.767852	-1.964181	2.061543
H	1.633542	-3.306953	1.733091
H	0.005285	-2.744750	3.542370
H	1.198979	-1.541357	4.117164
H	-0.486910	-1.056093	3.826024
H	2.324125	2.709479	2.243310
H	2.234660	5.169175	1.810722
H	-3.058194	-4.474958	1.002919
H	-2.115317	-4.629787	-0.487655
H	2.143227	1.850091	-1.064297
H	1.988703	1.316829	-2.792634
H	3.441486	-0.468175	-3.684550
H	5.488037	-1.843739	-3.462473
H	6.674753	-1.968260	-1.277831
H	5.787045	-0.715516	0.682695
H	3.739024	0.645775	0.466115
H	0.517868	-2.225239	-1.532898
O	0.711352	-3.179385	-1.607449
H	0.479313	-3.530312	-0.733246

Quartet Intermediate, 1 explicit H_2O, gas

C	0.567119	2.221682	1.048268
C	-0.492466	2.826588	0.312778
C	-0.505132	4.214507	0.112419
C	0.525920	4.987012	0.650274
C	1.561037	4.394454	1.381835
C	1.591993	3.012919	1.587068
N	-1.436343	1.891269	-0.112030
C	-2.633325	2.139432	-0.728662
O	-3.058017	3.243770	-1.065920
N	0.412377	0.832771	1.144265
C	1.140471	-0.030827	1.916654
O	2.132543	0.264598	2.586908
Fe	-0.936364	0.093947	0.074275
N	-0.665930	-1.454191	1.078181
C	-1.303489	-2.634223	0.837066
N	-2.515988	-2.615575	0.113359
C	-3.079756	-3.952560	-0.110986
O	-0.061263	-0.285059	-1.443042
N	-2.696519	-0.287992	-0.374322
C	-3.458626	0.849726	-0.949487
C	-4.806065	1.072185	-0.226126
C	-3.269850	-1.528650	-0.405139
O	-4.392869	-1.755949	-0.870622
C	-3.664339	0.686861	-2.471185
C	0.582098	-1.473530	1.882409
C	1.693407	-2.378343	1.299316
C	0.276944	-1.872559	3.342997
O	-0.883106	-3.741817	1.210454
C	3.002214	1.243198	-1.722613
C	4.058453	0.337291	-1.498283
C	4.489862	0.015150	-0.175508
C	5.540562	-0.865552	0.033323
C	6.202599	-1.459549	-1.051292
C	5.791023	-1.165303	-2.359767
C	4.741196	-0.288569	-2.583877
O	0.397288	-3.146686	-1.837160
H	0.836612	0.092920	-1.372880
H	-2.702277	0.508308	-2.964023
H	-4.100637	1.606198	-2.875192
H	-4.326268	-0.158040	-2.668525
H	-5.489147	0.249137	-0.434801
H	-5.235092	2.018935	-0.567804
H	-4.646354	1.135348	0.857030
H	-1.320417	4.656118	-0.445155
H	0.518209	6.063947	0.498094
H	-4.007750	-3.828225	-0.661810

H	1.799155	-2.228412	0.220433
H	2.641411	-2.129015	1.785898
H	1.453631	-3.427648	1.473384
H	-0.067627	-2.907919	3.375394
H	1.184003	-1.761215	3.944901
H	-0.501074	-1.223484	3.761222
H	2.375963	2.539492	2.163115
H	2.353386	5.011627	1.799013
H	-3.266855	-4.453215	0.842908
H	-2.371012	-4.559556	-0.681251
H	2.533396	1.776671	-0.901943
H	2.683223	1.488734	-2.731336
H	4.421319	-0.066540	-3.599201
H	6.294205	-1.631121	-3.203800
H	7.022842	-2.151580	-0.879361
H	5.845422	-1.101455	1.049775
H	3.966892	0.448923	0.672657
H	0.187377	-2.196015	-1.742470
H	0.192025	-3.518408	-0.965436

Doublet Reactant, 2 explicit H_2O, gas

C	5.882754	-1.451515	-0.020572
C	4.668877	-0.791201	-0.211361
C	4.443896	-0.008726	-1.356420
C	5.474022	0.084062	-2.302000
C	6.691451	-0.575856	-2.115511
C	6.901723	-1.346611	-0.971707
C	3.133338	0.715451	-1.550419
O	-0.228558	-0.204643	-1.312872
Fe	-1.003841	0.028878	0.109339
N	-1.280263	-1.681580	0.780425
C	-2.285734	-2.502320	0.359106
O	-2.257607	-3.739164	0.461542
N	-0.885133	1.911959	0.320932
C	-1.913486	2.654651	-0.229903
C	-3.111679	1.780808	-0.649749
C	-3.307051	1.966110	-2.171781
C	0.200381	2.368824	1.011478
C	0.976886	1.295542	1.598532
C	2.092091	1.603236	2.414775
C	2.431052	2.928442	2.617242
C	1.673464	3.976871	2.041307
C	0.566040	3.714079	1.255685
N	0.458549	0.064205	1.325642
C	0.865667	-1.157470	1.824186
O	1.891101	-1.347595	2.472770
O	-1.893124	3.872258	-0.382989
N	-2.789405	0.371147	-0.296570
C	-3.754565	-0.571540	-0.512688
O	-4.883120	-0.312105	-0.948148
N	-3.431892	-1.926185	-0.227848
C	-4.440022	-2.919173	-0.621887
C	-0.115850	-2.295579	1.472343
C	-0.542797	-2.939794	2.810117
C	0.658343	-3.312463	0.600382
C	-4.327190	2.320654	0.140387
O	0.221898	2.101468	-2.898428
H	2.272255	0.049047	-1.428923
H	-2.398553	1.682018	-2.712231
H	-3.513488	3.020713	-2.382891
H	-4.145296	1.354466	-2.509069
H	-5.236169	1.818932	-0.188491
H	-4.410112	3.399463	-0.023520
H	-4.193311	2.139988	1.214096
H	-0.022646	4.503572	0.808372
H	1.972900	5.007506	2.213748
H	-5.301940	-2.377975	-1.001172
H	0.826552	-2.913378	-0.404031
H	1.625361	-3.522116	1.068768
H	0.086176	-4.236692	0.512032
H	-1.200313	-3.787813	2.613609
H	0.345700	-3.275875	3.353318
H	-1.077136	-2.211357	3.431741
H	2.661390	0.791242	2.845985
H	3.300900	3.169959	3.222637
H	-4.716515	-3.534208	0.238170
H	-4.032892	-3.578835	-1.393832
H	3.014669	1.516039	-0.808205
H	3.054760	1.173966	-2.540335
H	5.315975	0.680471	-3.198211
H	7.473357	-0.489019	-2.867102
H	7.846757	-1.864277	-0.823628
H	6.030933	-2.054175	0.872647
H	3.883159	-0.887031	0.535161
H	0.091260	1.254955	-2.418570
H	0.025123	2.770400	-2.226684
H	-0.600786	-1.914956	-2.153171
O	-0.779780	-2.812169	-2.500442
H	-1.117351	-3.295981	-1.731785

Doublet TS1, 2 explicit H_2O, gas

C	-1.236271	2.634775	2.775031
C	-0.439488	2.020692	1.799939
C	-0.011648	2.755127	0.660105
C	-0.386664	4.096107	0.504647
C	-1.180834	4.695291	1.485646
C	-1.599723	3.973660	2.607462
N	0.031622	0.700450	1.783984
C	-0.058237	-0.221057	2.794038
O	-0.640421	-0.053586	3.865180
N	0.801668	1.986071	-0.177050
C	1.454108	2.387918	-1.304194
O	1.319623	3.479186	-1.865758
Fe	0.811848	0.142084	0.184151
N	2.243960	0.091740	-1.002959
C	3.031379	-0.993160	-1.276786
N	2.781561	-2.189139	-0.554417
C	3.469353	-3.391245	-1.041301
O	-0.543158	-0.432773	-0.711176
N	1.349085	-1.356307	1.156237

C	0.665614	-1.544153	2.458869
C	1.696907	-1.793476	3.580574
C	2.027806	-2.406359	0.617275
O	2.026568	-3.555422	1.090020
C	-0.405696	-2.660797	2.457441
C	2.428601	1.312985	-1.830661
C	2.095680	1.064245	-3.316879
C	3.846803	1.909259	-1.668711
O	3.920789	-0.996209	-2.135721
O	-1.408623	1.558694	-2.674169
O	-0.617162	-3.398969	-0.873721
C	-2.857856	0.088339	0.251222
C	-3.840739	-0.601031	-0.589263
C	-4.459765	-1.792402	-0.155491
C	-5.393806	-2.442020	-0.956118
C	-5.719304	-1.923724	-2.214070
C	-5.097070	-0.755138	-2.667877
C	-4.165081	-0.099124	-1.870030
H	-1.701122	-0.238102	-0.160193
H	-1.030195	-2.605130	1.560424
H	-1.035701	-2.542277	3.345139
H	0.071607	-3.641282	2.472630
H	2.196812	-2.749952	3.415298
H	1.184267	-1.802987	4.547223
H	2.447716	-0.994971	3.592726
H	-1.544885	2.063617	3.640281
H	-2.216898	4.454669	3.362790
H	2.736704	-4.179717	-1.230535
H	1.065406	0.709952	-3.425642
H	2.183224	2.010499	-3.860023
H	2.783165	0.329168	-3.737107
H	4.587305	1.239611	-2.106176
H	3.880180	2.884314	-2.164940
H	4.077959	2.050776	-0.606177
H	-0.048098	4.640630	-0.366974
H	-1.474012	5.736131	1.369409
H	4.178994	-3.759320	-0.294184
H	3.993876	-3.123152	-1.954159
H	-2.799656	1.169607	0.114388
H	-2.850118	-0.200635	1.303789
H	-4.199746	-2.198416	0.818803
H	-5.865583	-3.356059	-0.604490
H	-6.445689	-2.434258	-2.841777
H	-5.335624	-0.359563	-3.651950
H	-3.647946	0.785983	-2.232636
H	-1.055875	0.849906	-2.100085
H	-0.856922	2.328106	-2.461901
H	-0.570157	-2.424085	-0.879916
H	0.082353	-3.662590	-0.254970

Quartet Intermediate, 2 explicit H_2O, gas

C	-4.412759	-0.587499	-2.135634
C	-4.440628	-0.500120	-0.709598
C	-5.359925	-1.341457	-0.014457
C	-6.196280	-2.207815	-0.701886
C	-6.153258	-2.274839	-2.102614
C	-5.254962	-1.459540	-2.808329
C	-3.589081	0.392360	-0.028608
O	-0.339139	-0.568355	-0.816516
Fe	0.959996	0.163151	0.219015
N	1.837300	-1.310896	0.939318
C	2.690829	-2.103528	0.227293
O	2.944540	-3.284614	0.512035
N	0.099820	0.270360	1.872487
C	0.283314	-0.772231	2.748404
C	1.249427	-1.845202	2.193362
C	0.420454	-3.138208	1.996166
C	-0.655331	1.428526	2.082568
C	-1.554228	1.689940	3.126586
C	-2.222815	2.915083	3.151439
C	-2.007365	3.872144	2.152111
C	-1.113891	3.629559	1.108068
C	-0.427506	2.406940	1.072067
N	0.531754	1.986942	0.148966
C	1.000295	2.663798	-0.944027
C	2.184117	1.935744	-1.619246
C	3.434165	2.796857	-1.310666
O	-0.236996	-0.876475	3.856606
O	0.571466	3.741829	-1.361747
N	2.287838	0.583539	-1.011707
C	3.297925	-0.237335	-1.431273
O	4.153330	0.088796	-2.261491
N	3.330598	-1.556033	-0.903383
C	4.234468	-2.494934	-1.579342
C	2.346770	-2.065199	3.255953
C	1.916762	1.878375	-3.137127
O	-1.513644	1.314958	-2.630870
O	0.257677	-3.378323	-1.446677
H	-1.148315	-0.626913	-0.272911
H	-0.225826	-3.061920	1.115958
H	-0.198609	-3.299173	2.884804
H	1.083616	-3.991733	1.850580
H	3.016468	-2.865323	2.935170
H	1.877424	-2.329733	4.208094
H	2.928600	-1.147258	3.398783
H	-1.700852	0.942639	3.895209
H	-2.920010	3.124003	3.959373
H	3.682170	-3.396774	-1.852987
H	1.002398	1.314457	-3.346417
H	1.776561	2.897618	-3.510487
H	2.759725	1.409594	-3.645988
H	4.304164	2.384059	-1.821839
H	3.253740	3.823026	-1.646821
H	3.628386	2.811850	-0.231781
H	-0.933114	4.359569	0.330055
H	-2.540908	4.819008	2.185830
H	5.057033	-2.786129	-0.918578
H	4.627308	-1.997175	-2.461586
H	-2.925630	1.045613	-0.585472
H	-3.611210	0.482706	1.053191
H	-5.393712	-1.293768	1.071660

H	-6.887736	-2.841336	-0.150699
H	-6.807925	-2.958733	-2.636772
H	-5.213739	-1.514706	-3.893591
H	-3.707500	0.039870	-2.675057
H	-1.031797	0.646040	-2.099067
H	-1.145837	2.164173	-2.338125
H	0.095712	-2.425007	-1.307394
H	1.007472	-3.578938	-0.865268

Doublet Reactant, 3 explicit H_2O, gas

C	-4.650296	-0.126712	-1.938399
C	-4.589557	-1.347510	-1.251119
C	-5.783746	-2.055014	-1.041550
C	-7.004761	-1.561711	-1.501524
C	-7.054474	-0.343331	-2.184508
C	-5.873612	0.368598	-2.399841
C	-3.272570	-1.891391	-0.744048
O	0.062773	-0.275276	-1.034604
Fe	0.892344	0.236522	0.290060
N	2.173910	-1.069295	0.621257
C	3.385459	-1.136234	0.003283
O	4.138204	-2.123446	0.055745
N	-0.088651	-0.640721	1.665703
C	0.352591	-1.904478	2.024378
C	1.682914	-2.279316	1.336168
C	1.367878	-3.429589	0.351192
C	-1.132739	0.058022	2.184724
C	-2.077810	-0.383436	3.144706
C	-3.041475	0.499470	3.590541
C	-3.088648	1.837362	3.122416
C	-2.173591	2.309466	2.200998
C	-1.183308	1.428144	1.703609
N	-0.169355	1.715741	0.839915
C	0.178097	2.947658	0.314123
C	1.556939	2.927911	-0.376448
C	2.435768	3.938220	0.399222
O	-0.232170	-2.659263	2.792313
O	-0.516572	3.957206	0.378152
N	2.093109	1.541845	-0.285828
C	3.338995	1.309480	-0.795070
O	4.053904	2.179836	-1.306023
N	3.823564	-0.028128	-0.756757
C	5.098544	-0.266679	-1.454448
C	2.640158	-2.742650	2.455884
C	1.348832	3.382268	-1.838529
O	1.724551	-1.521371	-2.923354
O	-1.673153	1.583673	-2.217585
O	3.825220	-3.454930	-2.485760
H	0.637301	-3.098628	-0.393855
H	0.947779	-4.277622	0.902156
H	2.272287	-3.746069	-0.170696
H	3.553010	-3.151207	2.025700
H	2.134559	-3.499709	3.062480
H	2.903774	-1.897721	3.103811
H	-2.026050	-1.406285	3.492008
H	-3.784388	0.161647	4.308322
H	5.017075	-1.184491	-2.040102
H	0.643273	2.719381	-2.349044
H	0.928634	4.393344	-1.844055
H	2.306906	3.381149	-2.359912
H	3.399174	4.047369	-0.098086
H	1.922838	4.904036	0.440883
H	2.605203	3.587536	1.424565
H	-2.197898	3.326713	1.834274
H	-3.866468	2.501426	3.490251
H	5.919214	-0.382675	-0.738912
H	5.290530	0.592249	-2.091828
H	-3.276462	-1.988373	0.349663
H	-3.071667	-2.890760	-1.151530
H	-5.752932	-3.005468	-0.511008
H	-7.917427	-2.128311	-1.328280
H	-8.004598	0.044013	-2.545734
H	-5.898617	1.316467	-2.932865
H	-3.734217	0.435422	-2.115232
H	-1.068196	0.896333	-1.853757
H	-1.811767	2.183269	-1.469125
H	3.019015	-2.925429	-2.656203
H	4.076841	-3.174821	-1.587792
H	1.072359	-1.217107	-2.251537
H	2.344481	-0.777890	-2.967222
H	-2.432134	-1.246166	-1.014564

Doublet catalyst

C	1.854237	-2.131254	1.486704
C	2.527085	-2.246150	0.262174
C	3.230664	-3.435851	-0.056055
C	3.255657	-4.505945	0.848643
C	2.588224	-4.375593	2.067538
C	1.897524	-3.200870	2.383564
N	2.582108	-1.305711	-0.777619
C	1.941441	-0.089016	-0.806256
C	2.194613	0.691277	-2.103724
N	2.975869	-0.187409	-2.992395
C	3.258149	0.256134	-4.237926
O	2.937774	1.365723	-4.688402
N	3.789853	-3.376678	-1.327771
C	4.216687	-4.424874	-2.077875
C	4.501172	-4.002868	-3.532908
C	3.699824	-4.962334	-4.436401
Fe	3.808189	-1.652785	-2.120642
N	4.054824	-2.589546	-3.686170
C	4.240646	-2.000938	-4.918832
O	4.673734	-2.626598	-5.894748
O	5.199981	-1.065915	-1.651308
N	3.965966	-0.637439	-5.089494
C	4.297822	-0.130168	-6.424016
O	1.245994	0.359243	0.102356
O	4.354894	-5.589619	-1.699633
C	0.808744	1.041953	-2.688803
C	2.975843	1.970196	-1.723811

C	6.022246	-4.151062	-3.756597
H	3.957281	1.703053	-1.316413
H	2.419098	2.528345	-0.963713
H	3.117170	2.587678	-2.612640
H	0.920835	1.686328	-3.560711
H	0.214655	1.542980	-1.918535
H	0.285269	0.126622	-2.989698
H	1.318147	-1.220194	1.712416
H	1.385910	-3.111757	3.339270
H	4.158852	0.947623	-6.406701
H	6.565366	-3.435427	-3.128624
H	6.323327	-5.163962	-3.469506
H	6.272520	-3.969895	-4.802729
H	3.953927	-4.803235	-5.483933
H	3.927489	-5.990141	-4.138288
H	2.624624	-4.795382	-4.301418
H	3.782878	-5.410528	0.576020
H	2.610135	-5.199698	2.777327
H	3.648098	-0.574611	-7.186397
H	5.329337	-0.392198	-6.667993

Quartet catalyst

C	6.164681	12.289205	13.460940
C	4.905542	12.350671	14.064242
C	4.825648	12.414064	15.460559
C	6.007951	12.412356	16.244922
C	7.263219	12.347246	15.628350
C	7.329411	12.287512	14.233633
N	3.667507	12.464371	16.248224
C	2.380867	12.241491	15.843236
O	2.020509	12.026750	14.686345
N	5.732591	12.461490	17.618254
C	6.605427	12.234736	18.645825
O	7.810792	12.016817	18.527661
Fe	3.929227	12.834686	18.095777
N	2.132327	12.340882	18.276780
C	1.365109	12.269611	17.010983
C	0.480491	13.519470	16.801279
O	3.813179	14.454633	18.271404
N	4.460468	12.339149	19.821336
C	3.626588	12.493683	20.890061
N	2.244290	12.708495	20.635647
C	1.472318	12.495682	19.460845
O	0.242109	12.435372	19.575047
C	5.924708	12.262970	20.035763
C	6.312628	10.967323	20.773046
C	6.465665	13.510263	20.770857
O	3.999754	12.431445	22.067758
C	1.443228	12.939124	21.842628
C	0.531930	10.976091	16.937438
H	6.156318	14.419087	20.242931
H	7.559612	13.468742	20.788217
H	6.077876	13.542192	21.790184
H	5.932860	10.991740	21.795589
H	7.402747	10.873126	20.773582
H	5.889320	10.098012	20.256942
H	8.152657	12.332635	16.243829
H	8.302453	12.239172	13.749729
H	2.050659	13.490556	22.557834
H	1.089251	14.426685	16.883273
H	0.039205	13.481340	15.800001
H	-0.307915	13.551452	17.554822
H	-0.262329	11.000743	17.685073
H	0.107230	10.885140	15.933148
H	1.169971	10.104848	17.124757
H	3.992645	12.338722	13.484065
H	6.232122	12.242184	12.376251
H	1.130415	11.994857	22.305296
H	0.552658	13.498687	21.562486

Singlet Fe^{IV}(OH)

C	3.219779	1.445064	-2.988621
C	3.195680	0.066447	-3.333195
C	2.211869	-0.773741	-2.795128
C	1.253611	-0.237239	-1.932360
C	1.270634	1.121030	-1.602464
C	2.253373	1.969433	-2.119125
N	4.248131	-0.287707	-4.176396
C	4.860739	-1.495165	-4.190958
O	4.415492	-2.562661	-3.758621
N	4.294687	2.133171	-3.586461
C	4.531658	3.493964	-3.504176
O	3.825151	4.287469	-2.887685
Fe	5.251896	1.222688	-4.846336
N	6.351249	2.766057	-4.934132
C	7.553030	2.877594	-5.527777
N	8.160097	1.645492	-5.932181
C	9.433922	1.765170	-6.647279
O	4.324951	1.213641	-6.316081
N	6.609946	0.034604	-4.997204
C	6.278987	-1.412571	-4.808718
C	7.236890	-2.092230	-3.809866
C	7.834139	0.328975	-5.586272
O	8.648378	-0.558242	-5.870269
C	6.236434	-2.174867	-6.151748
C	5.766098	3.955941	-4.298081
C	5.288019	4.979530	-5.351860
C	6.717107	4.622478	-3.277473
O	8.172546	3.931619	-5.739237
H	3.729261	0.441056	-6.252981
H	5.600812	-1.642976	-6.870008
H	5.805214	-3.165910	-5.974832
H	7.236820	-2.273125	-6.574282
H	8.238710	-2.167421	-4.232309
H	6.845098	-3.085133	-3.571804
H	7.284060	-1.511711	-2.880868
H	2.230944	-1.826753	-3.045051
H	0.487496	-0.887788	-1.515561
H	9.436477	1.090805	-7.506502
H	4.617755	4.492488	-6.068978

H	4.746381	5.794901	-4.861147
H	6.154615	5.372262	-5.887860
H	7.577915	5.050096	-3.791886
H	6.173380	5.402448	-2.735547
H	7.072562	3.879886	-2.552721
H	2.282592	3.020546	-1.868804
H	0.514763	1.529200	-0.935286
H	10.276238	1.490700	-6.002220
H	9.534082	2.801854	-6.958130

Triplet Fe^{IV}(OH)

C	3.164092	1.495636	-2.987588
C	3.302821	0.086285	-3.149886
C	2.344419	-0.782195	-2.608513
C	1.259294	-0.245299	-1.912775
C	1.122345	1.138585	-1.754193
C	2.067288	2.017700	-2.287017
N	4.457228	-0.248424	-3.863899
C	4.978589	-1.496662	-4.071816
O	4.478302	-2.559685	-3.703694
N	4.216486	2.198268	-3.579906
C	4.464940	3.541942	-3.515847
O	3.769727	4.379488	-2.940289
Fe	5.323946	1.185005	-4.702760
N	6.410692	2.695053	-4.751088
C	7.604619	2.803309	-5.403804
N	8.197100	1.611007	-5.899214
C	9.443464	1.789703	-6.650871
O	4.405856	1.262782	-6.226327
N	6.693090	-0.029918	-5.034043
C	6.324369	-1.452652	-4.836333
C	7.353279	-2.200965	-3.961107
C	7.868211	0.251794	-5.668459
O	8.670943	-0.603254	-6.067105
C	6.108319	-2.178863	-6.182676
C	5.767825	3.937044	-4.253992
C	5.366865	4.875093	-5.413942
C	6.649551	4.673909	-3.222145
O	8.195514	3.875307	-5.594178
H	3.483517	1.053934	-5.992688
H	5.393080	-1.621151	-6.797746
H	5.705611	-3.179584	-5.993967
H	7.055275	-2.252337	-6.720261
H	8.299870	-2.297844	-4.493104
H	6.953408	-3.187988	-3.709781
H	7.525061	-1.649411	-3.029015
H	2.474567	-1.849256	-2.732701
H	0.514565	-0.915718	-1.489342
H	9.435676	1.132281	-7.521513
H	4.759489	4.328023	-6.143674
H	4.776382	5.708056	-5.018078
H	6.261703	5.254282	-5.910436
H	7.538997	5.078142	-3.705541
H	6.063610	5.478097	-2.766971
H	6.959852	3.981196	-2.430623
H	1.985283	3.089890	-2.166177
H	0.271286	1.539762	-1.208141
H	10.314751	1.526779	-6.039331
H	9.508509	2.834226	-6.943923

Appendix B

Gas chromatography (GC) was performed on a Perkin Elmer Arnel Clarus500 instrument equipped with a hydrogen flame ionization detector and HP-5 (30 m × 0.32 mm × 0.25 μm) column. Helium was used as carrier gas at a flow rate of 30 mL min^{-1}.

a) GC method for 4-methoxystyrene, styrene, 4-chlorostyrene, 4-cyanostyrene 4-nitrostyrene and *cis*-cyclooctene

Oven temperature program:-

Initial temperature: 60 °C for 0.00 min

Ramp1: 10.0 °C / min to 200 °C, hold for 0.00 min

Ramp2: 20.0 °C / min to 250 °C, hold for 2.00 min

Injector temperature: 250 °C

Detector temperature: 280 °C

b) GC method for methyl *trans*-cinnamate, *cis*-stilbene and *trans*-stilbene

Oven temperature program:-

Initial temperature: 80 °C for 0.00 min

Ramp 1: 20.0 °C / min to 180 °C, hold for 0.00 min

Ramp 2: 10.0 °C / min to 220 °C, hold for 0.00 min

Ramp 3: 20.0 °C / min to 280 °C, hold for 2.00 min

Injector temperature: 280 °C

Detector temperature: 300 °C

c) GC method for norbornene

Oven temperature program:-

Initial temperature: 50 °C for 0.00 min

Ramp 1: 10.0 °C / min to 200 °C, hold for 0.00 min

Ramp 2: 20.0 °C / min to 250 °C, hold for 1.00 min

Injector temperature: 200 °C

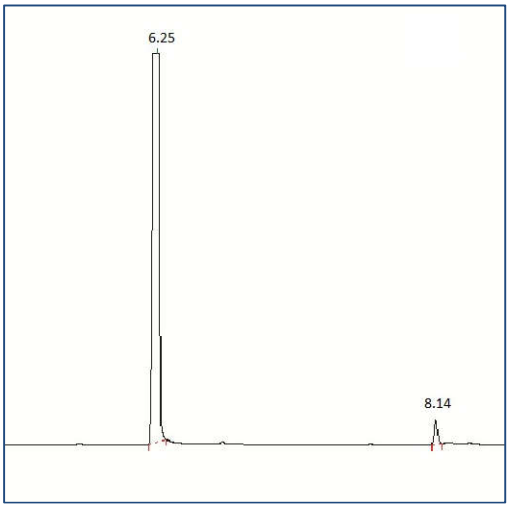

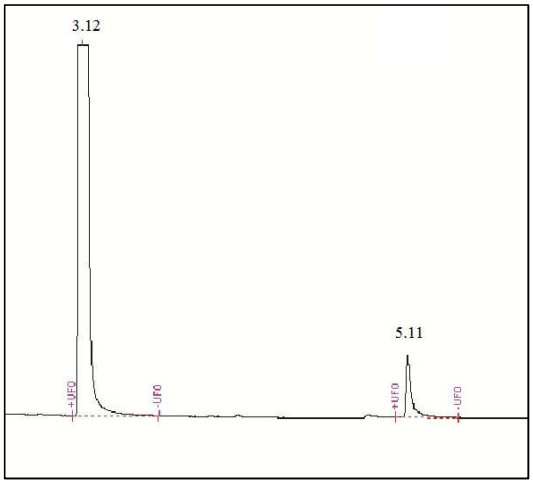

4-methoxystyrene, R_t = 6.25. 4-methoxystyrene oxide, R_t = 8.14 (left)

Styrene, R_t = 3.12. Styrene oxide, R_t = 5.11 (right)

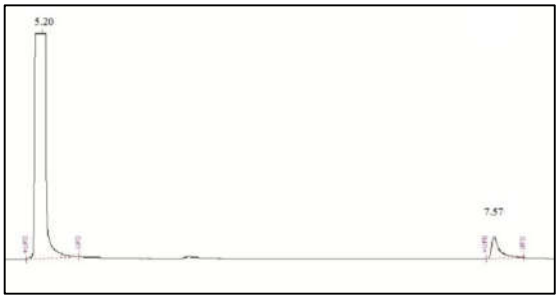

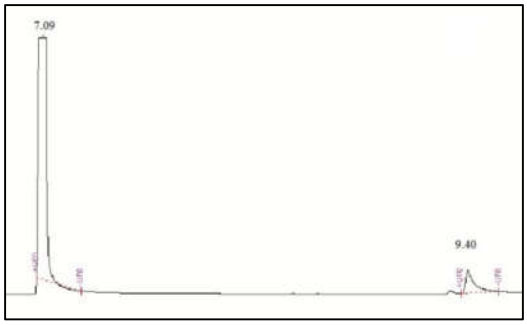

4-chlorostyrene, R_t = 5.20. 4-chlorostyrene oxide, R_t = 7.57 (left)

4-cyanostyrene, R_t = 7.09. 4-cyanostyrene oxide, R_t = 9.40 (right)

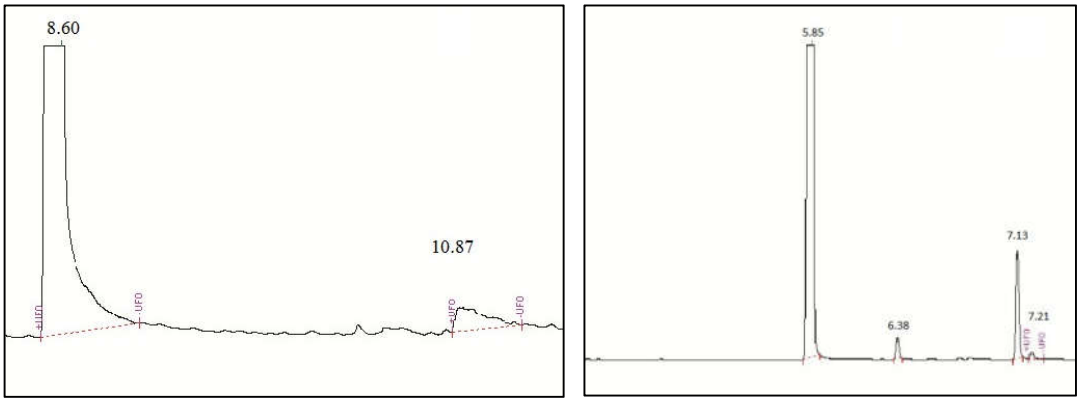

4-nitrostyrene, R_t = 8.60. 4-nitrostyrene oxide, R_t = 10.87 (left). *cis*-stilbene, R_t = 5.85. *cis*-stilbene oxide, R_t = 6.38. Isomer of *cis*-stilbene (*trans*-stilbene), R_t = 7.13. *trans*-stilbene oxide, R_t = 7.21 (right)

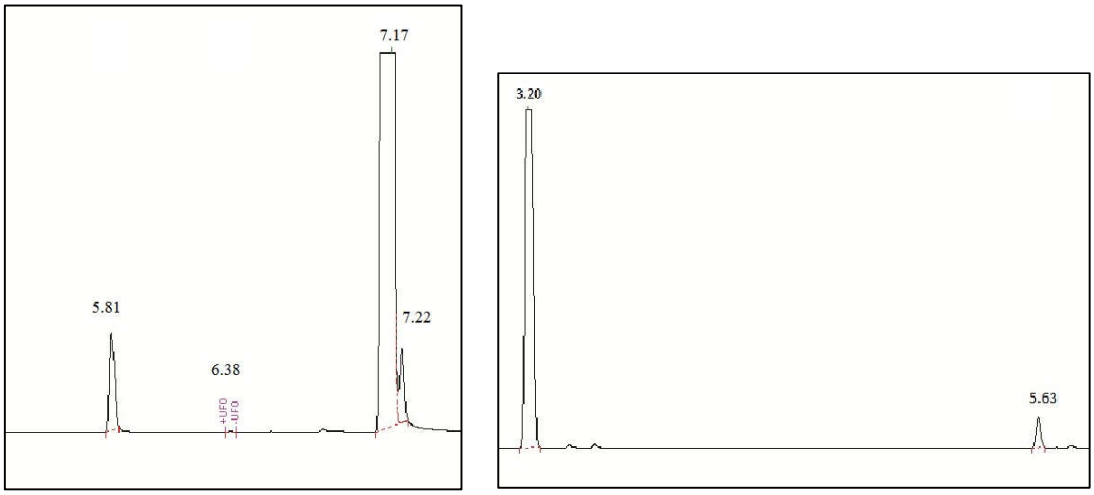

Benzaldehyde, R_t = 2.39 *cis*-stilbene, R_t = 5.81. *cis*-stilbene oxide, R_t = 6.38. Isomer of *cis*-stilbene (*trans*-stilbene), R_t = 7.17. *trans*-stilbene oxide, R_t = 7.22 (left).
cis-cyclooctene, R_t = 3.20. *cis*-cyclooctene oxide, R_t = 5.63(right)

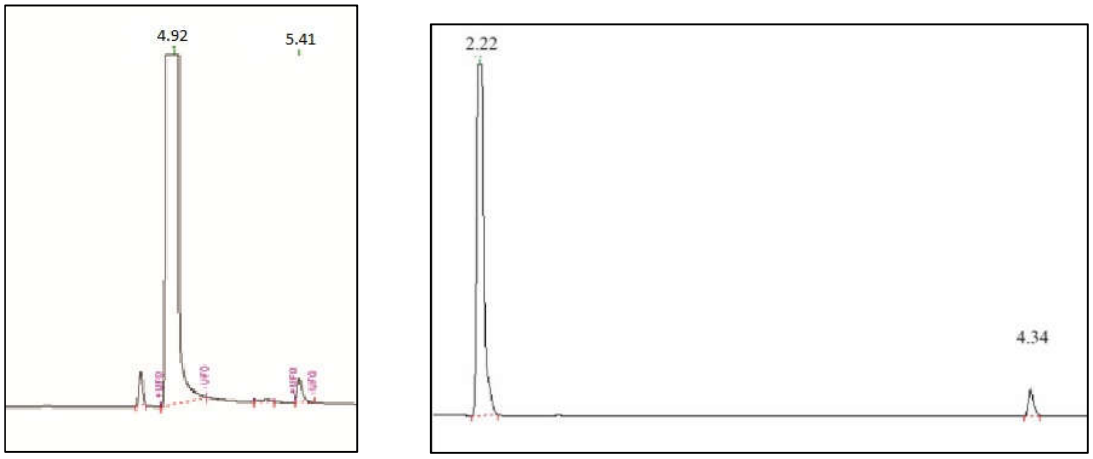

Methyl *trans*-cinnamate, $R_t = 4.92$. Epoxide, $R_t = 5.41$ (left).

Norbornene, $R_t = 2.22$. Norbornene oxide, $R_t = 4.34$ (right).

Appendix B1. GC trace of products given in table 3.1.

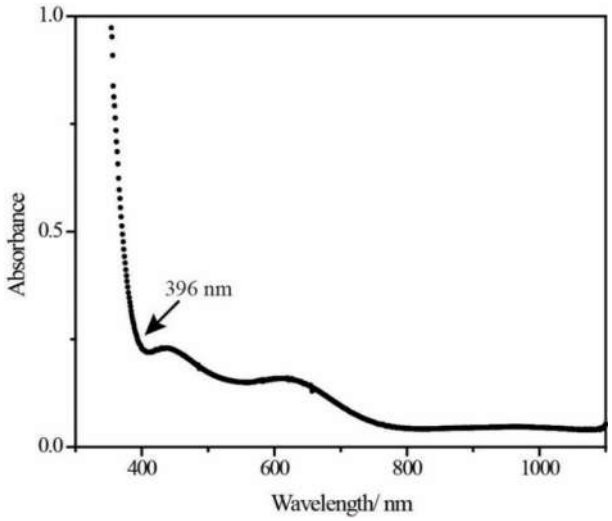

Appendix B2. UV-vis spectrum just after mixing of 4-nitrostyrene to complex **2** (4x10-5M) showing higher absorbance at Fe $^{III/IV}$ isosbestic point 396 nm.

	ΔE (UB3LYP)	Δ(E+ZPE) (UB3LYP)	ΔG (UB3LYP)
Neutral styrene + monoanionic doublet $Fe^{V}(O)$ complex	0.0	0.0	0.0
cationic styrene + dianionic triplet $Fe^{IV}(O)$ complex	35.5	34.6	34.4
TS1 (doublet) for Pathway A	9.2	9.4	21.4

Appendix B3. The solvent phase relative reaction energies in kcal/mol at the UB3LYP/6-31G*, LANL2DZ (Fe) level of theory for the Pathway B.

	ΔE (UB3LYP)	Δ(E+ZPE) (UB3LYP)	ΔG (UB3LYP)
Reactant (*S*=1/2)	0.0	0.0	0.0
TS1 (*S*=1/2)	12.4	12.2	25.0

Appendix B4. The gas phase relative reaction energies in kcal/mol at the UB3LYP/6-31G*, LANL2DZ (Fe) level of theory for *para*-chlorostyrene epoxidation catalyzed by $[Fe^{V}(O)(\text{biuret-TAML})]^{-}$.

	ΔE (UB3LYP)	Δ(E+ZPE) (UB3LYP)	ΔG (UB3LYP)
para-methoxy styrene	8.8	9.2	20.8
styrene	9.2	9.4	21.4
para-chloro styrene	12.7	13.0	25.6

Appendix B5. The solvent phase rate determining barrier (^{2}TS1) in kcal/mol at the UB3LYP/6-31G*, LANL2DZ (Fe) level of theory for epoxidation of the styrene derivatives catalyzed by $[Fe^{V}(O)(\text{biuret-TAML})]^{-}$ complex.

	ΔE (UB3LYP)	Δ(E+ZPE) (UB3LYP)	ΔG (UB3LYP)
S=1/2	0.0 (0.0)	0.0 (0.0)	0.0 (0.0)
S=3/2	3.0 (11.5)	2.1 (10.8)	1.3 (10.3)

Appendix B6. The relative energies of the $[Fe^{V}(O)(biuret\text{-}TAML)]^{-}$ catalyst in doublet and quartet electronic states in kcal/mol at the UB3LYP/6-31G*, LANL2DZ (Fe) level of theory

A **B**

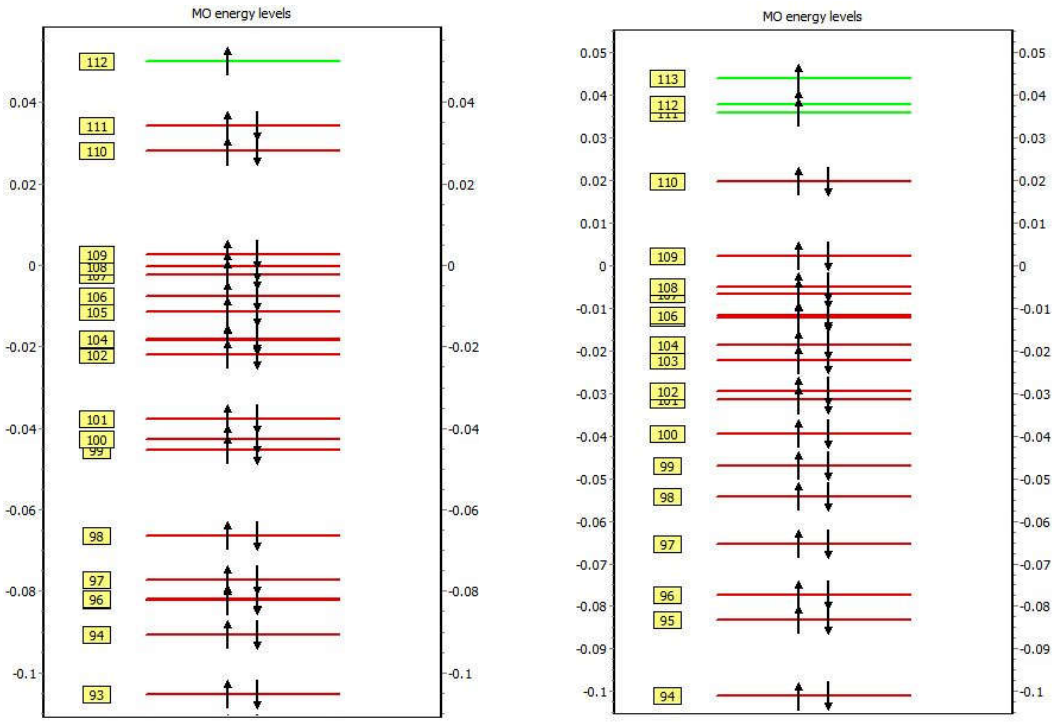

Appendix B7. Molecular orbitals energy diagram of some of the occupied orbitals of highest energies of product complex $[Fe^{III}(Cl)(biuret\text{-}TAML)]^{2-}$ in (A) *S*= 1/2 (B) *S*= 3/2. The values on Y-axis represent orbital energy in hartree.

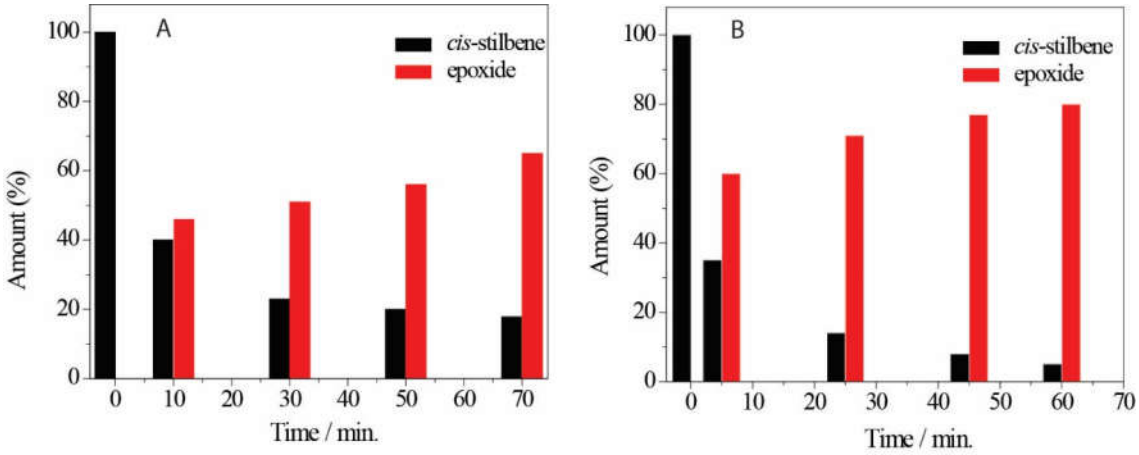

Appendix B8. Influence of the catalyst concentration *cis*-stilbene epoxidation. (A) Complex **1** / *cis*-stilbene = 1.0 %, Catalyst (**1**) (1×10^{-4} M): NaOCl (2×10^{-2} M, pH = 11.4) : Substrates (1×10^{-2} M) = 1 : 200 : 100). (B) Complex **1** / *cis*-stilbene = 1.5 %, Catalyst (**1**) (1.5×10^{-4} M) : NaOCl (3×10^{-2} M, pH = 11.4) : Substrates (1×10^{-2} M) = 1.5 : 300 : 100). *trans*-/ *cis*- epoxide = 1.7. Reaction were performed at room temperature in CH_3CN under air (10% error).

XYZ coordinates of all the stationary points obtained by full optimization at UB3LYP/6-31G*, LANL2DZ (Fe) level of theory

$Fe^{V}O$ doublet, gas

C	1.854237	-2.131254	1.486705
C	2.527085	-2.246150	0.262174
C	3.230663	-3.435851	-0.056056
C	3.255656	-4.505946	0.848642
C	2.588223	-4.375593	2.067538
C	1.897524	-3.200870	2.383564
N	2.582108	-1.305711	-0.777619
C	1.941441	-0.089016	-0.806255
C	2.194613	0.691277	-2.103723
N	2.975869	-0.187410	-2.992395
C	3.258148	0.256134	-4.237926
O	2.937773	1.365723	-4.688403
N	3.789852	-3.376678	-1.327772
C	4.216687	-4.424874	-2.077875
C	4.501172	-4.002868	-3.532908
C	3.699825	-4.962334	-4.436401
Fe	3.808189	-1.652785	-2.120642
N	4.054824	-2.589546	-3.686170
C	4.240646	-2.000939	-4.918832
O	4.673735	-2.626598	-5.894748
O	5.199981	-1.065916	-1.651308
N	3.965965	-0.637440	-5.089494
C	4.297821	-0.130168	-6.424017
O	1.245995	0.359244	0.102357
O	4.354895	-5.589619	-1.699632
C	0.808744	1.041954	-2.688803
C	2.975844	1.970196	-1.723811
C	6.022247	-4.151061	-3.756596
H	3.957281	1.703052	-1.316413
H	2.419099	2.528345	-0.963713
H	3.117171	2.587678	-2.612640
H	0.920836	1.686329	-3.560710
H	0.214656	1.542981	-1.918534
H	0.285269	0.126623	-2.989697
H	1.318148	-1.220194	1.712416
H	1.385910	-3.111757	3.339270
H	4.158850	0.947622	-6.406701
H	6.565366	-3.435427	-3.128623
H	6.323328	-5.163961	-3.469506
H	6.272521	-3.969894	-4.802729
H	3.953929	-4.803235	-5.483933
H	3.927491	-5.990141	-4.138288
H	2.624626	-4.795383	-4.301419
H	3.782876	-5.410529	0.576020
H	2.610134	-5.199699	2.777326
H	3.648097	-0.574612	-7.186397
H	5.329336	-0.392198	-6.667994

$Fe^{V}O$ quartet, gas

C	1.851075	-2.111473	1.544454
C	2.477628	-2.216514	0.279900
C	3.101046	-3.469793	-0.109929
C	3.073426	-4.570140	0.779468
C	2.450129	-4.430252	2.006861
C	1.843035	-3.209113	2.386823
N	2.564525	-1.259259	-0.687390
C	1.999167	-0.001552	-0.713220
C	2.228645	0.728113	-2.064981
N	2.876257	-0.222410	-3.007560
C	3.134393	0.199510	-4.276777
O	2.809472	1.311780	-4.720054
N	3.642465	-3.424454	-1.360682
C	4.211808	-4.444419	-2.094638
C	4.585461	-4.003262	-3.536026
C	3.932257	-5.025698	-4.491390
Fe	3.656145	-1.704425	-2.188436
N	4.070536	-2.626248	-3.749754
C	4.248162	-2.045533	-4.969820
O	4.760592	-2.606993	-5.949818
O	5.100178	-1.154703	-1.635571
N	3.811301	-0.704581	-5.148927
C	4.080198	-0.197805	-6.499143
O	1.366566	0.514543	0.205287
O	4.406748	-5.589244	-1.693049
C	0.836983	1.182495	-2.556777
C	3.139047	1.942641	-1.772856
C	6.126801	-4.052131	-3.640984
H	4.120739	1.594971	-1.433587
H	2.689998	2.563963	-0.990354
H	3.264024	2.529504	-2.684930
H	0.941206	1.787112	-3.457192
H	0.344188	1.756959	-1.766488
H	0.215552	0.308962	-2.789224
H	1.390951	-1.170845	1.816985
H	1.363122	-3.132810	3.359716
H	3.765291	0.841524	-6.528551
H	6.567009	-3.314929	-2.960965
H	6.486899	-5.050036	-3.367987
H	6.427225	-3.817654	-4.664198
H	4.235643	-4.819106	-5.517431
H	4.233725	-6.036586	-4.200406
H	2.839366	-4.957667	-4.426786
H	3.541373	-5.495895	0.471583

H	2.427220	-5.272983	2.693842
H	3.531561	-0.782542	-7.244989
H	5.145541	-0.289518	-6.726722

Fe^{III} O doublet, gas

C	5.015623	0.680538	-0.001835
C	3.825740	1.401268	-0.003298
C	2.601847	0.707457	-0.001769
C	2.595826	-0.733925	0.001492
C	3.814183	-1.437234	0.002793
C	5.009704	-0.725713	0.001098
N	1.322269	1.242005	-0.003017
Fe	-0.049486	-0.000108	-0.000028
N	1.312561	-1.257927	0.002971
C	0.920370	-2.579560	0.002356
O	1.666504	-3.556083	0.003087
C	0.942878	2.569119	-0.002067
O	1.700975	3.535928	-0.002878
C	-0.607236	2.756016	0.000439
C	-0.961932	3.562692	-1.268049
N	-1.242901	1.409474	0.001521
C	-2.601877	1.328181	0.001791
N	-3.183391	0.017051	-0.000701
C	-4.650329	-0.017715	-0.001221
C	-0.957941	3.562533	1.270113
O	-3.364741	2.306812	0.003776
C	-0.632441	-2.748397	0.000092
C	-0.996766	-3.549860	-1.268716
C	-1.000465	-3.548819	1.268518
N	-1.248427	-1.393177	-0.001555
C	-2.609728	-1.287789	-0.001833
O	-3.394305	-2.248218	-0.002896
H	-0.713174	2.983462	-2.165564
H	-0.386154	4.493609	-1.285591
H	-2.030426	3.782963	-1.277421
H	-2.026485	3.782442	1.282833
H	-0.382402	4.493629	1.285946
H	-0.706211	2.983280	2.166781
H	3.811087	2.483660	-0.005529
H	5.963314	1.214542	-0.003025
H	-5.003253	1.009677	-0.002313
H	-0.737408	-2.975175	-2.166114
H	-0.434782	-4.489176	-1.284212
H	-2.068490	-3.754314	-1.280055
H	-2.072133	-3.753647	1.276911
H	-0.438210	-4.487930	1.286458
H	-0.743920	-2.973283	2.166182
H	3.790920	-2.519521	0.005051
H	5.953076	-1.267389	0.002112
H	-5.017827	-0.550499	0.881281
H	-5.016783	-0.552416	-0.882912

Fe^{III} O quartet, gas

C	5.030473	0.675225	-0.001695
C	3.830966	1.395926	-0.003190
C	2.616785	0.702178	-0.001799
C	2.610168	-0.725899	0.001322
C	3.817816	-1.430936	0.002659
C	5.023992	-0.721413	0.001114
N	1.319717	1.249212	-0.003117
Fe	-0.052533	0.000578	-0.000027
N	1.307925	-1.260768	0.002716
C	0.920358	-2.573473	0.001555
O	1.664513	-3.554625	0.001693
C	0.944613	2.564912	-0.001518
O	1.697931	3.539187	-0.001666
C	-0.606895	2.753961	0.000805
C	-0.961017	3.558514	-1.267692
N	-1.252132	1.409323	0.002197
C	-2.614040	1.323807	0.001879
N	-3.197970	0.016841	-0.001003
C	-4.665776	-0.017035	-0.001515
C	-0.957379	3.559016	1.269951
O	-3.369731	2.305160	0.003581
C	-0.632700	-2.746658	-0.000156
C	-0.995151	-3.547800	-1.268340
C	-0.997919	-3.546199	1.268293
N	-1.260688	-1.395762	-0.001879
C	-2.621287	-1.287611	-0.001905
O	-3.402725	-2.248089	-0.002558
H	-0.721800	2.974899	-2.165282
H	-0.370252	4.479589	-1.288758
H	-2.026210	3.794770	-1.276146
H	-2.022617	3.794967	1.281280
H	-0.366776	4.480238	1.288997
H	-0.715513	2.975800	2.167082
H	3.814539	2.478464	-0.005335
H	5.975357	1.214563	-0.002790
H	-5.017639	1.010802	-0.003953
H	-0.744177	-2.969756	-2.166291
H	-0.419632	-4.478572	-1.286225
H	-2.064260	-3.766349	-1.278902
H	-2.067001	-3.764953	1.276820
H	-0.422310	-4.476872	1.288614
H	-0.748986	-2.966972	2.166051
H	3.791386	-2.513275	0.004800

H	5.963830	-1.269490	0.002179
H	-5.034635	-0.546336	0.882220
H	-5.033366	-0.550624	-0.883064

Styrene, gas

C	0.041782	0.000000	0.042481
H	0.081069	0.000000	1.128500
C	1.219649	0.000000	-0.704791
C	-1.124708	0.000000	-5.069761
H	0.927434	0.000000	-4.698128
H	-0.994145	0.000000	-6.147533
H	-2.150336	0.000000	-4.710915

Doublet TS1, styrene beta attack, gas

C	3.984507	-3.767163	-0.876393
C	3.785073	-2.416650	-1.170004
C	2.742497	-1.729022	-0.533439
C	1.907661	-2.402807	0.400837
C	2.126095	-3.756788	0.690817
C	3.164718	-4.429537	0.043992
N	2.400191	-0.380670	-0.663096
C	3.105304	0.588089	-1.319178
C	2.513852	1.997122	-1.097812
N	1.323572	1.860187	-0.225631
C	0.675575	2.990813	0.162229
O	1.000245	4.140191	-0.171457
N	0.945367	-1.552948	0.950993
C	0.136238	-1.811711	2.020619
C	-0.727078	-0.592973	2.414261
C	-0.440561	-0.304879	3.903726
Fe	0.746458	0.099296	0.082770
O	-0.341639	-0.219469	-1.138621
N	-0.319850	0.547746	1.556426
C	-0.928445	1.749104	1.749350
O	-1.854749	1.939630	2.553592
N	-0.483797	2.853912	0.972627
C	-1.171170	4.124002	1.230604
O	0.072205	-2.873621	2.641091
C	-2.201261	-1.005664	2.209797
O	4.119388	0.414243	-1.996260
C	2.156091	2.578676	-2.481926
C	3.629169	2.828658	-0.423985
C	-1.761212	1.116686	-1.807023
C	-2.878170	0.847158	-1.058562
C	-3.885311	-0.157790	-1.363405
H	-1.636516	0.705949	-2.802248
H	1.364931	1.980883	-2.949542
H	3.039505	2.544424	-3.127721
C	1.162144	0.000000	-2.097837
C	-0.068070	0.000000	-2.777349
C	-1.246086	0.000000	-2.007678
C	-1.191225	0.000000	-0.617213
H	2.184397	0.000000	-0.204215
H	2.084190	0.000000	-2.675040
C	-0.066321	0.000000	-4.249624
H	-2.213833	0.000000	-2.501040
H	-2.114374	0.000000	-0.043356
H	1.810968	3.608829	-2.375761
H	3.312245	3.866076	-0.315142
H	4.535055	2.769003	-1.035132
H	3.853195	2.419613	0.568472
H	4.414927	-1.884260	-1.870197
H	4.788501	-4.306291	-1.372972
H	-1.281204	4.670601	0.293045
H	-2.395849	-1.206554	1.151359
H	-2.396190	-1.921868	2.776868
H	-2.863766	-0.208776	2.550819
H	-1.100613	0.482975	4.269080
H	-0.592692	-1.223310	4.478723
H	0.600224	0.015408	4.032146
H	1.489741	-4.247956	1.414812
H	3.333578	-5.482030	0.261657
H	-0.596888	4.753979	1.920208
H	-2.137571	3.897449	1.673678
H	-3.022491	1.400583	-0.132939
H	-1.141431	1.968937	-1.564144
C	-5.091061	-0.171582	-0.630314
C	-6.092833	-1.098094	-0.906772
C	-5.911640	-2.046683	-1.916678
C	-4.714097	-2.061693	-2.640612
C	-3.713993	-1.133886	-2.369738
H	-5.231547	0.559685	0.161940
H	-7.013724	-1.085505	-0.328869
H	-6.689221	-2.775795	-2.130101
H	-4.555946	-2.810357	-3.413036
H	-2.776817	-1.179069	-2.915355

Quartet TS1, styrene beta attack, gas

C	-4.279875	-3.599012	-0.657516
C	-3.069491	-3.368988	-0.010307
C	-2.514523	-2.076813	-0.034449
C	-3.198755	-1.016412	-0.715568
C	-4.421037	-1.272799	-1.361127
C	-4.948858	-2.560586	-1.326841
N	-1.339269	-1.651394	0.562072
C	-0.545003	-2.342613	1.440193
C	0.623010	-1.487612	1.995566

N	0.442316	-0.091192	1.516275
C	1.342646	0.849912	1.903063
O	2.340542	0.627274	2.607331
N	-2.535311	0.194371	-0.609261
C	-2.978403	1.430619	-0.990782
C	-2.057507	2.571865	-0.486402
C	-2.922320	3.411004	0.484302
Fe	-0.795810	0.096485	0.127344
O	0.070312	-0.339263	-1.269242
N	-0.892887	1.958345	0.205455
C	0.008414	2.784753	0.808293
O	-0.049764	4.022367	0.801798
N	1.130650	2.189560	1.452254
C	2.109333	3.173090	1.931346
O	-4.008226	1.673518	-1.621319
H	-4.709976	-4.598012	-0.645149
H	3.011092	2.637005	2.215179
H	-1.044358	2.822214	-2.402566
H	-2.532368	3.769863	-2.226553
H	-1.041909	4.274715	-1.370833
H	-2.367139	4.287072	0.820500
H	-3.839638	3.717404	-0.027654
H	-3.197260	2.808664	1.358554
H	-4.924105	-0.459887	-1.868064
H	-5.892493	-2.763056	-1.828789
H	1.725332	3.722239	2.799245
H	2.308306	3.897175	1.140234
H	2.294102	-0.124541	-3.606541
H	0.767071	1.409609	-2.520638
C	4.610271	-1.064304	-2.845134
C	5.828900	-1.539498	-2.371198
C	6.199668	-1.315548	-1.041935
C	5.332047	-0.614409	-0.196360
C	4.114550	-0.135774	-0.666898
H	4.325802	-1.242643	-3.880039
H	6.490505	-2.088228	-3.037679
H	7.149512	-1.688170	-0.666640
H	5.600058	-0.444992	0.843211
H	3.457531	0.385474	0.020530

Doublet TS1, styrene alpha attack, gas

C	2.781202	-1.452775	-2.904406
C	2.922179	-0.596202	-1.800039
C	3.955799	-0.846876	-0.884171
C	4.839957	-1.908508	-1.076577
C	4.698212	-2.744760	-2.185273
C	3.661683	-2.515147	-3.095223
C	2.019818	0.553459	-1.570600
C	-1.636821	3.421873	-1.702224
O	-0.704151	-3.512501	1.787663
C	1.926628	-2.131628	1.475923
C	0.547154	-1.569611	3.535175
C	1.528855	0.917001	-1.932045
C	2.484353	0.157180	-2.571514
C	3.722427	-0.346178	-2.010420
H	1.719903	1.348377	-0.957347
H	1.979976	-2.046851	0.385828
H	1.935280	-3.193079	1.745236
H	2.791523	-1.632322	1.914916
H	1.405295	-1.063308	3.978812
H	0.530797	-2.620622	3.838388
H	-0.371537	-1.090855	3.895027
H	-2.542414	-4.153918	0.515649

O	0.461181	-0.453380	-0.987061
Fe	-0.594908	0.077640	0.222064
N	-0.791506	-1.371373	1.375375
C	-1.597182	-2.452327	1.156654
N	-2.535284	-2.389130	0.099034
C	-3.286330	-3.633415	-0.093491
N	-0.805125	1.897247	-0.174443
C	-1.773742	2.220794	-1.082085
O	-1.926139	3.324728	-1.609845
C	0.125594	2.758489	0.419087
C	0.330052	4.118614	0.149426
C	1.301039	4.817804	0.873127
C	2.064474	4.174941	1.851413
C	1.875618	2.817827	2.129527
C	0.904992	2.102774	1.414788
N	0.556962	0.755704	1.551173
C	0.972069	-0.111667	2.519294
O	1.827420	0.113248	3.378175
C	-2.713983	1.033971	-1.393339
C	-4.139346	1.501791	-1.023363
N	-2.279321	-0.119791	-0.570938
C	-2.986587	-1.278699	-0.664053
O	-3.992143	-1.427160	-1.374360
C	-2.603910	0.739220	-2.905117
C	0.224528	-1.463812	2.452637
C	1.275678	-2.556848	2.158876
C	-0.422110	-1.674898	3.839169
O	-1.555014	-3.498760	1.818894
C	1.427061	1.279059	-2.589687
H	1.385446	0.903889	-3.607689
H	-1.594791	0.383126	-3.140919
H	-2.793390	1.658750	-3.468844
H	-3.325859	-0.028989	-3.186798
H	-4.867654	0.740881	-1.304751
H	-4.352605	2.442608	-1.540341
H	-4.207669	1.676266	0.057112

H	-0.278988	4.601086	-0.603657
H	1.458504	5.874420	0.667805
H	-3.817741	-3.558834	-1.038739
H	1.715239	-2.401157	1.167173
H	2.072783	-2.498326	2.907604
H	0.806658	-3.541782	2.189041
H	-0.882335	-2.661562	3.893791
H	0.348061	-1.569710	4.609403
H	-1.192245	-0.913905	4.013857
H	2.449097	2.304297	2.890184
H	2.816179	4.731701	2.406845
H	-4.008272	-3.791984	0.716793
H	-2.591709	-4.474433	-0.092430
H	0.906477	2.205375	-2.376937
H	2.167594	1.063830	-0.624640
H	4.060275	-0.204503	-0.013335
H	5.634010	-2.085776	-0.355643
H	5.382100	-3.576683	-2.334633
H	3.533505	-3.173295	-3.951171
H	1.961816	-1.298801	-3.600016
C	0.007590	4.132188	0.365669
C	0.990517	4.846597	1.047820
C	1.891301	4.194912	1.903592
C	1.827373	2.815883	2.096503
C	0.842684	2.075069	1.420268
N	0.601377	0.708622	1.494788
C	1.245397	-0.218800	2.270986
O	2.209662	-0.001426	3.005928
C	-2.954295	0.924936	-1.105671
C	-4.370323	1.279009	-0.598288
N	-2.380798	-0.237304	-0.382646
C	-3.008876	-1.438768	-0.496054
O	-4.070388	-1.614496	-1.113667
C	-2.954462	0.710311	-2.635719
C	0.611848	-1.630183	2.156850
C	1.699602	-2.594868	1.638008
C	0.167450	-2.019354	3.585309
O	-1.089978	-3.754887	1.553261
C	1.152233	1.380318	-2.838896
H	1.211633	0.971073	-3.842699
H	-1.947473	0.442325	-2.974300
H	-3.260853	1.636326	-3.133799
H	-3.641547	-0.097243	-2.893847
H	-5.064280	0.476005	-0.847189
H	-4.693715	2.218076	-1.058113
H	-4.357483	1.411653	0.490346
H	-0.697707	4.617087	-0.296576
H	1.058653	5.923464	0.910642
H	-3.854767	-3.701069	-0.816051
H	1.989149	-2.321135	0.618372
H	2.581721	-2.529562	2.283671
H	1.314212	-3.615985	1.636224

Quartet TS1, styrene alpha attack, gas

C	2.861162	-1.142797	-2.994571
C	2.829138	-0.253087	-1.907361
C	3.833137	-0.353732	-0.930535
C	4.852895	-1.298309	-1.047860
C	4.881886	-2.166336	-2.140864
C	3.877431	-2.087731	-3.110614
C	1.783036	0.781159	-1.763534
O	0.333484	-0.375599	-1.105208
Fe	-0.647006	0.038732	0.257895
N	-0.538557	-1.542890	1.222197
C	-1.302548	-2.656504	1.019389
N	-2.408030	-2.564400	0.139448
C	-3.102313	-3.842955	-0.045157
N	-0.985800	1.859706	-0.026811
C	-2.067544	2.162147	-0.815692
O	-2.345815	3.277055	-1.257999
C	-0.075510	2.740278	0.543898
H	-0.212426	-3.041157	3.592893
H	1.021908	-1.927071	4.262863
H	-0.624292	-1.344126	3.932183
H	2.509093	2.296597	2.757424
H	2.652361	4.770590	2.425763
H	-3.579851	-4.166283	0.886651
H	-2.382492	-4.612363	-0.333213
H	0.492444	2.226919	-2.684621
H	1.835544	1.353559	-0.843233
H	3.802410	0.306323	-0.067201
H	5.619060	-1.360752	-0.279240
H	5.672658	-2.907110	-2.231333
H	3.881684	-2.772961	-3.955000
H	2.070582	-1.107813	-3.738096

Doublet intermediate, styrene beta attack, gas

C	-4.378255	-3.486505	-0.402648
C	-3.468874	-2.974603	0.524726
C	-2.748567	-1.815982	0.202122
C	-2.951448	-1.174464	-1.052705
C	-3.870714	-1.699504	-1.971677
C	-4.576791	-2.856357	-1.636770
N	-1.815089	-1.139478	0.990206
C	-1.507840	-1.380545	2.300280
C	-0.518116	-0.338974	2.875979
N	-0.208388	0.644819	1.807052
C	0.593476	1.704025	2.118728
O	1.116033	1.885106	3.226910
N	-2.169082	-0.025349	-1.184519
C	-2.233454	0.911209	-2.177402
C	-1.302808	2.118941	-1.909895

C	-2.215664	3.364350	-1.853452
Fe	-0.839425	0.191135	0.112534
O	0.480213	-0.762634	-0.591111
N	-0.601355	1.885433	-0.621582
C	0.217276	2.869489	-0.145868
O	0.451818	3.932318	-0.736477
N	0.877403	2.643497	1.090319
C	1.821828	3.700291	1.468398
O	-2.949591	0.865444	-3.178116
C	-0.316214	2.213247	-3.093401
O	-1.954562	-2.291779	2.997387
C	0.740751	-1.105770	3.335479
C	-1.232218	0.319434	4.077465
C	1.806567	-0.284931	-0.596781
C	2.663112	-1.286980	-1.308642
C	4.057529	-1.457851	-1.146830
H	2.164911	-0.115598	0.430588
H	1.233340	-1.575672	2.476274
H	0.446378	-1.894717	4.034870
H	1.439453	-0.420529	3.818687
H	-0.553721	0.995649	4.597922
H	-1.580087	-0.465672	4.755511
H	-2.103302	0.887988	3.730267
H	-3.307905	-3.442607	1.486882
H	-4.937160	-4.387277	-0.158258
H	2.517056	3.291660	2.198635
H	0.323669	1.323692	-3.124372
H	-0.881386	2.261717	-4.029550
H	0.310257	3.100746	-2.988421
H	-1.615485	4.270284	-1.765946
H	-2.824533	3.398432	-2.761974
H	-2.887638	3.298769	-0.989253
H	-4.016590	-1.193006	-2.916673
H	-5.289245	-3.269477	-2.347583
H	1.307144	4.558866	1.917406
H	2.338115	4.042885	0.572847
H	2.144623	-1.906802	-2.036510
H	1.860201	0.693365	-1.109318
C	4.749587	-2.437267	-1.921538
C	6.116570	-2.627329	-1.795260
C	6.862302	-1.852915	-0.893784
C	6.208664	-0.883625	-0.120656
C	4.840272	-0.683701	-0.238166
H	4.177994	-3.042182	-2.621667
H	6.612438	-3.383418	-2.399980
H	7.934156	-2.003302	-0.795641
H	6.777318	-0.278661	0.581822
H	4.357517	0.073168	0.372278

Quartet intermediate, styrene beta attack, gas

C	-2.979153	-4.505929	0.198561
C	-2.158599	-3.681085	0.968480
C	-1.925350	-2.364799	0.543305
C	-2.523641	-1.885080	-0.659617
C	-3.346798	-2.728446	-1.420520
C	-3.566766	-4.034794	-0.982748
N	-1.159565	-1.385045	1.174255
C	-0.570720	-1.452452	2.407323
C	0.127491	-0.126984	2.803137
N	-0.095313	0.858605	1.716200
C	0.385978	2.122784	1.875307
O	1.020869	2.510928	2.866837
N	-2.198203	-0.552470	-0.910251
C	-2.710163	0.261439	-1.883606
C	-2.194682	1.717418	-1.766901
C	-3.445284	2.599478	-1.547002
Fe	-0.809636	0.141353	0.142570
O	0.662183	-0.357069	-0.774431
N	-1.262358	1.789165	-0.615125
C	-0.733450	2.999286	-0.280380
O	-0.955926	4.056360	-0.887813
N	0.165245	3.053324	0.820416
C	0.771643	4.372951	1.025587
O	-3.514914	-0.065223	-2.756296
C	-1.501313	2.074437	-3.098666
O	-0.581585	-2.421705	3.166340
C	1.625891	-0.443019	3.002303
C	-0.518568	0.326663	4.131041
C	1.736330	0.535686	-1.003983
C	2.694782	-0.206533	-1.879479
C	3.992438	-0.665325	-1.547049
H	2.194235	0.856566	-0.060065
H	2.070702	-0.774018	2.056405
H	1.731419	-1.253343	3.730833
H	2.149318	0.447573	3.355344
H	-0.001374	1.203401	4.521614
H	-0.468335	-0.496958	4.849734
H	-1.572923	0.580050	3.968264
H	-1.702636	-4.023706	1.887957
H	-3.162117	-5.527858	0.523622
H	1.647178	4.249227	1.658805
H	-0.618484	1.441380	-3.247158
H	-2.194299	1.895334	-3.926955
H	-1.192476	3.121183	-3.087862
H	-3.167799	3.653990	-1.549979
H	-4.169618	2.394395	-2.341334
H	-3.909754	2.357856	-0.583511
H	-3.797969	-2.344376	-2.325969
H	-4.203518	-4.692875	-1.570138
H	0.075244	5.063863	1.516868
H	1.036179	4.793301	0.055753

H	2.303235	-0.482049	-2.856956
H	1.384518	1.443461	-1.519614
C	4.755138	-1.377160	-2.521088
C	6.039917	-1.821882	-2.251905
C	6.624089	-1.584089	-0.999355
C	5.894723	-0.894229	-0.021091
C	4.609134	-0.441046	-0.280590
H	4.305593	-1.567483	-3.492851
H	6.594702	-2.361269	-3.016189
H	7.630278	-1.935877	-0.787374
H	6.336398	-0.713404	0.955839
H	4.060763	0.081347	0.496146

Doublet intermediate, styrene alpha attack, gas

C	2.369108	-2.401960	-1.928649
C	2.822853	-1.141729	-1.521682
C	4.201529	-0.927176	-1.391973
C	5.110620	-1.949127	-1.666262
C	4.651376	-3.204048	-2.074841
C	3.278843	-3.425901	-2.202708
C	1.852999	0.006675	-1.265101
O	0.566881	-0.542957	-0.940331
Fe	-0.589379	0.153541	0.196826
N	-1.113103	-1.228220	1.321899
C	-2.069948	-2.167178	1.051044
N	-2.905560	-1.966874	-0.072053
C	-3.842873	-3.068970	-0.310932
N	-0.444780	1.963116	-0.259012
C	-1.282599	2.425097	-1.237044
O	-1.222491	3.532090	-1.774229
C	0.541913	2.684918	0.417730
C	0.990459	3.986816	0.152391
C	1.981503	4.541880	0.965728
C	2.525719	3.814827	2.029709
C	2.092596	2.515537	2.305654
C	1.097367	1.943936	1.500550
N	0.520737	0.676728	1.617931
C	0.680421	-0.209565	2.645447
O	1.447743	-0.082379	3.600526
C	-2.377007	1.399475	-1.611564
C	-3.729628	2.100867	-1.351038
N	-2.193612	0.201238	-0.756160
C	-3.094721	-0.815062	-0.880678
O	-4.052720	-0.803684	-1.666543
C	-2.208237	1.064683	-3.109554
C	-0.245145	-1.441055	2.507592
C	0.661092	-2.680098	2.332713
C	-1.056423	-1.528104	3.818710
O	-2.243862	-3.197728	1.715302
C	1.712491	0.884521	-2.462916
H	1.573482	0.427148	-3.438545
H	-1.255615	0.548101	-3.270260
H	-2.205322	1.994068	-3.688482
H	-3.024125	0.419884	-3.440187
H	-4.551781	1.469145	-1.687208
H	-3.741943	3.056607	-1.883585
H	-3.850268	2.300060	-0.279360
H	0.549484	4.536983	-0.668356
H	2.329770	5.552604	0.764784
H	-4.288887	-2.920597	-1.290924
H	1.214393	-2.613607	1.389202
H	1.380315	-2.718678	3.157517
H	0.053269	-3.586570	2.324874
H	-1.653494	-2.439732	3.834633
H	-0.362743	-1.511405	4.664484
H	-1.726038	-0.663727	3.904735
H	2.493699	1.940927	3.130085
H	3.296246	4.261972	2.653952
H	-4.633341	-3.089097	0.448813
H	-3.303589	-4.015682	-0.258034
H	1.497117	1.942155	-2.353534
H	2.227724	0.593600	-0.418540
H	4.561550	0.048391	-1.071790
H	6.177248	-1.767753	-1.554584
H	5.358023	-4.003604	-2.284904
H	2.911970	-4.401842	-2.512405
H	1.300677	-2.571613	-2.009816

Quartet intermediate, styrene alpha attack, gas

C	2.501150	-2.283897	-1.958927
C	2.818976	-0.965123	-1.611639
C	4.167278	-0.596058	-1.515706
C	5.179529	-1.523307	-1.764905
C	4.855660	-2.836627	-2.114860
C	3.513962	-3.212557	-2.208421
C	1.726717	0.080783	-1.387658
O	0.534060	-0.578727	-0.977030
Fe	-0.608534	0.135939	0.211425
N	-1.025891	-1.334827	1.282948
C	-1.924116	-2.312386	0.972971
N	-2.784177	-2.095416	-0.135394
C	-3.663453	-3.225281	-0.450183
N	-0.562038	1.974718	-0.157122
C	-1.466956	2.452573	-1.069124
O	-1.479053	3.587066	-1.546466
C	0.447180	2.689497	0.488302
C	0.864438	4.006683	0.242995
C	1.892110	4.546873	1.017288

C	2.506763	3.791468	2.024057
C	2.108010	2.478895	2.280094
C	1.072979	1.919820	1.514705
N	0.520719	0.643074	1.621812
C	0.767017	-0.292355	2.591899
O	1.566867	-0.175072	3.519721
C	-2.541715	1.402816	-1.436632
C	-3.901356	2.018221	-1.031729
N	-2.254288	0.164269	-0.675535
C	-3.094152	-0.898468	-0.831797
O	-4.100585	-0.895380	-1.555082
C	-2.473366	1.179946	-2.962950
C	-0.107883	-1.557658	2.425846
C	0.846672	-2.746681	2.177747
C	-0.877817	-1.734564	3.753708
O	-2.034494	-3.382282	1.588070
C	1.478681	0.859078	-2.644225
H	1.267911	0.320607	-3.563643
H	-1.515383	0.721634	-3.232593
H	-2.552892	2.146374	-3.471404
H	-3.283736	0.521321	-3.278791
H	-4.713777	1.359660	-1.340052
H	-4.006081	2.999252	-1.505510
H	-3.945244	2.151557	0.055810
H	0.370581	4.577697	-0.532235
H	2.216472	5.568627	0.832844
H	-3.951723	-3.155926	-1.497451
H	1.369694	-2.616784	1.223936
H	1.588952	-2.787888	2.981695
H	0.277630	-3.677366	2.146784
H	-1.443639	-2.666227	3.736733
H	-0.162253	-1.737605	4.581483
H	-1.573170	-0.899199	3.899748
H	2.562918	1.883303	3.060534
H	3.305747	4.229829	2.617929
H	-4.574352	-3.211164	0.161904
H	-3.125031	-4.148471	-0.243959
H	1.307319	1.930411	-2.617513
H	2.073426	0.766361	-0.603559
H	4.422441	0.425174	-1.240267
H	6.221189	-1.222244	-1.678777
H	5.642970	-3.562477	-2.304795
H	3.252650	-4.235285	-2.470709
H	1.456751	-2.573316	-2.011020

Doublet TS2, styrene beta attack, gas

C	0.517189	2.657178	0.727032
C	0.465165	2.691786	-0.699321
C	1.087369	3.733270	-1.399216
C	1.758329	4.729993	-0.685205
C	1.809801	4.696599	0.712015
C	1.192199	3.666614	1.426541
N	-0.263924	1.620865	-1.232343
C	-0.640463	1.427135	-2.531311
C	-1.550431	0.179751	-2.709499
C	-0.852294	-0.761256	-3.714050
N	-0.172502	1.563823	1.259754
C	-0.476603	1.323664	2.566429
C	-1.435542	0.111903	2.740270
C	-2.743240	0.687305	3.332061
Fe	-0.715566	0.288545	-0.009051
O	0.907479	-0.795517	-0.087401
C	2.019022	-2.120857	0.691730
C	0.828171	-2.204379	-0.167127
C	3.386964	-2.090100	0.251921
C	3.761448	-2.227380	-1.106066
C	5.101010	-2.234431	-1.474161
C	6.104788	-2.108884	-0.505984
C	5.753608	-1.964954	0.840341
C	4.414912	-1.949151	1.214106
N	-1.662775	-0.503294	1.407602
C	-2.527148	-1.546291	1.309125
O	-3.113034	-2.080013	2.263732
N	-1.732440	-0.460263	-1.382374
C	-2.554676	-1.540797	-1.281899
O	-3.131956	-2.082382	-2.236475
N	-2.736050	-2.115141	0.011595
C	-3.563295	-3.326296	0.017402
O	-0.343028	2.137111	-3.494080
O	-0.101545	1.978497	3.542978
C	-2.887895	0.695632	-3.285384
C	-0.785711	-0.870805	3.734792
H	0.965722	-2.594901	-1.181294
H	0.099779	-1.116116	-3.299871
H	-0.639210	-0.212901	-4.637340
H	-1.490323	-1.621088	-3.926371
H	-3.545416	-0.142860	-3.519221
H	-2.688941	1.283886	-4.186550
H	-3.385317	1.341925	-2.552226
H	1.027032	3.746337	-2.479804
H	2.243664	5.538843	-1.227562
H	-3.350457	-3.894481	-0.886517
H	0.132209	-1.293194	3.306381
H	-0.517661	-0.334720	4.650576
H	-1.476068	-1.685600	3.958984
H	-3.453486	-0.118787	3.521743
H	-2.516937	1.218517	4.261985
H	-3.192080	1.398425	2.628268
H	1.211779	3.628901	2.508140
H	2.335212	5.480147	1.254379
H	-4.634765	-3.089038	0.030794
H	-3.330085	-3.899665	0.912961

H	1.828515	-2.001231	1.753028
H	-0.066712	-2.630541	0.293937
H	4.142988	-1.828457	2.259755
H	6.526407	-1.856714	1.596962
H	7.150920	-2.114477	-0.800489
H	5.368063	-2.332768	-2.523130
H	2.994334	-2.306607	-1.869118

Quartet TS2, styrene beta attack, gas

C	-4.180860	-1.330129	-0.405367
C	-3.658150	-0.832050	-1.626423
C	-4.546034	-0.157222	-2.502921
C	-5.889169	-0.004456	-2.185483
C	-6.385821	-0.507800	-0.977427
C	-5.523084	-1.165468	-0.091039
C	-2.296668	-1.011973	-2.018746
C	-1.211007	-1.595232	-1.198246
O	-0.911379	-0.307298	-0.727346
Fe	0.771488	0.100868	0.174928
N	2.028993	-0.738493	-0.932357
C	2.379799	-2.051536	-0.892828
N	1.809964	-2.867684	0.129436
C	2.167537	-4.284849	0.008050
N	0.165981	1.261832	1.517946
C	-0.221045	0.699110	2.698896
O	-0.745042	1.280915	3.651597
C	0.132327	2.613808	1.157216
C	-0.434425	3.675279	1.874630
C	-0.350674	4.970650	1.356723
C	0.291114	5.214181	0.138198
C	0.863686	4.167549	-0.589846
C	0.786757	2.862212	-0.087034
N	1.307312	1.694799	-0.658122
C	2.118245	1.585609	-1.750765
O	2.472129	2.502478	-2.495629
C	0.089482	-0.823061	2.766475
C	1.015256	-1.025925	3.985964
N	0.749490	-1.225960	1.499066
C	1.164985	-2.512125	1.353716
O	0.998150	-3.403751	2.200556
C	-1.254087	-1.553471	2.975276
C	2.613902	0.130638	-1.983396
C	2.161458	-0.292593	-3.396952
C	4.155791	0.179177	-1.899296
O	3.133251	-2.609107	-1.705561
H	-1.527218	-2.291898	-0.412084
H	-1.904220	-1.389755	2.107104
H	-1.755809	-1.147060	3.859342
H	-1.081534	-2.624236	3.098729
H	1.197561	-2.088986	4.148348
H	0.546310	-0.581233	4.869145
H	1.975364	-0.524513	3.814471
H	-0.918488	3.467748	2.820239
H	-0.791199	5.795794	1.912704
H	1.515371	-4.853506	0.666469
H	1.065741	-0.319267	-3.449727
H	2.520925	0.437900	-4.128830
H	2.553687	-1.284072	-3.630939
H	4.576593	-0.797264	-2.142898
H	4.529315	0.938053	-2.593889
H	4.466524	0.455519	-0.884528
H	1.371765	4.336205	-1.530555
H	0.348473	6.228293	-0.252078
H	3.210576	-4.463063	0.297507
H	2.052729	-4.594844	-1.031269
H	-1.983825	-0.557291	-2.954491
H	-0.405665	-2.050175	-1.786552
H	-4.157440	0.242169	-3.436443
H	-6.551815	0.514877	-2.872955
H	-7.434996	-0.381319	-0.723766
H	-5.902370	-1.544606	0.854095
H	-3.519970	-1.825312	0.297752

Doublet TS2, styrene alpha attack, gas

C	-0.214257	2.741402	0.474398
C	-0.993590	2.014557	1.425957
C	-2.002472	2.665204	2.148825
C	-2.233636	4.026241	1.926893
C	-1.473612	4.737317	0.993183
C	-0.464277	4.105435	0.261523
N	-0.608106	0.670577	1.513882
C	-0.980015	-0.234137	2.468023
C	-0.183377	-1.560147	2.366985
C	0.506537	-1.756762	3.735160
N	0.757772	1.946650	-0.134403
C	1.719193	2.328893	-1.019026
C	2.721785	1.187320	-1.335392
C	4.099052	1.684458	-0.837187
Fe	0.607179	0.091870	0.208858
N	0.798918	-1.423545	1.261932
C	1.671013	-2.454692	1.041158
O	1.666388	-3.522224	1.670246
O	-0.502205	-0.256160	-1.229763
C	-1.278884	0.997713	-2.624066
C	-1.800497	0.303062	-1.432861
C	-2.870069	-0.741643	-1.665223
C	-4.219014	-0.406669	-1.494423
C	-5.220042	-1.344000	-1.751545
C	-4.880991	-2.631266	-2.175557
C	-3.536822	-2.973730	-2.337367
C	-2.535170	-2.034141	-2.085291
N	2.280084	-0.033579	-0.613821

C	3.056634	-1.147512	-0.698581
O	4.097480	-1.228485	-1.367818
N	2.628736	-2.309027	0.009410
C	3.445231	-3.508166	-0.203531
O	-1.831296	-0.062697	3.342622
O	1.840024	3.447833	-1.529113
C	-1.197474	-2.692079	2.095229
C	2.739771	0.982511	-2.864848
H	-0.768055	1.947250	-2.513435
H	-2.089402	0.986831	-0.630953
H	-1.666772	-2.552709	1.114431
H	-1.979899	-2.665607	2.860732
H	-0.690133	-3.658250	2.111037
H	1.010598	-2.722986	3.768221
H	-0.247229	-1.694031	4.525742
H	1.246834	-0.964436	3.899849
H	-2.572704	2.099574	2.874290
H	-3.015113	4.531956	2.490026
H	2.793675	-4.382284	-0.242548
H	1.772746	0.592693	-3.202316
H	2.919106	1.945152	-3.354617
H	3.520784	0.270608	-3.136609
H	4.875028	0.963350	-1.096234
H	4.316356	2.654615	-1.294973
H	4.081114	1.811533	0.251943
H	0.141416	4.640441	-0.458618
H	-1.665239	5.795904	0.830544
H	4.158281	-3.657216	0.616461
H	3.992130	-3.378728	-1.133969
H	-1.175885	0.446990	-3.552577
H	-4.484150	0.592111	-1.153915
H	-6.263553	-1.072509	-1.610808
H	-5.659617	-3.365240	-2.369064
H	-3.265093	-3.977608	-2.654714
H	-1.486947	-2.294697	-2.191214

Quartet TS2, styrene alpha attack, gas

C	-3.143514	-0.505880	-0.383934
C	-2.557802	-1.663589	0.211654
C	-3.270077	-2.869794	0.253643
C	-4.552454	-2.921918	-0.297839
C	-5.126383	-1.788190	-0.884521
C	-4.433077	-0.576860	-0.930899
N	-1.280439	-1.406963	0.721815
C	-0.553315	-2.192990	1.574464
C	0.690530	-1.457698	2.134795
C	0.426316	-1.290003	3.651293
N	-2.301987	0.605880	-0.319757
C	-2.586807	1.892076	-0.686450
C	-1.398680	2.855152	-0.431858
C	-1.929917	3.987062	0.473345
Fe	-0.529671	0.230923	0.188574
N	0.792173	-0.138835	1.460304
C	1.792312	0.708397	1.834476
O	2.669215	0.435896	2.665591
O	0.225722	-0.149887	-1.489362
C	0.354412	-1.371517	-3.252463
C	0.898459	-1.335019	-1.866221
C	2.415833	-1.245774	-1.820971
C	3.182981	-2.406467	-1.989069
C	4.576465	-2.342088	-2.000169
C	5.219830	-1.111971	-1.839493
C	4.460003	0.046517	-1.667905
C	3.064572	-0.018032	-1.661515
N	-0.312022	2.088009	0.223721
C	0.830546	2.740294	0.574809
O	1.041689	3.945642	0.377861
N	1.858591	1.980007	1.200343
C	3.077232	2.734247	1.507666
O	-0.837973	-3.338016	1.928674
O	-3.648729	2.295152	-1.163584
C	1.925878	-2.351269	1.904813
C	-0.961708	3.406671	-1.807920
H	-0.656565	-1.731512	-3.416583
H	0.554035	-2.197500	-1.280129
H	2.151490	-2.434531	0.836458
H	1.717196	-3.352738	2.294562
H	2.794648	-1.924072	2.407068
H	1.290767	-0.825687	4.128137
H	0.233918	-2.272419	4.094163
H	-0.453612	-0.656546	3.814562
H	-2.814830	-3.731822	0.723777
H	-5.107703	-3.856976	-0.267358
H	3.917995	2.041716	1.530335
H	-0.561896	2.594380	-2.425603
H	-1.828480	3.840458	-2.317459
H	-0.187753	4.164743	-1.675152
H	-1.161797	4.748625	0.612260
H	-2.820849	4.424573	0.012246
H	-2.210732	3.583741	1.453739
H	-4.864904	0.313135	-1.369724
H	-6.126111	-1.845651	-1.309842
H	3.014626	3.229808	2.484634
H	3.209265	3.495065	0.740793
H	0.810742	-0.747936	-4.014846
H	2.683711	-3.366558	-2.108121
H	5.159476	-3.251679	-2.125260
H	6.306022	-1.059621	-1.839098
H	4.952878	1.005848	-1.530661
H	2.466464	0.874039	-1.512626

Styrene epoxide, gas

C	1.184540	-0.082999	2.338627
C	1.076684	1.291016	2.092585
C	1.930154	2.174891	2.764627
C	2.884438	1.688336	3.657145
C	2.996444	0.315354	3.889411
C	2.142436	-0.569490	3.228664
C	0.068673	1.792177	1.112942
C	0.434234	2.671285	-0.017291
O	-0.237848	3.193841	1.131080
H	3.739679	-0.061906	4.586680
H	1.474366	2.977298	-0.131255
H	-0.804267	1.150183	0.977956
H	-0.153739	2.649322	-0.935833
H	0.515775	-0.774883	1.830705
H	2.217072	-1.638457	3.410129
H	3.538258	2.383053	4.178031
H	1.820836	3.241874	2.595247

Styrene, acetonitrile (ε = 37.5)

C	0.041801	0.000000	0.043787
H	0.080954	0.000000	1.129607
C	1.220784	0.000000	-0.703941
C	1.163826	0.000000	-2.098209
C	-0.067754	0.000000	-2.777668
C	-1.247345	0.000000	-2.007863
C	-1.192316	0.000000	-0.616294
H	2.185366	0.000000	-0.203334
H	2.086124	0.000000	-2.674863
C	-0.065426	0.000000	-4.251064
H	-2.215581	0.000000	-2.500415
H	-2.115343	0.000000	-0.042501
C	-1.125614	0.000000	-5.070686
H	0.928366	0.000000	-4.699418
H	-0.994560	0.000000	-6.148649
H	-2.151714	0.000000	-4.711988

Styrene cation, acetonitrile

C	0.000000	0.000000	0.000000
H	0.000000	0.000000	1.008000
C	1.212436	0.000000	-0.700000
C	1.212436	0.000000	-2.100000
C	0.000000	0.000000	-2.800000
C	-1.212436	0.000000	-2.100000
C	-1.212436	0.000000	-0.700000
H	2.155537	0.000000	-0.155500
H	2.155537	0.000000	-2.644500
C	0.000000	0.000000	-4.250000
H	-2.155537	0.000000	-2.644500
H	-2.155537	0.000000	-0.155500
C	-1.156144	0.000000	-4.917500
H	0.943102	0.000000	-4.794500
H	-1.156144	0.000000	-6.006500
H	-2.099246	0.000000	-4.373000

$Fe^{V}O$ doublet, acetonitrile

C	1.886729	-2.118852	1.503752
C	2.553065	-2.234338	0.273825
C	3.250194	-3.428164	-0.049158
C	3.282927	-4.495124	0.860269
C	2.626975	-4.361551	2.084562
C	1.936852	-3.185298	2.402600
N	2.607939	-1.293558	-0.765160
C	1.946484	-0.088174	-0.807665
C	2.174616	0.681656	-2.113513
N	2.996469	-0.180963	-2.985535
C	3.280436	0.255603	-4.233515
O	2.933188	1.351607	-4.699960
N	3.794284	-3.373845	-1.329771
C	4.193672	-4.425897	-2.089443
C	4.479645	-4.010827	-3.543765
C	3.636473	-4.938704	-4.443293
Fe	3.822353	-1.648899	-2.116430
N	4.077416	-2.581434	-3.684670
C	4.269112	-1.987775	-4.913601
O	4.683268	-2.617388	-5.895640
O	5.219830	-1.070961	-1.625691
N	4.033662	-0.614810	-5.065195
C	4.396233	-0.082518	-6.386370
O	1.249704	0.356698	0.102520
O	4.306420	-5.595139	-1.711488
C	0.777530	0.960573	-2.712301
C	2.896447	1.998547	-1.747257
C	5.992998	-4.209706	-3.781807
H	3.880954	1.787007	-1.315022
H	2.304821	2.550420	-1.010349
H	3.026554	2.608511	-2.642077
H	0.865522	1.589146	-3.597993
H	0.158813	1.462747	-1.963003
H	0.288760	0.020021	-2.991968
H	1.353478	-1.209173	1.739748
H	1.435159	-3.093726	3.361948
H	4.407883	1.001838	-6.319568
H	6.572195	-3.526629	-3.149858
H	6.262817	-5.236736	-3.516801
H	6.244145	-4.025363	-4.826506
H	3.878844	-4.779875	-5.493244

H	3.842785	-5.976596	-4.167217
H	2.567783	-4.747779	-4.291404
H	3.809446	-5.402084	0.595771
H	2.656971	-5.181271	2.797196
H	3.674331	-0.387829	-7.152157
H	5.378500	-0.461889	-6.666465
H	3.760487	-5.400430	0.567690
H	2.842016	-5.114864	2.867575
H	3.942031	-0.059780	-7.053483
H	5.593635	-0.436779	-6.521788

$Fe^{V}O$ quartet, acetonitrile

C	2.074014	-2.032742	1.620141
C	2.596412	-2.191416	0.330586
C	3.210126	-3.413739	-0.046263
C	3.297858	-4.470283	0.868624
C	2.773359	-4.299315	2.152872
C	2.168385	-3.094381	2.524366
N	2.595679	-1.255373	-0.715789
C	1.856971	-0.110270	-0.806414
C	2.046672	0.637537	-2.145473
N	2.872556	-0.223369	-3.027651
C	3.290489	0.236629	-4.241209
O	2.934893	1.317998	-4.726267
N	3.667056	-3.388897	-1.373581
C	4.036838	-4.453155	-2.145494
C	4.405130	-4.061286	-3.594302
C	3.567120	-4.938738	-4.544600
Fe	3.714056	-1.674441	-2.196550
N	4.077707	-2.624652	-3.768086
C	4.403171	-1.980652	-4.924920
O	4.874859	-2.547960	-5.918296
O	5.183389	-1.052456	-1.822061
N	4.173452	-0.580413	-4.997099
C	4.662244	0.046663	-6.234377
O	1.097246	0.315017	0.065298
O	4.078204	-5.624602	-1.766148
C	0.649915	0.873386	-2.752600
C	2.748388	1.974014	-1.814780
C	5.916364	-4.337580	-3.760954
H	3.744358	1.790127	-1.396577
H	2.155438	2.517224	-1.072774
H	2.848879	2.580654	-2.715142
H	0.731480	1.475779	-3.658298
H	0.024221	1.391734	-2.020382
H	0.174772	-0.081981	-3.001871
H	1.601006	-1.099367	1.893711
H	1.767691	-2.975107	3.527287
H	4.822745	1.105960	-6.044601
H	6.498850	-3.697652	-3.088741
H	6.120610	-5.382515	-3.508697
H	6.224421	-4.144525	-4.788865
H	3.858977	-4.755414	-5.579502
H	3.730075	-5.991495	-4.296694
H	2.500439	-4.715591	-4.430494

Dianionic $Fe^{IV}O$ singlet, acetonitrile

C	1.892669	-2.117027	1.502107
C	2.560410	-2.234116	0.276189
C	3.256768	-3.425592	-0.046156
C	3.278856	-4.497587	0.854681
C	2.615384	-4.366294	2.075519
C	1.932715	-3.188919	2.396177
N	2.617913	-1.292953	-0.766931
C	1.949460	-0.090027	-0.803217
C	2.180421	0.677813	-2.111917
N	3.014221	-0.180818	-2.976558
C	3.287582	0.260825	-4.227355
O	2.930341	1.349880	-4.695609
N	3.815893	-3.362651	-1.321749
C	4.205033	-4.422011	-2.080405
C	4.486263	-4.001806	-3.536136
C	3.621526	-4.911856	-4.431922
Fe	3.854985	-1.635343	-2.100236
N	4.101841	-2.566775	-3.669792
C	4.285948	-1.983938	-4.906793
O	4.693102	-2.613608	-5.889518
O	5.243268	-1.048306	-1.619978
N	4.041181	-0.611585	-5.060174
C	4.389315	-0.085006	-6.383047
O	1.242029	0.350964	0.098322
O	4.309443	-5.591636	-1.710663
C	0.784602	0.939262	-2.719355
C	2.885636	2.004654	-1.753185
C	5.991983	-4.226641	-3.791709
H	3.878210	1.804622	-1.334818
H	2.293256	2.542425	-1.005777
H	2.997892	2.613490	-2.651670
H	0.873002	1.559928	-3.610914
H	0.157549	1.435068	-1.972194
H	0.310072	-0.010202	-2.994221
H	1.362416	-1.203638	1.731890
H	1.425118	-3.098779	3.353870
H	4.371900	1.000245	-6.322198
H	6.587590	-3.556461	-3.161031
H	6.242217	-5.258957	-3.526726
H	6.233606	-4.040002	-4.838513
H	3.857093	-4.749003	-5.483268
H	3.809697	-5.953255	-4.154728
H	2.558492	-4.699651	-4.268001

H	3.800808	-5.404584	0.580447
H	2.635804	-5.191841	2.783550
H	3.673948	-0.415322	-7.145488
H	5.377225	-0.451482	-6.663473

Dianionic $Fe^{IV}O$ triplet, acetonitrile

C	1.892669	-2.117027	1.502107
C	2.560410	-2.234116	0.276189
C	3.256768	-3.425592	-0.046156
C	3.278856	-4.497587	0.854681
C	2.615384	-4.366294	2.075519
C	1.932715	-3.188919	2.396177
N	2.617913	-1.292953	-0.766931
C	1.949460	-0.090027	-0.803217
C	2.180421	0.677813	-2.111917
N	3.014221	-0.180818	-2.976558
C	3.287582	0.260825	-4.227355
O	2.930341	1.349880	-4.695609
N	3.815893	-3.362651	-1.321749
C	4.205033	-4.422011	-2.080405
C	4.486263	-4.001806	-3.536136
C	3.621526	-4.911856	-4.431922
Fe	3.854985	-1.635343	-2.100236
N	4.101841	-2.566775	-3.669792
C	4.285948	-1.983938	-4.906793
O	4.693102	-2.613608	-5.889518
O	5.243268	-1.048306	-1.619978
N	4.041181	-0.611585	-5.060174
C	4.389315	-0.085006	-6.383047
O	1.242029	0.350964	0.098322
O	4.309443	-5.591636	-1.710663
C	0.784602	0.939262	-2.719355
C	2.885636	2.004654	-1.753185
C	5.991983	-4.226641	-3.791709
H	3.878210	1.804622	-1.334818
H	2.293256	2.542425	-1.005777
H	2.997892	2.613490	-2.651670
H	0.873002	1.559928	-3.610914
H	0.157549	1.435068	-1.972194
H	0.310072	-0.010202	-2.994221
H	1.362416	-1.203638	1.731890
H	1.425118	-3.098779	3.353870
H	4.371900	1.000245	-6.322198
H	6.587590	-3.556461	-3.161031
H	6.242217	-5.258957	-3.526726
H	6.233606	-4.040002	-4.838513
H	3.857093	-4.749003	-5.483268
H	3.809697	-5.953255	-4.154728
H	2.558492	-4.699651	-4.268001
H	3.800808	-5.404584	0.580447
H	2.635804	-5.191841	2.783550
H	3.673948	-0.415322	-7.145488
H	5.377225	-0.451482	-6.663473

Doublet TS1, styrene beta attack, acetonitrile

C	-3.770453	3.947989	-0.909045
C	-3.635608	2.589492	-1.208162
C	-2.653711	1.837658	-0.547972
C	-1.811897	2.456429	0.417806
C	-1.963505	3.818763	0.711192
C	-2.943236	4.556255	0.040843
N	-2.376181	0.471712	-0.689351
C	-3.115663	-0.454683	-1.360193
C	-2.585045	-1.891139	-1.170455
N	-1.397642	-1.822866	-0.283239
C	-0.780780	-2.982156	0.064668
O	-1.140362	-4.110022	-0.311025
N	-0.910085	1.548727	0.987332
C	-0.131291	1.741682	2.087298
C	0.636408	0.468635	2.502723
C	0.200162	0.146447	3.949711
Fe	-0.754429	-0.093895	0.078021
O	0.351686	0.222325	-1.111096
N	0.246189	-0.620073	1.571004
C	0.781529	-1.856399	1.755791
O	1.620269	-2.131107	2.630063
N	0.370875	-2.901859	0.890567
C	1.066673	-4.179554	1.096901
O	-0.033895	2.791487	2.731180
C	2.142709	0.802344	2.447389
O	-4.124251	-0.224593	-2.035080
C	-2.243002	-2.451021	-2.567975
C	-3.737998	-2.692018	-0.522870
C	1.869438	-1.181659	-1.835156
C	2.962057	-0.886037	-1.069112
C	3.982347	0.110447	-1.354261
H	1.723935	-0.756269	-2.821166
H	-1.425174	-1.880042	-3.022271
H	-3.120657	-2.369574	-3.216652
H	-1.943000	-3.496896	-2.490442
H	-3.466700	-3.744049	-0.435849
H	-4.635867	-2.590998	-1.139613
H	-3.958800	-2.298639	0.476623
H	-4.273802	2.106354	-1.935614
H	-4.526513	4.533978	-1.424988
H	1.009787	-4.758563	0.177574
H	2.452929	1.025615	1.421154
H	2.337820	1.684170	3.065527
H	2.728366	-0.039936	2.816900
H	0.766412	-0.702518	4.333764
H	0.373546	1.021626	4.582652
H	-0.868493	-0.096901	3.979402

H	-1.323369	4.275484	1.453869
H	-3.057705	5.614128	0.262287
H	0.612648	-4.763754	1.906343
H	2.102528	-3.972742	1.357306
H	3.085417	-1.426295	-0.132378
H	1.235840	-2.018218	-1.574234
C	5.064732	0.250096	-0.457512
C	6.073709	1.181825	-0.687465
C	6.023424	2.001346	-1.819081
C	4.955847	1.880239	-2.718242
C	3.948677	0.948359	-2.492501
H	5.105396	-0.385865	0.423083
H	6.898038	1.270576	0.014359
H	6.808384	2.729805	-2.001010
H	4.912456	2.516485	-3.597691
H	3.128921	0.870072	-3.199907

***para*-chloro Styrene, gas**

C	0.035595	0.000000	0.031385
Cl	0.094443	0.000000	1.788528
C	1.222117	0.000000	-0.698134
C	1.159352	0.000000	-2.090072
C	-0.067501	0.000000	-2.774793
C	-1.245178	0.000000	-2.005143
C	-1.202104	0.000000	-0.615280
H	2.178142	0.000000	-0.185490
H	2.085545	0.000000	-2.659796
C	-0.063649	0.000000	-4.246054
H	-2.214005	0.000000	-2.495537
H	-2.117969	0.000000	-0.033724
C	-1.122663	0.000000	-5.065148
H	0.930338	0.000000	-4.693342
H	-0.992583	0.000000	-6.142813
H	-2.148311	0.000000	-4.706087

Doublet TS1, *para*-chloro styrene beta attack, gas

C	3.698333	0.406493	-0.527662
C	3.372536	0.220056	-1.891125
C	4.343614	-0.389709	-2.716341
C	5.583025	-0.783649	-2.223696
C	5.869377	-0.574196	-0.874499
C	4.931951	0.013750	-0.022115
C	2.116371	0.641189	-2.482441
C	1.082253	1.299973	-1.858522
O	-0.242897	-0.147162	-1.290551
Fe	-1.212896	0.042064	0.053622
N	-1.556156	1.879242	0.205184
C	-0.747436	2.794665	0.805948
N	0.446451	2.335543	1.426450
C	1.307447	3.422109	1.908641
N	-1.599554	-1.719826	0.555963
C	-0.770773	-2.320667	1.464218
O	-0.834354	-3.493752	1.830939
C	-2.703697	-2.293458	-0.077162
C	-3.100705	-3.638530	-0.062528
C	-4.258808	-4.009932	-0.746916
C	-5.024720	-3.058774	-1.431786
C	-4.649537	-1.714759	-1.447622
C	-3.483658	-1.326137	-0.771942
N	-2.961632	-0.040493	-0.633741
C	-3.570555	1.134592	-0.971191
O	-4.637666	1.253776	-1.574128
C	0.304681	-1.357877	2.011064
C	0.217927	-1.409075	3.550883
N	-0.002447	-0.001023	1.497498
C	0.799304	1.027043	1.868156
O	1.827370	0.905977	2.557033
C	1.666487	-1.896020	1.519432
C	-2.791022	2.364702	-0.458271
C	-2.492729	3.273508	-1.668118
C	-3.734502	3.076079	0.539813
O	-0.952791	4.016756	0.810334
H	1.194730	1.707082	-0.861636
H	1.728002	-1.829719	0.427970
H	1.761720	-2.947358	1.810361
H	2.478994	-1.315318	1.957644
H	1.026196	-0.825049	3.993240
H	0.282886	-2.451580	3.876573
H	-0.741700	-0.999982	3.888290
H	-2.502641	-4.357212	0.481381
H	-4.564923	-5.053813	-0.746477
H	2.262651	2.989145	2.194036
H	-1.837019	2.756619	-2.378609
H	-3.431059	3.506832	-2.181111
H	-2.007565	4.193232	-1.337073
H	-3.282114	4.004563	0.888834
H	-4.688188	3.281176	0.043677
H	-3.924867	2.426768	1.402551
H	-5.234245	-0.962959	-1.960805
H	-5.923909	-3.366502	-1.961168
H	0.862943	3.923664	2.776059
H	1.428153	4.165335	1.119102
H	1.985306	0.374722	-3.530532
H	0.293329	1.734888	-2.457585
H	4.115246	-0.552558	-3.766985
H	6.318057	-1.248590	-2.872538
Cl	7.437662	-1.065276	-0.237389
H	5.158072	0.155352	1.029278
H	2.982040	0.840195	0.161176
C	1.161501	0.000000	-2.090399
C	-0.066560	0.000000	-2.774646

C	-1.246096	0.000000	-2.006367
C	-1.204100	0.000000	-0.615515
H	2.180932	0.000000	-0.187062
H	2.088216	0.000000	-2.658463
C	-0.061763	0.000000	-4.247097
H	-2.215409	0.000000	-2.495316
H	-2.121722	0.000000	-0.036915
C	-1.123929	0.000000	-5.063537
H	0.931943	0.000000	-4.694371
H	-0.994670	0.000000	-6.141537
H	-2.148983	0.000000	-4.702240

Doublet TS1, 4-chloro styrene beta attack; CPCM

C	3.251530	1.623875	-0.780956
C	2.425869	2.449090	0.033412
C	2.671538	3.827417	0.112632
C	3.726559	4.375333	-0.621398
C	4.537517	3.564245	-1.422804
C	4.309978	2.188371	-1.507040
N	1.439676	1.711768	0.701207
C	0.627363	2.145431	1.706946
C	-0.260409	1.023578	2.284986
C	-1.728722	1.437629	2.047411
N	2.880588	0.276778	-0.708325
C	3.589798	-0.797507	-1.150395
C	2.956901	-2.140797	-0.728799
C	4.019690	-2.866046	0.128370
Fe	1.195907	-0.044383	0.076785
N	0.100163	-0.239200	1.595316
C	-0.536501	-1.381584	1.956569
O	-1.440729	-1.447005	2.806745
O	0.149507	0.150765	-1.196583
N	1.732479	-1.840096	0.057337
C	1.026028	-2.878856	0.579340
O	1.331333	-4.073438	0.434523
N	-0.156221	-2.588051	1.309118
C	-0.941145	-3.769232	1.694495
O	0.580885	3.296461	2.151275
O	4.644997	-0.757453	-1.791436
C	0.052676	0.947944	3.795991
C	2.653880	-2.937123	-2.015457
C	-1.175166	-1.427959	-1.830927
C	-2.181085	-0.749584	-2.469633
C	-3.431028	-0.292328	-1.892970
C	-3.801122	-0.529378	-0.548601
C	-5.017617	-0.081938	-0.049535
C	-5.889174	0.613855	-0.893911
C	-5.559683	0.868235	-2.226424
C	-4.338305	0.415259	-2.713069
Cl	-7.429026	1.178341	-0.262710
H	-1.284869	-1.808176	-0.823191
H	-1.950349	1.470125	0.975118
H	-1.895552	2.435514	2.465174
H	-2.402690	0.724726	2.523599
H	-0.600829	0.221742	4.280070
H	-0.093934	1.934011	4.246243
H	1.095207	0.647242	3.953920
H	2.043240	4.443102	0.741857
H	3.913455	5.444587	-0.567360
H	-1.970032	-3.460496	1.865518
H	1.922136	-2.405993	-2.634664
H	3.573936	-3.049099	-2.597337
H	2.257949	-3.921887	-1.764770
H	3.678152	-3.868052	0.387646
H	4.954471	-2.927939	-0.436462
H	4.209755	-2.306237	1.051755
H	4.935504	1.549597	-2.115957
H	5.353384	4.004670	-1.989884
H	-0.556619	-4.231263	2.611633
H	-0.888566	-4.499693	0.889771
H	-2.031240	-0.492209	-3.516741
H	-0.357011	-1.838598	-2.407841
H	-4.076203	0.609401	-3.749450
H	-6.245678	1.409587	-2.868649
H	-5.291187	-0.268607	0.983183
H	-3.133516	-1.064522	0.118312

4-methoxystyrene, CPCM, acetonitrile

C	0.113753	0.000000	-0.013898
O	0.086792	0.000000	1.349041
C	1.277203	0.000000	-0.791751
C	1.170945	0.000000	-2.184557
C	-0.069534	0.000000	-2.839838
C	-1.227139	0.000000	-2.032660
C	-1.141008	0.000000	-0.649590
H	2.258865	0.000000	-0.332556
H	2.082993	0.000000	-2.777134
C	-0.107204	0.000000	-4.310071
H	-2.210463	0.000000	-2.493949
H	-2.035729	0.000000	-0.034090
C	-1.188110	0.000000	-5.103578
H	0.874624	0.000000	-4.784441
H	-1.083871	0.000000	-6.184469
H	-2.204809	0.000000	-4.718769
C	1.329193	0.000000	2.049034
H	1.073751	0.000000	3.109586
H	1.918884	-0.894665	1.815929

H	1.918884	0.894665	1.815929

Doublet TS1, 4-methoxy styrene beta attack; CPCM, acetonitrile

C	3.832912	0.028200	-2.112451
C	3.571859	-0.840128	-1.022366
C	4.569925	-0.953892	-0.031574
C	5.768965	-0.252134	-0.104819
C	6.001467	0.601926	-1.194387
C	5.017950	0.733735	-2.197222
C	2.350040	-1.607503	-0.884433
C	1.295773	-1.639064	-1.750187
O	-0.026199	0.080897	-1.074585
Fe	-1.220654	0.000874	0.053342
N	-0.463346	-0.824997	1.554741
C	-0.264592	-2.163310	1.691391
N	-0.855092	-3.031404	0.738334
C	-0.497866	-4.448519	0.889051
N	-2.621847	0.984504	-0.729616
C	-3.526043	0.302159	-1.485189
O	-4.419389	0.805619	-2.174508
C	-2.565673	2.368603	-0.516514
C	-3.311476	3.368315	-1.156512
C	-3.126634	4.702787	-0.783830
C	-2.214368	5.044661	0.219548
C	-1.467546	4.058730	0.870571
C	-1.637428	2.716475	0.504264
N	-1.005020	1.590725	1.046911
C	-0.272880	1.531050	2.191575
O	0.045065	2.491820	2.901102
C	-3.348138	-1.228102	-1.390472
C	-4.697909	-1.796011	-0.898239
N	-2.250708	-1.496294	-0.429098
C	-1.933070	-2.786804	-0.151973
O	-2.510552	-3.774170	-0.637013
C	-3.018074	-1.742610	-2.809138
C	0.120542	0.087420	2.571647
C	1.662213	0.030905	2.627616
C	-0.484938	-0.176466	3.968905
O	0.415771	-2.679023	2.594139
H	1.318220	-1.137978	-2.710998
H	-2.063871	-1.328893	-3.154569
H	-3.802354	-1.427622	-3.504617
H	-2.950073	-2.831446	-2.805504
H	-4.674349	-2.885553	-0.901008
H	-5.497240	-1.440780	-1.555107
H	-4.907606	-1.448765	0.120499
H	-4.019852	3.091284	-1.925511
H	-3.699501	5.479110	-1.284277
H	-0.598212	-4.937921	-0.077776
H	2.094836	0.215125	1.638630
H	2.023348	0.806461	3.310312
H	1.991818	-0.947128	2.979269
H	-0.171941	-1.153733	4.337912
H	-0.150407	0.602403	4.660360
H	-1.579949	-0.149667	3.920148
H	-0.765540	4.308899	1.654588
H	-2.079151	6.086340	0.498693
H	-1.151225	-4.958649	1.607143
H	0.527468	-4.511818	1.246489
H	2.274206	-2.202233	0.024230
H	0.476067	-2.324566	-1.582142
H	4.398018	-1.612448	0.815812
H	6.506997	-0.372342	0.679110
O	7.125189	1.335771	-1.374112
H	5.215592	1.399480	-3.031551
H	3.094493	0.149712	-2.898798
C	8.164947	1.249535	-0.397440
H	8.954379	1.915422	-0.747145
H	7.812872	1.582264	0.585484
H	8.553232	0.227530	-0.322596

4-chlorostyrene; CPCM, acetonitrile

C	0.034999	0.000000	0.028120
Cl	0.093374	0.000000	1.791399
C	1.223834	0.000000	-0.697555

Appendix C

O_2 pressure	TON (after 20 h)
1 bar	8
5 bar	40
10 bar	34
20 bar	26

Appendix C1. The effect of O_2 pressure on styrene epoxide formation (TON) for reaction of styrene (40 mM) with complex **1**(0.25 mM) in dichloromethane at RT.

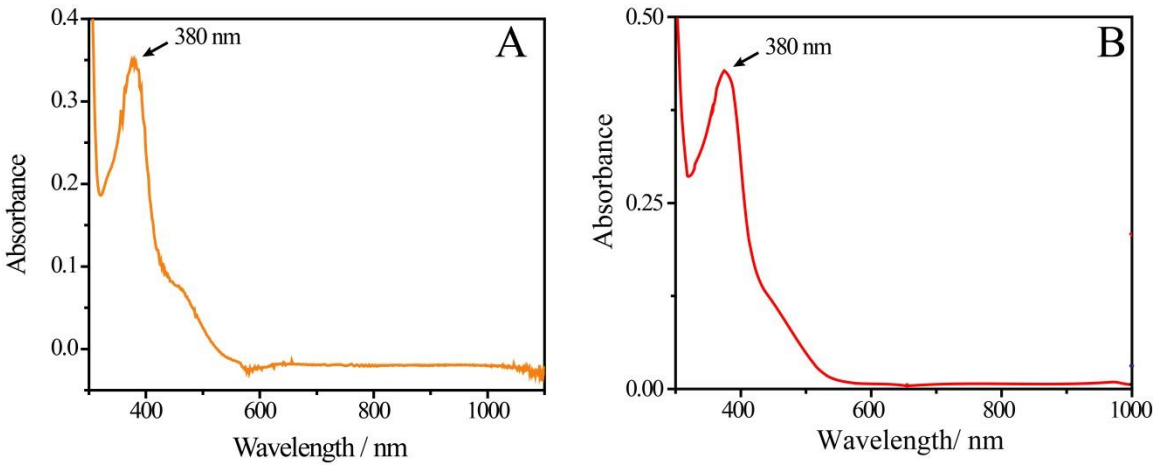

Appendix C2. (A) The UV-vis spectra of the acetonitrile solution of precipitate formed after reaction of complex **1** (1 mM) with styrene in DCB; the spectral features are identical to the solution of (bTAML)Fe^{III} complex in acetonitrile. (B) UV-vis spectra of (bTAML)Fe^{III} complex in acetonitrile.

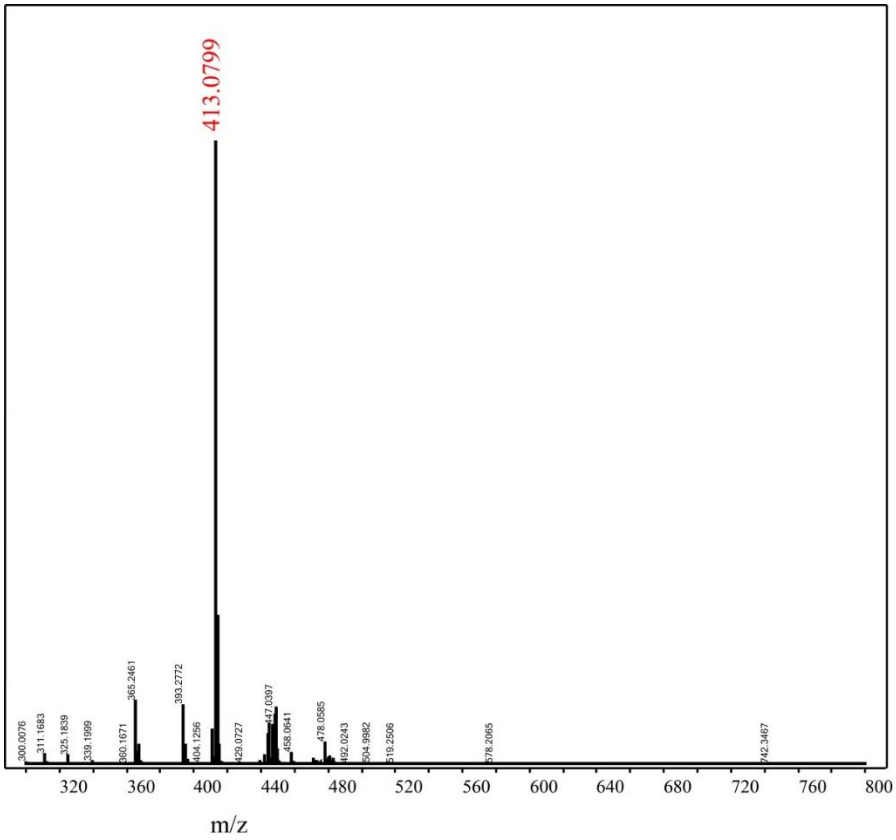

Appendix C3. HR-MS of acetonitrile solution of precipitate formed after reaction of complex **1** (1 mM) with styrene in DCB. Calculated m/z of $[(bTAML)Fe^{III}]^-$ is 413.0786.

Fe^{III}-OH_2	ΔE (gas) (B3LYP)	ΔE (DCM) (B3LYP)
S=3/2	0.0	0.0
S=1/2	22.9	22.2
(Fe^{III}-O_2)		
S=1/2	0.0	0.0
S=3/2	0.68	-1.1
S=5/2	8.3	10.4

Appendix C4. The gas phase relative reaction energies in kcal/mol at the B3LYP/6-31G*, LANL2DZ (Fe) level of theory for different spin state of catalyst $[(bTAML)Fe^{III}(OH_2)]^-$ and its O_2 adduct after substitution of H_2O with O_2, $[(bTAML)Fe^{III}(O_2)]^-$.

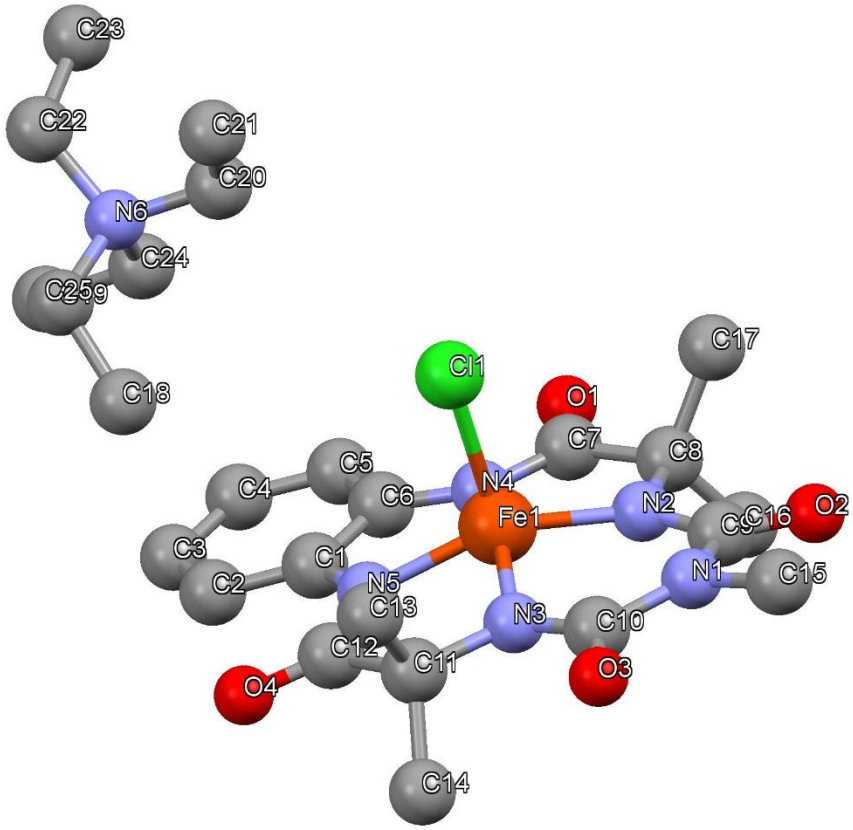

Table 1. Crystal data and structure refinement for C25 H29 Cl Fe N6 O4 at 296(2) K.

Empirical formula	C25 H29 Cl Fe N6 O4
Formula weight	568.84
Temperature	296(2) K
Wavelength	0.71073 Å
Crystal system	$P2_1/c$
Space group	Monoclinic
Unit cell dimensions	a = 8.8258(16) Å, α = 90° b = 26.470(5) Å, β = 100.399(4)° c = 13.291(3) Å, γ = 90°
Volume	3054.0(10) $Å^3$
Z	4
Density (calculated)	1.237 g/cm^3
Absorption coefficient	0.618 mm^{-1}
F(000)	1184
Crystal size	0.500 x 0.400 x 0.300 mm^3
θ range for data collection	1.539 to 27.309°
Index ranges	-11<=h<=10, -34<=k<=29, -17<=l<=17

Reflections collected	27643
Independent reflections	6812 [R_{int} = 0.0987]
Completeness to θ = 25.242°	100%
Refinement method	Full-matrix least-squares on F^2
Data / restraints / parameters	6812 / 0 / 344
Goodness-of-fit	1.278
Final R indices [I > 2σ(I)]	R_{obs} = 0.1162, wR_{obs} = 0.3451
R indices [all data]	R_{all} = 0.1813, wR_{all} = 0.3754
Extinction coefficient	0.013(3)
Largest diff. peak and hole	4.077 and -0.479 e·Å^{-3}

$R = \Sigma||F_o|-|F_c|| / \Sigma|F_o|$, $wR = \{\Sigma[w(|F_o|^2 - |F_c|^2)^2] / \Sigma[w(|F_o|^4)]\}^{1/2}$ and $w=1/[\sigma^2(Fo^2)+(0.2000P)^2]$ where $P=(Fo^2+2Fc^2)/3$

Table 2. Bond lengths [Å] for C25 H29 Cl Fe N6 O4 at 296(2) K with estimated standard deviations in parentheses.

Label	Distances
C(1)-N(5)	1.382(10)
C(1)-C(2)	1.393(11)
C(1)-C(6)	1.448(12)
C(2)-C(3)	1.387(12)
C(3)-C(4)	1.412(15)
C(4)-C(5)	1.359(14)
C(5)-C(6)	1.402(11)
C(6)-N(4)	1.393(11)
C(7)-O(1)	1.228(10)
C(7)-N(4)	1.378(10)
C(7)-C(8)	1.520(13)
C(8)-N(2)	1.490(10)
C(8)-C(16)	1.509(12)
C(8)-C(17)	1.539(13)
C(9)-O(2)	1.227(9)
C(9)-N(2)	1.360(11)
C(9)-N(1)	1.416(11)
C(10)-O(3)	1.241(9)
C(10)-N(3)	1.332(10)
C(10)-N(1)	1.421(11)
C(11)-N(3)	1.472(9)
C(11)-C(13)	1.532(11)
C(11)-C(12)	1.537(11)

C(11)-C(14)	1.563(10)
C(12)-O(4)	1.216(9)
C(12)-N(5)	1.371(10)
C(15)-N(1)	1.485(12)
C(18)-C(19)	1.518(12)
C(19)-N(6)	1.531(9)
C(20)-N(6)	1.504(10)
C(20)-C(21)	1.506(13)
C(22)-N(6)	1.499(10)
C(22)-C(23)	1.524(12)
C(24)-C(25)	1.523(11)
C(24)-N(6)	1.536(9)
Cl(1)-Fe(1)	2.253(2)
Fe(1)-N(4)	1.858(6)
Fe(1)-N(2)	1.865(6)
Fe(1)-N(3)	1.871(6)
Fe(1)-N(5)	1.872(6)

Table 3. Bond angles [°] for C25 H29 Cl Fe N6 O4 at 296(2) K with estimated standard deviations in parentheses.

Label	Angles
N(5)-C(1)-C(2)	128.2(8)
N(5)-C(1)-C(6)	111.8(7)
C(2)-C(1)-C(6)	120.0(7)
C(3)-C(2)-C(1)	119.7(9)
C(2)-C(3)-C(4)	119.4(8)
C(5)-C(4)-C(3)	122.5(8)
C(4)-C(5)-C(6)	119.3(9)
N(4)-C(6)-C(5)	130.0(8)
N(4)-C(6)-C(1)	111.0(6)
C(5)-C(6)-C(1)	119.1(8)
O(1)-C(7)-N(4)	124.6(8)
O(1)-C(7)-C(8)	122.3(8)
N(4)-C(7)-C(8)	113.1(7)
N(2)-C(8)-C(16)	111.7(7)
N(2)-C(8)-C(7)	107.9(7)
C(16)-C(8)-C(7)	107.3(8)
N(2)-C(8)-C(17)	109.9(8)

C(16)-C(8)-C(17)	112.7(8)
C(7)-C(8)-C(17)	107.1(7)
O(2)-C(9)-N(2)	125.1(8)
O(2)-C(9)-N(1)	117.5(8)
N(2)-C(9)-N(1)	117.3(7)
O(3)-C(10)-N(3)	125.2(8)
O(3)-C(10)-N(1)	117.1(7)
N(3)-C(10)-N(1)	117.7(7)
N(3)-C(11)-C(13)	111.4(6)
N(3)-C(11)-C(12)	108.4(6)
C(13)-C(11)-C(12)	106.3(6)
N(3)-C(11)-C(14)	113.6(6)
C(13)-C(11)-C(14)	110.0(6)
C(12)-C(11)-C(14)	106.8(6)
O(4)-C(12)-N(5)	124.4(7)
O(4)-C(12)-C(11)	123.6(7)
N(5)-C(12)-C(11)	112.0(6)
C(18)-C(19)-N(6)	116.1(7)
N(6)-C(20)-C(21)	115.8(7)
N(6)-C(22)-C(23)	115.0(6)
C(25)-C(24)-N(6)	114.3(6)
N(4)-Fe(1)-N(2)	85.3(3)
N(4)-Fe(1)-N(3)	153.0(3)
N(2)-Fe(1)-N(3)	95.0(3)
N(4)-Fe(1)-N(5)	82.5(3)
N(2)-Fe(1)-N(5)	152.0(3)
N(3)-Fe(1)-N(5)	84.8(3)
N(4)-Fe(1)-Cl(1)	101.3(2)
N(2)-Fe(1)-Cl(1)	105.0(2)
N(3)-Fe(1)-Cl(1)	104.6(2)
N(5)-Fe(1)-Cl(1)	102.09(19)
C(9)-N(1)-C(10)	131.0(7)
C(9)-N(1)-C(15)	113.5(8)
C(10)-N(1)-C(15)	115.2(8)
C(9)-N(2)-C(8)	118.8(7)
C(9)-N(2)-Fe(1)	125.9(5)
C(8)-N(2)-Fe(1)	114.9(5)
C(10)-N(3)-C(11)	117.9(6)

C(10)-N(3)-Fe(1)	125.5(5)
C(11)-N(3)-Fe(1)	113.9(4)
C(7)-N(4)-C(6)	127.0(7)
C(7)-N(4)-Fe(1)	116.5(6)
C(6)-N(4)-Fe(1)	116.4(5)
C(12)-N(5)-C(1)	127.0(7)
C(12)-N(5)-Fe(1)	116.9(5)
C(1)-N(5)-Fe(1)	116.0(5)
C(22)-N(6)-C(20)	111.2(6)
C(22)-N(6)-C(19)	105.8(6)
C(20)-N(6)-C(19)	111.3(6)
C(22)-N(6)-C(24)	112.3(6)
C(20)-N(6)-C(24)	105.9(5)
C(19)-N(6)-C(24)	110.5(6)

Table 4. Atomic coordinates ($x10^4$) and equivalent isotropic displacement parameters ($Å^2x10^3$) for C25 H29 Cl Fe N6 O4 at 296(2) K with estimated standard deviations in parentheses.

Label	x	y	z	Occupancy	U_{eq}^*
C(1)	5509(9)	5659(3)	4768(6)	1	31(2)
C(2)	4919(11)	5483(3)	3789(6)	1	39(2)
H(2)	3970	5598	3445	1	47
C(3)	5752(12)	5135(4)	3329(7)	1	50(2)
H(3)	5378	5022	2669	1	60
C(4)	7174(12)	4956(3)	3872(8)	1	54(3)
H(4)	7724	4723	3556	1	65
C(5)	7770(10)	5110(3)	4838(7)	1	39(2)
H(5)	8704	4982	5177	1	47
C(6)	6960(9)	5466(3)	5317(6)	1	32(2)
C(7)	8498(9)	5535(3)	7069(7)	1	38(2)
C(8)	8397(9)	5782(3)	8087(7)	1	43(2)
C(9)	6681(10)	6380(3)	8738(6)	1	36(2)
C(10)	4209(10)	6770(3)	7694(6)	1	37(2)
C(11)	3094(8)	6576(3)	5952(5)	1	28(2)
C(12)	3446(8)	6230(3)	5094(6)	1	30(2)
C(13)	3070(9)	7116(3)	5536(6)	1	37(2)
H(13A)	2611	7338	5969	1	56
H(13B)	2480	7126	4855	1	56

H13C()	4105	7225	5524	1	56
C(14)	1456(9)	6427(4)	6145(7)	1	42(2)
H(14A)	1523	6121	6536	1	63
H(14B)	779	6377	5502	1	63
H14C()	1061	6693	6517	1	63
C(15)	5300(16)	7049(5)	9436(8)	1	79(4)
H(15A)	4910	6854	9944	1	119
H(15B)	4609	7323	9214	1	119
H15C()	6297	7180	9724	1	119
C(16)	8225(12)	5364(4)	8830(7)	1	55(3)
H(16A)	7986	5507	9447	1	82
H(16B)	9170	5177	8987	1	82
H16C()	7407	5142	8530	1	82
C(17)	9883(10)	6090(4)	8413(8)	1	56(3)
H(17A)	9957	6342	7905	1	84
H(17B)	10758	5869	8479	1	84
H17C()	9862	6251	9057	1	84
C(18)	5855(10)	6750(4)	2877(8)	1	57(3)
H(18A)	5679	6393	2911	1	85
H(18B)	4901	6918	2614	1	85
H18C()	6258	6876	3550	1	85
C(19)	7003(9)	6851(3)	2177(7)	1	38(2)
H(19A)	6969	7208	2012	1	45
H(19B)	6670	6668	1543	1	45
C(20)	9266(9)	6971(3)	3594(6)	1	37(2)
H(20A)	10295	6847	3859	1	44
H(20B)	8616	6876	4079	1	44
C(21)	9326(11)	7539(4)	3546(7)	1	49(2)
H(21A)	9985	7639	3080	1	74
H(21B)	9725	7670	4215	1	74
H21C()	8308	7669	3313	1	74
C(22)	9574(9)	6860(3)	1790(6)	1	35(2)
H(22A)	9455	7221	1680	1	42
H(22B)	9131	6693	1155	1	42
C(23)	11289(10)	6738(4)	2035(7)	1	49(2)
H(23A)	11754	6913	2645	1	73
H(23B)	11769	6843	1476	1	73
H23C()	11426	6381	2137	1	73

C(24)	8809(9)	6139(3)	2832(6)	1	31(2)
H(24A)	9863	6064	3148	1	37
H(24B)	8157	6058	3324	1	37
C(25)	8359(10)	5801(3)	1899(7)	1	44(2)
H(25A)	7275	5833	1642	1	66
H(25B)	8595	5456	2089	1	66
H25C()	8925	5900	1378	1	66
Cl(1)	7409(2)	6870(1)	6013(2)	1	30(1)
Fe(1)	6120(2)	6220(1)	6558(1)	1	25(1)
N(1)	5427(9)	6721(3)	8548(5)	1	42(2)
N(2)	7038(7)	6126(3)	7923(5)	1	33(2)
N(3)	4317(7)	6509(2)	6853(4)	1	28(2)
N(4)	7313(7)	5674(2)	6294(5)	1	33(2)
N(5)	4863(7)	6006(2)	5346(5)	1	27(2)
N(6)	8678(7)	6707(2)	2597(4)	1	28(2)
O(1)	9526(7)	5237(3)	6970(5)	1	55(2)
O(2)	7401(7)	6352(3)	9618(4)	1	48(2)
O(3)	3119(7)	7050(2)	7797(5)	1	47(2)
O(4)	2569(7)	6168(2)	4286(4)	1	42(2)

*U_{eq} is defined as one third of the trace of the orthogonalized U_{ij} tensor.

Appendix C4. Data of single crystal structure of $[(bTAML)Fe^{IV}(Cl)]^-$

Appendix D

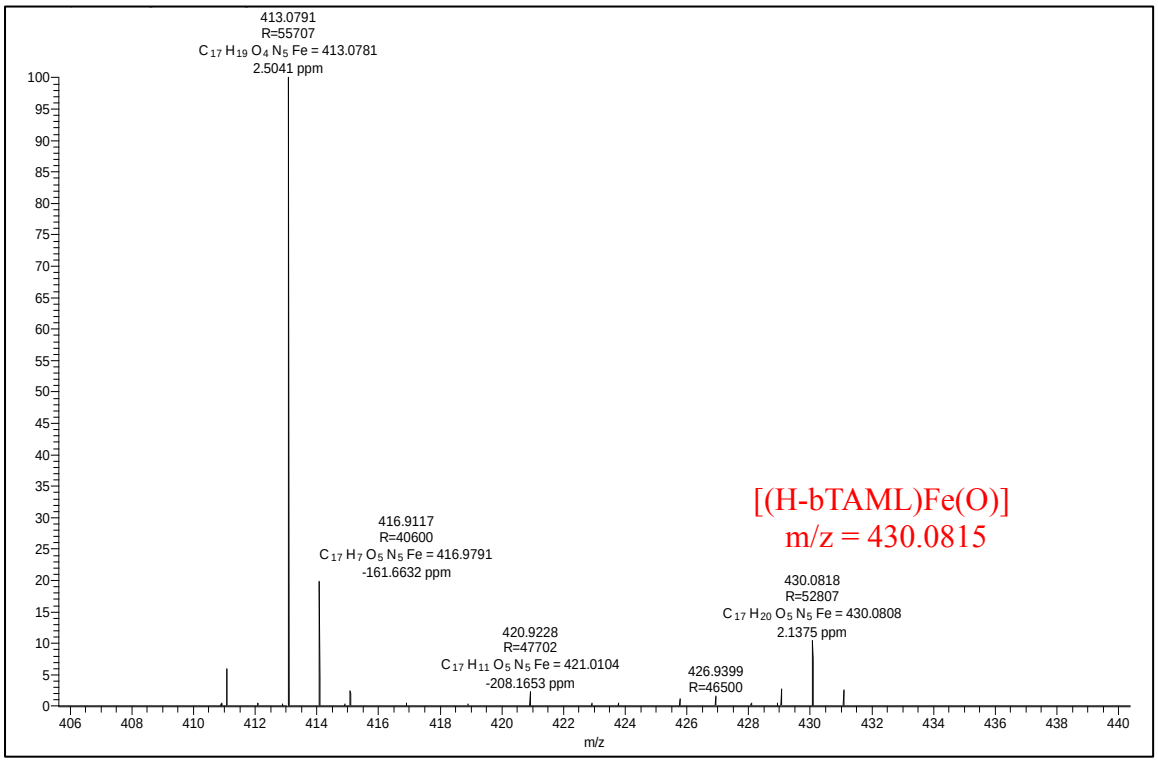

Appendix C1. HR-MS spectrum of solution mixture after addition of $(B(C_6F5)_3)$ in $[(bTAML)Fe^{V}(O)]^{-}$ displayed a mass peak at m/z = 430.0808 (calculated m/z = 430.0815).

List of Research Credentials, Awards and Conferences

List of Publications

1. Tuning the Reactivity of FeV(O) toward C −H Bonds at Room Temperature: Effect of Water. **Kundan K. Singh**, Mrityunjay k. Tiwari, Munmun Ghosh, Chaka Dola Panda, Andrew Weitz, Michael P. Hendrich, Basab B. Dhar, Kumar Vanka and Sayam Sen Gupta. *Inorg. Chem*. **2015**, *54*, 1535-1542.

2. Mechanism of Oxygen Atom Transfer from FeV(O) to Olefins at Room Temperature. **Kundan K. Singh**, Mrityunjay k. Tiwari, Basab B. Dhar, Kumar Vanka and Sayam Sen Gupta. *Inorg. Chem.* **2015**, *54*, 6112-6121.

3. Reductive Activation of O2 by a Bio-inspired Fe-Complex for Catalytic Epoxidation Reaction. **Kundan K. Singh**, and Sayam Sen Gupta, *Chem. Commun*. **2017**, *53*, 5914-5917.

4. Formation of a Room Temperature Stable $Fe^{V}(O)$ Complex: Reactivity Toward Unactivated C −H Bonds. Munmun Ghosh, **Kundan K Singh**, Chaka Dola Panda, Andrew Weitz, Michael P. Hendrich, Terrence J. Collins, Basab B. Dhar and Sayam Sen Gupta. *J. Am. Chem. Soc.* **2014,** *136*, 9524-9527.

5. Homogeneous Photochemical Water Oxidation by Biuret-Modifi ed Fe-TAML: Evidence of $Fe^{V}(O)$ Intermediate. Chaka Dola Panda, Joyashish Debgupta, David Díaz Díaz, **Kundan K. Singh**, Sayam Sen Gupta and Basab B. Dhar. *J. Am. Chem. Soc.* **2014,** *136*, 12273-12282.

6. Electrocatalytic water oxidation by a molecular cobalt complex through a high valent cobalt oxo intermediate. Debasree Das, Santanu Pattanayak, **Kundan K. Singh**, Bikash Garai and Sayam Sen Gupta. *Chem. Commun*. **2016**, *52*, 11787-11790.

7. Electrochemical formation of $Fe^{V}(O)$ and mechanism of its reaction with water during O-O bond formation. Santanu Pattanayak, Debarati Roy Chowdhury, Bikash Garai, **Kundan K. Singh**, Amit Paul, Basab B. Dhar and Sayam Sengupta. 2016, *Chem. Eur. J.* **2017**, *23*, 3414-3424.

8. Spectroscopic and Reactivity Comparison of a pair of bTAML Complexes with Fe^{V}=O and Fe^{IV}=O Units. Santanu Pattanayak, Andrew J. Jasniewski, Atanu Rana, Apparao Draksharapu, **Kundan K. Singh**, Andrew Weitz, Michael Hendrich, Lawrence Que, Jr., Abhishek Dey, and Sayam Sen Gupta, *Inorg. Chem*. **2017**, *56*, 6352-6361.

Awards

1. **CSIR-UGC National Eligibility Test (NET) for Lectureship and Junior Research Fellowship (India)** in Chemical Sciences for the period July 2011 to July 2016.
2. **Secured All India Rank 212 in Graduate Aptitude Test in Engineering (GATE-2011) (**Department of Higher Education-India) for the Subject Chemistry in the year 2011.

Conferences/Symposia/Workshop attended

1. Poster presentation in **"International Conference on Structural and Inorganic Chemistry"** during December 4-5, 2014. Hosted by CSIR-NCL, IISER-Pune and SP Pune University, India.
2. Poster presentation in **"17th CRSI National Symposium in Chemistry"** during February 6-8, 2015. Hosted by CSIR-National Chemical Laboratory, Pune, India.
3. Poster presentation in **"5th Symposium on Advanced Biological Inorganic Chemistry (SABIC)"** held in Kolkata during January 7-11, 2017. Hosted by TIFR-Mumbai and IACS-Kolkata, India.
4. Participant in National Conference on **"Chemistry Interfacing with Biology and Physics"** during January 27-28, 2017. Hosted by IISER-Kolkata, India.
5. Participant in workshop on **"ESR Spectroscopy Techniques & Applications"** under Continuing Education & Quality Improvement Programme, conducted by Indian Institute of Technology Bombay, India, during February 04-06,2013.
6. Participant in **"Workshop on Electronic Structure of Coordination Complexes (WESCC)"** conducted by Department of Chemistry, Indian Institute of Technology Bombay, India, during 16^{th} -18^{th}, May 2016.

About the Author

Kundan Kumar Singh Sagar, son of Sri Ajay Kishor Singh and Smt. Manikraj Devi was born in Chikanee village of Adapur tehsil, East Champaran (Motihari) district and the Bihar state of India. He persuaded his B.Sc. (Hons) with the honours subject of Chemistry from Faculty of Science, Banaras Hindu University-Varanasi in the year of 2006-2009 and M.Sc. in Chemistry from Department of Chemistry (Faculty of Science), Banaras Hindu University-Varanasi in the year of 2009-2011. He qualified Joint CSIR-UGC National Eligibility Test for Lectureship and Junior Research Fellow (JRF-NET)-Dec 2010 in the subject of Chemical Sciences and awarded fellowship for the period of the year 2011-2016. He joined Department of Chemical Engineering and Process Development Division, CSIR-NCL, Pune to pursue his Ph.D. degree in July 2011 under the supervision of Dr. Sayam Sen Gupta.